UNCLASSIFIED

AD NUMBER
AD904472
LIMITATION CHANGES
TO: **Approved for public release; distribution is unlimited.**
FROM: **Distribution authorized to U.S. Gov't. agencies only; Test and Evaluation; JUL 1972. Other requests shall be referred to Naval Ship Systems Command, Washington, DC 20360.**
AUTHORITY
USNSSC ltr dtd 21 Jun 1979

THIS PAGE IS UNCLASSIFIED

UNCLASSIFIED
Security Classification

DOCUMENT CONTROL DATA - R & D

(Security classification of title, body of abstract and indexing annotation must be entered when the overall report is classified)

1. ORIGINATING ACTIVITY *(Corporate author)* Naval Undersea Center San Diego, California 92132	2a. REPORT SECURITY CLASSIFICATION UNCLASSIFIED 2b. GROUP

3. REPORT TITLE

HANDBOOK OF UNDERWATER IMAGING SYSTEM DESIGN

4. DESCRIPTIVE NOTES *(Type of report and inclusive dates)*
Test and Evaluation – July 1971 to July 1972

5. AUTHOR(S) *(First name, middle initial, last name)*

C. J. Funk, S. B. Bryant, and P. J. Heckman, Jr.

6. REPORT DATE July 1972	7a. TOTAL NO. OF PAGES 344	7b. NO. OF REFS 37
8a. CONTRACT OR GRANT NO. b. PROJECT NO. Project order 1-0005 c. Project S4636 Task 12623 d.	9a. ORIGINATOR'S REPORT NUMBER(S) NUC TP 303 9b. OTHER REPORT NO(S) *(Any other numbers that may be assigned this report)*	

10. DISTRIBUTION STATEMENT
Distribution limited to U. S. Government agencies only; test and evaluation; July 1972. Other requests for this document must be referred to the Naval Ship Systems Command, Washington, D.C. 20360.

11. SUPPLEMENTARY NOTES	12. SPONSORING MILITARY ACTIVITY Naval Ship Systems Command Washington, D. C. 20360

13. ABSTRACT

The resources necessary to reliably predict optical viewing system performance in various water conditions have been summarized in handbook format. Multiple scattering effects are included. The handbook introduces the basic optical properties of seawater, conventional underwater television systems, and extended-range techniques. A nomogram is provided as a simple graphical tool for the design of conventional underwater television systems. A more general method, consisting of sets of formulas and data tables, is developed for predicting the performance of a variety of viewing systems as functions of hardware components (sources and receivers), practical viewing geometries, and water conditions. The formulas are summarized in a simple table, and sample calculations are presented. Finally, the analytical model is verified by comparison with experimental data.

DD FORM 1 NOV 65 1473 (PAGE 1)
0102-014-6600

UNCLASSIFIED
Security Classification

14. KEY WORDS	LINK A		LINK B		LINK C	
	ROLE	WT	ROLE	WT	ROLE	WT
Images						
Underwater cameras						
Underwater communication						
Optical properties						

TP 303

HANDBOOK OF UNDERWATER IMAGING SYSTEM DESIGN

by

C. J. Funk S. B. Bryant

P. J. Heckman, Jr.

Ocean Technology Department

Naval Undersea Center

July 1972

NAVAL UNDERSEA CENTER, SAN DIEGO, CA. 92132

AN ACTIVITY OF THE NAVAL MATERIAL COMMAND

ROBERT H. GAUTIER, CAPT, USN
Commander

Wm. B. McLEAN, Ph.D.
Technical Director

ADMINISTRATIVE INFORMATION

Work on this handbook was performed from July 1971 to July 1972 by members of the Advanced Systems Division. The work was sponsored by the Deep Ocean Technology Project, NAVSHIPS Project Order 1-0005, Project S4636, Task 12623. The report was reviewed for technical accuracy by T. J. Keil, Jr., and A. R. Waltz.

Released by
I. P. LEMAIRE, Head
Advanced Systems Division

Under authority of
H. R. TALKINGTON, Head
Ocean Technology Department

SUMMARY

PROBLEM

Develop, in handbook form, methods which designers can use to accurately predict the performance of a wide variety of undersea optical imaging systems under a broad spectrum of water conditions. Include sufficient background information, analytical resources, and input data (specification of typical hardware components and the optical properties of seawater) so that designers previously unfamiliar with undersea imaging systems can hypothesize practical systems, perform quantitative tradeoff analyses, and assess system potential.

RESULTS

1. A comprehensive handbook has been written to systematically describe the procedure used to predict the performance of underwater optical imaging systems. Analyses of both conventional and advanced extended-range imaging systems are included in the outlined procedure, which consists of sets of formulas, tables, and nomograms. In addition, a large body of engineering information, acquired from the development and testing of experimental systems and their components, is summarized in this handbook.

2. The system performance analysis is based on a mathematical model of the propagation of light in ocean water; this model has been developed and experimentally verified at the Naval Undersea Center. Monte Carlo techniques are used to simulate the multiple scattering of the light by the water.

RECOMMENDATIONS

Engineers should use the analysis procedure described in this handbook for the following.

1. Perform quantitative tradeoff analyses between competitive types of optical viewing systems.

2. Optimize the design of viewing systems selected for development.

3. Compare the performance of different optical imaging systems when they are tested under different water conditions.

CONTENTS

SECTION 1.	INTRODUCTION TO UNDERWATER IMAGING SYSTEM DESIGN	1-1
SECTION 2.	BASIC OPTICAL PROPERTIES OF SEAWATER	2-2
SECTION 3.	CONVENTIONAL UNDERWATER TELEVISION SYSTEMS	3-3
SECTION 4.	EXTENDED-RANGE UNDERWATER IMAGING SYSTEMS	4-4
SECTION 5.	SYSTEM PERFORMANCE NOMOGRAMS	5-5
SECTION 6.	SYSTEM PERFORMANCE ANALYSIS	6-6
APPENDIX A.	PERFORMANCE ANALYSIS WORKSHEETS	A-1
APPENDIX B.	SAMPLE CALCULATIONS	B-1
APPENDIX C.	EXPERIMENTAL VALIDATION OF THE SYSTEM PERFORMANCE ANALYSIS	C-1

METHOD OF UPDATING AND REVISING THE HANDBOOK

This handbook is designed to be periodically revised to reflect new information on undersea imaging system technology and related analytical techniques acquired through the Deep Ocean Technology (DOT) Program. Maintenance and expansion of the handbook is the responsibility of the Naval Ship Systems Command utilizing the Naval Ship Engineering Center as Technical Agent.

Because the handbook is published in loose-leaf form, revisions and additions can be easily made. A "User Comment Return Form" is included as a convenient method of obtaining feedback for additions or amendments. Individuals within the Navy and the nonmilitary community are encouraged to submit comments and additional data for future revisions of the handbook. Material received will be reviewed by NAVSEC and considered for possible inclusion in the handbook at a later date.

SECTION 1

INTRODUCTION TO UNDERWATER IMAGING SYSTEM DESIGN

1.1 Viewing System Requirements 1-4

1.1.1 Environment 1-4

1.1.2 Vehicle 1-4

1.1.3 System Use 1-5

1.1.4 Summary 1-5

1.2 Scope of Handbook 1-6

1.3 Organization of Handbook 1-7

1.4 Reference 1-8

SECTION 1

INTRODUCTION TO UNDERWATER IMAGING SYSTEM DESIGN

The military and civilian necessity for effective underwater imaging* is extensive. Present goals include the following.

- Long-range search.
- Close-range classification and inspection.
- The extension of vision to remote undersea work systems.
- Large-area mapping of the ocean floor.
- Pollution monitoring.
- The extension of diver viewing ranges for increased safety and work efficiency.
- Maintenance inspection of in-sea installations.
- Salvage operations, from initial surveys of salvage sites to eventual monitoring of recovery operations.

Unfortunately, formidable environmental problems challenge progress in underwater imaging. Light is both scattered and absorbed in water, resulting in poor resolution, reduced contrast, and limited viewing ranges. High pressures and the corrosive action of seawater pose challenges to hardware design, and changing conditions and an inadequate data bank make it difficult to accurately predict system performance.

To the program manager, engineer, or scientist responsible for in-ocean systems development, underwater imaging is an additional problem. Although imaging components often comprise only a fraction of the total in-ocean system, such as a manned or unmanned submersible, they affect the total system in a number of significant ways.

- Imaging systems often limit the useful range of the work of the total system.
- Imaging systems are critical to the survival of the total system, particularly when used for close-in maneuvering.
- Components selected to meet specified viewing ranges and resolutions place size, weight, and power requirements on the total system.

Significant errors in the initial design phase can later be costly. The frustration facing the designer is that it has often been difficult, if not impossible, to predict how well a combination of imaging components will perform in a given body of water or, conversely, to develop an appropriate combination of components to meet a specified performance. Even the specialist in imaging system design has been faced with inadequate resources to reliably predict the performance of an optical system in the undersea environment.

"Imaging" in this handbook refers to optical imaging. Although acoustic imaging is a rapidly developing field, the capabilities of field-operational equipment have not yet been demonstrated.

This handbook is one approach to this problem. For several years, the Naval Undersea Center (NUC), under the sponsorship of the Deep Ocean Technology Program, has been developing an analytical model for accurately predicting the performance of underwater optical imaging systems. A major feature of this model is its capability to describe the most significant effects of multiple scattering on imaging system performance. (The role of multiple scattering increases dramatically as viewing ranges are increased.) The results of this theoretical research have been summarized in this handbook as nomograms, sets of equations, and tables of input data which can be used to calculate the performance of various types of imaging systems. These formulas and tables permit the designer to consider a variety of conventional and advanced system components (sources and receivers), targets, practical viewing geometries, and water conditions and to determine system performance under any combination of these parameters. In addition, a large body of engineering information derived from the development and testing of underwater imaging systems and their components is summarized in this handbook. This engineering data describes factors such as system cost, complexity, reliability, maintenance, safety, and operability.

This section of the handbook discusses basic viewing system requirements, defines the scope of the handbook as it applies to these requirements, and describes the organization of the handbook.

1.1 VIEWING SYSTEM REQUIREMENTS

The design of any underwater viewing system will depend upon the environment, the platform or vehicle on which the system is used, and the specific use or purpose of the viewing system.

1.1.1 ENVIRONMENT – Primary environmental parameters or effects which must be considered in the design of an undersea optical viewing system are listed below.

- Light scattering and absorption effects.
- Refraction at optical interfaces due to the differences in the refractive indices of water and air.
- Pressure effects.
- Low-temperature environment and resulting humidity and condensation problems.
- Corrosion and marine fouling if long submersion times are involved.

1.1.2 VEHICLE – If the viewing system is to be operated from a submarine, small submersible, cable-controlled vehicle, or self-contained remotely operated vehicle, the power consumption and mechanical configuration must be considered. Other features, which are important regardless of vehicle type, are system reliability and ease of operation.

Operating Power. Small submersibles or self-contained remotely operated vehicles are generally battery operated. Energy (power $\times$ time) is at a premium because unnecessary power consumption reduces the maximum duration of the mission. Although cable-operated

vehicles are not energy limited, they are generally power limited due to cable size. When long cablelengths are involved, the hydrodynamic drag due to the cross-sectional area (and the corresponding power capacity) of the cable becomes critical.

Size. Minimum size is required for both internal components, such as displays and control consoles, and externally mounted hardware. Space is generally at a premium inside any submersible vehicle, and large external size can critically increase drag and reduce speed and vehicle maneuverability.

Weight. On a small submersible, any substantial weight increase must be compensated by buoyancy material which can adversely affect the speed/maneuverability characteristics of the vehicle.

Reliability. For most underwater vehicles, viewing system failure results in abortion of the dive, and for some critical operations, viewing system failure can also lead to complete mission failure.

Ease of Operation. Because submersible operators will generally be occupied with vehicle control, work system operation, etc., operation should be as simple as possible and require minimum effort and time.

Maintainability. When missions require that vehicles be used in remote locations or when they impose rigid time schedules, maintainability becomes critical to mission success.

1.1.3 SYSTEM USE – The intended use of the viewing system dictates the relative importance of the various system parameters.

Range and Resolution. If the system is to be primarily used for vehicle guidance and target classification, maximum range and resolution will be desired. This system will probably have a relatively small field-of-view to provide high angular resolution and low source-spreading losses.

Field-of-View. For general viewing or close-in observation, the advantages of a wide field-of-view take precedence over high resolution. Because an increase in field-of-view degrades the angular resolution capability of the system, these features must be traded-off for any given application. Some situations might need pan-and-tilt mechanisms to provide the desired angular coverage while high resolution is maintained.

Viewing Technique. The optimum system type or viewing technique for a given vehicle will depend upon system use and the water characteristics which will be encountered. For example, extended-range techniques would neither be necessary nor practical for close-in viewing.

1.1.4 SUMMARY – Although the relative order of importance will depend upon the intended use of the system, the basic system requirements are listed below.

1. High reliability.
2. Ease of operation.
3. Low power input.
4. Minimum size and weight.
5. Good range and resolution characteristics.
6. Adequate field-of-view.
7. Low cost for development and production.
8. Low maintenance.

1.2 SCOPE OF HANDBOOK

The information in subsequent sections of this handbook is restricted to electro-optical receivers, i.e., television cameras and scanning photomultiplier tubes using artificial illumination sources. Both conventional and extended-range imaging systems are described. (The extended-range systems have special components for implementing the backscatter-reduction techniques of polarization discrimination, range gating, and volume scanning.)

The emphasis of the handbook is on performance analysis, which allows the designer to perform quantitative system tradeoffs. Parameters available for use in the analysis are listed below.

1. Source power, beam pattern, and spectral characteristics.
2. Source-receiver separation and the orientation of the optical axes of the source and receiver.
3. Target reflectance and contrast.
4. Receiver field-of-view and depth-of-field.
5. The f/ and transmission coefficient of the receiver's optical system.
6. Threshold sensitivity, spectral response, and other performance specifications for various types of television tubes.
7. Performance characteristics of polarizers and analyzers, electrooptical shutters and gated image intensifiers, beamscanning optics, and the other specialized equipment used in the backscatter-reduction systems.

Several analytical resources are available to the user: a simple set of nomograms for the performance evaluation of conventional systems, worksheets for the evaluation of a large variety of systems for a simple viewing geometry, and sets of algebraic equations for the evaluation of a large variety of systems for both the simple and more complex geometries. In addition, the basic properties of underwater light sources and television cameras are compiled in a series of tables and graphs. These resources are outlined in the following section.

1.3 ORGANIZATION OF HANDBOOK

This handbook has been organized into six main sections and three appendices. The specific organization is as follows.

Section 1. Introduction to Underwater Imaging System Design.

Section 2. Basic Optical Properties of Seawater. This section introduces the basic physics of imaging in the sea, provides a glossary of commonly used underwater imaging terminology, describes the instrumentation for measuring the optical properties of seawater, and tabulates the data essential for subsequent performance analyses.

Section 3. Conventional Underwater Television Systems. This section introduces the four most common light sources and the five most common television cameras used in underwater viewing systems. Considerations involved in successful combinations of these sources and receivers are established, and the data essential to subsequent performance analyses is tabulated.

Section 4. Extended-Range Techniques. This section discusses three principal techniques for extending underwater viewing ranges by the reduction of backscattered light: polarization discrimination, range gating, and volume scanning. Methods of implementing the techniques are presented, and adequate component data is tabulated to facilitate subsequent analyses.

Section 5. Conventional System Nomogram. This section provides a simple graphical description of the major tradeoffs involved in the design of a conventional underwater television system. This first-order approach to viewing system design can be read and used independently of the remainder of the handbook.

Section 6. System Performance Analysis. In this section, the fundamental analytical resources of the handbook are developed. Three sets of formulas are developed for conventional, polarization-discrimination, range-gated, and volume-scanning systems. The first set of formulas describes the signal and noise photocurrents generated by imaging and non-imaging scattered light which is incident on the receiver from conventional illumination sources. The second set of equations describes the signal and noise photocurrents produced by lasers or other narrow spectral bandwidth sources. To facilitate hand calculations, the logarithm is taken of both sets of equations to obtain complementary sets of decibel equations which are similar to the "sonar equation" of underwater acoustics. These first two sets of equations and their decibel counterparts are simplifications and approximations of the third set of equations which describe a more general viewing system geometry. This final set of more complex equations is derived in reference 1.1. Sufficient data is provided in this section so that the designer can evaluate a large range of hypothetical imaging systems without reliance on external information.

Appendix A. Performance Analysis Worksheets. This appendix consists of two sets of worksheets designed to facilitate hand calculations of the performance analysis described in section 6. The first set of worksheets is for evaluating systems that use conventional light sources, and the second set is for systems that use lasers.

Appendix B. Sample Calculations. This appendix contains sample evaluations of several practical imaging systems. The samples illustrate proper execution of the analysis scheme developed in section 6, display the range of information that can be derived, and demonstrate the applicability of the analysis to realistic imaging systems.

Appendix C. Experimental Validation of the System Performance Analysis. The appendix establishes the validity of the preceding analysis by comparing analytical predictions with experimental data obtained by the Visibility Laboratory of Scripps Institute of Oceanography and by the Ocean Technology Department of the Naval Undersea Center.

1.4 REFERENCE

1.1 Naval Undersea Research and Development Center, NUC TP 273. *Comparison of Advanced Underwater Television Systems,* by S. Bryant, D. Cozen, R. Fugitt, and C. Funk, San Diego, California. January 1972.

SECTION 2. BASIC OPTICAL PROPERTIES OF SEAWATER

2.1 Imaging in the Sea: Basic Physics 2-3

2.2 Glossary 2-4

2.3 Water Characteristics Instrumentation 2-7

- 2.3.1 Transmissometer 2-7
- 2.3.2 Nephelometer 2-8
- 2.3.3 Small-Angle Forward-Scattering Meter 2-8
- 2.3.4 Modulation-Transfer-Function (MTF) Meter 2-8
- 2.3.5 Polarization Meter 2-9
- 2.3.6 Absorption Meter 2-9

2.4 Data 2-9

2.5 References 2-10

Figures

2.1 Block Diagram of Basic Imaging Situation 2-11
2.2 Marine Advisors Transmissometer 2-12
2.3 SRI Transmissometer 2-12
2.4 Operation of Nephelometer 2-13
2.5 Scripps Nephelometer 2-13
2.6 Small-Angle Scattering Meter 2-14
2.7 Diver Aligning SRI Small-Angle Forward-Scattering Meter 2-14
2.8 MTF Meter 2-15
2.9 Tetra Tech Modulation-Transfer-Function (MTF) Meter 2-16
2.10 Breadboard Polarization Meter 2-17
2.11 NUC Polarization Meter and Waterproof Polyvinyl Chloride (PVC) Housing . 2-18
2.12 Absorption Meter 2-19
2.13 SRI Absorption Meter 2-19

Tables

2.1 Typical Water Characteristics Instrumentation 2-20
2.2 Spectral Variation of the Total Attenuation Coefficient for Light in Seawater (ln/m) 2-21
2.3 Spectral Variation of the s/a Ratio for Light in Seawater 2-22

SECTION 2. BASIC OPTICAL PROPERTIES OF SEAWATER

This section describes the most important optical properties of seawater, contains a glossary of the most commonly used terms, introduces common water characteristics instrumentation, and summarizes important data.

2.1 IMAGING IN THE SEA: BASIC PHYSICS

Seawater and its complex effects on light transmission pose formidable problems to the designers of underwater imaging systems. The imaging situation in figure 2.1 shows some of the more important problems. These problems are listed below.

1. Some source light is scattered out of the beam, and does not reach the target.
2. Some source light is absorbed or converted to a different form of energy, such as thermal kinetic energy or chemical potential energy, and does not reach the target.
3. Some source light, scattered backwards into the receiver's field-of-view, does not reach the target and tends to reduce the contrast at the receiver.
4. Some reflected light is absorbed, and does not contribute to the image.
5. Some reflected light is scattered out of the receiver's field-of-view, and does not contribute to the image.
6. Some reflected light undergoes small-angle forward scattering, introducing resolution losses.

These six problems are special cases of three more general problems – attenuation, backscatter, and small-angle forward scattering – which will be discussed in this section.

The first of these problems that the system designer must consider is the attenuation of image-forming radiation due to absorption and scattering. Water selectively attenuates light as a function of wavelength or color. Near 4800 Å in the blue-green region of the electromagnetic spectrum, light is transmitted with less attenuation through clear water than it is at other wavelengths. This peak transmission normally shifts to longer wavelengths as the amount of dissolved organic material in the water is increased. However, even at peak transmission, the ability to transmit light over long distances is severely limited. In clear ocean water, the maximum viewing ranges for advanced imaging systems are a few hundred feet; in turbid water, imaging is often limited to a few feet. Increasing these distances is difficult because the light is exponentially attenuated as a function of range.

The second imaging problem for the designer is backscatter. When source light is scattered into the receiver's field-of-view by particles in the water, image contrast is degraded. As more light is backscattered, a visibility condition arises which is similar to that encountered when automobile headlights are used in fog. Finally, the image contrast becomes so low that

the image is no longer detectable or recognizable. A variety of techniques and systems have been devised to combat this phenomenon and are discussed in later sections of this handbook.

The remaining problem, small-angle forward scattering, can introduce serious resolution losses. The significance of these losses depends on the nature of the water, the imaging system and its geometry, and resolution requirements.

These three problems can be quantitatively characterized by a set of optical measurements. The measured parameters are defined in section 2.2, and typical instruments for performing these measurements are discussed in section 2.3

2.2 GLOSSARY

The following terms describe the major and minor phenomena which influence underwater imaging systems.

Absorption. This is the thermodynamically irreversible process by which light energy is converted to a different form, such as thermal kinetic energy or chemical potential energy, and is thereby lost from the image-forming process.

Absorption Coefficient, a. This coefficient, which describes the attenuation of light for a particular wavelength by the absorption mechanism alone, strongly depends on the optical wavelength. It is related to the attenuation coefficient α and the scattering coefficient s according to

$$a = \alpha - s. \tag{2.1}$$

(Typical units: 1n/m.)

Absorption Limit. (The alternate terminology is photon limit or shot-noise limit.) For a given light source, this is the range between the target and the receiver at which the number of arriving photons per resolution element is so small that the photon statistics affect and degrade the image quality. Insufficient light is collected at the receiver at this limit to form an image. (Typical units: m.)

Attenuation. This is the process by which light is lost from a collimated beam by two independent processes: absorption and scattering.

Attenuation Coefficient, α. This coefficient describes the total decrease in the intensity of the unscattered light of a particular wavelength in a collimated beam according to the formula

$$H^* = H^*_0 e^{-\alpha x}. \tag{2.2}$$

The parameter H^*_0 is the initial intensity of the unscattered light, and H^* is the intensity of the unscattered light a distance x away (the water is assumed to be macroscopically homogeneous). Theoretically, the coefficient α is related to the absorption coefficient a and the scattering coefficient s according to

$$\alpha = a + s. \tag{2.3}$$

However, the measurement of α is complicated by the necessity of distinguishing unscattered light from the light which has been scattered by very small angles. Because some scattered light is always collected at the receiver of even the best instruments, the measured attenuation is actually given by

$$\alpha' = a + ks, \tag{2.4}$$

where k is some number less than one whose value depends on the instrument. Because the value of the measured attenuation coefficient depends on the instrument's design as well as the properties of the water, the accuracy of reported measurements of the attenuation coefficient must be carefully evaluated. (Typical units: 1n/m.)

Attenuation Length. The attenuation length, the reciprocal of the attenuation coefficient α, is the range at which the unscattered light of a particular wavelength in a collimated beam is decreased in macroscopically homogeneous water by a factor of $1/e = 0.3679$. As a general rule, large dark objects, such as swimmers in black wet suits, are just visible at a horizontal distance of about 4 attenuation lengths when there is sufficient underwater daylight. (Typical units: m.)

Backscatter. Backscatter is that portion of source illumination reflected into the receiver's field-of-view by particles and inhomogeneities in the water (exclusive of light reflected by the target).

Backscatter Coefficient, b. This is the coefficient which describes the amount of light scattered in the interval: $90 \text{ deg} \leqslant \theta \leqslant 180 \text{ deg}$. The coefficient b is related to the volume scattering function $\sigma(\theta)$ by

$$b = 2\pi \int_{\pi/2}^{\pi} \sigma(\theta) \sin\theta \, d\theta. \tag{2.5}$$

(Typical units: 1n/m.)

Backscatter Fraction, η. This parameter is defined by

$$\eta = b/s, \tag{2.6}$$

where b is the backscatter coefficient and s is the scattering coefficient. (Typical units: dimensionless.)

Backscatter Limit. (The alternate terminology is contrast limit.) For a given light source, this is the range between the target and the receiver at which the amount of backscatter is so large that the image contrast is degraded to the point where the image is no longer detectable or recognizable. (Typical units: m.)

Diffuse Attenuation Coefficient, k. This coefficient describes the vertical attenuation of daylight in seawater according to the equation

$$H(z_2) = H(z_1)e^{-k(z_2 - z_1)}. \tag{2.7}$$

The parameter $H(z_1)$ is the total irradiance, both scattered and unscattered, which is detected by an integrating sphere at depth z_1, while $H(z_2)$ is the total irradiance measured at depth z_2. (The water is assumed to be macroscopically homogeneous, and the light is assumed to have its asymptotic radiance distribution at depths z_1 and z_2 (see ref. 2.1).) An integrating sphere detects the light which is incident from all directions on a small volume element. By using the appropriate spectral filters, the wavelength dependence of k can also be measured. (Typical units: 1n/m.)

Irradiance. This is the radiant power per unit area. (Typical units: W/m^2.)

Polarization Coefficient of Backscattered Light, ψ_b. This parameter gives the fraction of light which is backscattered from a collimated, linearly polarized beam of light which retains its original polarization. Operationally, ψ_b is defined by

$$\psi_b = \frac{H_{max} - H_{min}}{H_{max} + H_{min}}, \tag{2.8}$$

where H_{max} and H_{min} are the maximum and minimum values of received backscattered irradiances when a linear analyzer is rotated in front of the receiver.

Scattering. Scattering is the process by which the direction of individual photons is changed without any other alteration. Because most scattering of light in seawater is the result of the different sizes of the particles, scattering is nearly independent of wavelength.

Scattering Coefficient, s. The scattering coefficient, which describes the attenuation of light of a particular wavelength by the scattering mechanism alone, is related to the volume scattering function $\sigma(\theta)$ by

$$s = 2\pi \int_0^{\pi} \sigma(\theta) \sin\theta \, d\theta. \tag{2.9}$$

(Typical units: 1n/m.)

Small-Angle Forward Scattering. This scattering is caused by the refractive deviations of light passing through transparent plankton and by temperature and salinity fluctuations. These processes, which produce a significant amount of light which is scattered by angles less than 1 deg, degrade the resolution of the imaging system.

Volume Scattering Function, $\sigma(\theta)$. This function describes the angular dependence of the light scattered from a small volume element. Operationally, $\sigma(\theta)$ is defined by the equation

$$dJ(\theta) = \sigma(\theta) H dV, \tag{2.10}$$

where $dJ(\theta)$ is the radiant intensity (power/solid angle) of the light scattered from a collimated beam in the volume element dV. The polar angle θ describes the direction of the

scattered light with respect to the axis of the collimated beam. The irradiance H gives the power per unit area of the light incident on dV. (Typical units: ln/(sr · m).)

Water Window. This is the spectral bandwidth (λ_1, λ_2) for which light penetrates seawater with the lowest attenuation losses. For clear water, the window is centered near 4800 Å.

2.3 WATER CHARACTERISTICS INSTRUMENTATION

Water can be characterized by a few unique parameters which can then be used to predict the performance of real or hypothetical imaging systems in a particular type of water. This section of the handbook discusses the instrumentation used to measure these water characteristics. The list of instruments is not inclusive; in fact, some of the instruments are not necessarily ideal, and more development in the ability to measure certain functions is required. The following discussion, however, should acquaint imaging system designers with current instrumentation and its associated problems.

Typical measuring meters are listed in table 2.1. General and specific properties of these meters are discussed in the following sections.

2.3.1 TRANSMISSOMETER – Transmissometers, or α-meters, are used to measure the spectral volume attenuation coefficient. A basic transmissometer consists of a light source with a very narrow, highly collimated beam and a receiver with a very narrow field-of-view. The source and detector are separated by a fixed, known pathlength x. Photocells measure the radiant output of the source and the irradiance detected at the receiver. From these measurements, the percent transmission T of unscattered light over the pathlength x can be determined. The attenuation coefficient is then calculated using

$$\alpha = -\ln(T)/x. \tag{2.11}$$

Color filters can be used to determine the dependence of α on the wavelength.

The main problem with transmissometers is the physical impossibility of excluding all of the scattered light from the irradiance measured by the receiver. The result is a reduced α as defined in equation 2.4:

$$\alpha' = a + ks, \tag{2.4}$$

where $0 < k < 1$. By inspection, $\alpha' < \alpha$. The value of k is determined by the acceptance angle θ_0 of the transmissometer. Light scattered by angles less than θ_0 is not distinguished from the unscattered light by the transmissometer. Because the volume scattering function is strongly peaked in the forward direction (small angles) and because α is a coefficient in an exponential function, large values of θ_0 can introduce considerable error in viewing range calculations. The Marine Advisors transmissometer (fig. 2.2) accepts all the scattered light in a 1-deg cone surrounding its optical axis, i.e., θ_0 = 1 deg. The value of the acceptance angle for the SRI transmissometer (fig. 2.3) is θ_0 = 0.17 deg.

2.3.2 NEPHELOMETER – The nephelometer, or large-angle scattering meter, is used to determine the volume scattering function $\sigma(\theta)$. From this function, the scattering coefficient s and the backscatter coefficient b can be determined by equations 2.9 and 2.5. The basic operation of the nephelometer is shown in figure 2.4. The light scattered from an elemental scattering volume is recorded by a photodetector that rotates in a semicircle at a fixed radius from the scattering volume.

One problem with the nephelometers has been a difficulty in defining the elemental scattering volume. Another problem occurs because the instruments were not designed to measure scattering at very small angles: Because the volume scattering function is strongly peaked at small angles, errors occur in attempting to evaluate s by integrating the volume scattering function that is determined by this instrument.

The Scripps Institute of Oceanography (SIO) nephelometer is shown in figure 2.5.

2.3.3 SMALL-ANGLE FORWARD-SCATTERING METER – Small-angle forward-scattering meters are used to determine $\sigma(\theta)$ for very small angles (generally less than 1 deg). Several of these meters are in either the proposal stages or in operation. A typical design is shown in figure 2.6. In this design, a collimated beam from a laser is passed through the scattering medium. It then passes through a long focal-length lens (450 mm), and is imaged on a photographic plate at the focal plane of the lens. Effectively, the laser provides an infinitely distant point source, and the camera is focused at infinity. In the absence of a scattering medium, the illuminating beam, depending on how well it has been collimated, will be focused to a diffraction-limited spot on the film. When a scattering medium is present, the focused spot will diverge, yielding a distribution of energy distance versus distance from the beam center. For single-scattered light, the distance from the center of the beam is directly related to the angle at which the light is scattered.

Problems inherent in such meters are diffraction effects due to finite optical apertures, multiple scattering, beam alignment problems, and extraneous scattering from optical surfaces in proximity to the beam.

The SRI meter (fig. 2.7) is described in reference 2.2. The most widely used small-angle scattering meter has been developed by SIO and is described in reference 2.3.

2.3.4 MODULATION-TRANSFER-FUNCTION (MTF) METER – Modulation-transfer-function (spatial frequency response) meters, which measure the MTF of a fixed pathlength of water, can be used to determine $\sigma(\theta)$ for small angles. One design works by shining a light beam through a transparent, variable-frequency bar pattern laid on a rotating disk; recording the light output at the opposite end of a calibrated pathlength of water; and displaying the output on an oscilloscope (fig. 2.8). Reference 2.4 relates the measured MTF to the volume scattering function for small angles.

The Tetra Tech MTF meter is shown in figure 2.9.

2.3.5 POLARIZATION METER – The polarization-meter design, shown in figure 2.10, is designed to measure the degree of polarization, as defined in equation 2.8, of backscattered light in seawater. The laser output is passed through a rotating beam chopper, a linear polarizer, and an aperture (to block spurious reflections) into the scattering medium. A portion of the backscattered light is intercepted by an analyzer-detector module, and the detector output is displayed on an oscilloscope. The rotating polarizer produces a modulation of the signal at twice the rotational frequency. The maximum signal H_{max} occurs when the polarizer and analyzer are in the "aligned" position, and the minimum signal H_{min} occurs when they are "crossed." This meter, designed and constructed at NUC, is shown in figure 2.11.

2.3.6 ABSORPTION METER – The absorption coefficient can be found by direct substitution into equation 2.1 if s and α are known (s is found by integrating a nephelometer output). However, if either of these quantities is unknown or, more commonly, if the accuracy of s is questionable, the absorption coefficient can be directly measured with an absorption meter. A simple design is shown in figure 2.12. The operation of the meter can be understood if the irradiance detector is considered to be an element of a sphere that is concentric about the source. Because of the symmetry of the source, the total radiant flux through the sphere can be determined from the flux detected by the irradiance meter. Thus, because the scattered light also passes through the spherical surface, the instrument only measures the loss in light intensity that is the result of absorption. The meter can be calibrated by measuring the flux for two distances between the source and the irradiance detector.

Although there are a few sources of error in the measurements made by this meter, they can be minimized by careful design. One type of error, an intrinsic error, results because scattered light travels farther between the source and the irradiance meter than unscattered light does. Thus, the scattered light is more attenuated than the unscattered light because there is a greater probability that it will be absorbed because of its longer pathlength. The amount of this intrinsic error can be estimated, and it is quite small if the distance between the source and the irradiance meter is considerably less than 1/s, the mean free scattering length. The meter must also be calibrated to account for a lack of uniformity in the omnidirectional characteristics of the source. Slight mechanical misalignments also introduce significant errors, and, with some models, proximity to the surface or submerged objects introduces reflections that cause errors.

The SRI absorption meter is shown in figure 2.13, and is described in reference 2.5.

2.4 DATA

The data in this section, which is duplicated for convenience in section 6, has been gathered from the work of several researchers. The distilled water data is from Clark, James, and LeGrand (ref. 2.1); the bay water data is from Hulbert (ref. 2.6); the coastal water data is from Pelevin (ref. 2.7); and the deep ocean data is from Matlack (ref. 2.8). Based on these sources, tables 2.2 and 2.3 were compiled.

2.5 REFERENCES

2.1 Jerlov, N. G. *Optical Oceanography.* Elsevier Publishing Co., Amsterdam, The Netherlands. 1968.

2.2 Stanford Research Institute, SRI Project 6572. *Underwater Visibility Meter Concept Study, Final Report,* by Glenn P. Sorenson and Richard C. Honey. Menlo Park, California. February 1968.

2.3 Scripps Institute of Oceanography, Visibility Laboratory, SIO Ref. 71-1. *Underwater Lighting by Submerged Lasers and Incandescent Sources*, by Seibert Q. Duntley. San Diego, California. June 1971.

2.4 Wells, Willard H. "Loss of Resolution in Water as a Result of Multiple Small-Angle Scattering," *Journal of the Optical Society of America.* Vol. 59, no. 6, pp. 686-691. June 1969.

2.5 Stanford Research Institute, SRI Project 7440. *Optical Absorption Meter, Final Report,* by G. D. Gilbert, R. C. Honey, R. E. Meyers, and G. P. Sorenson. Menlo Park, California. April 1969.

2.6 Hulbert, E. O. "Optics of Distilled and Natural Waters," *Journal of the Optical Society of America.* Vol. 35, pp. 698-705. November 1945.

2.7 Pelevin, V. N. "Some Experimental Results of the Determination of the True Absorption Coefficient of Light at Sea," *Research in Hydrooptics – USSR.* Joint Publications Research Service, Washington, D. C. Vol. 36, no. 816, pp. 45-53. 3 August 1966.

2.8 Naval Ordnance Laboratory, NOLTR 70-165. *The Deep Ocean Optical Measurement (DOOM) Project,* by D. Matlack. Silver Springs, Maryland. 18 January 1971.

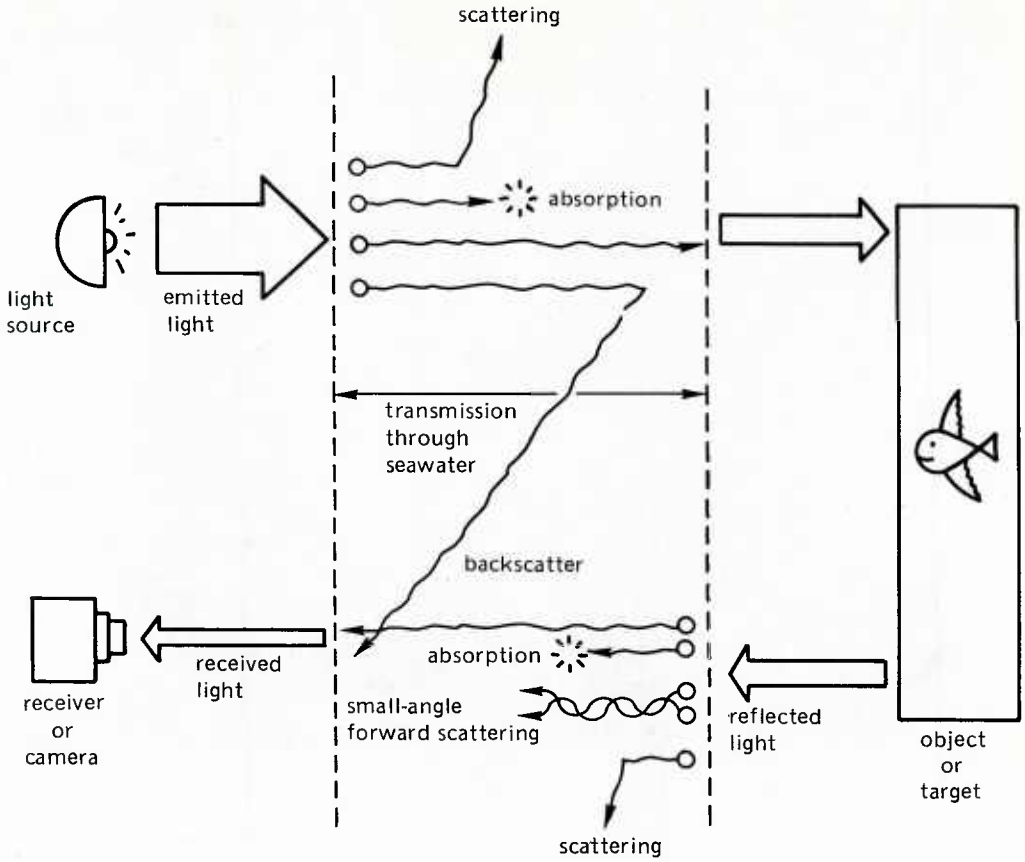

Figure 2.1. Block diagram of basic imaging situation.

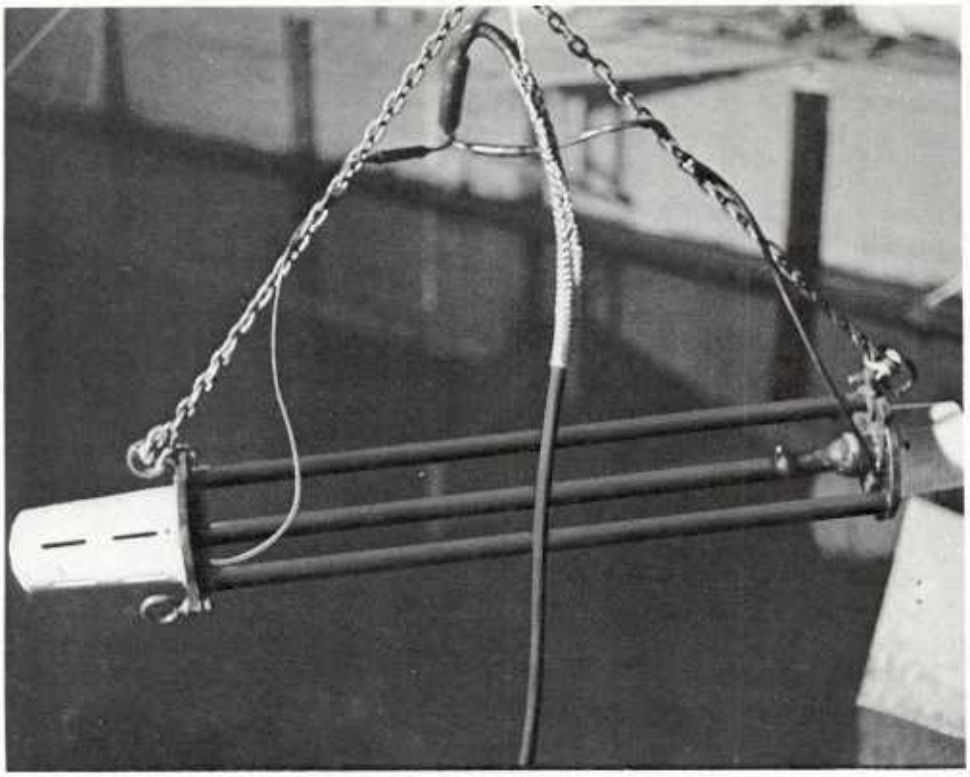

Figure 2.2. Marine Advisors transmissometer.

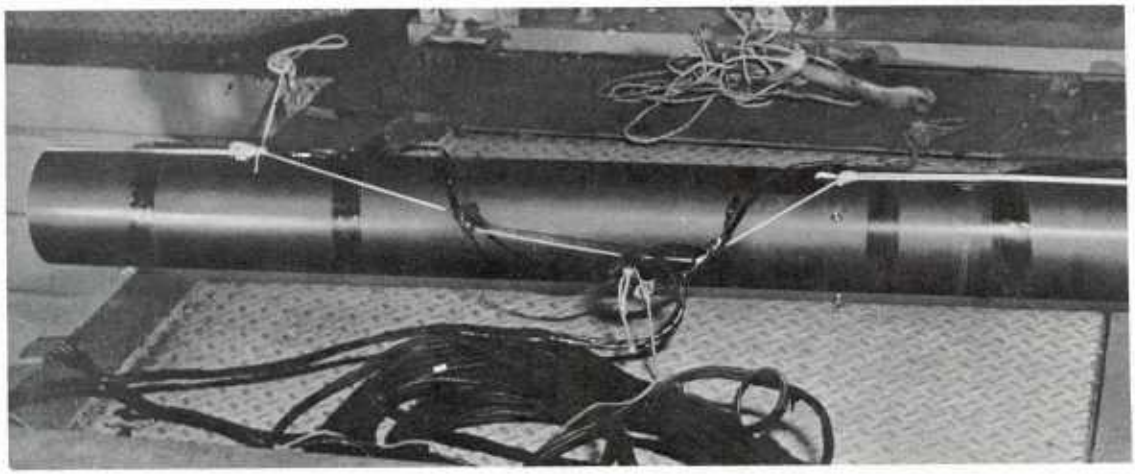

Figure 2.3. SRI transmissometer.

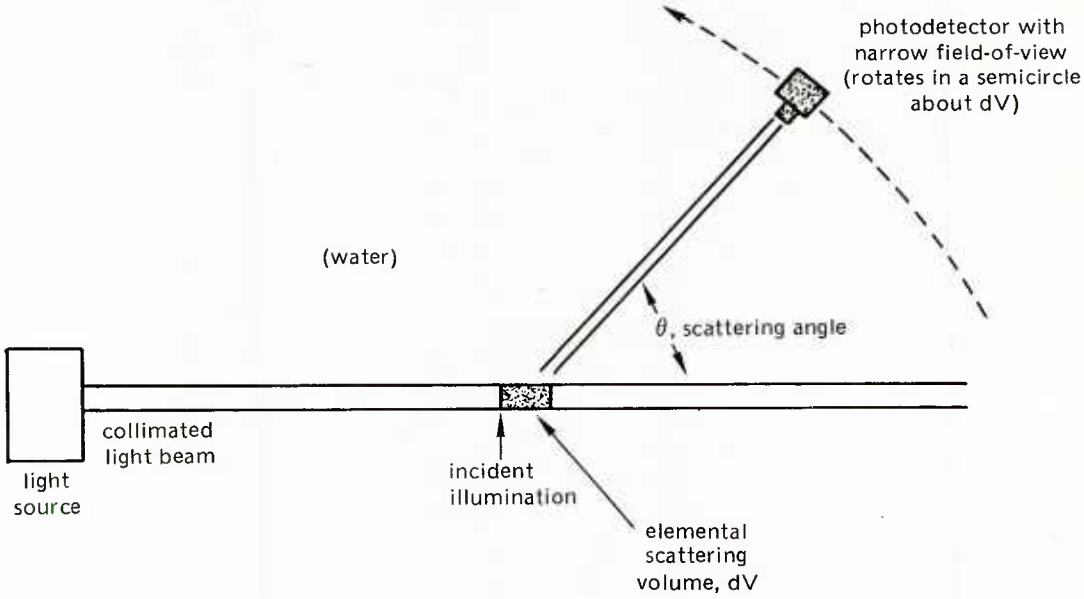

Figure 2.4. Operation of nephelometer.

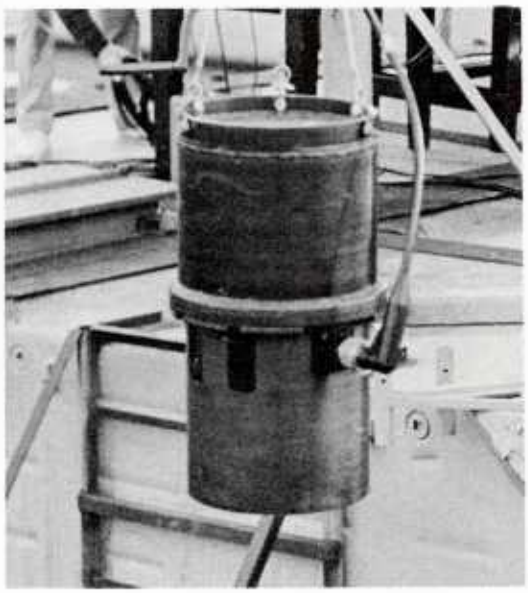

Figure 2.5. Scripps nephelometer.

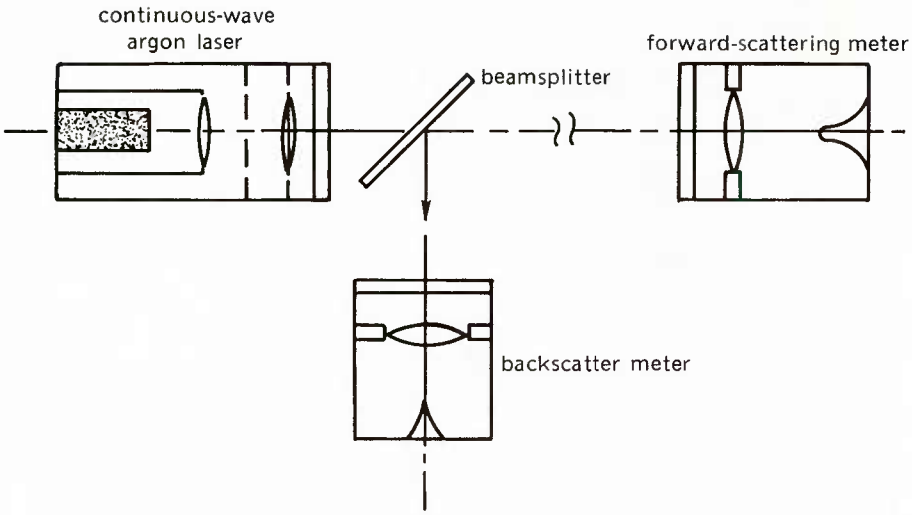

Figure 2.6. Small-angle scattering meter.

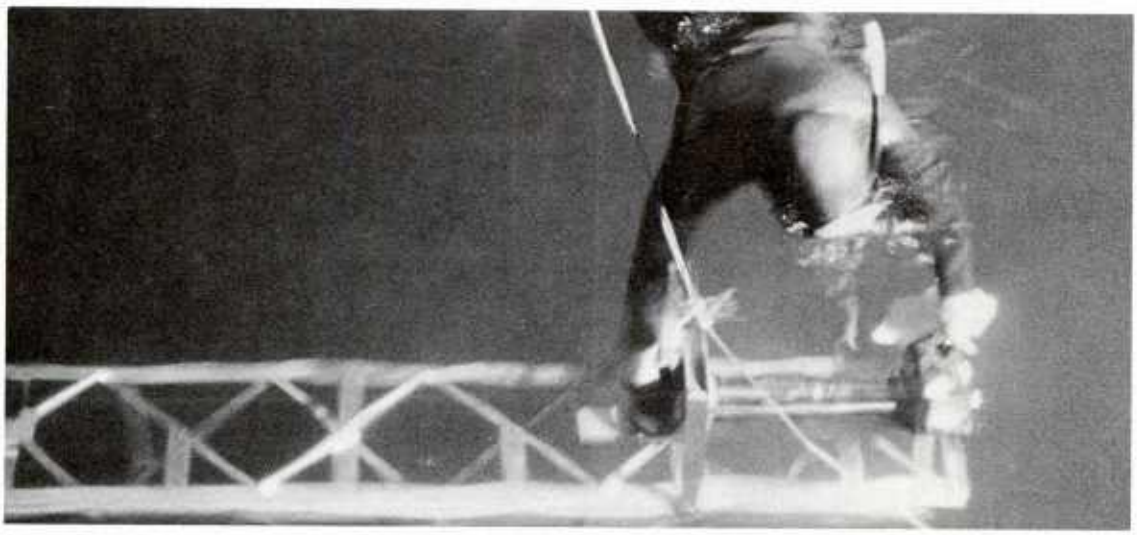

Figure 2.7. Diver aligning SRI small-angle forward-scattering meter.

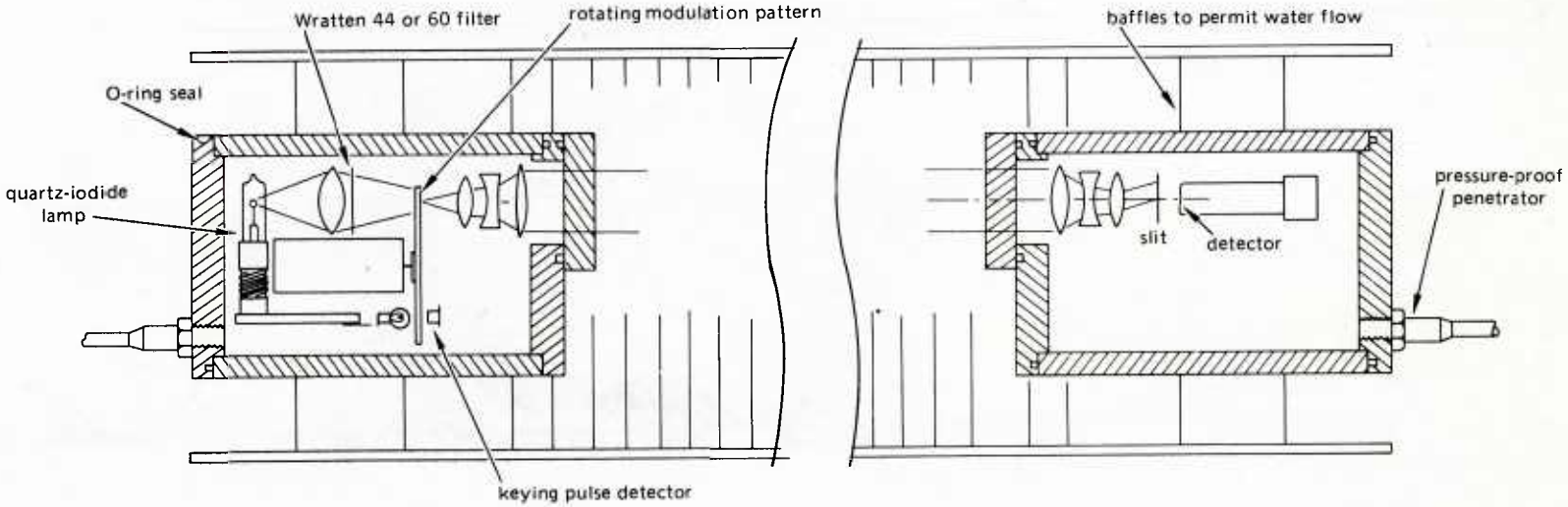

Figure 2.8. MTF meter.

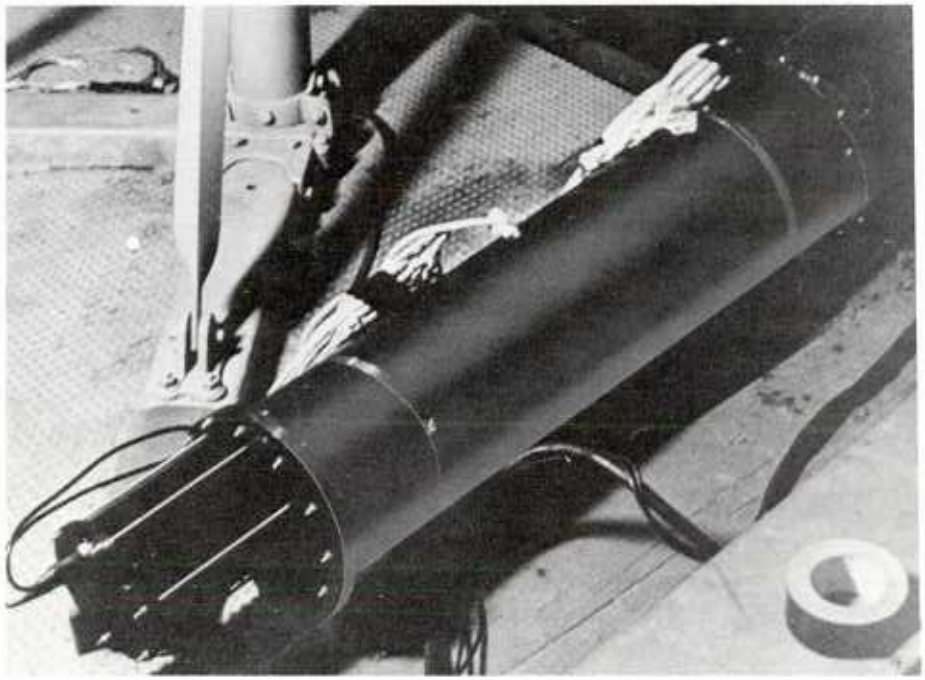

Figure 2.9. Tetra Tech modulation-transfer-function (MTF) meter.

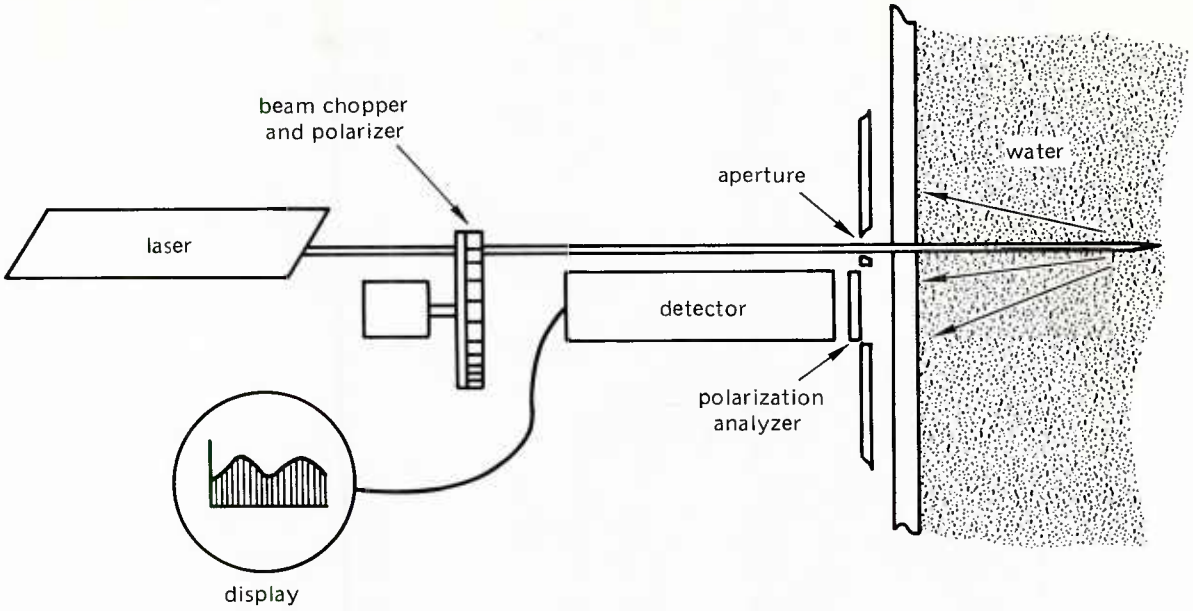

Part A. Schematic diagram.

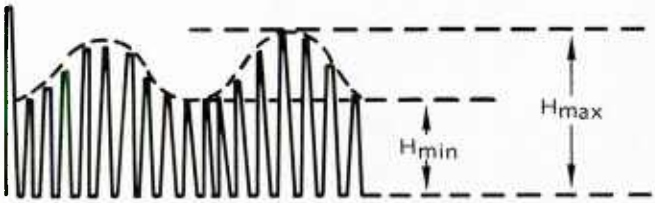

$$\psi_b = \frac{H_{max} - H_{min}}{H_{max} + H_{min}}$$

Part B. Detector output.

Figure 2.10. Breadboard polarization meter.

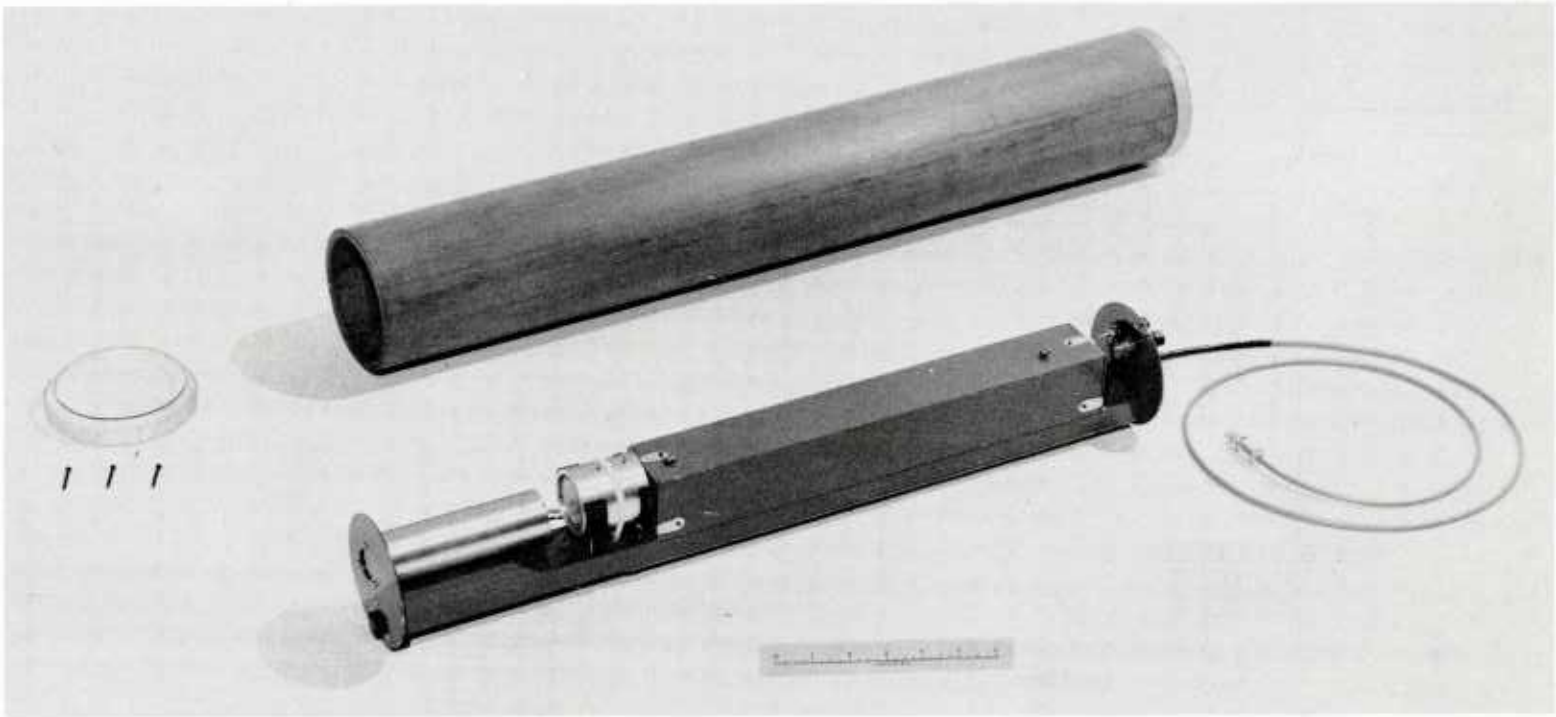

Figure 2.11 NUC polarization meter and waterproof polyvinyl chloride (PVC) housing.

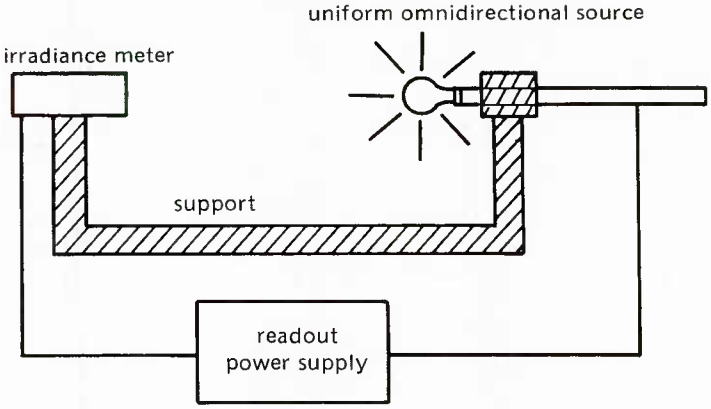

Figure 2.12. Absorption meter.

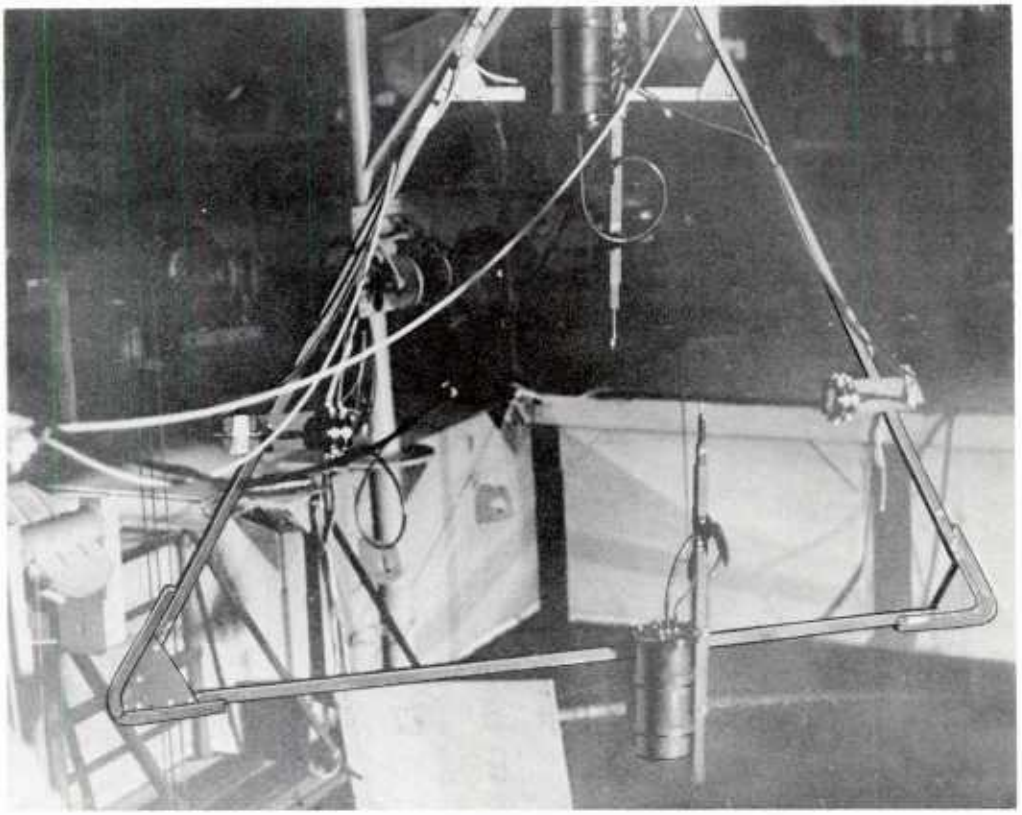

Figure 2.13. SRI absorption meter.

Table 2.1. Typical Water Characteristics Instrumentation.

Meter Type	Function Measured	Function Calculated	Manufacturer
Transmissometer	Percent transmission	α	SRI Marine Advisors
Nephelometer	$\sigma(\theta)$	$\sigma(\theta)$, s, b	SIO
Small-angle forward scattering	$\sigma(\theta)$	$\sigma(\theta)$, s	SRI SIO
Modulation transfer function (MTF)	MTF	$\sigma(\theta)$	Tetra Tech
Polarization	ψ_b	ψ_b	NUC
Absorption	a	a	SRI

Table 2.2. Spectral Variation of the Total Attenuation Coefficient for Light in Seawater (ln/m).*

Lambda	Distilled Water	Deep Ocean Water	Coastal Water	Bay Water
400.	.430E–01	.680E–01	.410E 00	.100E 01
410.	.400E–01	.630E–01	.395E 00	.905E 00
420.	.350E–01	.600E–01	.375E 00	.805E 00
430.	.300E–01	.560E–01	.360E 00	.705E 00
440.	.210E–01	.540E–01	.343E 00	.628E 00
450.	.190E–01	.520E–01	.330E 00	.556E 00
460.	.180E–01	.500E–01	.320E 00	.512E 00
470.	.180E–01	.490E–01	.310E 00	.475E 00
480.	.200E–01	.490E–01	.296E 00	.447E 00
490.	.250E–01	.500E–01	.288E 00	.417E 00
500.	.360E–01	.560E–01	.282E 00	.388E 00
510.	.380E–01	.670E–01	.273E 00	.368E 00
520.	.400E–01	.730E–01	.263E 00	.351E 00
530.	.440E–01	.770E–01	.257E 00	.337E 00
540.	.530E–01	.850E–01	.252E 00	.331E 00
550.	.690E–01	.920E–01	.253E 00	.323E 00
560.	.800E–01	.990E–01	.254E 00	.323E 00
570.	.880E–01	.106E 00	.263E 00	.323E 00
580.	.100E 00	.113E 00	.272E 00	.331E 00
590.	.122E 00	.119E 00	.282E 00	.365E 00
600.	.186E 00	.125E 00	.288E 00	.429E 00

* .400E–01 equals 0.400×10^{-1},
.400E 02 equals 0.400×10^{2}, etc.

Table 2.3. Spectral Variation of the s/a Ratio for Light in Seawater.*

Lambda	Distilled Water	Deep Ocean Water	Coastal Water	Bay Water
400.	.132E 00	.789E 00	.412E 01	.218E 00
410.	.128E 00	.909E 00	.449E 01	.248E 00
420.	.132E 00	.100E 01	.495E 01	.288E 00
430.	.140E 00	.115E 01	.532E 01	.343E 00
440.	.196E 00	.125E 01	.560E 01	.402E 00
450.	.191E 00	.136E 01	.602E 01	.479E 00
460.	.183E 00	.150E 01	.611E 01	.542E 00
470.	.164E 00	.158E 01	.638E 01	.610E 00
480.	.131E 00	.158E 01	.659E 01	.674E 00
490.	.927E–01	.150E 01	.678E 01	.759E 00
500.	.576E–01	.115E 01	.706E 01	.865E 00
510.	.500E–01	.811E 00	.680E 01	.957E 00
520.	.436E–01	.698E 00	.611E 01	.105E 01
530.	.365E–01	.638E 00	.559E 01	.115E 01
540.	.281E–01	.545E 00	.515E 01	.119E 01
550.	.197E–01	.484E 00	.462E 01	.126E 01
560.	.156E–01	.435E 00	.418E 01	.126E 01
570.	.132E–01	.395E 00	.378E 01	.126E 01
580.	.107E–01	.361E 00	.339E 01	.119E 01
590.	.810E–02	.337E 00	.303E 01	.973E 00
600.	.503E–02	.316E 00	.260E 01	.723E 00

*.400E–01 equals 0.400×10^{-1},

.400E 02 equals 0.400×10^{2}, etc.

SECTION 3. CONVENTIONAL UNDERWATER TELEVISION SYSTEMS

		Page
3.1	Light Sources	3-3
	3.1.1 Common Light Sources	3-3
	3.1.2 Light Source Data	3-6
3.2	Receivers	3-8
	3.2.1 Common Receiver Types	3-8
	3.2.2 Receiver Data	3-10
3.3	System Geometry	3-12
3.4	Conclusions	3-12
3.5	References	3-12

Figures | Page

3.1	Spectral Output of the 3400 °K Tungsten Incandescent Source	3-14
3.2	Lumen Output and Power Consumption with Input Voltage Variation for the Tungsten Incandescent Light	3-14
3.3	Spectral Output of the Mercury-Vapor Arc Light	3-15
3.4	Spectral Output of the Thallium-Iodide-Doped Mercury-Vapor Arc Source	3-15
3.5	Spectral Output of the Xenon Arc Source	3-16
3.6	Normalized Radiant Output Power for the 3400 °K Tungsten Incandescent Source	3-16
3.7	Normalized Radiant Output Power for the Mercury-Vapor Arc Source	3-17
3.8	Normalized Radiant Output Power for the Thallium-Iodide-Doped Mercury-Vapor Arc Source	3-17
3.9	Conventional Imaging System Geometry	3-18

Tables

3.1	Summary of Conventional Light Source Characteristics	3-19
3.2	Radiant Conversion Efficiencies	3-20
3.3	Radiant Conversion Efficiencies for Different Spectral Bandwidths	3-21
3.4	Summary of Input Power, Beam Pattern, and Expected Lifetime of Conventional Light Sources	3-22
3.5	Typical Parameters for Television Cameras	3-23

SECTION 3

CONVENTIONAL UNDERWATER TELEVISION SYSTEMS

This section discusses light sources and television cameras and the basic considerations involved in combining these components into successful underwater viewing systems. The systems in this section are distinguished from advanced systems because techniques involving specialized hardware, such as polarization discrimination, range gating, and volume scanning, are not used to discriminate against backscattered light. Systems incorporating these special techniques are discussed in section 4.

The relationships between light-source and camera-performance characteristics and the viewing problems described in section 2.1 are fully defined in section 6. To facilitate the analysis of conventional-system performance, adequate resources are available in this handbook to evaluate the most common light sources and cameras. These sources and receivers are defined in the following sections, including the corresponding performance data. The data in this section is useful by itself and as an input to the analysis in section 6.*

3.1 LIGHT SOURCES**

The light sources in this section represent the most common sources used in underwater viewing systems. If a designer wants to evaluate a different type of light source, or a more specialized version of one of the following sources, additional data is needed. Lasers, which are more often used in advanced systems than in conventional systems, are discussed in section 4.

3.1.1 COMMON LIGHT SOURCES – Four general categories of light sources are currently being used in conventional underwater viewing systems. These are the tungsten filament incandescent light, the mercury-vapor arc light, the thallium-iodide-doped mercury-vapor arc light, and the xenon arc light.

Tungsten Filament Incandescent Light. The tungsten light is characterized by radiant emission properties which closely approximate those of a blackbody radiator. The tungsten light is typically designed to operate as a source of blackbody radiation between 2800 and 3400 °K. The visible radiation produced by such a light is shown in figure 3.1. The operating behavior of this light has been studied by manufacturers, and data is available (refs. 3.2 and 3.3).

**The conventional-system data that is useful only in section 6 is presented in section 6.*
***Most of the material in section 3.1 originally appeared in reference 3.1.*

Figure 3.2 shows that the nominal lifetime of a tungsten light is severely curtailed by overpower operation; the power supply should, therefore, be regulated to obtain maximum lifetime and luminous output. For example, a 10 percent increase in the supply voltage will increase the luminous output by 38 percent, but it will decrease the lifetime to 29 percent of its nominal value. Two other factors which affect the life of tungsten lights are concerned with control of the evaporation of the tungsten onto the wall of the light envelope. The first is the darkening of the envelope wall which causes the light output to decay and ultimately the light to fail because of excessive heat absorption within the envelope. Second, the addition of iodide to the envelope's atmosphere creates a cyclic reaction which reduces the accumulation of tungsten on the envelope wall. Because the rate of evaporation is less with DC power than with AC power, the lifetime of the source is increased.

Mercury-Vapor Arc Light. The mercury-vapor arc light is one of a group of light sources that uses a current discharge through an ionized gas. As the electrons, which have gained sufficient energy from the arc to exist in excited energy levels about the atoms or to be completely free, return to the lower atomic energy levels, they radiate energy in the form of light. Their wavelength is determined by the net difference in the energy of the electron transition. A complete description of the mechanics of discharge radiation is in references 3.2 and 3.4. The radiation produced by such a discharge is, among other factors, a function of the excited-electron, transition-energy level that is characteristic of gaseous atoms and the operating vapor pressure of gas.

The mercury arc light is useful for illumination applications because a high percentage of its radiant emission is in the visible region. (Other gases which are commonly used to produce visible radiation are argon, xenon, neon, and sodium.) The mercury arc is most commonly used for commercial lighting applications because of its high input-to-output conversion efficiency (luminous efficiency).

The mercury arc light has been extensively used underwater because its spectral output is concentrated in small spectral bandwidths or lines, two of which are transmitted fairly well by seawater. Figure 3.3 shows the mercury spectral lines and their relative intensity; the blue line at 4358 Å and the green line at 5461 Å are the mercury lines least attenuated by seawater. Because the spectral output is not continuous, true color rendition is not achieved with this light. For this reason, the light is usually used as an efficient source of illumination for monochrome, closed-circuit, underwater television systems where color rendition is not of primary importance.

The types of mercury arc lights used in existing underwater light systems were developed for commercial use, and are designed to operate with a ballast unit (current limiter) specifically tailored to the voltage level of the AC supply source. These lights are also designed to be self-starting when the supply voltage is applied. For those submersibles which have only DC power, the voltage is converted to AC and is reactively ballasted.

Mercury arc lights can generally be operated with either AC or DC sources of current, but are generally designed specifically for one or the other source for optimum performance. The choice of AC or DC operation is generally dictated by the type of power available and the type of stabilization technique selected to regulate the light.

The starting and operating voltages, the energy requirements, and the current levels of an arc discharge light are governed by factors such as the type of material used as the radiating source, the initial and steady-state operating vapor pressure of the material, the volume of the arc discharge envelope, and the electrode separation distance. These factors can be traded-off to determine the final configuration. Consider the following example. The mercury arc tubes on Navy submersibles have a relatively large electrode spacing, relatively low operating pressure, and a third electrode that allows the light to self-start on the available supply voltage. This commercial configuration results in a relatively large light source (requiring a large reflector for projection) and a long inherent operating life for the light element. To reduce the required size of the reflector, it is necessary to use a compact or short arc configuration. However, existing versions of these lights require a starting voltage much higher than the operating (steady-state) voltage, and the inherent operating life of these arc sources is lower. Neither of these difficulties is intolerable, but they do indicate the tradeoffs required to specify any one particular characteristic of an arc discharge source.

Thallium-Iodide-Doped Mercury-Vapor Arc Light. It has been found that the spectral radiation characteristics of a mercury discharge can be modified by adding metal halides to the material in the arc volume. The emission spectrum of the resulting arc discharge contains the normal emission lines of the mercury spectrum and the spectral lines that are characteristic of the added metal. (The mercury lines are usually reduced in intensity.) Several metal halides have been found to increase the visible output of these hybrid mercury arc lights; among these halides are thallium iodide, sodium iodide, dysprosium iodide, and indium iodide. The resulting lights have electrical characteristics very similar to those of the mercury arc light, but their net visible radiation is increased and their color rendition is improved. Several investigators have parametrically varied the concentration and composition of the dopant, pressure, power level, and various arc design parameters in an attempt to increase the luminous efficiency of these doped lights (refs. 3.5, 3.6, and 3.7). They have concluded that the thallium-iodide-doped mercury-vapor arc yields the highest efficiency light now known for underwater application. This efficiency is gained at the expense of color rendition; however, this problem can be solved by adding other additives to the thallium iodide to improve the color rendition with only a slight loss of luminous efficiency. The spectral output of a thallium-iodide-doped mercury-vapor arc light is shown in figure 3.4.

One of the undesirable operating characteristics of mercury arc lights is the start-up time required to produce full output radiation. This time depends on the ambient temperature and the arc tube configuration. The relatively long arc configuration requires up to 13 min to produce peak output when the ambient temperature of the water is 32 °F, and as little as 6 min when the water temperature is 90 °F. This thermal influence on starting time is explained by the fact that mercury is almost completely condensed at the ambient temperature of water (100 °F or less) and operating conditions are achieved only when the arc volume has been sufficiently heated to vaporize all of the mercury. The rate at which the temperature of the arc increases is initially a function of the ambient temperature of the arc tube. This start-up time is a hindrance to submersible operations because the television cameras, with which the mercury lights are being used, are relatively insensitive to the low illumination levels offered by the light as it is warmed up. This situation can lead to operational difficulties unless the lights remain on during the entire mission.

This problem is aggravated with existing lights because additional time is required when the light is turned off in which the vapor pressure of the mercury decreases (as the arc cools) before the available ballast supply voltage is sufficient to reignite the arc. If a light is inadvertently turned off, 2 to 4 min are required to achieve full radiant output from the light (this is in addition to the nominal 6- to 13-min warm-up time). This cooling-time problem has been solved in short arc lights by using a pulse of voltage and energy that is sufficient to restrike the arc in a hot light; the same technique can be applied to the existing underwater mercury lights after circuit and packaging modifications.

Xenon Arc Light. The xenon arc light, which has been used as a source of high-intensity illumination in light projection systems, operates as a vapor-discharge light with a continuous spectral emission in the visible region. Its spectral output approximates that of a 6000 °K blackbody radiator (this output also approximates the light produced by the noonday sun). Because the output radiation of this light is strong in the violet and blue spectral regions, it provides a better rendition of these colors than tungsten filament lights do (fig. 3.5).

The xenon light is generally packaged in a compact arc configuration so that the effective size of the radiating arc is approximately a few millimeters. This configuration allows smaller reflector geometries and better control of the resulting projected beam.

Because the current must be limited to maintain stable operation of the light, the electrical properties of the xenon light are similar to those of the mercury arc light. In addition, it is necessary to provide sufficient energy (approximately 10 to 20 kV for most existing configurations) to initially ionize the xenon and start the conduction of current. This starting pulse can be used to restart a hot light if its amplitude is greater than the minimum required to initially start a cold light.

The metal halide additives previously mentioned can be added to the xenon arc to modify its spectral emission. Although the addition of thallium iodide to the xenon arc results in an improved luminous efficiency, the light is still not as efficient as the thallium-iodide-mercury arc light. However, the thallium-iodide-xenon arc light produces more light output, both initially and during start up, than does the thallium-iodide-mercury arc light.

Summary. A summary of some of the various light source characteristics is given in table 3.1

3.1.2 LIGHT SOURCE DATA – The following data is of general interest to designers who want to create a viewing system with one or more of the sources discussed in section 3.1.1. Additional data appears in section 6.

3.1.2.1 Spectral Radiant Output – The radiant output of each light system considered has been indicated in figures 3.2 through 3.5. The radiant spectral output curves indicate the general trend of the light's power distribution, and can be used to evaluate the effective radiating power over the bandwidths of interest. To make possible a relatively quick assessment of a given light's output power within a portion of the water-transmission spectrum, the data in figures 3.2 through 3.5 has been integrated with respect to wavelength to obtain a normalized cumulative power curve for the lights within the visible region of the spectrum

(figs. 3.6 through 3.8). To obtain an absolute evaluation, the radiant power conversion efficiency (ratio of radiant power emitted in the 4000- to 7000-Å region to electrical power input) of each of the lights is shown in table 3.2.

By using table 3.2 and figures 3.6 through 3.8, it is possible to compute the radiant power emitted by these light sources in a given bandwidth. For example, the bandwidth determined by the combined receiver response and the water-transmission spectral characteristics is appropriate for a comparison of relative light source effectiveness in illuminating, spectrally nonselective reflectors (gray bodies).

A rigorous analytical comparison of the effectiveness of these lights in an underwater application requires a computation of the resultant sensor signals, including the effects of light source output, water transmission, object reflectivity, and sensor response. Because water characteristics vary with location and time, no one light source will be the optimum for use in all situations.

Table 3.3 compares the radiant conversion efficiency of the four types of light sources for various spectral bandwidths. These bandwidths, calculated in section 6.1.2, are from table 6.5. The bandwidths are defined so that the transmission loss for a given range at the wavelengths λ_1 and λ_2 is twice as great as the transmission loss at the wavelength λ_0. Transmission loss is a minimum at λ_0, and the wavelengths λ_1 and λ_2 represent the smallest and largest wavelengths in the bandwidth, respectively. The radiant conversion efficiency is defined as the percent of input electrical power which is converted to radiant output power for a given spectral bandwidth, i.e.,

$$\left\{\begin{matrix}\text{radiant conversion}\\ \text{efficiency } (\lambda_1,\lambda_2)\end{matrix}\right\} = 100 \text{ percent} \left\{\frac{\text{radiant output power } (\lambda_1,\lambda_2)}{\text{input electrical power}}\right\}.$$

The basic spectral properties of the three different types of water – bay, coastal, and deep – are in tables 2.2 and 2.3. The values for the radiant conversion efficiencies for the different bandwidths can be obtained directly from the data in table 3.2 and figures 3.6, 3.7, and 3.8.

Assuming that the receiver has the same spectral responsiveness and that the objects or background under observation are nonselective reflectors over the different bandwidths, the information in table 3.3 indicates that the thallium-iodide-doped mercury-vapor arc light is generally the most efficient underwater source. (The regular mercury arc lamp has higher efficiency for long viewing ranges in deep ocean water.) The effect of increasing viewing ranges is readily apparent in table 3.3. As the viewing distance is increased, the transmission bandwidth becomes narrower and the radiant conversion efficiency decreases.

3.1.2.2 Input Data for Section 6 – In addition to the previous light source data and to that presented in section 6, two specific characteristics are required as inputs to the analysis in section 6: electrical input power and beam half-angle. Obviously, light sources are available with a variety of input powers, and reflectors can be designed to give a wide range of beam angles. (A detailed definition of the half-angle of the beam pattern appears in section 6.2.)

The designer should choose a source power appropriate to his needs and constraints and a reflector matched to the general system geometry. Section 3.3 discusses the selection of an appropriate beam pattern. The collection efficiency of the projection optics used to produce a given beam pattern is described in section 4.3.2.2. Table 3.4 summarizes the input power, beam pattern, and expected lifetime characteristics of conventional light sources.

3.2 RECEIVERS

Critical tradeoff factors associated with underwater receivers include spectral response and sensitivity.

Spectral response is important because light can efficiently penetrate water only in a narrow-band of the visible spectrum. For extended-range viewing, the receiver must respond well in this band. Fortunately, the spectral response of the common photosensitive materials used in television cameras is high in the blue-green region. The response depends upon the type of material used to construct the photosensitive surface, the band gap and the ionization energies of the surface, the thickness of the surface, and the absorption by the surface of protective materials.

Sensitivity in image tubes can vary by three to four orders of magnitude. Therefore, under absorption-limited conditions, viewing systems using the most sensitive television cameras can see about 3 attenuation lengths farther than systems that use a standard vidicon. This increase in range improvement often makes sensitivity the determining criterion in practical receiver tradeoff studies.

Additional tradeoff considerations are resolution capabilities, cost, ease of operation, and power input requirements.

Common receivers are discussed in the following section.

3.2.1 COMMON RECEIVER TYPES

– The common receiver types that can be applied to underwater viewing situations are image intensifiers and television cameras.

3.2.1.1 Image Intensifiers. The image intensifier, a light-in light-out device that can be used alone, is usually used as an input amplifier stage to television cameras. Any number of these devices can, in principle, be used in series as an input to a television camera, but resolution losses prohibit such a scheme. The image intensifier consists of a photoemissive cathode, focusing electron optics, and a screen which is usually a phosphor. When photons strike the photocathode, a number of electrons equal to the product of the number of incident photons and the surface quantum efficiency is emitted. These electrons are accelerated by an electric field until they strike the phosphor. Because the electrons gain energy from the field, more photons are emitted by the phosphor than were incident on the photocathode, constituting a gain in image brightness. Unlike those produced by the television systems, these images are produced without scanning. For remote viewing, image intensifiers are usually coupled to a television tube by fiber optics or other arrangements.

The overall gain of the standard intensifier is between 30 and 50 times, requiring approximately 10 kV to produce the necessary electron acceleration. This gain depends on the luminous efficiency of the photocathode, the coupling efficiency between the photocathode and the phosphor, the voltage on the intensifier, and the gain of the phosphor. Microchannel plates have recently been used in image intensifiers to produce an overall gain of nearly 10,000.

3.2.1.2 **Television Cameras.** The following receivers represent the most common television cameras. All television cameras use a scanning process, developing at each instant a voltage that is proportional to the light intensity of a small portion of the image incident on the camera tube. The varying voltage is transmitted to a display device either by a hardwire link or by modulation of a transmitted rf carrier wave.

Vidicon Tube. The essential components of a vidicon are a photoconductive target and an electron gun. When light strikes the target, conductivity increases in the immediate area of exposure. Because of the increased conductivity, the charge leaks-off, and the areas become positive with respect to the electron gun. When the electron beam scans the target, it returns precisely enough electrons to return a given portion of the target to the same potential as the electron gun. As these new electrons leak-off the given target portion, the current passing through a load resistance produces the output signal. The sensitivity of vidicon tubes is orders of magnitude lower than competing varieties of television cameras. (Using a Type V (silicon diode) photoconductor in the vidicon increases its sensitivity by a factor of three over that of the standard vidicon which uses a Type II (antimony trisulfide) photoconductor in underwater applications.) The vidicon's performance is also impaired by a tendency to smear moving images (lag) and by the nonuniformity of the photoconductive surface. It is, however, generally smaller, simpler, less expensive, and more reliable than other image tubes.

Image Orthicon (IO). The image orthicon is a complex television camera which uses a photocathode as its initial sensor. Electrons emitted from the photocathode are accelerated by an electric field towards a thin, moderately insulating target surface. As these primary electrons strike the target, they produce secondary electrons which are collected by a fine mesh screen, leaving positive areas on the target proportional to the intensity pattern of the image incident on the photocathode. A beam from an electron gun scans the target, loses some electrons to the positively charged areas, and then returns (reflects back) to an electron multiplier which surrounds the electron gun. The output signal is the current from the anode of the electron multiplier.

The image orthicon is a highly sensitive camera. Problems associated with it are its complexity and associated unreliability, its size, weight, and power consumption, and its sensitivity to environmental conditions such as noise, humidity, vibration, and rough handling.

Image Isocon (II). In the image isocon (an improved version of the image orthicon), the electrons arriving at the electron multiplier are those which land on the target and are reflected at various angles rather than those which are reflected directly back along the electron beam. Although the signal-to-noise ratio is inherently better because the DC term of the beam is not involved, fragility and reliability problems are significant.

Secondary Electron Conduction (SEC). The SEC vidicon uses a photocathode as its input sensor. Electrons emitted from the photocathode are accelerated by an electric field towards the SEC target, which usually consists of a supporting layer of Al_2O_3, a layer of aluminum (the signal plate), and a layer of KCl. The primary electrons dissipate their energy in the KCl by generating low-energy, secondary-emission electrons. The secondary emissions are collected by the aluminum plate, leaving the KCl positively charged in areas that correspond to the exposed areas on the photocathode. Operation of the camera now approximates that of the standard vidicon. The beam from an electron gun fills-in the positive areas with a negative charge, and the dissipation of the charge through a load resistor is the output voltage.

The SEC vidicon has excellent low-light-level capabilities. Because of its relative simplicity and reliability, compared with the image orthicon, it has dominated the low-light-level television field. Its major operating difficulty has been overheating and destruction of the target when the camera has been exposed to intense light. Westinghouse, however, has recently developed a more rugged version in which a supporting mesh structure conducts excess heat from the target.

Silicon-Electron-Bombardment-Induced-Response (SEBIR) Tube. (This tube is also called the Silicon Intensifier Target (SIT) Tube.) The SEBIR tube operates similarly to the SEC vidicon; however, a thin silicon wafer, upon which a fine matrix of p-n junctions has been formed, replaces the SEC's KCl layer. In operation, primary electrons accelerated up to 10 kV cause multiple dissociation of the electron-hole pairs. The holes are collected at the p-side of the diode until the charge is neutralized by the beam from the electron gun. The dissipation of these electrons through a load resistor is the output voltage.

Although the SEBIR tube is more sensitive than the SEC tube, it does not have the SEC's problem of burnout due to high-intensity light, and the gain can be manually controlled by varying the target voltage from 2 to 10 kV.

3.2.2 RECEIVER DATA – The spectral responses of the three most common photosensitive surfaces used in underwater television cameras are indicated in figure 6.5. The Type II (antimony trisulfide) and Type V (silicon diode) photoconductors are used in the vidicon camera tubes, while the S-20 (multialkali) photocathode is used in the image intensifiers and the IO, II, SEC, and SEBIR camera tubes. All of these photosensitive surfaces have good responses for the spectral bandwidths transmitted through water. In sections 6.1.2 and 6.2.2, a method is outlined for combining the spectral characteristics of the light source, water medium, and receiver so that the spectral response of total imaging system can be determined.

The noise-limited resolutions of the various types of television receivers are indicated by the signal response curves which are given in figure 6.4. These curves, which show the interrelationship of resolution, image contrast, and photocurrent level, are required for a precise analysis of image system performance. Image contrast is defined as

$$C = \frac{i_2 - i_1}{i_2}, \tag{3.1}$$

where i_2 is the photocurrent which corresponds to the brighter areas of the image and i_1 is the photocurrent corresponding to the darker area. In detail,

$$i_2 = i_s + i_n \tag{3.2}$$

and

$$i_1 = \frac{\rho_1}{\rho_2} i_s + i_n, \tag{3.3}$$

where i_s is the signal photocurrent produced by light reflected from the brighter area on the target, i_n is the noise photocurrent produced by the backscattered light, and ρ_2 and ρ_1 are the reflectances of the brighter and darker areas of the target, respectively. The signal-to-noise ratio of the output from the receiver depends on both the image contrast and the photocurrent level, and the resolution is a measure of the information content. Therefore, the greater the image contrast and the photocurrent levels are, the greater the noise-limited resolution of the receiver will be.

Often, only an approximate estimate of system performance is necessary to evaluate a particular tradeoff, and the designer will not want to spend the time required for a detailed calculation. The system performance nomograms described in section 5 can be used for this purpose. For these nomograms, the properties of the different television cameras have been reduced to threshold sensitivity ranges. These sensitivities correspond to the minimum number of footcandles from a standard 2854 °K incandescent source* which must be incident on the faceplate of the camera tube** if the receiver is to function properly. The lower sensitivity in the range corresponds to the high contrast images, and the higher sensitivity corresponds to the low contrast images. Table 3.5 lists the threshold sensitivity ranges for the different television cameras described in section 3.2.1. In using the nomograms, the image illuminance E_s and the image contrast C are usually calculated. Based on these values, it can be determined from the data in table 3.5 if a particular television camera has sufficient sensitivity. Table 3.5 also provides typical values of other input parameters which are required for a detailed analysis; these parameters include the camera's field-of-view, the f/ and transmission coefficient of the receiver's optics, and the image format area on the photosensitive surface. Because the values in table 3.5 are only examples, the designer should always use his own data when it is available. (In the nomograms, the values of f/1.5 and $\tau = 1.0$ are assumed.)

**It should be noted that the values of the image illuminance E_s given by the nomograms do not correspond to the number of footcandles which are actually incident on the faceplate of the receiver. The value of E_s is, instead, the number of footcandles from the standard 2854 °K incandescent source which produces the same photocurrent level as the light from the underwater source. This distinction is quite important for underwater television systems because the spectral characteristics of underwater sources are quite different from those of the standard source. Also, typical photosensitivity surfaces have an appreciable response for light with wavelengths greater than 600 nm, while the value of λ_2, the maximum wavelength in the transmission bandwidths in table 3.3, is less than or equal to 600 nm. The procedure for evaluating E_s for a particular photosensitive surface is described in section 6.4.3.*

***The photosensitive surface.*

3.3 SYSTEM GEOMETRY

In addition to component characteristics, such as source power, receiver sensitivity, and the degree to which both the source output and the receiver sensitivity match the spectral transmission window of the water, system performance also depends on geometrical parameters. These parameters include the source-receiver separation, the beam pattern of the source, and the field-of-view of the receiver.

For viewing situations where reliability, low power input, and ease of operation are primary considerations, conventional television systems are strong contenders against those which use more sophisticated imaging techniques. To achieve maximum image contrast with a conventional system, source-receiver separation should be exploited as fully as possible within the context of the given application.

The conventional imaging system shown in figure 3.9 consists of a light source and receiver separated by a distance d and located in a plane a distance R from the target. The half-angle of source's beam pattern is given by the angle θ_1, while the angle θ_3 specifies the half-angle of the receiver's field-of-view. The backscatter volume (the cross-hatched area) is defined by the intersection of the source's beam pattern and the receiver's field-of-view. By increasing the source-receiver separation d and decreasing the angles θ_1 and θ_3, the backscatter volume is reduced and moved farther from the source-receiver plane. Both of these effects significantly reduce the amount of backscatter and increase the image contrast. However, maximizing d introduces a longer optical pathlength from the source to the target and back to the receiver, thereby incurring greater attenuation losses. Also, minimizing the angles θ_1 and θ_3 reduces the observed target area and increases alignment requirements. The nomograms in section 5 permit the designer to estimate the effects of these system tradeoffs, while the detailed analysis in section 6 provides a more accurate evaluation.

3.4 CONCLUSIONS

The following conclusions have been found to be valid for most conventional imaging systems using the source-receiver-separation technique (ref. 3.8).

1. In an absorption-limited environment, the maximum underwater viewing range is strongly dependent on the threshold sensitivity of the detector. Source-receiver separation has only a minor effect on the maximum viewing range.

2. In a backscatter- or contrast-limited environment, the maximum underwater viewing range is strongly dependent on source-receiver separation.

3. In either type of environment, image contrast is strongly dependent on source-receiver separation. For a fixed viewing range, a factor of two increase in source-receiver separation generally yields about a tenfold increase in image contrast.

3.5 REFERENCES

3.1 Naval Undersea Research and Development Center, NUC TP 265. *A Study of Light Sources for Underwater Use*, by A. R. Waltz. San Diego, California. October 1971.

3.2 Illuminating Engineering Society. *IES Lighting Handbook*. Waverly Press, Inc. Baltimore, Maryland. 1966.

3.3 Kingslake, R. *Applied Optics and Optical Engineering.* Academic Press, New York, New York. 1965.

3.4 Bourne, H. K. *Discharge Lamps for Photography and Projection.* Chapman and Hall, Ltd., London. 1948.

3.5 Reiling, G. H. "Characteristics of Mercury Vapor-Metallic Iodide Arc Lamps," *Journal of the Optical Society of America.* Vol. 54, no. 4, p. 532. April 1964.

3.6 Tetra Tech, Inc., Contract No. N00019-67-C-0613. *Investigation of Improved Light Sources for Underwater Photography, Final Report.* Pasadena, California. 26 February 1968.

3.7 Larson, D. A., and F. H. Rixton. "Underwater Lighting and New Light Sources," *Undersea Technology.* p. 38. September 1969.

3.8 Naval Undersea Research and Development Center, NUC TP 237. *The Effect of Source-Receiver Separation on Conventional Underwater Imaging,* by R. P. Bocker. San Diego, California. June 1971.

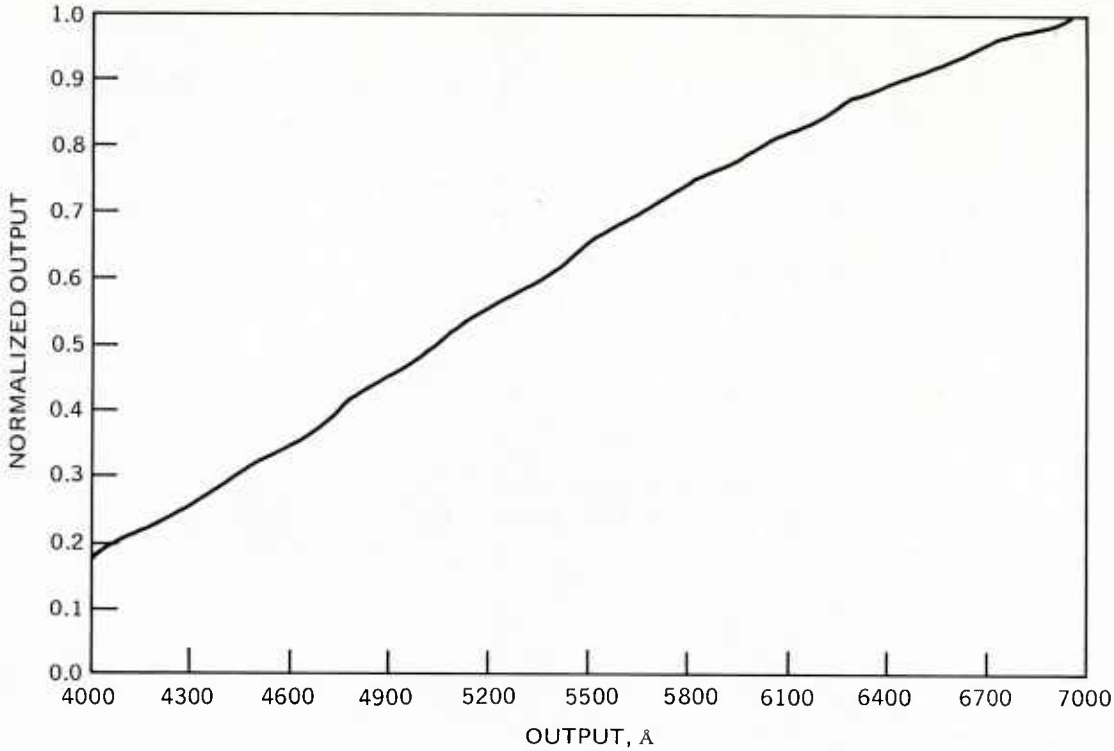

Figure 3.1. Spectral output of the 3400 °K tungsten incandescent source.

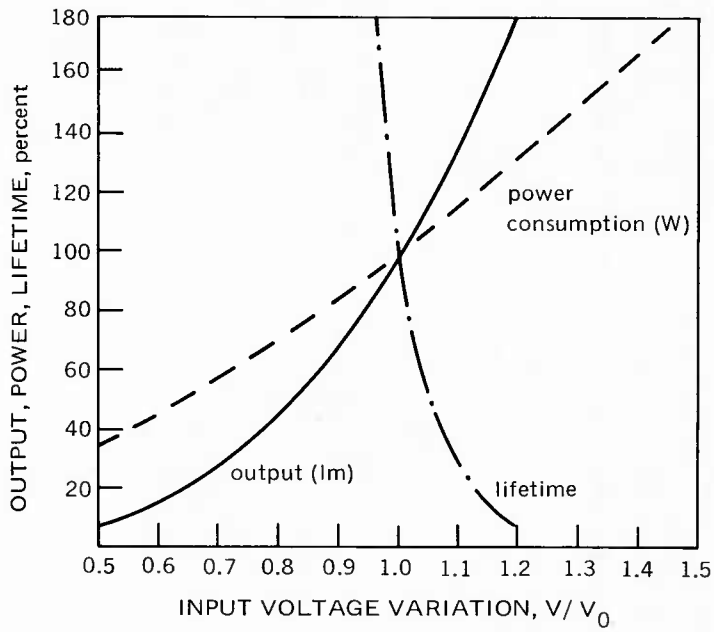

Figure 3.2. Lumen output and power consumption with input voltage variation for the tungsten incandescent light.

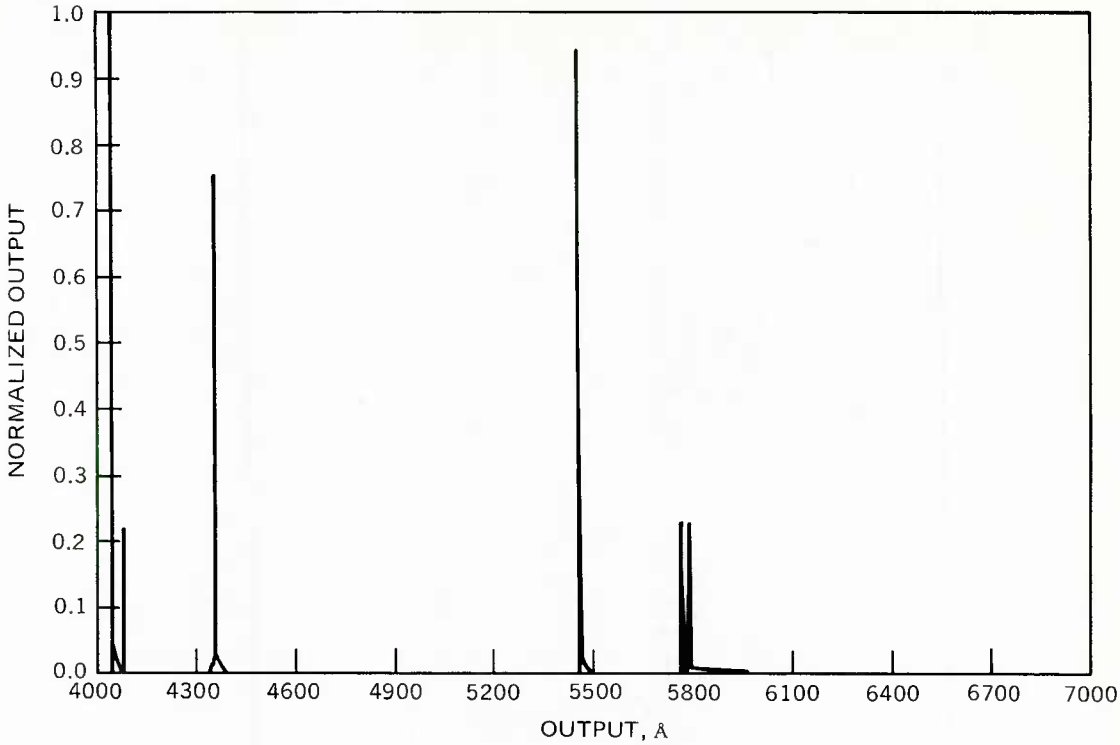

Figure 3.3. Spectral output of the mercury-vapor arc light.

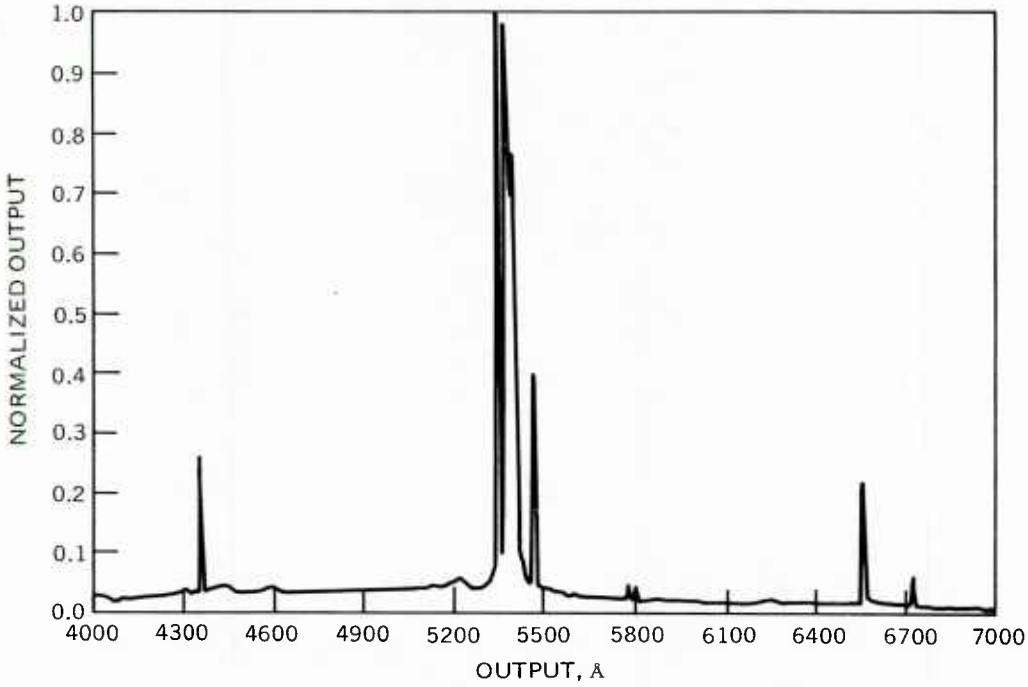

Figure 3.4. Spectral output of the thallium-iodide-doped mercury-vapor arc source.

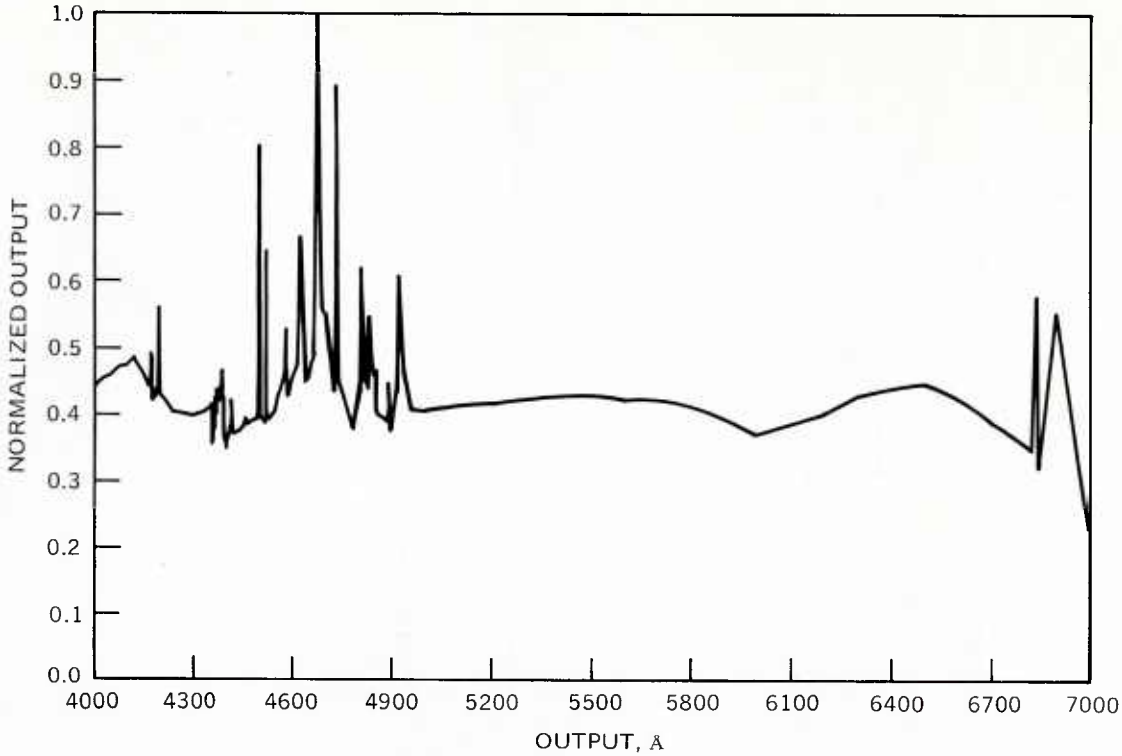

Figure 3.5. Spectral output of the xenon arc source.

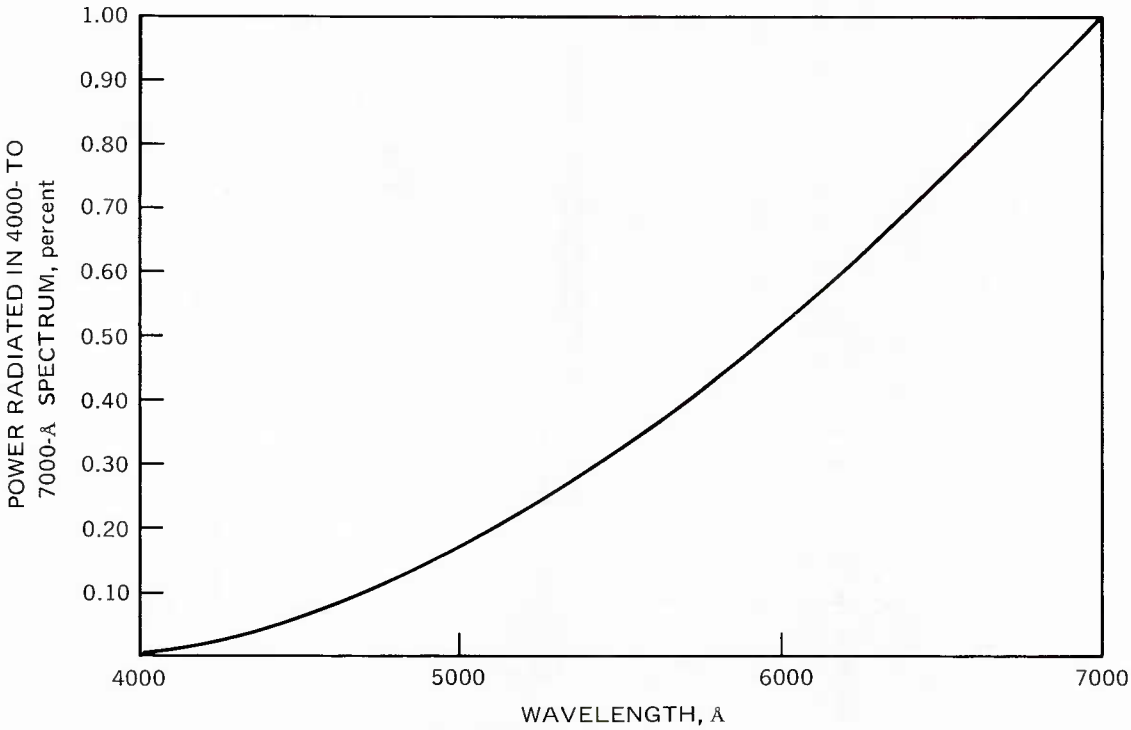

Figure 3.6. Normalized radiant output power for the 3400°K tungsten incandescent source.

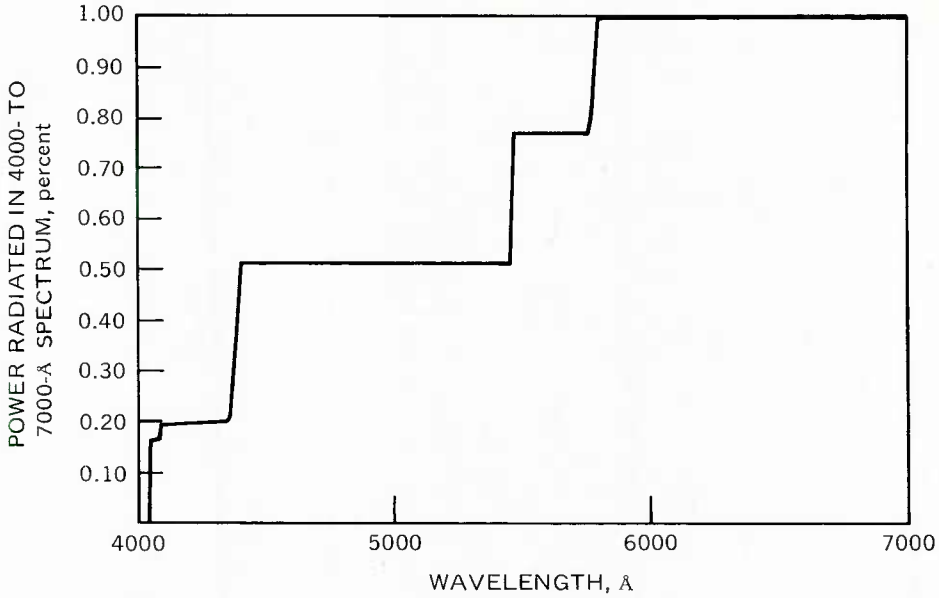

Figure 3.7. Normalized radiant output power for the mercury-vapor arc source.

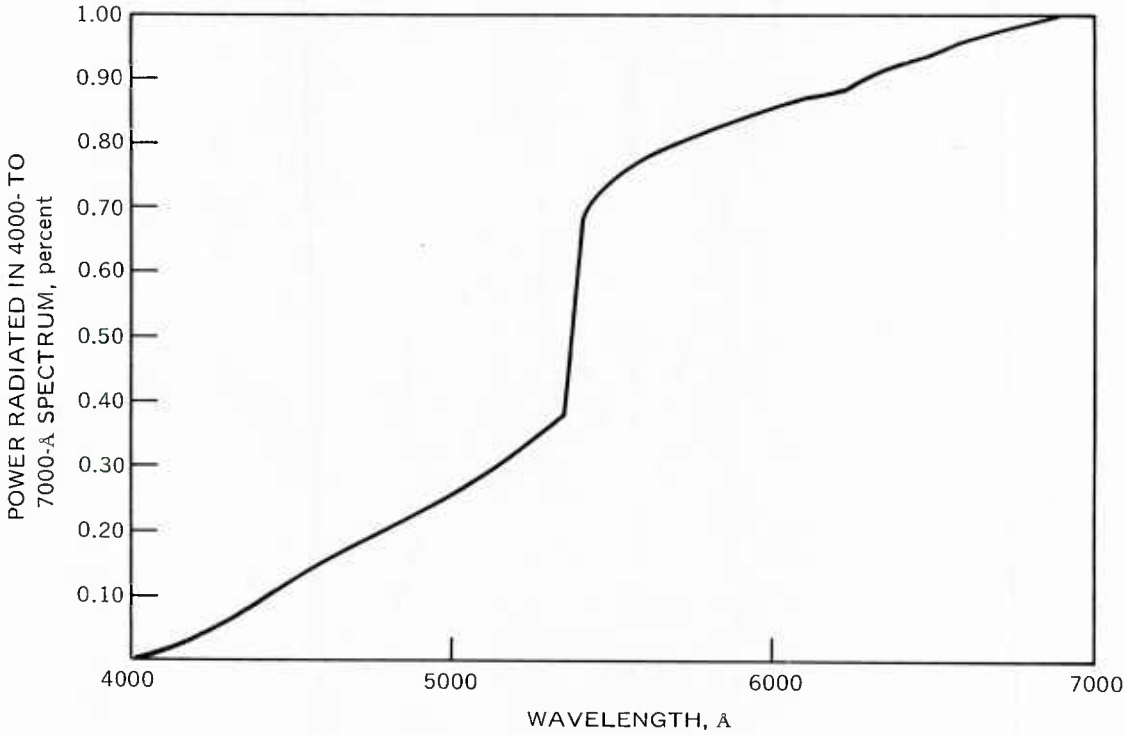

Figure 3.8. Normalized radiant output power for the thallium-iodide-doped mercury-vapor arc source.

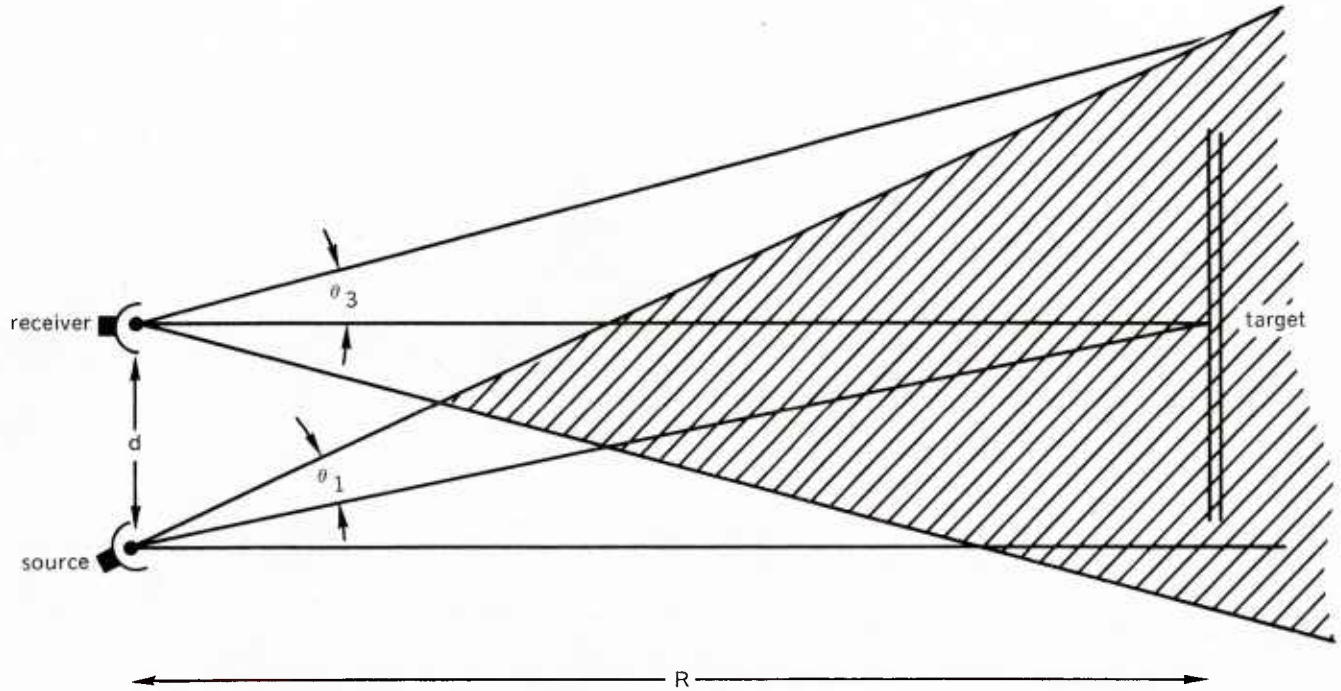

Figure 3.9. Conventional imaging system geometry.

Table 3.1. Summary of Conventional Light Source Characteristics.

Light Type	Optical Characteristics	Power Source Requirements	Advantages	Deficiencies
Mercury-vapor arc	Lines in violet, blue, green, and yellow; deficient elsewhere	Current-limited supply; regulated power input	Relatively high efficiency (45 to 50 lm/W)	Relatively long start time (6 min) and restart time (10 min); poor color rendition
Thallium-iodide-doped mercury-vapor arc	Green line of thallium dominates the visible output; mercury lines are suppressed	Current-limited supply; regulated power input	Very high efficiency source of green light (85 to 90 lm/W)	Relatively long start time (5 min) and restart time (10 min)
Incandescent tungsten filament	Continuous output throughout the visible spectrum increases from the blue to the red end of the spectrum	Regulated power input	Fast start time (1 sec) and good color rendition	Relatively low efficiency (24 lm/W)
Xenon arc	Continuous output throughout the visible spectrum	Current-limited supply; regulated power input	Fast start time (80 percent output instantaneously) and immediate restart; excellent color rendition	Relatively low efficiency (22 lm/W)

Table 3.2. Radiant Conversion Efficiencies.

Light	Radiant Watts/Electrical Watts (4000 to 7000 Å)
Xenon arc	9.1 percent
Tungsten incandescent	11.5 percent
Mercury-vapor arc	14.6 percent
Thallium-iodide-doped mercury-vapor arc	22.1 percent

Table 3.3. Radiant Conversion Efficiencies for Different Spectral Bandwidths.

Bay Water

Range	Bandwidth		Radiant Conversion Efficiencies, percent			
	λ_1	λ_2	Tungsten Incandescent	Mercury Arc	T1I-Doped Hg Arc	Xenon Arc
2	460	600	5.00	7.08	15.4	4.21
4	490	600	4.43	7.08	13.7	3.16
6	500	590	3.66	7.08	12.8	2.51
8	510	590	3.31	7.08	12.1	2.22
10	520	590	2.93	7.08	11.3	1.94

Coastal Water

Range	Bandwidth		Radiant Conversion Efficiencies, percent			
	λ_1	λ_2	Tungsten Incandescent	Mercury Arc	T1I-Doped Hg Arc	Xenon Arc
5	430	600	5.50	11.6	17.4	5.15
10	470	590	4.32	7.08	14.5	3.60
15	480	580	3.68	6.08	13.6	3.00
20	490	580	3.49	6.08	13.1	2.64
25	500	570	2.77	3.68	12.1	2.00

Deep Ocean Water

Range	Bandwidth		Radiant Conversion Efficiencies, percent			
	λ_1	λ_2	Tungsten Incandescent	Mercury Arc	T1I-Doped Hg Arc	Xenon Arc
10	400	540	3.33	7.52	14.9	4.70
20	400	510	2.16	7.52	6.25	3.88
30	420	500	1.52	4.61	4.82	2.73
40	430	500	1.36	4.56	4.27	2.38
50	430	500	1.36	4.56	4.27	2.38

Table 3.4. Summary of Input Power, Beam Pattern, and Expected Lifetime of Conventional Light Sources.

Light Type	Expected Life	Half-Angle of Source Beam Angle (θ_1)	Maximum Input Power (w)
Gas argon laser (continuous wave)		Can be designed to be any fixed angle from 2 to 90 deg	10 kW
Xenon arc (continuous)	1000 hr (short arc)		
Xenon arc (pulsed)	5×10^5 to 5×10^6 pulses (i.e., 5 to 50 hr at 30 pps)	Can be designed to be any fixed angle from 2 to 90 deg	5 J per pulse $<$ 60 pps
Mercury-vapor arc (continuous)	$>$ 15,000 hr (long arc) 1000 hr (short arc)	10 to 90 deg (long arc) 2 to 90 deg (short arc)	2 kW
Thallium-iodide-doped mercury-vapor arc (continuous)	7000 hr (long arc) 1000 hr (short arc)	10 to 90 deg (long arc) 2 to 90 deg (short arc)	1 kW
Tungsten lamp (quartz iodide lamp)	1000 hr	5 to 90 deg	2 kW

Table 3.5. Typical Parameters for Television Cameras.

Camera	Threshold Sensitivity, fc	
	Low-Contrast Image	High-Contrast Image
Standard vidicon	10^{-1}	10^{-2}
Silicon-diode vidicon	3×10^{-2}	3×10^{-3}
IO	10^{-5}	10^{-6}
II	10^{-4}	10^{-5}
SEC	10^{-5}	10^{-6}
SEBIR or SIT	10^{-6}	10^{-7}

Term	Symbol	Unit	Typical Values
Half-angle of receiver's field-of-view (in water)	θ_3	deg	19, 26, 27.5
Image format on photo-sensitive surface of receiver	A_0	m^2	7.7×10^{-5} (1/2-in.-image diagonal) 3.1×10^{-4} (1-in.-image diagonal)
f number of receiver's optics	f/		1.4, 1.5, 1.8, 2.8
Transmission coefficient of receiver's optics	τ		Generally about 1.0.

SECTION 4. EXTENDED-RANGE UNDERWATER IMAGING SYSTEMS

		Page
4.1	Description of Extended-Range Techniques	4-3
	4.1.1 Polarization Discrimination	4-3
	4.1.2 Volume Scanning	4-4
	4.1.3 Range Gating	4-4
	4.1.4 System Components	4-5
4.2	Polarization Discrimination	4-5
	4.2.1 Design Considerations	4-5
	4.2.2 Source Polarizer	4-5
	4.2.3 Receiver Analyzer	4-6
	4.2.4 Polarization Properties of Targets	4-6
	4.2.5 Polarization Properties of Seawater	4-8
4.3	Volume Scanning	4-8
	4.3.1 Design Considerations	4-9
	4.3.2 Light Sources	4-9
	4.3.3 Scanning Techniques	4-13
	4.3.4 Receivers	4-14
4.4	Range Gating	4-15
	4.4.1 Design Considerations	4-16
	4.4.2 Light Sources	4-16
	4.4.3 Post-Source Processing	4-20
	4.4.4 Prereceiver Processing	4-20
	4.4.5 Receivers	4-20
4.5	References	4-21

Figures | Page

4.1	Polarization-Discrimination System	4-23
4.2	Comparison of Conventional- and Volume-Scanning-System Geometries	4-24
4.3	Range-Gating-System Operation	4-25
4.4	Typical Spectral Characteristics for Common Dichroic Polarizers	4-26
4.5	Polarization Characteristics of Underwater Targets for Incident Circularly Polarized Light	4-27
4.6	Paraboloidal Projection Optics Design	4-28
4.7	Geometry for the Volume-Scanning Imaging System	4-29

Tables

4.1	Possible Components for Extended-Range Underwater Imaging Systems	4-30
4.2	Properties of Typical Polarizers	4-31
4.3	Polarization Coefficients ψ_s of Various Targets	4-32
4.4	Light Detectors for a Volume-Scanning System	4-33
4.5	Sources of Underwater Range-Gating Systems	4-34

SECTION 4

EXTENDED-RANGE UNDERWATER IMAGING SYSTEMS

This section introduces three principal techniques that extend underwater viewing ranges by discriminating against backscattered light: polarization discrimination, volume scanning, and range gating. Design considerations, component descriptions, and problems involved in building workable systems from various components are presented. Adequate design data is also included to provide input parameters for the detailed analysis of the performance of these systems according to the methods outlined in section 6.

4.1 DESCRIPTION OF EXTENDED-RANGE TECHNIQUES

The basic problems of optical imaging in seawater were introduced in section 2. Of these problems, backscatter – the light reflected from particles and biological organisms in the water into the receiver's field-of-view – is often the limiting factor in achieving longer viewing ranges. The following sections discuss three techniques which use specialized hardware to reduce the effects of backscatter on imaging system performance. The geometrical technique of source-receiver separation, which is discussed in section 3 for use with conventional imaging systems, can be used to additionally reduce the effects of backscatter in extended-range imaging systems.

4.1.1 POLARIZATION DISCRIMINATION – This technique uses the polarization differences between the backscattered light and the light reflected from the target to improve visibility (fig. 4.1). If a polarized source of illumination is used underwater, much of the backscattered light will also be polarized and can be blocked with a properly oriented analyzer which is placed in front of the receiver. Ideally, the light which is reflected from diffuse underwater targets is depolarized, and approximately 37 percent of this light will pass through a dichroic analyzer. Because this analyzer attenuates the light reflected from the target less than it attenuates the backscattered light, the image contrast will be enhanced. However, the image irradiance (radiant power/area) is decreased by a factor whose value varies between 4 and 10, depending upon the type of polarizer used, when compared with the image irradiance produced in an "equivalent" conventional system (same light source, receiver, and system geometry). The tradeoff between the increase in image contrast and the corresponding decrease in image irradiance is crucial in determining the effectiveness of this technique in extending viewing range (ref. 4.1). This tradeoff depends on the radiant intensity of the light source, the sensitivity of the receiver, the polarization characteristics of the target, and the values of the polarization coefficient and the other optical properties of seawater. Source-receiver separation also has a significant impact on the performance of polarization-discrimination systems.

The primary advantages of the polarization-discrimination technique are simplicity, low cost, ease of implementation on existing hardware, and the fact that it does not reduce the depth-of-field* of the viewing system.

4.1.2 VOLUME SCANNING – This technique, which is also called synchronous or raster scanning, reduces backscatter by reducing the volume of illuminated water which can be seen by the receiver (fig. 4.2) and by making this volume as distant as possible from the receiver. Volume scanning uses a narrow, well collimated light source and a receiver with a narrow field-of-view. Because the instantaneous field-of-view is too small for practical use, the source and receiver must be synchronously scanned across the desired target area.

The major advantage of a volume-scanning system is its large backscatter reduction, especially for systems with a wide field-of-view. Disadvantages of this system include (1) the difficulty in collimating efficient sources to the narrow-beam angles required, (2) the complexity introduced by the requirement for synchronous scanning, (3) the power limitations of sources suitable for this system, (4) the reduced depth-of-field, and (5) the residual backscatter caused by second- and higher-order backscatter.

4.1.3 RANGE GATING – This technique improves image contrast by rejecting all the backscattered light except that produced by a small volume of water immediately in front of the target. The special components for a range-gating imaging system are a light source which produces high-intensity, short-duration pulses of light and a receiver shutter which can be "opened" and "closed" very rapidly. As illustrated in figure 4.3, the target is illuminated with a short pulse of light from the source, and the receiver's shutter is opened only when the reflected light pulse returns from the target. While the light pulse is traveling to and from the target, the returning scattered light is blocked by the closed shutter. For range gating to be effective, the duration Δt of the light pulse must be much less than the time t for the light to travel between the source and the target.

Range gating, unlike volume scanning and polarization discrimination, provides good discrimination against second- and higher-order backscatter because all light rays must travel at least some minimal distance which is determined by the duration of the light pulse and the timing of the receiver's shutter. Because the range-gating system does not depend on source-receiver separation, the structural position constraints are not as crucial for this system as they are for the other techniques. The range-gating system is also a distance-measuring system, which permits target size to be inferred from image size. The principal drawbacks of range gating are the system's complexity and cost, the low average power output of state-of-the-art pulsed sources, and the small depth-of-field. In addition, range gating becomes less efficient for systems with wide fields-of-view because more backscatter arrives from the edges of the picture than from the center.

**Depth-of-field, as defined in this handbook, must be distinguished from the normal definition used in photography. Depth-of-field is defined in this handbook as the variation in viewing range over which a target can be imaged because of the overlap of the source beam and the receiver's field-of-view. As shown in figure 4.2, the depth-of-field is identical to the depth of the common volume.*

4.1.4 SYSTEM COMPONENTS – These backscatter-reduction techniques will be discussed from an engineering design approach in the remainder of this section. Table 4.1 summarizes the basic components used to construct these systems: components to provide illumination; components to shape and/or shutter the illumination sources; components to optically process and shutter the illumination arriving at the receiver; and components for detecting and converting the returned light into a form of information suitable for electronic processing.

4.2 POLARIZATION DISCRIMINATION

Polarization discrimination, the backscatter-reduction technique whose effectiveness is most dependent on local water and target characteristics, is the simplest and least expensive to operate. For these reasons, there has been an attempt to develop polarization-discrimination systems that will aid the underwater viewing system when water and target conditions permit, but will not detract from the viewing system's effectiveness when water conditions and target characteristics prohibit its use.

4.2.1 DESIGN CONSIDERATIONS – Practical implementation of the polarization-enhancement system simply involves attaching a polarizer to the underwater source and an analyzer to the receiver. The effectiveness of the technique will depend upon the following.

1. The polarization properties of the particular water in which the system is to be used.
2. The polarization properties of the target.
3. The ability of the system to combat the absorption losses caused by the polarizer and analyzer which are used to implement the technique.

Because the polarization characteristics of the target and of the medium at any given location are generally uncontrollable, the primary concern of the designer will be to determine whether this technique will improve his system. The basic hardware specification decisions are reduced to selecting polarizers and analyzers which have minimal absorption losses. Properties of various polarizers are listed in table 4.2 and illustrated in figure 4.4.

The design of polarization-discrimination systems should also include techniques for the rapid removal of the polarizer from the light source and the analyzer from the receiver. With this capability, the performance of the imaging system will not be degraded under conditions where polarization discrimination is not effective in improving target contrast and viewing range.

4.2.2 SOURCE POLARIZER – It is recommended that the polarizer not be a dichroic (absorption) type. Dichroic polarizers waste power, and tests at Morris Dam showed that these polarizers warped when placed in front of a 1000-W tungsten lamp because of overheating (ref. 4.2). Dichroic polarizers have transmission efficiencies of 21 to 38 percent for unpolarized light. Although very sensitive television camera tubes, such as the SEC or SEBIR (table 3.5), can overcome these absorption losses, these tubes are quite expensive.

For these reasons, an advanced type of polarizer, which uses reflectance and interference effects to obtain polarized beams which contain nearly 90 percent of the original light (ref. 4.3), is recommended.

Although these high-efficiency polarizers are not commercially available, they can be easily built to produce either linearly polarized or circularly polarized light. The tradeoff between the two types of polarization involves alignment problems, target characteristics, and the rejection of some of the second-order backscattered light. There are no alignment problems with circular polarizers and analyzers, while the axes of the linear polarizers and analyzers must be orthogonal to within a few degrees to provide good rejection of the polarized backscattered light. Also, experimental measurements indicate that most diffuse targets tend to depolarize circularly polarized light better than they depolarize linearly polarized light. However, the linear polarizers and analyzers are able to discriminate against rays of backscattered light which have been scattered twice by angles nearly equal to 90 deg.

4.2.3 RECEIVER ANALYZER – The analyzer placed on the receiver should be aligned to reject all of the polarized backscattered light. A dichroic polarizing filter with a transmission efficiency of 38 percent is recommended.

4.2.4 POLARIZATION PROPERTIES OF TARGETS – Ideally, if the target has a diffuse or optically rough surface, the incident polarized light will be unpolarized when it is reflected. "This depolarization can be visualized as resulting from multiple reflections at the diffuse surface. Randomness of the diffuse surface will produce about equal numbers of odd and even reflections and thus equal left and right circularly polarized components. If the target surface has high specular reflectance, there will be very little depolarization" (ref. 4.4).

Experimental Measurements of the Polarization Coefficients of Targets. Because physical targets are neither perfectly diffuse nor specular, the actual polarization characteristics of real targets are much more complex than the ideal characteristics. Experimental measurements also indicate that the polarization coefficients are correlated with the target's reflectance coefficients, i.e., "white" targets depolarize better than "black" targets.

Polarization coefficients of the light reflected from a variety of targets are compiled in table 4.3. These coefficients, calculated from a set of measurements,* describe how well the target depolarizes the incident polarized light. The polarization coefficient ψ_s of the light reflected from the target is defined as the ratio of the polarized reflected light to the total reflected light which is incident on the receiver, i.e.,

$$\psi_s = \frac{W_p}{W_t} = \frac{W_1 - W_2}{W_1 + W_2} \quad , \tag{4.1}$$

**Private communication from D. L. Phillips, RCA Service Company, Patrick Air Force Base, Florida.*

where

W_1 is the amount of reflected light that has the same polarization as the light emitted by the source,

W_2 is the amount of reflected light whose polarization state is orthogonal to the polarization of the light emitted by the source,

$W_p = W_1 - W_2$ is the amount of polarized reflected light,

and

$W_t = W_1 + W_2$ is the total amount of reflected light which is incident on the receiver.

The angle β in table 4.3 gives the orientation of the normal to the target's surface with respect to the optical axis of the source. As equation 4.1 indicates, the smaller the value of ψ_s is, the better the target depolarizes the light from the source. Ideally, the bright resolution elements on the target would have a value of ψ_s equal to 0.0, while the dark resolution elements would have a value of ψ_s equal to 1.0 for maximum contrast enhancement. (If ψ_s was equal to 1.0, the reflected light from the dark resolution elements would be blocked by the analyzer, and the image contrast would, therefore, be greater.)

Cooperative Targets. In underwater viewing situations, targets can be classified as either uncooperative or cooperative. Uncooperative targets are objects which have not been treated for ease of optical detection, e.g., enemy hardware, and cooperative targets have special surface coatings for ease in optical detection and/or recognition. If objects are coated with a retroreflector such as Scotchlite, the image irradiance and contrast will be greatly increased because the reflected light is not spread-out. In addition, if the objects can reflect light whose polarization is orthogonal to the polarization of the incident light from the source, the image irradiance can be doubled and the image contrast significantly improved.

Two different approaches have been used to construct cooperative targets for right-handed circularly polarized light (RHCP) (ref. 4.5). The first involves the use of a two-reflection retroreflector which reflects the incident light back towards the source for a variety of target orientations (fig. 4.5, part B). The polarization characteristics of this target can be explained by resolving the incident RHCP light beam into two linearly polarized light beams. (The electric vectors of these two orthogonal components of the light beam are 90-deg out of phase with respect to each other.) For a single reflection from a metal of near-normal incidence, the phase difference between the two beams is increased by 180 deg. Because 90 deg + 180 deg = 270 deg and because 270 deg is equivalent to –90 deg, the reflected light is left-handed circularly polarized (LHCP). At the second reflection of the light from the target, the LHCP light is converted into RHCP light by a process similar to that previously described, and this RHCP light is then retroreflected back to the light source. The second approach uses birefringent quarter-wave materials* and single reflections. One target

---

**A birefringent material has different indices of refraction for the two orthogonal polarization states into which a beam of unpolarized light can be resolved. The quarter-wave plate is a sheet of birefringent material whose thickness is such that a 90 deg or quarter wavelength phase shift occurs between these two polarized components when the unpolarized beam passes through the sheet.*

consists of a quarter-wave plate and a dimpled metallic reflector (fig. 4.5, part C). The polarization of this target is explained by again resolving the incident RHCP light into two linearly polarized components which are 90-deg out of phase. The two-way path through the quarter-wave plate produces two 90-deg phase shifts between these components, and one 180-deg phase shift occurs when the light is reflected at near-normal incidence. Because the total phase shift produced by the target is 360 deg and because 360 deg is equivalent to 0 deg, the returning light will be RHCP. Because the dimpled reflecting surface partially spreads the reflected light, the target is visible for more than one viewing position and source-receiver separation can be used to a limited extent.

A target which uses a quarter-wave plate and Scotchlite retroreflective material is shown in figure 4.5, part D. The Scotchlite is composed of tiny glass spheres of high refractive index which are partially imbedded in a reflective substrate. The incident light passes through the quarter-wave plate, is focused onto the reflecting substrate by the spheres, and returns back through the quarter-wave plate in a direction approximately parallel to the incident beam. Although the polarization characteristics are the same as for the previously described model, this target is much more efficient because of its retroreflective action.

4.2.5 POLARIZATION PROPERTIES OF SEAWATER – The polarization coefficient ψ_b of backscattered light is defined by equation 2.8. This coefficient describes how much of the backscattered light remains polarized and can thus be rejected by using the polarization-discrimination technique. Published measurements of data from which ψ_b can be determined are quite rare. From the limited information that is available, the value of ψ_b appears to vary between 60 to 75 percent in clear ocean water. When the water becomes more turbid and contains large particles, the value of ψ_b decreases. In San Diego Bay, values of ψ_b as low as 10 percent were measured when grains of sand were suspended in the water. Reference 4.6 describes a set of measurements from which the relationship of ψ_b and particle size can be calculated. Estimates of the polarization properties of different types of seawater are also given in reference 4.6.

4.3 VOLUME SCANNING

As described in section 4.1.2, the volume-scanning technique reduces backscatter by using a narrow beam of light and a receiver with a narrow field-of-view to synchronously scan the target. The volume-scanning approach to backscatter reduction has the following advantages.

- Only one source and one receiver are required for imaging a large field-of-view.
- It can significantly increase the absorption- or photon-limited viewing range when imaging static scenes (slowing the scan rate increases the number of photons per resolution element).

Two general types of underwater volume-scanning techniques can be used: dot-scanning and fan-beam-scanning systems. In the dot-scanning system, a small pencil beam of light is transmitted, and a matching, narrow, circular field-of-view receiver is synchronously scanned in a two-dimensional pattern with the beam. Two-dimensional rectilinear scanning can be

accomplished by using a two-dimensional raster pattern or by scanning in one dimension and using a moving vehicle's forward motion to supply the vertical scan, e.g., an airborne radiometer. In the fan-beam-scanning system, a fan beam of light is scanned across the target and a conventional television camera is used as the receiver. Complex post-detection signal processing is used to reduce the effects of the backscattered light. Because a detailed discussion of signal processing is beyond the scope of this handbook, the engineering design information in this section and the system performance calculations in section 6 are restricted to the dot-scanning system.

4.3.1 DESIGN CONSIDERATIONS – Volume-scanning systems are complex and require sophisticated components. There are many design decisions to be made which have a crucial effect on the system's performance. The choice of the proper light source, scanning mechanism, and receiver depends on many interrelated variables. This section discusses some of the engineering tradeoffs between the various types of possible system components, and provides input variables for use in the system performance analysis described in section 6.

4.3.2 LIGHT SOURCES – The choice and the design of the light source are influenced by factors such as the spectral characteristics, the collection efficiency of the projection optics used to collimate or focus the beam pattern of the source, and the overall conversion efficiency between the input electrical power and the output radiant power. Because volume-scanning systems are generally absorption or photon limited, the output radiant power should be as high as possible. In addition, the spectral output of the source should be matched to the spectral characteristics of the particular types of water in which the system is designed to operate. Collimation and focusing of the beam pattern of the source are critical because the fundamental resolution of the dot-scanning system is limited by the spot-size of the source beam as it intersects the target.

There are three types of light sources which can be used in volume-scanning systems: lasers, gas discharge lamps with collimating optics, and high-intensity CRT's (flying spot scanners) with focusing optics.

4.3.2.1 Laser Sources – For many applications, lasers are the ideal sources for volume-scanning systems. They are inherently collimated, and they present a relatively small cross-section for ease in packaging. However, their overall conversion efficiency between the input electrical power and the output radiant power is usually less than 0.10 percent. Candidate lasers for underwater use are the frequency-doubled Nd:YAG (neodymium:yttrium-aluminum-garnet), the argon ion, and the xenon ion lasers.

<u>Nd:YAG Laser</u>. These lasers produce a frequency-doubled output at 5320 Å which is suitable for underwater transmission. In the Q-switch pulse mode, average powers of 1 to 10 W have been obtained. However, the pulsed mode cannot be used for most volume-scanning systems because the maximum pulse rates (5000 pps) for existing lasers are not high enough for high-resolution imaging. In the CW mode, average powers are limited to the milliwatt

range by the capabilities of the pumping lamp and by the crystal damage which is caused by the residual absorption, nonhomogeneities, and other crystalline defects of the doubling crystal.

Argon Ion Lasers. Although argon ion lasers have an overall power conversion efficiency of only 0.05 to 0.10 percent, they are probably the best source for volume-scanning systems. They have the highest blue-green CW power output of any ion laser including xenon. (The characteristics of CW xenon ion lasers are similar to those of CW argon ion lasers, and will not be separately discussed in this section.) Several companies are currently producing argon ion lasers with a total radiant output of 4 to 6 W in all lines. (The spectral lines of the argon and xenon ion lasers and the distribution of the radiant power among these lines are given in table 6.6.) Laboratory argon ion lasers with a total output of 10 W have been built in the last few months. However, doubling the source output power provides only a small increase in viewing range, i.e., less than 1 attenuation length, for an imaging system which is photon limited. Typical head sizes for the 4- to 6-W CW argon ion laser are 8-in. wide, 6-in. high, and 48-in. long; typical weight is 90 lb in air. The multiple wavelengths of the argon ion laser are beneficial when operating in different types of water. The spectral line at 4880 Å is most effective in clear ocean water, and the 5145-Å line is most effective in more turbid water.

The divergence of the light beam from the argon ion laser is 0.2 to 1.0 mrad with initial beam diameters of approximately 1 mm. In air at a 50-m range, the 1-mrad divergence beam produces a spot approximately 50 mm (2 in.) in diameter. Forward scattering in water has a large effect on the beam pattern of a collimated source. Even with severe beam spreading, the unscattered light within the geometrical beam pattern will produce a spot of maximum intensity, and some high-resolution data will be available in the image. Sophisticated signal processing might be required to enhance the quality of the image produced by a spot-scanning system. Precise evaluation of the resolution capabilities of a spot-scanning system depends upon detailed knowledge of the volume scattering function at small angles and the ratio of the scattering coefficient to the absorption coefficient at the wavelengths of interest.

4.3.2.2 Gas Discharge Sources – Gas discharge lamps, such as the xenon and the thallium-iodide-doped mercury-vapor (TlI Hg) arc lamps, have several advantages. Compared with other light sources, their overall power conversion efficiency is high (2.0 to 17.0 percent depending on the required spectral bandwidth – see table 3.3), and large input powers (1000 W) can be used. In addition, both lamps are relatively rugged, simple, and inexpensive sources that can withstand exposure to fairly high ambient pressure. Their major disadvantages are the size and collection efficiency of the projection optics required to produce the highly collimated beam patterns required by volume-scanning systems.

Projection Optics for Arc Lamps. The collection efficiency e_4 and the diameter D of the projection optics required to form a narrow-beam pattern can be determined by some simple geometrical calculations. Consider the projection optics illustrated in figure 4.6. The paraboloidal reflector determines the beam pattern, while the secondary spherical

mirror, which is concentric with the arc, is used to redirect forward radiation into the paraboloid. The focal length f required to achieve a beam pattern with a prescribed divergence is given by

$$f = \frac{x}{2 \tan \theta_1} , \tag{4.2}$$

where x is the length of the discharge arc and θ_1 is the required half-angle of the beam pattern. The diameter of the paraboloidal reflector is given by

$$D = \frac{4 f \sin \theta_0}{1 + \cos \theta_0} , \tag{4.3}$$

where θ_0 is the half-angle of the initial beam pattern of the arc and is determined by the obstruction of the electrodes. The diameter D_s of the spherical reflector is given by

$$D_s = 2R \sin \theta_0 , \tag{4.4}$$

where R is the radius of curvature of this mirror. The collection efficiency of the projection optics is approximately given by*

$$e_4 \cong \frac{\Omega_c}{\Omega_r} \frac{\left(A_p - A_s - A_b\right)}{A_p} , \tag{4.5}$$

where

$$\Omega_c = 4\pi (1 - \cos \theta_0) \tag{4.6}$$

is the solid angle subtended by both reflectors;

$$\Omega_r \cong 4\pi - 4\pi \left\{1 - \cos\left(\frac{\pi}{2} - \theta_0\right)\right\} = 4\pi \sin \theta_0 \tag{4.7}$$

is the solid angle into which the arc radiates;

**The collection efficiency is equal to the product of the fraction,*

$$f_1 \cong \frac{\Omega_c}{\Omega_r} ,$$

of the emitted light which is collected by the paraboloidal and spherical reflectors and the fraction,

$$f_2 \cong \frac{A_p - A_s - A_b}{A_p} ,$$

of the collected light which is not blocked by the electrodes and the spherical reflector.

$$A_p = \frac{\pi D^2}{4} \tag{4.8}$$

is the cross-section of the paraboloidal reflector;

$$A_s = \frac{\pi D_s^2}{4} \tag{4.9}$$

is the cross-section of the spherical reflector;

and

$$A_b \cong \frac{x}{2}(D - x) \tag{4.10}$$

is the area blocked by the electrodes.

4.3.2.3 High-Intensity CRT Sources – High-intensity projection cathode ray tubes have been used in a dot-scanning-system design for the Navy by Westinghouse (ref. 4.1). The spot produced by the electron beam on the phosphor serves as a point source of light which is focused on the target with a large collecting lens. The advantages of this source are listed below.

- An inherent electrical to optical conversion efficiency.
- A small source spot which allows high optical collection efficiencies for producing a narrow-beam angle.
- Ease of scanning through electrostatic or electromagnetic deflection, i.e., no moving parts.

Its disadvantages, compared with other sources adaptable for use with the volume-scanning system, include the following.

- Relatively low power outputs because of the practical limitations of the electron energy densities impacting a small phosphor surface (this limits the output to approximately 0.1-W continuous output in the blue-green region of the spectrum).
- Extremely short tube life (approximately 100 hr) because of the strain on the phosphor and the high demands on the electron gun.
- Packaging for pressure environments requires heavy, large housings because of the large vacuum tube and the large focusing optics necessary to create the scanning spot.

Substantial increases in output power are not likely to be attained in the near future. As more power is put into the electron beam, the light output from the phosphor reaches a saturation point. In addition, as output power increases, the tube life decreases.

4.3.3 SCANNING TECHNIQUES – Three methods can be used in volume-scanning systems: mechanical scanning, electromechanical scanning, and electrical scanning.

4.3.3.1 Mechanical Scanning – These systems use sets of spinning mirrors, prisms, and/or lenses to simultaneously scan the narrow-beam pattern of the source and the narrow, instantaneous field-of-view of the receiver over the target. Either the same components should be used to scan both the source and the receiver, or the separate components which individually scan the source and the receiver should be mechanically slaved together so that the scanning system is automatically self-synchronized. In mechanical-scanning systems, the physical configuration of the scanner must be continually sensed and converted into an electrical signal to drive the scanning raster of the television monitor.

Simple operation and the capability to physically synchronize the source and receiver are the primary advantages of mechanical-scanning systems using rotating mirrors. In each system, the source and receiver are stationary; only the scanning components (mirrors, prisms, lenses, etc.) have any motion, and this motion is constant and uniform. Various gearing or phase-lock techniques can achieve the proper speeds without excessive complexity. The inertia of the spinning parts assures smooth, uniform scanning, assuming that the parts can be manufactured with sufficient accuracy. In most mechanical scanners, it is possible to use the same mirrors for both source-beam and receiver field-of-view scanning by geometrically placing the various units in proper position. Instantaneous synchronization is maintained by the scanner itself. Source-receiver separation can be attained by placing a mirror at some distance from the scanner and reflecting the light from the scene to the scanner and then from the scanner to the receiver. Range parallax adjustment can be accomplished by moving either the detector's aperture, or source, or by rotating the source-receiver-separation mirror.

Drawbacks include mechanical wear, gyroscopic reactions, and the necessity of converting the physical position of the scanner into an electrical signal for the monitor. For the system to work at standard television rates, one mirror must scan at 15,750 lines per second. This speed can be reduced with multifaceted mirrors, prisms, or lenses; however, the angular speed will still be hundreds of revolutions per second. These speeds imply that the system should be surrounded by a vacuum, which might necessitate a bulky pressure housing, and that care will be needed to prevent excessive wear or damage caused by gyroscopic reactions.

4.3.3.2 Electromechanical Scanning – These systems use scanning mirrors or prisms mounted on a torsional spring or piezoelectric crystals. Electrical signals are used to deflect the mirrors so that they can scan the source beam and the receiver field-of-view in a simple raster pattern.

Electromechanical systems have the following advantages.

- Scanning smoothness due to the physical inertia of the scanning mirror.
- Reliability because of the lack of moving parts (except for expansion and contraction within the spring and crystals).

- The capability to use the same scanner for both the source and the receiver to achieve automatic self-synchronization.
- The inherent connection between the physical position of the scanning mirror and the driving electrical signals, which can also be used to control the television monitor.
- Smaller pressure housings than those required for mechanical systems.

A disadvantage of the piezoelectric-scanning system is the limited size of the angles through which it can scan. Other drawbacks might exist, but testing will be required to determine them.

A major difference between electromechanical and other scanning systems is that the scan is sinusoidal in time across the target rather than linear. This is an advantage because radiant energy is concentrated in those directions for which the pathlength is greatest in the normal imaging system geometry. (In the sinusoidal scan, the scanning beam moves slowest at the edges of the target and fastest at the center of the target.)

4.3.3.3 Electrical Scanning – These systems use a high-intensity CRT light source and an image dissector receiver. The source, receiver, and monitor are driven by the same electrical signals.

The all-electrical-scanning system has no moving parts, except the range focus control, and the signals controlling its scanning are always synchronized. Because the circuits are standard closed-circuit television modules, parts and sophisticated design are available. The major drawbacks are the low power output and the short lifetime of the light source and the complex electronics necessary to achieve and maintain source-receiver tracking. In addition, there is no inherent feedback in the system to insure that the transmitted beam and receiver field-of-view always overlap at the range of interest. To introduce this feedback would cause additional complexity.

4.3.4 RECEIVERS – Because the scene is scanned by the techniques previously described, conventional television cameras are not used for the receiver in a dot-scanning system. The only equipment needed is a light-detection element.

4.3.4.1 Light Detectors – Two basic types of detectors appear applicable to volume scanning: photomultiplier tubes and solid-state photodetectors. The photomultiplier-tube category includes the image-dissector tube (scanning photomultiplier) as well as conventional photomultiplier tubes.

Photomultiplier tubes are generally the most sensitive, linear, and noise immune of the detectors. Minimum sensitivities of approximately 10^{-6} fc are possible with rugged photomultiplier tubes, and sensitivities of 5×10^{-8} fc can be achieved with the more sensitive tubes. Photomultiplier tubes are also characterized by high bandwidth and good linearity. The tubes, however, are vacuum tubes which must be packaged inside pressure housings and require high voltages (1 to 2 kV). They are also more complicated and expensive than solid-state detectors.

Solid-state detectors include photosensitive field-effect-transistors (FET's), transistors, diodes, photoconductors, and photovoltaic cells; however, all but the photosensitive FET's have severe disadvantages. The chief advantages of the photosensitive FET's, when compared with the photomultiplier tubes, are their cost, ruggedness, and ability to withstand pressurization. Table 4.4 lists some of the characteristics of several detectors.

4.3.4.2 Receiver Optics – The depth-of-field of a volume-scanning system is determined by the narrow, instantaneous field-of-view of the receiver (fig. 4.7). Mathematically, the relationship is approximated by the expression

$$\Delta \cong \frac{\theta_3 R^2}{d+\theta_3 R}, \tag{4.11}$$

where Δ is the depth-of-field above (in front of) the average target location, θ_3 is the half-angle of the instantaneous field-of-view, and R is the average distance to the target. The instantaneous field-of-view of the receiver is determined by a field stop or aperture in the image plane; the image-dissector tube has an internal aperture which can be used for this field stop. The aperture diameters in image-dissector tubes vary from 0.0005 to 0.010 in. The exact aperture size required for a dot-scanning system depends on the field-of-view and the focal length of the receiver's optical system. The requirement of a constant depth-of-field* demands a different field-of-view (value of θ_3) for different values for the viewing range R. Because the aperture size is fixed, a zoom-lens system is required to vary the value of θ_3.

The power utilization efficiency of the volume-scanning system is directly proportional to the area A_e of the entrance pupil of the receiver's optics. This area can be quite large. In a proposed volume-scanning system (ref. 4.7), the value of A_e was specified to be 66 in^2.

4.4 RANGE GATING

With the range-gating technique described in section 4.1.3, only the target and a small amount of backscatter in front of the target are imaged.

The range-gating system, however, is extremely complex. Although it is the best method** to reduce the detrimental effects of backscatter at long ranges, it is difficult to produce sufficient source power and receiver sensitivities to combat the absorption losses at these distances. The system does, however, appear to be useful in long-range, narrow field-of-view applications (ref. 4.2).

**A minimum depth-of-field Δ is required for an operational system because of the roughness of the ocean floor and the size of typical targets. Equation 4.11 can be inverted to determine the value of θ_3 which corresponds to this value of Δ at a given range R.*

***The range-gating technique is the best method for eliminating backscattered light which has been scattered more than one time.*

4.4.1 DESIGN CONSIDERATIONS – A range-gating system consists of a light source which provides short-duration, high-intensity pulses, a receiver with a fast shutter, and a method for synchronizing the source pulse and the receiver gate. Because the range-gating technique is effective in eliminating backscattered light, the designer should be primarily concerned with providing enough receiver sensitivity and average radiant power output from the source to attain the relatively long viewing ranges which are theoretically possible.* If the duration of the light pulse is less than 20 nsec, only a slight amount of backscattered light will be received under most circumstances. The depth-of-field for a range-gating system is determined by the pulselength and the duration of the receiver gate. The position of the depth-of-field in front of the receiver is determined by the time delay for the receiver gate.

Various factors limit the pulse repetition rate. For real-time television viewing, the rate must be at least as fast as the television frame rate (30 frames/sec). A maximum rate can be determined from the following premise: A pulse should not be initiated until the target reflection from the previous pulse reaches the camera. (This eliminates backscatter from new pulses by allowing only one light pulse at a time in the receiver's field-of-view.) For example, a 400-ft range imposes a maximum repetition rate of 1.8×10^6 pps; this rate, however, is beyond the practical limit of any near-future, range-gating system.

Range-gating systems are complex and require sophisticated components. There are many design decisions to be made which have a crucial effect on system performance. The choice of the proper light source, receiver, and electrooptical shutters depends on large numbers of interrelated variables. This section discusses some of the engineering tradeoffs between the various system components and provides input variables for the system performance analysis in section 6.

4.4.2 LIGHT SOURCES – A pulsed light source with a pulselength of approximately 20 nsec is normally required for a range-gating system.** This duration is a tradeoff between the depth-of-field and the amount of backscatter which is to be eliminated. Usually, the depth-of-field (feet) will be approximately 3/8 of the pulse duration (nanoseconds). Thus, a 20-nsec light pulse would produce a depth-of-field of 7-1/2 ft.

The light sources that can be considered for the range-gating system are lasers, short-pulse flashlamps, and shuttered conventional sources. Data on these sources is given in table 5.4 and section 3.1. It should be recognized that state-of-the-art laser technology is rapidly advancing and that changes in the relative merits of each source will occur. It should also be

---

**The ultimate viewing range for a range-gating system is determined by the degradation of resolution by small-angle scattering.*

***A larger pulse, e.g., 100 nsec, can also be used in a range-gating system if its trailing edge has a sharp cutoff. By keeping the receiver gate closed until most of the reflected light has passed and by then opening it for just the last portion of the reflected pulse, only the backscattered light from a small volume in front of the target will be received. Although a large fraction of the light reflected from the target is lost, the increase in image contrast should more than compensate for the loss in image illuminance.*

noted that these are special-purpose sources, and up to 6 months of development time might be required to ruggedize them to withstand the imposed operational and environmental requirements.

4.4.2.1 **Lasers** – For many applications, pulsed lasers are the ideal sources for range-gating systems. However, the overall conversion efficiency between the input electrical power and the output radiant power is usually less than 0.1 percent. Candidate lasers for the range-gating system are solid-state lasers, dye lasers, and gas ion lasers (table 4.5).

Solid State Lasers – The best known solid-state laser for underwater range-gating systems is the Nd:YAG laser. This laser produces a pulse of 10,640 Å, which is frequency doubled (with a loss of power) to 5320 Å using a nonlinear crystal, such as lithium niobate. A small fraction of the emitted light pulse is used to trigger a timing circuit for the receiver gate. The rest of the pulse passes through a diffuser and illuminates the target. The diffuser spoils the coherence of the light, thereby eliminating the speckle pattern in the image. (Objects illuminated by coherent light have a characteristic speckle pattern in their images.)

There are two methods of exciting or pumping laser rods. The first is to pulse pump with a gas flashlamp, such as xenon. Because of flashtube lifetimes, the pulse rate frequency cannot be much more than 100 pps. The second method is continuous pumping with a continuous xenon lamp and high-speed Q-switching with a sonic Q-switch. Pulse rates of 5000 pps can be achieved with this method.

The continuously pumped laser cannot produce as high an average power as the pulse-pumped laser because the doubling crystal and the pumping lamp cannot survive the operation needed to produce such continuous high power.

Dye Lasers – These lasers are another possible source for range-gating systems. The dye laser uses organic dyes which absorb in the ultraviolet and yield stimulated radiation in the visible. Because of the wide emission bands of these dyes, the lasing action can be tuned (e.g., by diffraction gratings) to occur at a desired place on a continuum of wavelengths. This feature is especially attractive for underwater applications because the optimal wavelength for underwater transmission varies for different kinds of water. The two most common means of pumping dye lasers are with flashlamps and nitrogen lasers. Flashlamps have been used to give outputs of a few hundred millijoules in pulselengths of approximately 1/2 μsec. These pulselengths are long when compared with the pulselengths needed for underwater range gating. Nitrogen lasers, however, can be used to produce short pulses of ultraviolet light. At these short pulselengths, the stimulated emission becomes competitive with the other relaxation processes in the dyes, and the dyes become very efficient lasers. Some dyes yield efficiencies as high as 50 percent in this mode,* although typical efficiencies are approximately 5 percent. Because of the small power available from even large nitrogen lasers (typical outputs are approximately 5 to 50 mJ at an efficiency of 10^{-3} to 10^{-4} percent), organic dye lasers pumped by these lasers have never been used in underwater range-gating systems.

**Private communication with T. G. Pavolpolous, Naval Electronics Laboratory Center, San Diego, California.*

Gas Ion Lasers – Although argon ion lasers are the most powerful lasers for the production of CW visible radiation, xenon ion lasers are the highest power-pulsed lasers available for blue-green radiation. The principal spectral wavelengths are 4954, 5008, 5159, 5260, 5353, and 5396 Å, which compare favorably with the spectral transmission characteristics of seawater. A pulsed xenon laser has been developed with an average power of 50 W (ref. 4.8). The minimum pulselength is 0.5 μsec, which is too long for underwater range-gating systems. However, it is now considered feasible to build a pulsed xenon laser with the following capabilities.

- Peak power: 200 kW.
- Pulse repetition rate: 5000 pulses/sec.
- Pulselength: 20 nsec.
- Average power: 20 W.

Despite these high-performance characteristics, there would be several disadvantages to this laser.

- Its overall power conversion efficiency would be low, which is typical of all lasers.
- There would be difficult engineering problems with heat dissipation.
- The length of the laser cavity would be 4 ft (the diameter would only need to be 1 mm).

4.4.2.2 Short-Pulse Flashlamps – Because flashlamps are normally used to excite lasers, flashlamps have been suggested as an alternative source for range-gating systems. Because the laser converts only a fraction of the light from the flashlamp into its radiant output, greater overall power conversion efficiency would result if the light from the flashlamp could be directly used in the range-gating system. However, there are several disadvantages to using flashlamps for underwater range-gating sources (ref. 4.9).

- The minimum pulselength is approximately 100 nsec which is too long for most applications.
- The expected lifetime of a single flashlamp under normal operating conditions is between 0.3 and 3.0 hr.
- Average radiant power output is estimated to be between 0.5 and 2.0 W in the spectral bandwidths which are optimal for transmission in seawater.

Some of these disadvantages can be overcome by proper engineering design of the system. One possibility would be to design a multiple-source system or a multiple-flashlamp single source.

4.4.2.3 Conventional Sources with Electrooptical Shutters –Another type of range-gating source uses a conventional light source followed by an electrooptical shutter. The high-power output and efficiency of a conventional source (e.g., a mercury arc or a thallium-iodide-doped mercury arc) and the short pulselength of the gate can be used to produce a range-gating source which is useful for some applications. The Pockels cell (ref. 4.10) and the Fabry-Perot

interferometer (ref. 4.11) have been studied as possible shutters for range-gating systems. The Kerr cell is another possibility, but it has the disadvantages of requiring a high bias voltage (approximately 40 kV) and of having a high capacitance.

The transmittance of the Pockels cell, including the transmittance of a pair of dichroic polarizers required for its operation, is approximately 10 percent. The voltage required to drive the Pockels cell is approximately 3 kV, and good contrast ratios* can be obtained for full-beam angles less than 5 deg. Calculations indicate that a Pockels-cell-gated, 200-W, TlI-doped Hg arc with a 0.3 duty cycle** will yield a 0.2-W radiant output in a beam pattern with a 2.5-deg half-angle. This gives an overall radiant power conversion efficiency of 0.1 percent, which is approximately the same as that of the Nd:YAG laser (this efficiency does not include the power required to drive the Pockels cell or that which is required by the control circuitry).

Pockels cells, tested at 3.3 MHz with a 0.3 duty cycle, yield a 90-nsec pulselength. When the Pockels cell is operated with a 0.3 duty cycle, the range-gating technique only eliminates backscatter from the first half of the range to the object. This allows more backscattered light to reach the receiver than is allowed by a laser range-gating system. (If there is sufficient source-receiver separation, a conventional imaging system also eliminates more backscattered light than does the Pockels-cell range-gating system which is operated with a 0.3 duty cycle.) By using a smaller duty cycle or by gating the receiver so that it only receives a fraction of the returning pulse, additional backscattered light can be eliminated. However, both these techniques waste power, and the 0.3 duty cycle is the result of driving the Pockels cell with a fixed, biased, sinusoidal voltage. To obtain a smaller duty cycle, it would be necessary to drive the Pockels cell with a train of square pulses with pulsewidths of approximately 20 nsec. However, because of the capacitive effects, the problems in using a driving voltage of this type are very severe, and an elaborate matching network would be required to keep the power needed to drive the Pockels cell at a reasonable level.

The maximum transmission efficiency of the experimental Fabry-Perot interferometer shutter is 6.1 percent, and its contrast ratio is only equal to 4.1 (ref. 4.11). Investigators predict that an improved shutter could be built, but it is questionable whether the performance characteristics of the new shutter would be better than those of the Pockels cell. Although conventional sources with electrooptical shutters appear to be less effective than pulsed lasers for range-gating sources, there are certain situations in which they have definite advantages. Reference 4.1 describes the possible use of a Pockels-cell range-gating system for divers. (Because the Pockels-cell-shuttered conventional source is small and compact, it is a more reasonable source for a diver to wear than a pulsed laser.)

**The contrast ratio for an electrooptical shutter is the ratio of its transmission coefficient in its "open" state to its transmission coefficient in its "closed" state.*

***The duty cycle of an electrooptical shutter is the fraction of time that it is in its "open" state.*

4.4.3 POST-SOURCE PROCESSING – When a pulsed laser is used for the source in a range-gating system, several post-source processing operations must be performed. First, the collimated laser beam must be spread to match the field-of-view of the receiver. Second, a diffuser is needed to spoil the coherence of the laser light and to remove any "hot spots" or spatial inhomogeneities in the beam pattern.

Synchronization of the laser pulse and the receiver gate has been a problem in range-gating systems. The most common method has been to sample a tiny fraction of the laser pulse and to use it to initiate a trigger circuit for the receiver gate (ref. 4.12). However, this method results in a minimum range limitation for the system. Because of the electrical time delay in the trigger circuit, the receiver gate cannot be opened immediately. Therefore, if the target is closer than the minimum distance determined by this electrical time delay, it cannot be seen. The use of a trigger pulse which is initiated prior to the laser output, such as a pulse from the laser Q-switch, has eliminated this problem. The success of this latter method depends upon the stability of the delay between the Q-switch initiation and the laser output in the particular laser chosen for the source.

4.4.4 PRERECEIVER PROCESSING – The range-gating system requires that the receiver as well as the source be gated. In addition, if the receiver is to exhibit high sensitivity, large aperture optics are necessary and the transmission coefficient of the receiver gate should be as high as possible. Pockels cells, Fabry-Perot interferometers, and image-intensifier tubes can be used as the receiver's shutter. The first two shutters have serious disadvantages: low transmission coefficients and poor contrast ratios for large fields-of-view (section 4.4.2.3). The image-intensifier, however, has an effective transmission coefficient* much greater than one.

There are several types of image intensifiers: electrostatic-focusing tubes, electromagnetic-focusing tubes, and proximity-focusing tubes. Electrostatic tubes with gating electrodes produce distortion and loss of resolution when gated with short pulses. (The loss of resolution is a result of a voltage-controlled focus.) The focusing properties of the proximity-focused tubes are not sensitive to voltage, and there are no gating electrodes; the gate voltage is applied directly between the planar anode and cathode.

All image-converter shutters have the problem of space-charge build up. The photoelectrons emitted by the unwanted backscatter build up a space-charge cloud and are accelerated to the anode with the arrival of the gate pulse, producing an unwanted background because of the backscatter. The solution has been to operate the image converter with a low forward bias.

4.4.5 RECEIVERS – To obtain the extended ranges which are theoretically possible with the range-gating technique, the receiver should be as sensitive as possible. The ideal receiver

---

**The transmission coefficient of an optical device is as the ratio of the number of output photons to the number of input photons.*

should be limited only by the fluctuation noise which is a result of the quantitization of the electromagnetic field, i.e., photon-noise limited. The receiver should also have low lag* at low-light input levels and a large format area so that large aperture lenses with low f/numbers can be used. The best television camera tube for meeting these requirements is the intensified silicon-electron-bombardment-induced-response (ISEBIR) tube (also known as the ISIT tube). The intensified image isocon (III) tube, the intensified image orthicon (IIO) tube, and the intensified secondary-electron-conduction (ISEC) tubes require approximately two to five times more irradiance to produce the same picture quality. The detailed resolution, contrast, and irradiance limitations of these tubes are illustrated in figure 6.4.

4.5 REFERENCES

4.1 Naval Undersea Center, NUC TP 302. *Performance Study of Present and Near-Future Diver Viewing Systems,* by S. B. Bryant and C. J. Funk. San Diego, California. July 1972.

4.2 Naval Undersea Research and Development Center, NUC TP 273. *Comparison of Advanced Underwater Television Systems,* by S. B. Bryant, D. Cozen, R. Fugitt, and C. J. Funk. San Diego, California. January 1972.

4.3 Naval Undersea Research and Development Center, NUC TP 269. *Experimental Optical Polarizer for Underwater Use,* by R. Bruce Fugitt. San Diego, California. February 1972.

4.4 Mertens, Lawrence E. *In-Water Photography.* Wiley Interscience, New York, New York. 1970.

4.5 Naval Undersea Research and Development Center, NUC TN 165. *Extended Range Polarization Targets,* by R. Bruce Fugitt. Pasadena, California. September 1968.

4.6 Gilbert, G. D. "The Effects of Particle Size on Contrast Improvement by Polarization Discrimination for Underwater Targets," *Applied Optics.* Vol. 9, pp. 421-428. February 1970.

4.7 Perkin-Elmer, Engineering Report No. 10706. *Undersea Laser Sensor.* Norwalk, Connecticut. 24 May 1971.

4.8 TRW. *Xenon Laser Review.* Redondo Beach, California. 9 October 1970.

4.9 Naval Undersea Research and Development Center, NUC TP 275. *Design Study of Advanced Underwater Optical Imaging Systems,* by A. Gordon, D. Cozen, C. Funk, and P. Heckman. San Diego, California. January 1972.

**In many television camera tubes, the stored image is not completely erased by a single readout by the scanning electron beam. Lag is a measure of the persistence of the stored image from one frame readout to another.*

4.10 Ocean Metrics, Inc., OMI TR70-004. *Study for Illumination-Modulated, Synchronized Shutter Underwater TV System – Final Report,* by M. Kerpchar and B. Lichtenstein. Fairfield, New Jersey. 3 August 1970.

4.11 Ocean Metrics, Inc., OMI TR72-007. *Design Study of Experimental Piezoelectric Fabry-Perot Light Modulators – Final Report,* by M. Kerpchar and B. Lichtenstein. Fairfield, New Jersey. 31 January 1972.

4.12 Heckman, P. J., and R. T. Hodgson. "Underwater Optical Range Gating," *IEEE Journal of Quantum Electronics.* Vol. QE-3, pp. 445-448. November 1967.

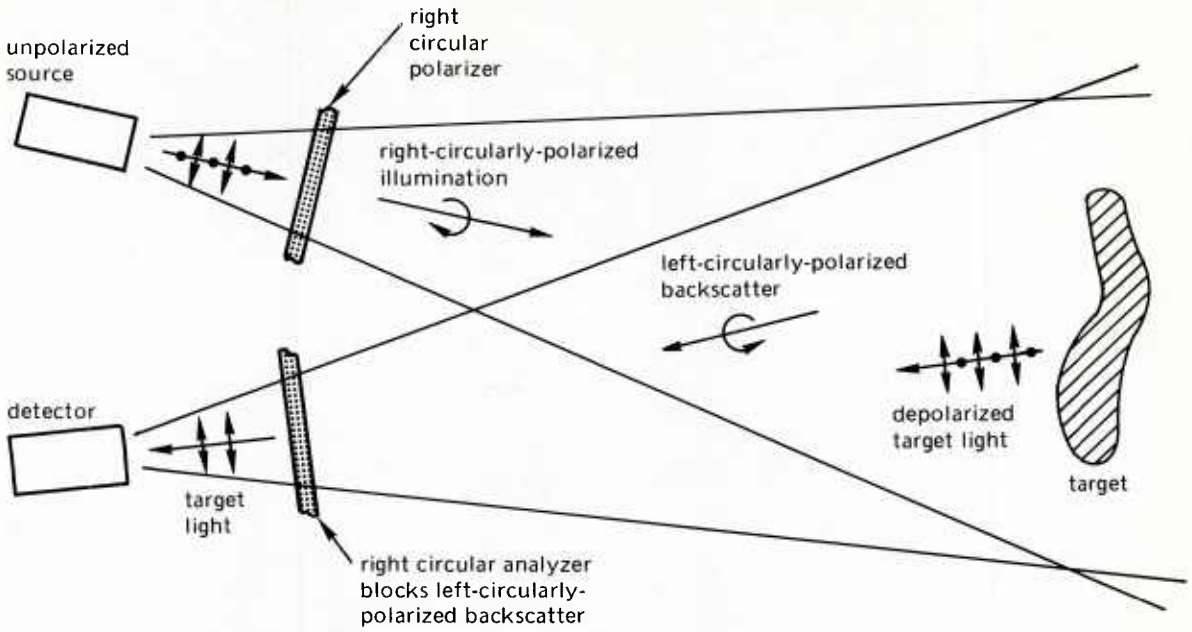

Figure 4.1. Polarization-discrimination system.

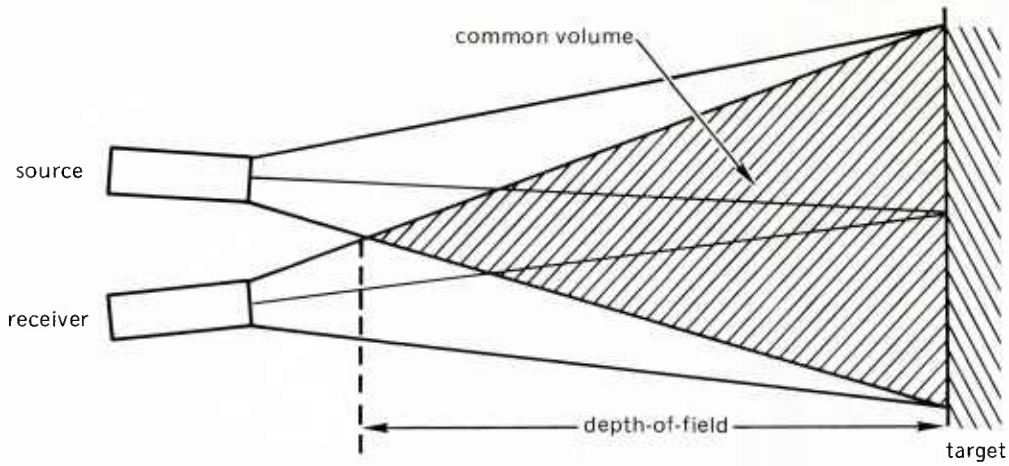

Part A. Common volume of backscatter using a conventional viewing system.

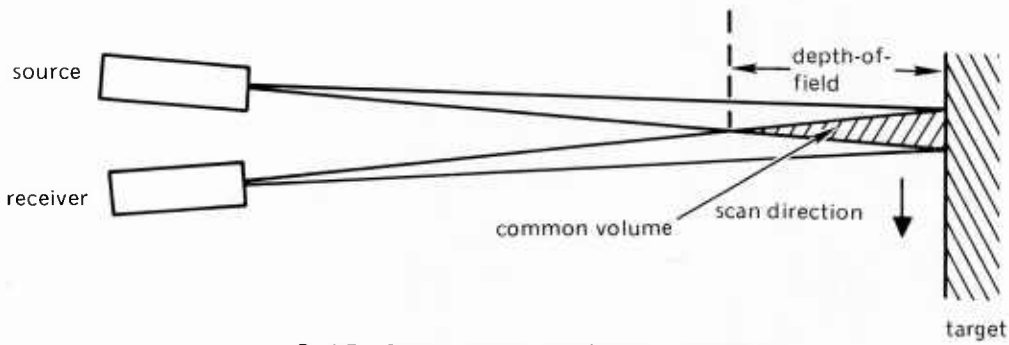

Part B. Common volume of backscatter using a volume-scanning system.

Figure 4.2. Comparison of conventional- and volume-scanning-system geometries.

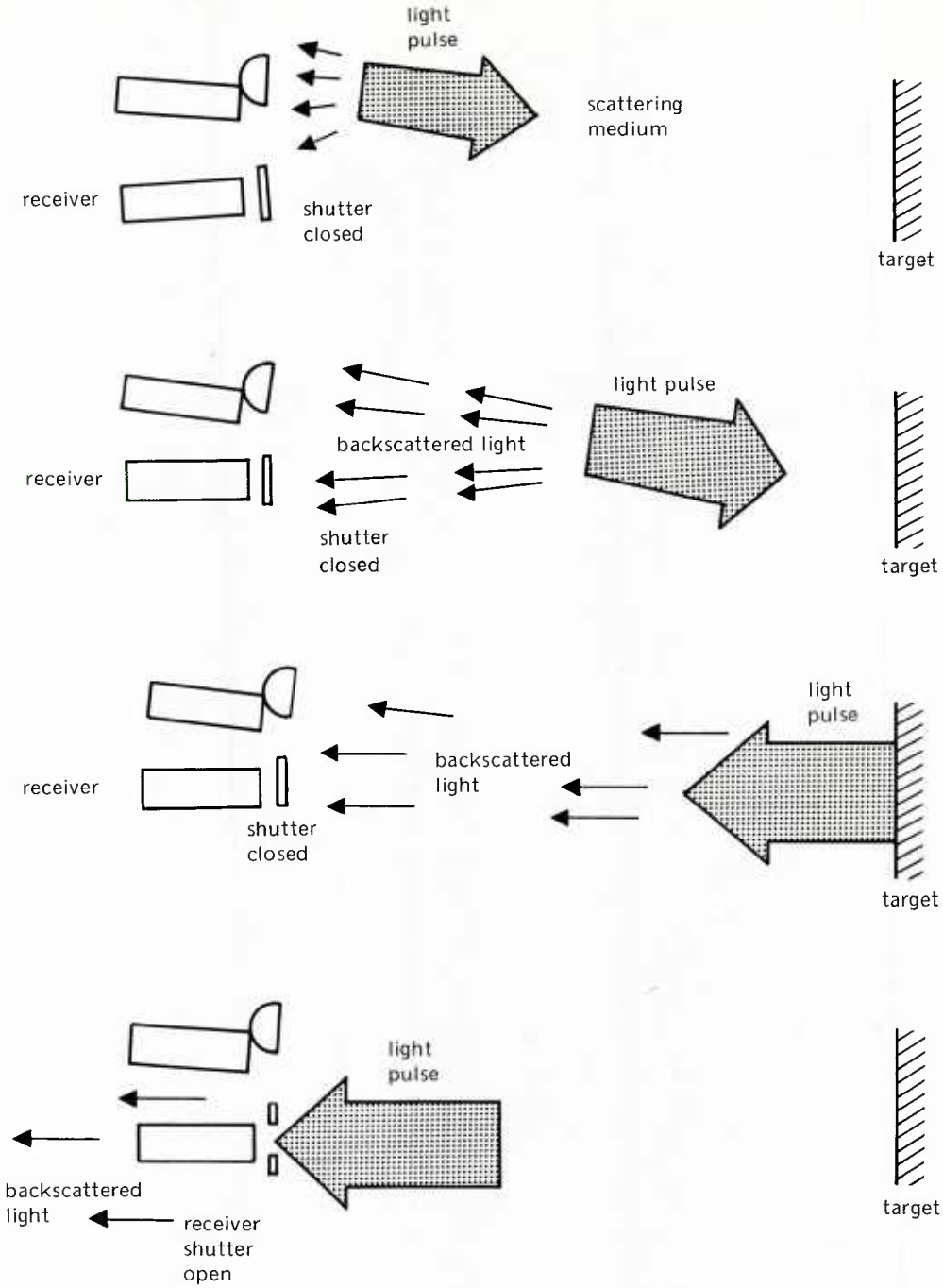

Figure 4.3. Range-gating-system operation.

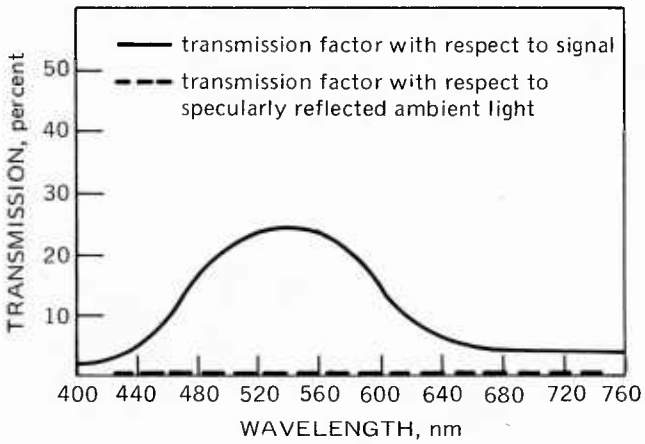

Part A. Circular dichroic polarizer.
HGCP 21 green.

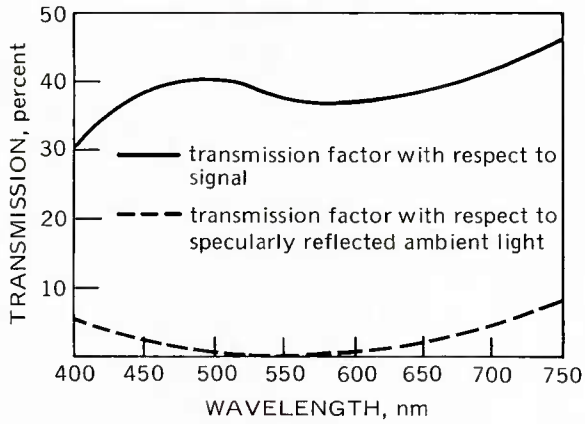

Part B. Circular dichroic polarizer.
HNCP 37 — a neutral-color circular polarizer with a total luminous transmittance of 35 percent.

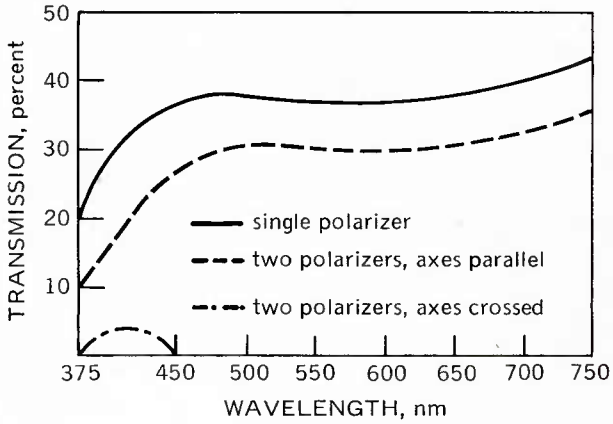

Part C. Linear dichroic polarizer.
HN 38 — a neutral-color linear polarizer with a total luminous transmittance of 38 percent, usually the practical maximum for commercial dichroic polarizers. This filter is noted for its freedom from color distortion.

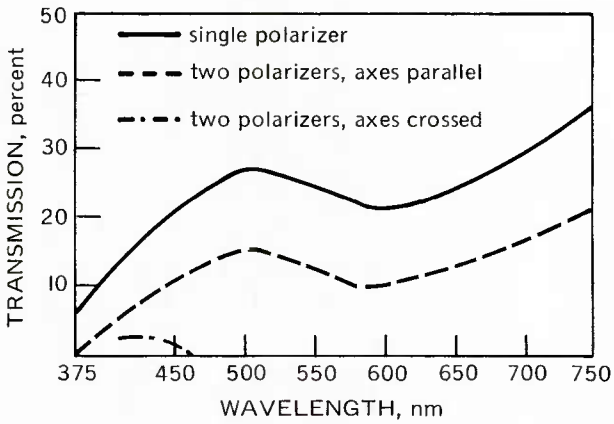

Part D. Linear dichroic polarizer.
HN 22 — a neutral-color linear polarizer with a total luminous transmittance of 22 percent for white light (C.I.E. illuminant C). It offers maximum extinction value (two filters, axes crossed, transmit only 0.0005 percent).

Figure 4.4. Typical spectral characteristics for common dichroic polarizers.

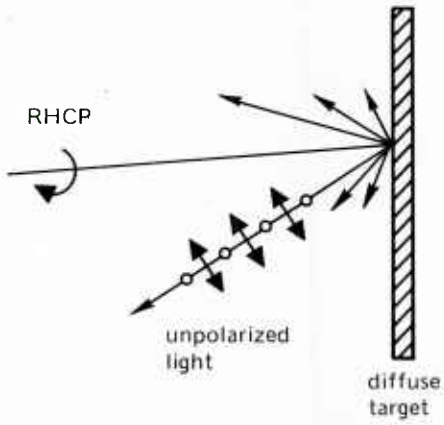

Part A. Target A.

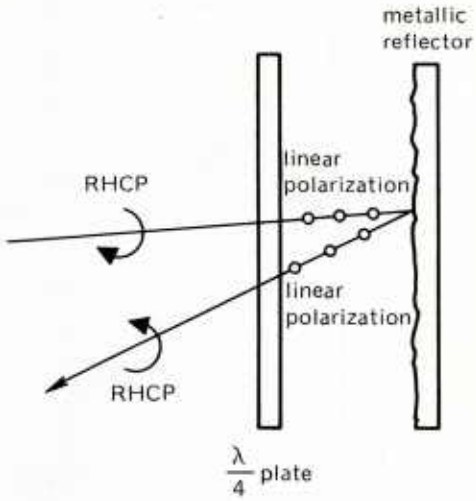

Part C. Target C.

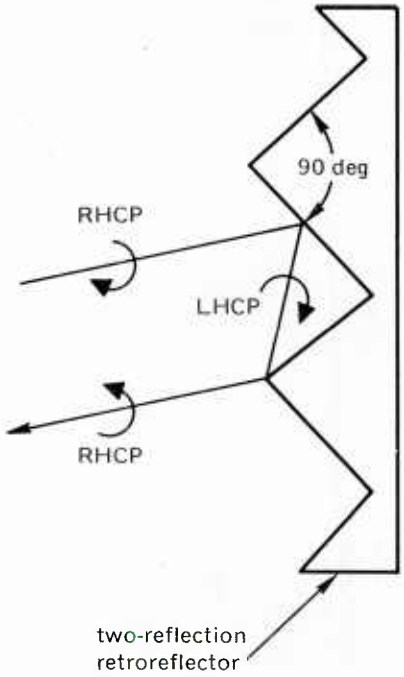

Part B. Target B.

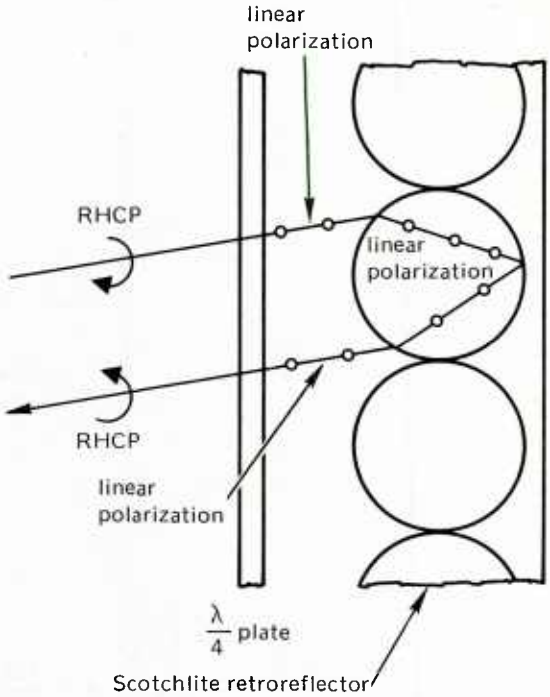

Part D. Target D.

Figure 4.5. Polarization characteristics of underwater targets for incident circularly polarized light.

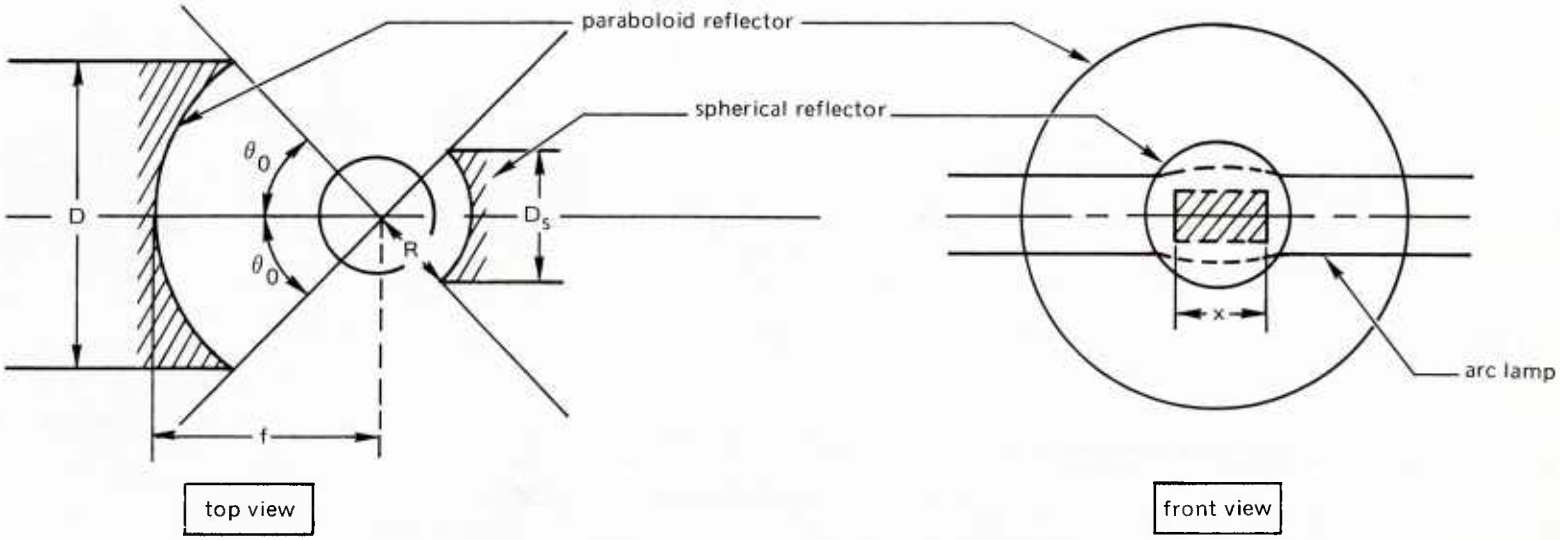

Figure 4.6. Paraboloidal projection optics design.

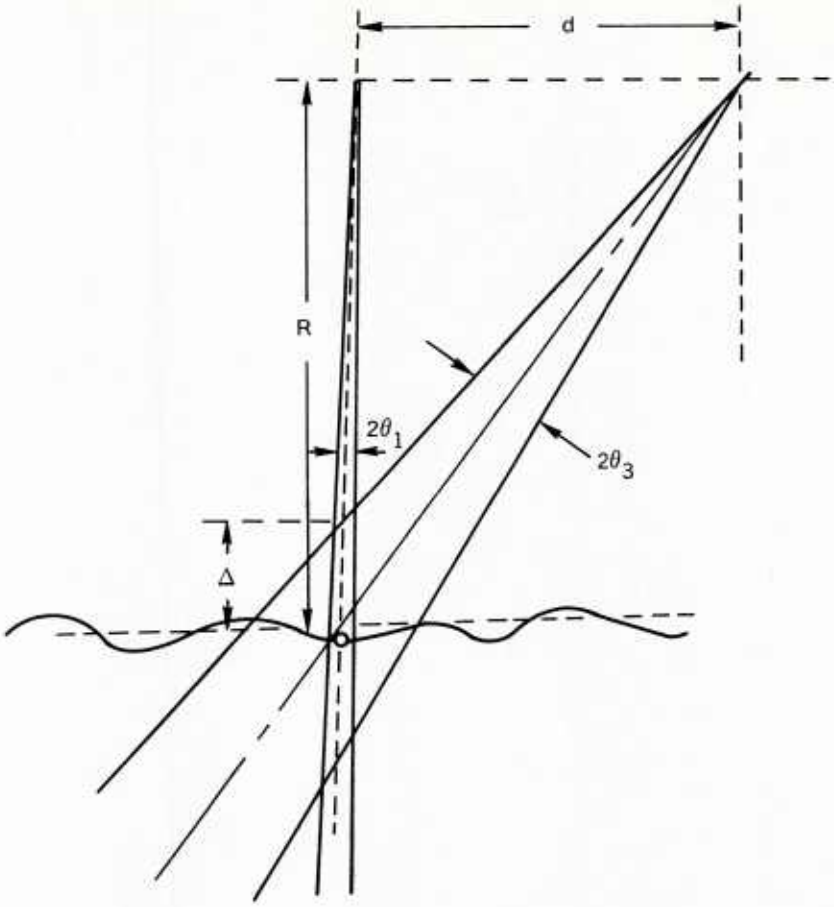

Figure 4.7. Geometry for the volume-scanning imaging system.

Table 4.1. Possible Components for Extended-Range Underwater Imaging System.

System Type	Light Sources	Post-Source Processing	Prereceiver Processing	Receiver
Polarization discrimination	Continuous gas arc – Hg, Xe, Hg + TlI Tungsten Pulsed Xe gas arc Continuous-wave argon laser	Projection optics Polarizer Pan-and-tilt unit	Receiver optics Analyzer Image intensifier Pan-and-tilt unit	Television tubes · Vidicon · Image orthicon · Image isocon · SEC · SEBIR (SIT)
Volume scanning	Continuous-wave argon laser Continuous gas arc – Hg, Xe, Hg + TlI Cathode ray tube	Projection optics Beam scanner · Mechanical · Electromechanical · Electrostatic Pan-and-tilt unit	Receiver optics Beam scanner · Mechanical · Electromechanical · Electrostatic Pan-and-tilt unit	Photomultiplier Image dissector FET's
Range gating	Nd:YAG laser Dye laser Xenon laser Flashlamp Argon laser Continuous gas arc – Hg, Xe, Hg + TlI	Projection optics Shutters · Pockels cell · Kerr cell · Fabry Perot Beam diffuser Pan-and-tilt unit	Receiver optics Shutters · Image intensifier · Pockels cell · Kerr cell · Fabry Perot Pan-and-tilt unit	Television tube · SEBIR (SIT) · Image orthicon · Image isocon · SEC

Table 4.2. Properties of Typical Polarizers.*

	Polarizer	Type	Polarization Efficiency (e_i)**	Color***	Degree of Polarization (ψ)+
Circular	Polaroid HNCP 37	Dichroic	0.37	Neutral	> 0.95
	Polaroid HGCP 21	Dichroic	0.21	Green (peak transmittance at 540 nm)	> 0.96
	Free-flooded experimental	Reflection recombination	0.57	Neutral	> 0.95
	Prism-divided system	Reflection recombination	0.88	Neutral	> 0.95
Linear	Polaroid HN 38	Dichroic	0.38	Neutral	> 0.95
	Polaroid HN 22	Dichroic	0.22	Neutral	> 0.96

*Polarizer is used as a polarizer when used with a light source; polarizer is used as an analyzer when used with a receiver.

**$e_i = \dfrac{\text{total radiance transmitted by polarizer}}{\text{total unpolarized radiance incident on polarizer}}$ = polarization efficiency. $i = 1$ for polarizer; $i = 2$ for analyzer.

***Transmittance of most polarizers is wavelength dependent.

+$\psi = \dfrac{k_2 - k_1}{k_2 + k_1}$ = degree of polarization, where $k_2 = k_2(\lambda)$ is the ratio of the transmitted intensity to the incident intensity when the incident polarized beam is oriented for maximum transmittance and $k_1 = k_1(\lambda)$ is the ratio obtained when the transmittance is minimum.

Table 4.3. Polarization Coefficients ψ_s of Various Targets.*

Circularly Polarized Light

Target	β = 0 deg**	β = 15 deg	β = 30 deg	β = 45 deg
Ba SO_4 paint (ultrawhite)	0.04	0.04	0.07	0.11
White paper (ρ = 0.90)	0.26	0.24	0.17	0.17
Gray paper (ρ = 0.18)	0.38	0.23	0.22	0.22
Flat black paint	0.77	0.74	0.70	0.65
Black anodized metal	0.91	0.80	0.55	0.14

Linearly Polarized Light

Target	β = 0 deg	β = 15 deg	β = 30 deg	β = 45 deg
Ba SO_4 paint (ultrawhite)	0.11	0.11	0.11	0.12
White paper (ρ = 0.90)	0.20	0.11	0.05	0.05
Gray paper (ρ = 0.18)	0.61	0.48	0.37	0.31
Flat black paint	0.95	0.94	0.93	0.90
Black anodized metal	0.98	0.97	0.94	0.91

*Type of polarized light (circular or linear) should agree with that which was used to to evaluate the polarization coefficients, e_1 and e_2.

**β = the angle between the direction of the incident light and the normal to the target.

Table 4.4. Light Detectors for a Volume-Scanning System.

Type	Sensitivity	Dark Current	Minimum Sensitivity, fc	Bandwidth	Comments
Photo-multiplier tube	1000 μA/fc	0.05 μA	10^{-7} to 10^{-5}	100 MHz	Linear and rugged High voltages (2 kV) Cannot be pressurized
FET	5 μA/fc	0.05 nA	2×10^{-5}	10 MHz	Solid-state ruggedness Nonlinear response Simple and inexpensive
Transistor	0.2 μA/fc	25 nA	0.25	50 kHz	Solid-state ruggedness Nonlinear response
Diode	0.3 nA/fc	2 nA	6	200 MHz	Fast but insensitive

Table 4.5. Sources for Underwater Range-Gating Systems.

Type	Spectral Characteristics	Overall Power Conversion Efficiency, percent	Peak Output Power per Pulse, kW	Average Power, W	Pulse Duration, nsec	Pulse Repetition Rate, pps
Nd:YAG laser (pulse pumped)	10640 Å doubled to 5320 Å	0.1	8000	4	17	30
Nd:YAG laser (continuously pumped)	10640 Å doubled to 5320 Å	0.002	1	0.13	25	5000
Pulsed xenon ion laser	4954 Å, 17 percent 5008 Å, 17 percent 5159 Å, 9 percent 5260 Å, 18 percent 5353 Å, 20 percent 5396 Å, 19 percent	0.1	20	50	500	5000
Dye laser (nitrogen laser pumped)	Tunable throughout the visible spectrum	10^{-3} to 10^{-4}	50	0.15 to 0.3	100 to 200	30
Flashlamp	Black-body radiator	< 0.5	< 20	0.05 to 0.2	> 100	100

SECTION 5

SYSTEM PERFORMANCE NOMOGRAMS

5.1 Nomograms: Input and Output Parameters 5-3

5.2 Uses of the Nomograms 5-4

5.2.1 Calculation of Image Illuminance and Contrast 5-5

5.2.2 Evaluation of Source-Receiver Separation 5-6

5.2.3 Tradeoff Between the Source Power and Divergence of the Beam Pattern of the Source 5-8

5.3 Mathematical Basis for the Nomograms 5-9

Figures

5.1 System Performance Nomogram (Conventional Imaging System) 5-14

5.2 Problem One – Evaluation of Image Illuminance and Contrast 5-15

5.3 Problem Two – Evaluation of Source-Receiver Separation 5-16

5.4 Problem Three – Tradeoff Between Source Divergence and Input Power 5-17

Table

5.1 Input and Output Parameters for System Performance Nomograms 5-18

SECTION 5

SYSTEM PERFORMANCE NOMOGRAMS

A simple procedure for evaluating the basic tradeoffs for a conventional underwater optical imaging system is described in this section. In this procedure, a set of nomograms is used to predict system performance which is determined by system components, system geometry, and the total attenuation coefficient of the water. These nomograms permit a designer to obtain insight into the type and relative importance of the tradeoffs which are possible when specifying an underwater imaging system. This is done by restricting the designer's attention to the most crucial variables and providing a simple and fast method for calculating system performance.

To construct a set of nomograms which satisfies these objectives, a number of simplifications and approximations were used. First, the nomograms were limited to describing a conventional system with a thallium-iodide-doped mercury-vapor arc lamp source. Second, the effects of multiple scattering were not included in the analysis. Third, geometrical parameters were approximated by the zero-order representation, i.e., if $\zeta_1 = (R^2 + d^2/4)^{1/2}$, then the value of ζ_1 is approximated by $\zeta_1 \cong R$ for $R >> d$. Fourth, fixed values, listed on pages 5-10 and 5-11, were assumed for the various system parameters. These parameters are the spectral transmission bandwidth (λ_1, λ_2), the transmission coefficient τ and the f/ of the receiver's optics, the backscatter fraction η, the ratio of the scattering coefficient s to the attenuation coefficient α, and the reflectance coefficient ρ_1 of the darker area on the target. Because of these approximations, the values given by the nomograms to describe system performance should only be considered as estimates (values for the image illuminance will be too low, and values for the image contrast will be too high). Section 6 describes a more accurate and sophisticated procedure for determining system performance which is not limited by these restrictions.

The information presented in this section can be summarized as follows.

- Section 5.1 describes the input and output parameters for the various nomograms.
- Section 5.2 explains how to use these nomograms by describing the solution of three typical problems.
- Section 5.3 records the mathematical formulas used to construct the nomograms. (This section is not essential for the use of the nomograms.)

5.1 NOMOGRAMS: INPUT AND OUTPUT PARAMETERS

The complete set of nomograms is presented in figure 5.1. The normal input parameters are listed below.

- Total attenuation coefficient – α (1n/m).
- Electrical input power to the source – w (W).

- Half-angle of the beam pattern of the source (the beam pattern is assumed to be conical) – θ_1 (deg).
- Source-receiver separation – d (m).
- Distance between receiver and target – R (m).
- Reflectance coefficient of the bright area of the target (the reflectance coefficient of the darker area is assumed to be 0.20) – ρ_2.

The geometrical parameters θ_1, d, and R are shown in figure 3.9.

Examples of the output parameters include the following.

- Equivalent image illuminance caused by light reflected from the bright area of the target – E_s (fc).*
- Image contrast – C.**

The user is not limited by this classification of parameters as being either input or output. For example, one might want to determine the source-receiver separation required to produce a given image contrast for fixed values of the other parameters.

For conciseness in identifying the input and output parameters for a particular nomogram, each nomogram is numbered in figure 5.1. Table 5.1 summarizes the input and output variables for each nomogram. (Graphs 2 and 7 are reflector nomograms. They simply change the vertical axis of one graph to the horizontal axis of another graph or *vice versa.*)

5.2 USES OF THE NOMOGRAMS

The basic procedure for using the nomograms in figure 5.1 for system performance analysis consists of three steps.

1. Input and output parameters are identified, and the selected values for the input parameters are inserted into the appropriate nomograms.
2. A set of straight horizontal and vertical lines is constructed to combine the input parameters and to determine the output parameters. (The only purpose of the internal grid marks on each nomogram is to assist in drawing these horizontal and vertical lines.)
3. The output parameters are read from the appropriate nomograms.

For example, both the image contrast, $C = C(R, d, \alpha, \theta_1, \rho_2)$, and the image illuminance, $E_s = E_s(R, \alpha, w, \theta_1, \rho_2)$, are functions of five independent variables. In solving for either

---

* *As described in section 3.2.2, the equivalent image illuminance is the number of footcandles incident on the faceplate of the receiver from a 2854 °K incandescent light which produces the same photocurrent as the light reflected from the target. This reflected light is produced by a thallium-iodide-doped mercury-arc lamp and has been spectrally filtered by the water. Threshold illuminance levels for different television cameras are given in table 3.5.*

** *As described in section 3.2.2, the noise-limited resolution of a television receiver depends on the image contrast and the image illuminance (the photocurrent level). The lower the image illuminance, the higher the image contrast must be for the same degree of resolution. Threshold values for image contrast lie between 0.05 and 0.10 for most applications. The mathematical definition of image contrast is given by equation 3.1.*

C or E_s, the values of the independent variables must be first determined by the user. These values are then inserted into the nomogram – the range R is entered at the top of nomogram 1; the source-receiver separation d is entered at the bottom of nomogram 10; the attenuation coefficient α determines a particular curve in nomograms 1, 5, and 10; the angle θ_1 determines a particular curve in nomograms 9 and 11; the reflectance coefficient ρ_2 determines a curve in nomograms 3 and 6; and the input power w is entered on the left-hand side* of nomogram 9. A series of vertical and horizontal lines is then constructed to connect these input parameters and to determine the output parameters E_s and C. The value of E_s is then read from the family of curves in nomogram 4, while the value of C is read from the right-hand side of nomogram 3. The parameter Γ is an internal variable for coupling nomograms 3 and 8.

Interpolations between pairs of curves in nomograms 4 and 8 are generally required to determine the values of E_s and Γ for a particular problem. Because there are many approximations in the nomograms, these interpolations should be as simple as possible, and "visual" estimates are usually sufficient. The ranges for the different variables in the nomograms have been selected to cover most of the situations for which the calculations are meaningful. If the user runs off-scale in a calculation, he should check the values of his input parameters to determine if they are physically meaningful in terms of the expected operation of a conventional imaging system. For certain problems, off-scale values of some parameters can be handled using inequalities (section 5.2.3). For other problems, it is necessary to use the more elaborate analysis method presented in section 6.

Perhaps the best method for describing the use of the set of nomograms is to demonstrate the detailed solution of three typical problems. In the first problem, image illuminance and contrast are evaluated for fixed values of the target range, attenuation coefficient, target reflectance, input source power, source-receiver separation, and the divergence of the light source. For the second problem, the amount of source-receiver separation required for a minimum value of image contrast is evaluated, and the amount of input source power needed to produce a minimum value of image illuminance is calculated. For the third problem, the tradeoff between source divergence and input power is demonstrated, and the image contrast which corresponds to the various values of the source divergence is evaluated.

5.2.1 CALCULATION OF IMAGE ILLUMINANCE AND CONTRAST – The following values are assumed for the input parameters.

- Target range: R = 15 m.
- Attenuation coefficient: $\alpha = 0.2$ 1n/m.
- Target reflectance: $\rho_2 = 0.5$.
- Input source power: w = 100 W.
- Source-receiver separation: d = 1.5 m.
- Half-angle of light source: $\theta_1 = 10$ deg.

**The right and left sides of the nomograms in this report refer to the reader when he is facing the nomogram.*

The following procedure is used to calculate the image illuminance due to the light reflected from the brighter area of the target (the procedure is illustrated in figure 5.2).

1. Enter the range R at the top of nomogram 1. Draw a vertical line from the value of R = 15 to the curve (straight line) for $\alpha = 0.2$. Then draw a horizontal line from this intersection point to the diagonal line in nomogram 2.
2. Draw a vertical line from the intersection point in nomogram 2 to the diagonal line in nomogram 7.
3. Find the intersection of the vertical line with the curve for $\alpha = 0.2$ in nomogram 5, and draw a horizontal line through nomogram 4.
4. Enter the input power w on the left-hand side of nomogram 9. Draw a horizontal line to the curve (straight line) for $\theta_1 = 10$ deg. Next draw a vertical line from this intersection point into nomogram 6.
5. Find the intersection of the vertical line with the curve for $\rho_2 = 0.5$. Draw a horizontal line from this intersection point to the diagonal line in nomogram 6, which connects the lower left-hand corner to the upper right-hand corner. Draw a vertical line from this second intersection point into nomogram 4.
6. The value of the image illuminance E_s is given by the intersection of this vertical line and the horizontal line constructed in step 3. The value of E_s is approximately 1.1×10^{-3} fc.

The following procedure is used to calculate the image contrast.

1. Enter the source-receiver separation d at the bottom of nomogram 10. Draw a vertical line from the point d = 1.5 to the curve for $\alpha = 0.2$. Draw a horizontal line from this intersection point into nomogram 11.
2. Find the intersection of the horizontal line with the curve for $\theta_1 = 10$ deg, and draw a vertical line from this intersection point into nomogram 8.
3. Draw a horizontal line from the intersection of the vertical and the diagonal lines in nomogram 7 into nomogram 8. (The vertical line was drawn in step 2 of the previous procedure for finding E_s.) Find the intersection of this horizontal line and the vertical line constructed in step 2. This intersection point determines the value of the parameter Γ. In the current problem, $\Gamma = 1.05$.
4. Enter the value of Γ at the bottom of nomogram 3. Draw a vertical line from this point to the curve for $\rho_2 = 0.5$. Draw a horizontal line from this intersection to the right side of nomogram 3, and read the value of image contrast C. The calculated value of C is approximately 0.51.

5.2.2 EVALUATION OF SOURCE-RECEIVER SEPARATION – Image contrast depends upon the parameters R, α, θ_1, ρ_2, and d. In this problem, the value of d is determined so that for fixed values of R, α, θ_1, and ρ_2 the image contrast is at least 0.1. In addition, the amount of input source power is calculated so that the image illuminance is at least equal to 10^{-4} fc. The assumed values for the fixed input parameters are listed on the next page.

- Target range: R = 20 m.
- Attenuation coefficient: $\alpha = 0.20$ 1n/m.
- Half-angle of light source: $\theta_1 = 10$ deg.
- Target reflectance: $\rho_2 = 0.5$.

The following procedure is used to determine the source-receiver separation (the procedure is illustrated in figure 5.3).

1. Enter the image contrast C = 0.1 on the right-hand side of nomogram 3, and draw a horizontal line from this point to the curve for $\rho_2 = 0.5$. Draw a vertical line from the intersection point to the bottom of the nomogram, and determine the value of Γ. For the current problem, Γ has a value of -0.4.
2. Enter the range R = 20 at the top of nomogram 1; draw a vertical line from this point to the curve for $\alpha = 0.2$; draw a horizontal line from the intersection point to the diagonal line in nomogram 2.
3. Draw a vertical line from this intersection point to the diagonal line in nomogram 7. From this intersection point, draw a horizontal line through nomogram 8. Interpolate the value of $\Gamma = -0.4$ along this horizontal line from the curves of constant Γ, and draw a vertical line from the selected point down through nomogram 11.
4. Find the intersection of this vertical line with the curve for $\theta_1 = 10$ deg, and draw a horizontal line from this point into nomogram 10.
5. Determine the intersection of this horizontal line with the curve for $\alpha = 0.2$; draw a vertical line; read the value of the source-receiver separation d. In this problem, the value of d is equal to 1.25 m.

The following procedure is used to calculate the minimum input source power required to produce an image illuminance equal to 10^{-4} fc.

1. Find the intersection of the vertical line drawn through nomogram 5 in step 3 of the previous procedure and the curve for $\alpha = 0.2$. Draw a horizontal line from this point into nomogram 4.
2. Find the intersection of this horizontal line with the curve for $E_s = 10^{-4}$, and draw a vertical line into nomogram 6.
3. Find the intersection of this line with diagonal line running from the lower left-hand to the upper right-hand corner of nomogram 6, and draw a horizontal line from this point to the curve for $\rho_2 = 0.5$. Draw a vertical line from this second intersection point into nomogram 9.
4. Determine the intersection of this vertical line with the curve for $\theta_1 = 10$ deg, and draw a horizontal line from this point to the left-hand side of the nomogram. The calculated input power required to produce a value of E_s equal to 10^{-4} fc is w = 70 W.

5.2.3 TRADEOFF BETWEEN SOURCE POWER AND THE DIVERGENCE OF THE BEAM PATTERN OF THE SOURCE – Image illuminance E_s, caused by the light reflected from the brighter area of the target, depends on the parameters R, α, ρ_2, w, and θ_1. In this problem, corresponding values of w and θ_1 are determined so that the value of E_s is at least equal to 1.0 fc for fixed values of R, α, and ρ_2. In addition, the image contrast C is determined for each of the corresponding pairs of w and θ_1. The following values are assumed for the fixed parameters.

- Target range: R = 1.5 m.
- Attenuation coefficient: α = 1.0 1n/m.
- Target reflectance: ρ_2 = 0.5.

The following procedure is used to calculate the corresponding pairs of w and θ_1 (the procedure is illustrated in figure 5.4).

1. Enter the range R = 1.5 at the top of nomogram 1, and draw a vertical line from this point to the curve for α = 1.0. Draw a horizontal line from the intersection point to the diagonal line in nomogram 2.
2. Draw a vertical line from the intersection point to the diagonal line in nomogram 7.
3. Find the intersection of this vertical line with the curve for α = 1.0 in nomogram 5, and draw a horizontal line into nomogram 4.
4. Find the intersection of this horizontal line with the curve for $E_s = 10^0$ fc in nomogram 4, and draw a vertical line into nomogram 6.
5. Find the intersection of this vertical line with the diagonal line which runs from the lower left-hand corner to the upper right-hand corner of nomogram 6, and draw a horizontal line from this intersection point to the curve for ρ_2 = 0.5. Draw a vertical line from this second intersection point into nomogram 9.
6. Find the intersections of this vertical line with the curves for θ_1 = 5, 10, 15, 25, and 50 deg, and draw a set of horizontal lines from these intersection points to the left-hand side of nomogram 9. The various values of w which correspond to the different values of θ_1 for E_s = 1.0 can now be read. The following pairs of values were obtained for this calculation.
   - θ_1 = 50 deg w = 1000 W
   - θ_1 = 25 deg w = 250 W
   - θ_1 = 15 deg w = 100 W
   - θ_1 = 10 deg w = 40 W
   - θ_1 = 5 deg w = 10 W

The following procedure is used to determine the image contrast which corresponds to the above values for θ_1 and a source-receiver separation equal to 0.4 m.

1. Enter the source-receiver separation d = 0.4 at the bottom of nomogram 10, and draw a vertical line from this point to the curve for α = 1.0. From this intersection point, draw a horizontal line into nomogram 11.

2. Find the intersections of the horizontal line with the curves for θ_1 = 50, 25, 15, 10, and 5 deg, and draw a set of vertical lines from these intersection points into nomogram 8.

3. Draw a horizontal line from the intersection of the vertical and diagonal lines in nomogram 7 into nomogram 8. (The vertical line was constructed during step 2 of the previous procedure.)

4. Find the intersection of this horizontal line with the set of vertical lines drawn in step 2 of the current procedure. From these intersection points, determine as set of values for the parameter Γ. (The values for Γ are obtained by interpolating between the curves of constant Γ.) The following values of Γ, which correspond to the various values of θ_1, were determined.

   - θ_1 = 50 deg $\Gamma = 0.3$
   - θ_1 = 25 deg $\Gamma = 1.5$
   - θ_1 = 15 deg $\Gamma > 2.0$ (off-scale value)
   - θ_1 = 10 deg $\Gamma > 2.0$ (off-scale value)
   - θ_1 = 5 deg $\Gamma > 2.0$ (off-scale value)

5. Enter these values of Γ at the bottom of nomogram 3, and draw a set of vertical lines between these points and the curve for $\rho_2 = 0.5$. Draw a set of horizontal lines from these intersection points and the right-hand side of the nomogram. The different values of the image contrast C can now be read; the following results were obtained.

   - θ_1 = 50 deg $\Gamma = 0.3$ $C = 0.30$
   - θ_1 = 25 deg $\Gamma = 1.5$ $C = 0.58$
   - θ_1 = 15 deg $\Gamma > 2.0$ $C > 0.59$ (off-scale value)
   - θ_1 = 10 deg $\Gamma > 2.0$ $C > 0.59$ (off-scale values)
   - θ_1 = 5 deg $\Gamma > 2.0$ $C > 0.59$ (off-scale values)

   (Note that the off-scale values are indicated by inequalities. The ranges of the parameters selected for the nomograms represent the physical values likely to be encountered in designing underwater optical imaging systems. Off-scale values frequently correspond to unrealistic values for one or more of the input parameters.)

5.3 MATHEMATICAL BASIS FOR THE NOMOGRAMS

The set of nomograms in figure 5.1 is based on simplifications of the system performance equations (developed in section 6) to describe conventional imaging systems. Six basic equations are used.

Equation 6.18

$$i_s = A_0 \tilde{h}_s (CON) [G(\lambda_2(S)) - G(\lambda_1(S))]. \tag{5.1}$$

Equation 6.19

$$\tilde{h}_s\,(\mathrm{CON}) = \rho_2 \cdot w \cdot (\tau/f/^2) \cdot \frac{4\pi}{2\pi(1-\cos\theta_1)} \cdot \frac{9}{256\pi R^2} \cdot \exp(-\alpha g_1 R). \tag{5.2}$$

Equation 6.36

$$i_n = A_0 \tilde{h}_n\,(\mathrm{CON})\left[G(\lambda_2[N]) - G(\lambda_1[N])\right]. \tag{5.3}$$

Equation 6.37

$$\tilde{h}_n\,(\mathrm{CON}) = \eta s \cdot w \cdot (\tau/f/^2) \cdot \frac{4\pi}{2\pi(1-\cos\theta_1)} \cdot \frac{9}{512\pi}\left[\frac{1}{r_0} E_2(\alpha g_3 r_0) - \frac{1}{R} E_2\,(\alpha g_3 R)\right]. \tag{5.4}$$

Equation 6.119

$$C = \frac{i_2 - i_1}{i_2} = \frac{i_s(1-\rho_1/\rho_2)}{i_s + i_n}\,. \tag{5.5}$$

Equation 6.125 and 6.126

$$E_s = i_s/(k_i A_0) \tag{5.6A}$$

and

$$E_n = i_n/(k_i A_0). \tag{5.6B}$$

The various parameters described in these formulas are explained in the text either preceding or following these equations in section 6.

To develop a simple set of interrelated nomograms, the number of variables in these six equations had to be reduced, and the relationships among these variables had to be simplified. For these reasons, the following assumptions and approximations were made.

$\lambda_1\,(S) = \lambda_1\,(N) = 470$ nm.

$\lambda_2\,(S) = \lambda_2\,(N) = 590$ nm.

$\tau = 1.0.$

$f/ = 1.5.$

$g_1 = 2.0.$

$g_3 = 2.0.$

$\eta = 0.02.$

$s = 0.6\alpha.$

$r_0 = d \cot\theta_1.$

$E_2(\alpha g_3 R) = 0.0.$

$\rho_1 = 0.20.$

Under these restrictions, equations 5.1, 5.2, and 5.6A can be combined to yield

$$E_s = 1.88 \times 10^{-2} \left\{ \rho_2 \cdot \frac{2w}{1-\cos\theta_1} \cdot \frac{\exp(-2\alpha R)}{R^2} \right\} \tag{5.7}$$

for the image illuminance of the light reflected from the brighter area of the target. In obtaining equation 5.7, the following values were determined from the data compiled in section 6 for the combination of a thallium-iodide-doped mercury-vapor arc lamp and an antimony-trisulfide photoconductor.

$G(470) = 2.52 \times 10^{-3}$ (table 6.8).

$G(590) = 1.70 \times 10^{-2}$ (table 6.8).

$k_i = 3.83 \times 10^{-3}$ (table 6.11).

Equations 5.3, 5.4, and 5.6B can be combined under the same conditions to yield

$$E_n = 1.13 \times 10^{-4} \left\{ \frac{2w}{1-\cos\theta_1} \cdot \frac{\alpha}{r_0} E_2(2\alpha r_0) \right\} \tag{5.8}$$

for the image illuminance of the backscattered light. Equations 5.5, 5.7, and 5.8 can be combined to yield

$$C = \left\{ \left(1 - \frac{0.2}{\rho_2}\right) E_s \right\} / \left\{ E_s + E_n \right\} \tag{5.9}$$

for the image contrast. By defining

$$\gamma = E_s/(\rho_2 E_n) = 167 r_0 \exp(-2\alpha R) / (\alpha R^2 E_2(2\alpha r_0)), \tag{5.10}$$

the image contrast can also be written as

$$C = \gamma(\rho_2 - 0.2) / (\rho_2 \gamma + 1). \tag{5.11}$$

By using the dimensionless parameters,

$$n = \alpha R, \tag{5.12}$$

$$m = \alpha r_0, \tag{5.13}$$

and

$$k = \alpha d. \tag{5.14}$$

Equations 5.7, 5.8, and 5.10 can be written as

$$E_s = 1.88 \times 10^{-2} \left\{ \rho_2 \cdot \frac{2w}{1-\cos\theta_1} \cdot \frac{\alpha^2 \exp(-2n)}{n^2} \right\}, \tag{5.15}$$

$$E_n = 1.13 \times 10^{-4} \left\{ \frac{2w}{1-\cos\theta_1} \cdot \frac{\alpha^2}{m} E_2\,(2m) \right\}, \tag{5.16}$$

and

$$\gamma = 167 \left\{ \frac{m \exp(-2n)}{n^2 E_2(2m)} \right\}. \tag{5.17}$$

The nomograms in figure 5.1 illustrate the interrelationships among equations 5.11 through 5.17. The following functions are specifically illustrated in each nomogram.

1. Nomogram 1. $n = n(\alpha, R) = \alpha R$; $0.05 \leqslant \alpha \leqslant 1.0$, $0 \leqslant R \leqslant 25$, and $0 \leqslant n \leqslant 5$.
2. Nomogram 2. Reflector – changes a horizontal axis into a vertical axis or *vice versa.*
3. Nomogram 3. $\log C = \log (10^{\Gamma} (\rho_2 - 0.2) / (\rho_2 10^{\Gamma} + 1))$,

   where

   $$\Gamma = 10 \log \gamma; \tag{5.18}$$

   $0.25 \leqslant \rho_2 \leqslant 1.0$, $-1.0 \leqslant \Gamma \leqslant 2.0$, and $0.01 \leqslant C \leqslant 1.0$.
4. Nomogram 4. $E_s = E_s\,(F_1(\alpha, n), F_2(\rho_2, w, \theta_1))$.

   where

   $$F_1 = \log \left(\alpha \frac{\exp(-n)}{n} \right), \tag{5.19}$$

   $$F_2 = \log \rho_2 + \log \frac{2w}{1-\cos\theta_1}, \tag{5.20}$$

   and

   $$E_s = 1.88 \times 10^{-2} \left(10^{2F_1 + F_2} \right); \tag{5.21}$$

   $-4 \leqslant F_1 \leqslant 0$, $1 \leqslant F_2 \leqslant 6$, and $10^{-5} \leqslant E_s \leqslant 10^2$.

5. Nomogram 5. $F_1 = F_1(\alpha, n) = \log\left\{\frac{\alpha}{n}\exp(-n)\right\}$;

$0.05 \leqslant \alpha \leqslant 1.0$, $0 \leqslant n \leqslant 5$, and $-4 \leqslant F_1 \leqslant 0$.

6. Nomogram 6. $F_2 = F_2(\rho_2, w, \theta_1) = \log \rho_2 + F_3(w, \theta_1)$,

where

$$F_3 = \log\left\{\frac{2w}{1-\cos\theta_1}\right\}; \tag{5.22}$$

$0.1 \leqslant \rho_2 \leqslant 1.0$, $1 \leqslant F_3 \leqslant 6$, and $1 \leqslant F_2 \leqslant 6$.

(A reflector is also used in this nomogram to exchange the vertical and horizontal coordinates.)

7. Nomogram 7. Reflector – changes a horizontal axis into a vertical axis and *vice versa.*

8. Nomogram 8. $n = n(\Gamma, m)$,

where

$$\Gamma = \log\left\{167\, m \exp(-2n) / (n^2 E_2(2m))\right\}; \tag{5.23}$$

$-1.0 \leqslant \Gamma \leqslant 2.0$, $0 \leqslant m \leqslant 3$, and $0 \leqslant n \leqslant 5$.

9. Nomogram 9. $F_3 = F_3(w, \theta_1) = \log\left\{\frac{2w}{1-\cos\theta_1}\right\}$;

$1 \leqslant w \leqslant 1000$, $5 \text{ deg} \leqslant \theta_1 \leqslant 50 \text{ deg}$, and $1 \leqslant F_3 \leqslant 6$.

10. Nomogram 10. $k = k(\alpha, d) = \alpha d$;

$0.05 \leqslant \alpha \leqslant 1.0$, $0 \leqslant d \leqslant 2.5$, and $0 \leqslant k \leqslant 0.5$.

11. Nomogram 11. $m = m(k, \theta_1) = k \cot\theta_1$;

$0 \leqslant k \leqslant 0.5$, $5 \text{ deg} \leqslant \theta_1 \leqslant 50 \text{ deg}$, and $0.0 \leqslant m \leqslant 3.0$.

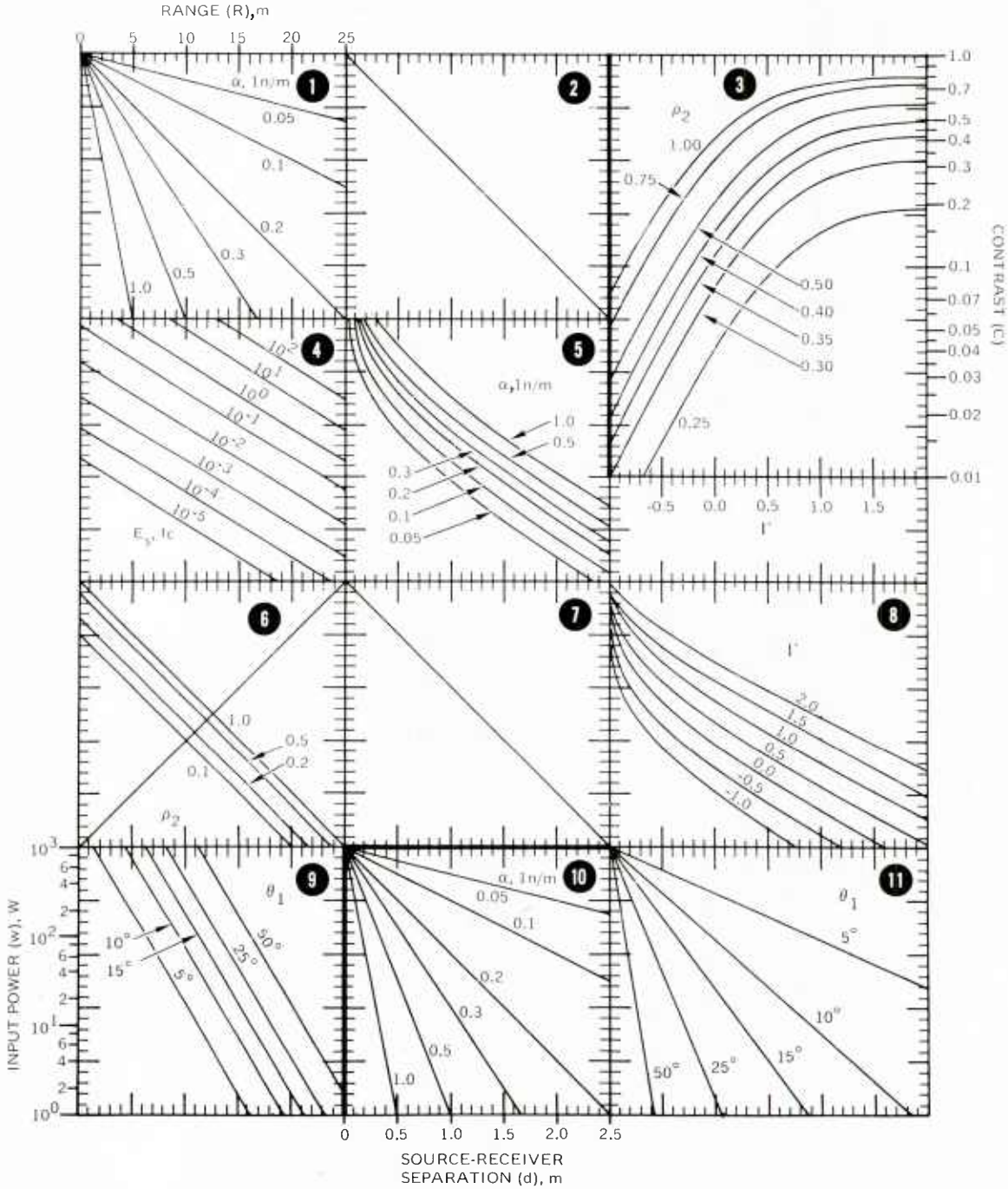

Figure 5.1. System performance nomogram (conventional imaging system).

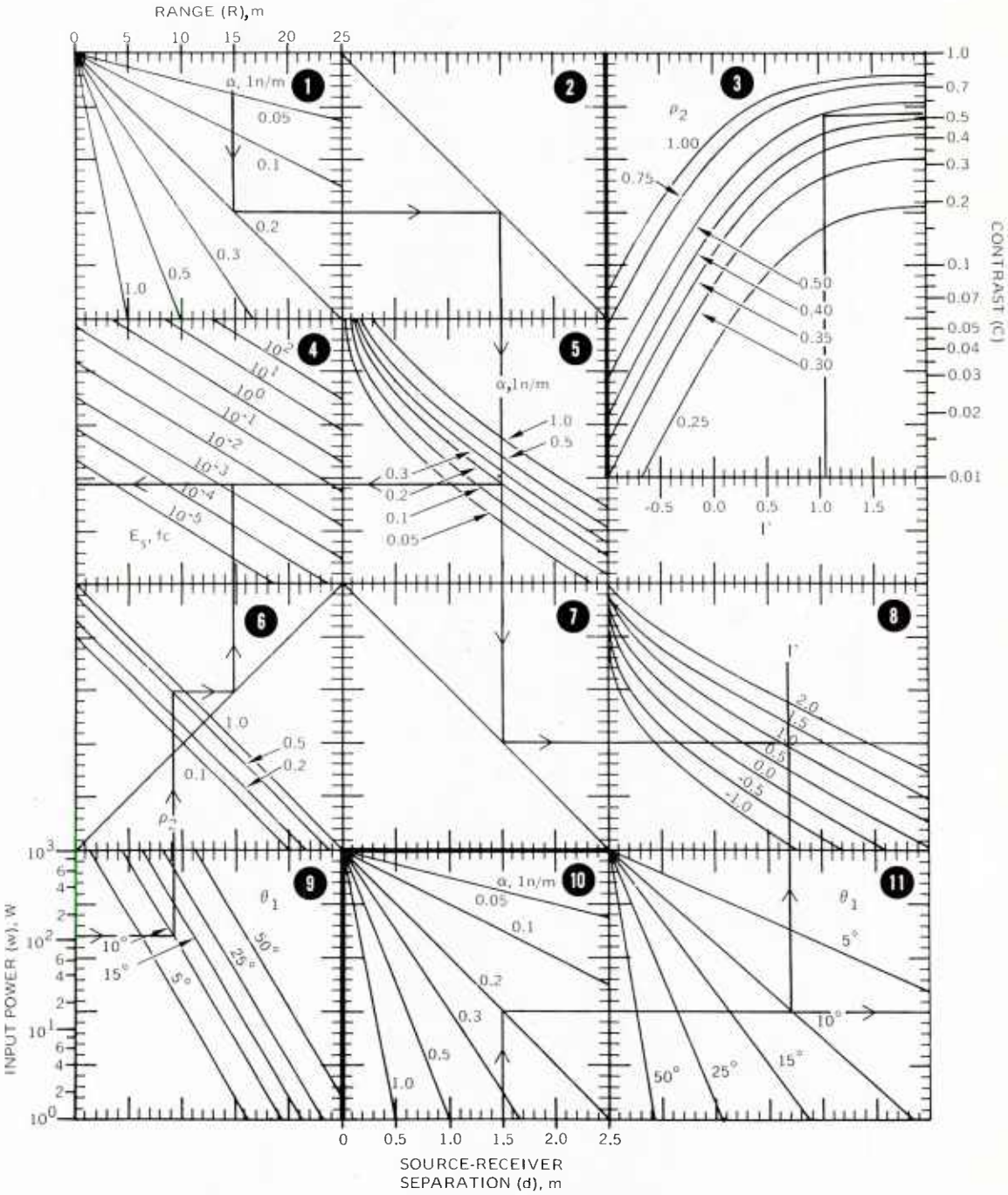

Figure 5.2. Problem one – evaluation of image illuminance and contrast.

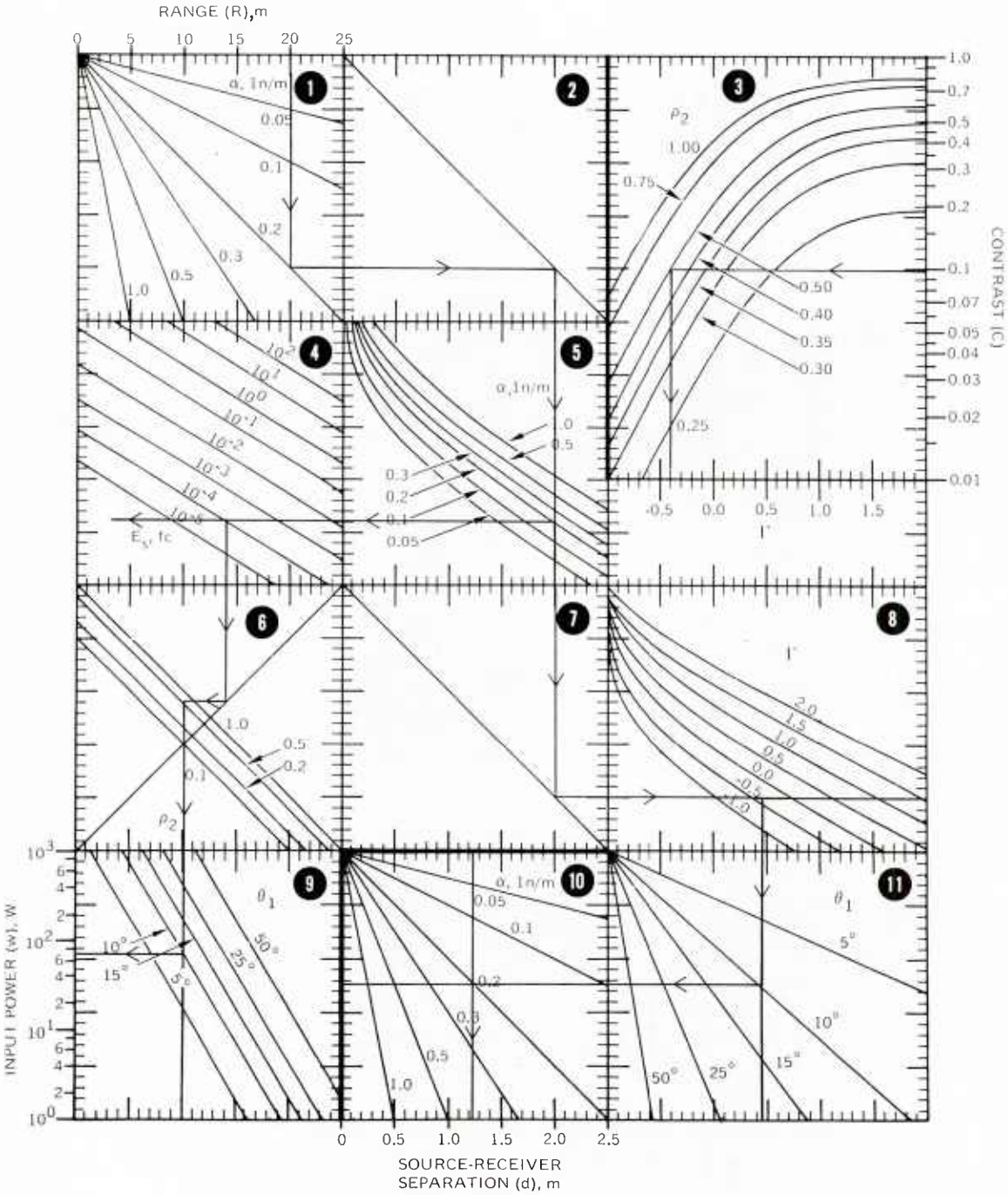

Figure 5.3. Problem two – evaluation of source-receiver separation.

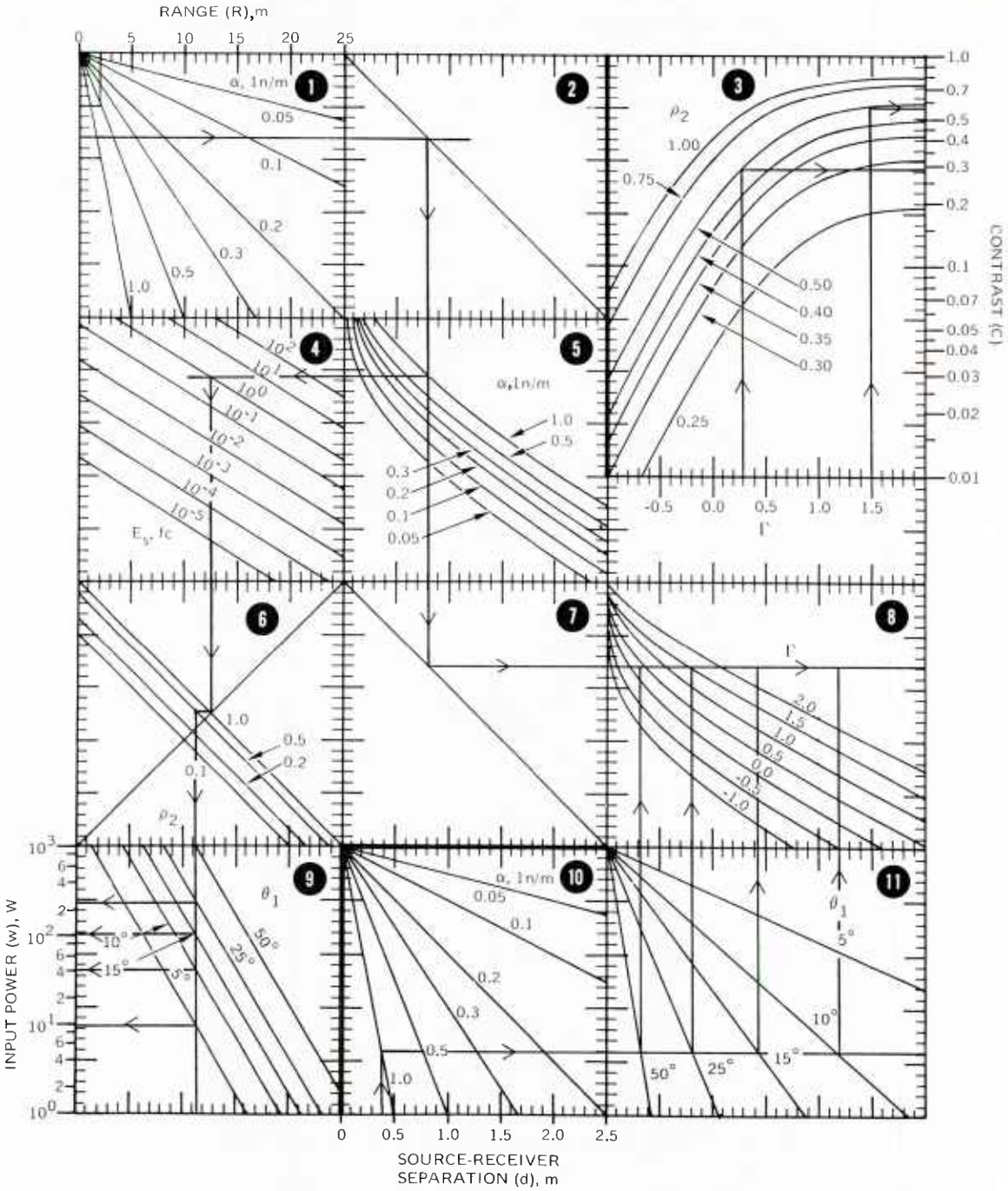

Figure 5.4. Problem three – tradeoff between source divergence and input power.

Table 5.1. Input and Output Parameters for the System Performance Nomogram.

Number of Nomogram	Symbol*	Meaning
1	R (m)	Distance between receiver and target
	α (1n/m)	Attenuation coefficient
2		Reflector nomogram
3	C	Image contrast
	Γ	Internal variable
	ρ_2	Reflectance coefficient
4	E_s (fc)	Image illuminance due to light reflected from the brighter area of the target
5	α (1n/m)	Attenuation coefficient
6	ρ_2	Reflectance coefficient
7		Reflector nomogram
8	Γ	Internal variable
9	θ_1 (deg)	Half-angle of source's beam pattern
	w (W)	Input power to the source
10	d (m)	Source-receiver separation
	α (1n/m)	Attenuation coefficient
11	θ_1 (deg)	Half-angle of source's beam pattern

*The symbols in parentheses refer to units (m, meter; ln, natural logarithm; fc, footcandle; deg, degree; and W, watt).

SECTION 6. SYSTEM PERFORMANCE ANALYSIS

		Page
6.1	Multiple-Scattering Analysis of Light Propagation	6-5
	6.1.1 Effective Attenuation Coefficients	6-6
	6.1.2 Effective Spectral Bandwidths	6-9
6.2	Conventional Imaging Systems	6-10
	6.2.1 System Geometry	6-12
	6.2.2 Signal-Current Equations	6-13
	6.2.3 Noise-Current Equations	6-15
6.3	Extended-Range Imaging Systems	6-19
	6.3.1 Polarization Discrimination	6-19
	6.3.2 Range Gating	6-23
	6.3.3 Volume Scanning	6-26
6.4	Relationship of Perception, Resolution, Image Contrast, and Photocurrent Level	6-29
	6.4.1 Ideal Receivers	6-30
	6.4.2 Real Receivers	6-31
	6.4.3 Equivalent Faceplate Illuminance	6-31
6.5	System Evaluation Procedure	6-32
	6.5.1 Glossary for System Performance Analysis	6-32
	6.5.2 Computational Procedure	6-36
6.6	References	6-38

Page

Figures

6.1	Variation of c_i with θ_i, i = 1 or 3, and the s/a Ratio	6-39
6.2	Spectral Variation of c_i, i = 1 or 3	6-41
6.3	Spectral Characteristics of Conventional Light Sources	6-44
6.4	Receiver-Signal-Response Curves	6-46
6.5	Spectral Responses of Photosensitive Surfaces	6-51
6.6	Simplified Geometry for Conventional and Extended-Range Imaging Systems	6-53
6.7	Variation of r_0/R with θ_1 and d/R	6-54
6.8	General Geometry for Undersea Viewing Systems	6-55
6.9	Variation of D with θ_1	6-56
6.10	Geometry for the Calculation of the Backscattered Light	6-57
6.11	Compensating Backscattered Rays of Light	6-57
6.12	Geometry for the Volume-Scanning Imaging System	6-58
6.13	Signal-Response Curves for an Ideal Photon-Limited Receiver	6-59
6.14	Procedure for Evaluating Underwater Viewing System Performance	6-60

Tables

6.1	Variation of c_i/α with θ_i, i = 1 or 3, and the s/a Ratio	6-61
6.2	Spectral Variation of the Total Attenuation Coefficient for Light in Seawater	6-63
6.3	Spectral Variation of the s/a Ratio for Light in Seawater	6-64
6.4	Effective Spectral Bandwidths for Image-Forming Light for Different Ranges and Beam Patterns	6-65
6.5	Effective Spectral Bandwidths for Backscattered Light for Different Ranges and Beam Patterns	6-66
6.6	Spectral Characteristics for Conventional and Laser Light Sources	6-67
6.7	Spectral Responses of Photosensitive Surfaces	6-70
6.8	Combined Spectral Characteristics of Light Sources and Receivers	6-71
6.9	Values of $E_2(x)$	6-74
6.10	Line Resolution Requirements for Varying Degrees of Perception	6-94
6.11	Conversion Factors Between Current Density and Illuminance	6-94
6.12	Selected Effective Attenuation Coefficients for Bay, Coastal, and Deep Ocean Water	6-95

SECTION 6

SYSTEM PERFORMANCE ANALYSIS

This section describes a procedure for calculating the performance of a specified optical imaging system. This method allows the designer to evaluate important system tradeoffs under a complex set of conditions imposed by mission requirements, the optical properties of the water, and the physical characteristics of light sources, targets, and receivers. The method has sufficient generality to include the evaluation of polarization-discrimination, range-gating, and volume-scanning imaging systems, as well as conventional systems. The analysis, however, is limited to the consideration of the imaging capabilities of systems using artificial illumination sources and electrooptical receivers.

Although the step-by-step computations required to evaluate an imaging system are quite simple, the large number of interrelated parameters required for a complete calculation makes the entire procedure lengthy and complex. A detailed set of work sheets is provided in appendix A to assist the user in organizing the required input data. These work sheets also describe the step-by-step calculations needed to evaluate the performance of the selected viewing system. There are three general classes of input parameters required for a calculation. The first set of variables describes the physical properties of the system components and the targets of interest; the following parameters are listed in this set.

- Input electrical power, output radiant power, beam pattern, and spectral characteristics of the illumination source.
- Target reflectance, contrast, and polarization coefficients.
- Field-of-view, depth-of-field, f/, transmission coefficient, spectral response, and noise characteristics of the receiver.
- Performance characteristics of polarizers and analyzers, electrooptical shutters, gated image intensifiers, beam-scanning optics, and other specialized equipment used in the backscatter-reduction techniques described in section 4.

Each parameter is carefully defined and explained in this section.

The second set of parameters describes the optical properties of seawater which determine system performance. These parameters, defined in section 2, include the following.

- The attenuation coefficient, α,
- The ratio of the scattering coefficient to the absorption coefficient, the s/a ratio.
- The volume scattering function, $\sigma(\theta)$.
- The polarization coefficient, ψ_b.

The third set of parameters describes the geometrical arrangement of the system, and includes the relative locations and orientations of the source, receiver, and target.

In a typical system tradeoff calculation, the first task of the designer is to identify the input parameters required to evaluate his system and to assign them definite numerical values. As mentioned previously, the work sheets in appendix A are designed to help in the systematic collection of the required data. Several values are often used for a few variables so that the designer can determine the relationship between some measure of system performance and the variation in these parameters, e.g., calculation of the change in image contrast as either the viewing range or the beam pattern of the source is varied for fixed values of other input parameters.

The second step is the determination of a set of output parameters which describes the performance of the system. These include the following.

- Image contrast.
- Signal photocurrent produced by the receiver from the image-forming light reflected from the target.
- Noise photocurrent produced by the receiver from backscattered light.
- Noise-limited resolution.*

These output parameters are calculated from the input parameters using a series of formulas developed in sections 6.2, 6.3, and 6.4. Section 6.5.2 briefly outlines the general procedure to be followed in evaluating these formulas; a step-by-step description of the computation is given in appendix A; and sample calculations which describe in detail the evaluation of realistic systems using this analysis technique are in appendix B.

The third step involves the determination of system tradeoffs from the calculated values of the output parameters. For example, one might want to determine how much improvement in system performance is gained by using an expensive, highly sensitive television camera rather than a standard vidicon camera in a particular imaging system. By selecting the appropriate values of the input parameters in the first step of the calculation, the output parameters can be used for a quantitative value judgment. Because of the large number of input parameters, the number of possible system tradeoffs is extremely large. Therefore, a formal procedure for evaluating system tradeoffs is not developed in this section. The designer should, however, have a well defined set of tradeoffs outlined before attempting to perform the first step of the calculation because the selection of input parameters depends upon the type of tradeoffs being considered.

**Noise-limited resolution is the maximum resolution that the system can achieve; it does not include the degradation of image quality due to small-angle scattering and the limitations of the receiver's optics. The point spread function of the combined seawater-receiver optics system must be determined to specify the actual resolution which is present in the display. Under many operating conditions, the degradation of image quality due to small-angle scattering is of minor importance when compared with the other sources of image degradation which are included in the performance analysis described in this section.*

A general method that can be used to evaluate system tradeoffs – the evaluation of a decision matrix – is described in reference 6.1. As illustrated in the following diagram, the different types of systems being considered are listed on the left-hand side of the matrix, while the criteria being used to select the optimal system are listed at the top of the matrix. The element, X_{ij}, of the matrix corresponds to a number between 0 and 10, and gives the relative merit of the ith system according to the jth criterion. By evaluating a set of n equations,

$$V_i = \sum_{j=1}^{m} X_{ij} W_j \, , \, i = 1, 2, \cdots, n, \tag{6.1}$$

and determining the value of i for which V_i is a maximum, the optimum system for a particular mission requirement can be selected. The weight W_j corresponds to the relative importance of the jth criterion of the designer. This matrix technique allows the designer to consider criteria such as cost, reliability, maintainability, and safety, in addition to the system performance factors that are determined in this section.

Decision Matrix

	Criterion 1	Criterion 2	Criterion 3	Criterion 4	Criterion 5	...	Criterion m-1	Criterion m
System 1	X_{11}	X_{12}	X_{13}	X_{14}	X_{15}	...	X_{1m-1}	X_{1m}
System 2	X_{21}	X_{22}	X_{23}	X_{24}	X_{25}	...	X_{2m-1}	X_{2m}
System 3	X_{31}	X_{32}	X_{33}	X_{34}	X_{35}	...	X_{3m-1}	X_{3m}
...	...	...	...	...	...	...	...	...
System n-1	X_{n-11}	X_{n-12}	X_{n-13}	X_{n-14}	X_{n-15}	...	X_{n-1m-1}	X_{n-1m}
System n	X_{n1}	X_{n2}	X_{n3}	X_{n4}	X_{n5}	...	X_{nm-1}	X_{nm}

6.1 MULTIPLE-SCATTERING ANALYSIS OF LIGHT PROPAGATION

This section outlines the mathematical model used to describe the basic physics of undersea imaging systems. Predicting the performance of sophisticated optical imaging systems for undersea applications requires an accurate description of the propagation of light in the sea. As innovations in imaging-device technology increase the viewing range, simplified theories of light propagation become insufficient for an accurate description of the effects of the medium. For long viewing ranges, it is essential that the effects of multiple scattering be evaluated. Monte Carlo techniques have been used to simulate the multiple scattering of

light by seawater (ref. 6.1). The results of these simulations have been reduced to a set of effective attenuation coefficients. These coefficients permit the most significant effects of multiple scattering to be expressed by relatively simple formulas that are suitable for system performance analysis. Appendix C presents experimental data to document the validity of the Monte Carlo simulations and the resulting formulas which are used to predict system performance.

6.1.1 EFFECTIVE ATTENUATION COEFFICIENTS – The fundamental problem in constructing a model of an underwater viewing system is relating the basic optical properties – α, a, s, and $\sigma(\theta)$ – to the propagation of light from sources with a wide variety of beam geometries and spectral contents. Typically, the basic optical properties are measured using specialized beam geometries, i.e., a source with a narrow collimated beam or an isotropic point source. The effective attenuation coefficients provide the essential connection between the light-propagation properties of these specialized beam geometries and those of the general beam patterns used in underwater imaging systems. These coefficients account for both the scattered and unscattered light originally emitted by a point source, and because they are factors in the arguments of exponential functions, accurate calculation of these values can greatly improve the prediction of system performance.

Three effective attenuation coefficients are used in the system performance analysis. The coefficient c_1 describes the attenuation of illuminating light, i.e., the light which travels from the source to the target. The attenuation of image-forming light between the target and the receiver is given by c_2, and the coefficient c_3 accounts for the attenuation of backscattered light.

6.1.1.1 Illuminating Light – The physical meaning of the coefficient c_1 is given by the relationship

$$h(0, R) = J(0) \exp(-c_1(\theta_1) R)/R^2 . \tag{6.2}$$

where h(0, R) is the on-axis irradiance (power/area) produced on a target a distance R from a noncollimated source. The source is assumed to be axial symmetric, and its radiant intensity (power/solid angle) is expressed by the function $J(\theta)$. The coefficient c_1 describes the attenuation of both the unscattered and scattered light which is incident on the target. (For a lossless medium, the value of c_1 is identically zero. In a nonscattering medium, c_1 is identically equal to the absorption coefficient a.) The value of c_1 depends upon the initial divergence of the beam pattern of the source, the ratio of the scattering coefficient to the absorption coefficient (s/a ratio), and the volume scattering function. For the conical beam pattern illustrated in the diagram on page 6-7, the divergence of the light source is specified by the half-angle θ_1. The ratio of the effective attenuation coefficient c_1 to the standard attenuation coefficient α is a convenient parameter for use in the system performance analysis. The value of this ratio is an excellent indicator of the significance of multiple scattering. (The smaller c_1/α is, the more important multiple scattering is.) The variation of c_1/α

with the angle θ_1 and the s/a ratio is shown in figure 6.1 and compiled in table 6.1. These values were determined from a Monte Carlo simulation which used the Morrison volume scattering function. This scattering function was selected because it was measured *in situ* for angles less than 1.0 deg (ref. 6.2). It can be observed from figure 6.1 that the coefficient c_1 is bounded by the inequality, $a<c_1<\alpha$, and that the c_1/α ratio decreases as either the s/a ratio or the angle θ increases.

The equation

$$c_1(\theta_1) = [-\ln\{H(\theta_1)\,\Theta(R)\}]/R \tag{6.3}$$

is used to determine c_1 from the Monte Carlo simulation data. The function $H(\theta_1)$ gives the probability that the angle θ is less than or equal to θ_1. As illustrated in the following diagram, θ is the angle between the original direction of a ray of light and the direction of a vector from the point source where the ray was emitted to the intersection of the ray with a spherical surface. This surface is centered on the point source and has a radius equal to R.

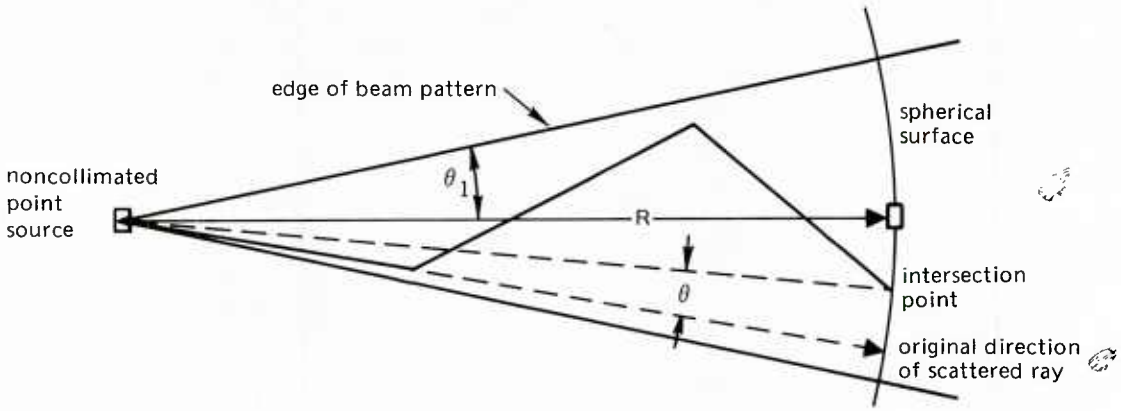

The function Θ (R) gives the probability that a ray of light emitted by the point source reaches the spherical surface without being absorbed. The equivalence of equations 6.2 and 6.3 is demonstrated in reference 6.3 for sources with conical beam patterns.

6.1.1.2 Image-Forming Light – The effective attenuation coefficient c_2 for image-forming light has been demonstrated by experimental measurements (ref. 6.4) to be equal to the total attenuation coefficient α, i.e., $c_2 = \alpha$. This implies that only the light which is either unscattered or scattered by angles less than the very small acceptance angle of a well designed transmissometer retains image-forming information. A discussion of significance of the transmissometer's finite acceptance angle is given an appendix C.

6.1.1.3 Backscattered Light – The physical meaning of the coefficient c_3 is given by the relationship

$$V = V_0 A \exp(-c_3(\theta_3) R)/4\pi R^2, \tag{6.4}$$

where V is the radiant flux accepted by a receiver with a conical field-of-view; V_0 is the initial radiant power emitted by an omnidirectional point source; and A is the area of the receiver's entrance pupil. As indicated in the following diagram, R is the distance between the source and the receiver, and θ_3 is the half-angle of the receiver's field-of-view. The coefficient c_3 describes the attenuation of both the unscattered light and scattered light which are incident on the receiver. This coefficient is determined from the Monte Carlo simulation data according to the equation

$$c_3 = [-\ln\{G(\theta_3)\Theta(R)\}]/R. \tag{6.5}$$

The function $G(\theta_3)$ gives the probability that the angle β is less than or equal to θ_3. As illustrated in the following diagram, β is the angle between the direction of a light ray as it intersects a spherical surface and the normal to the surface at the point of intersection. The spherical surface is centered on the point source from which the ray of light was originally emitted. The function $\Theta(R)$ again gives the probability that a ray of light emitted from the point source reaches the spherical surface without being absorbed.

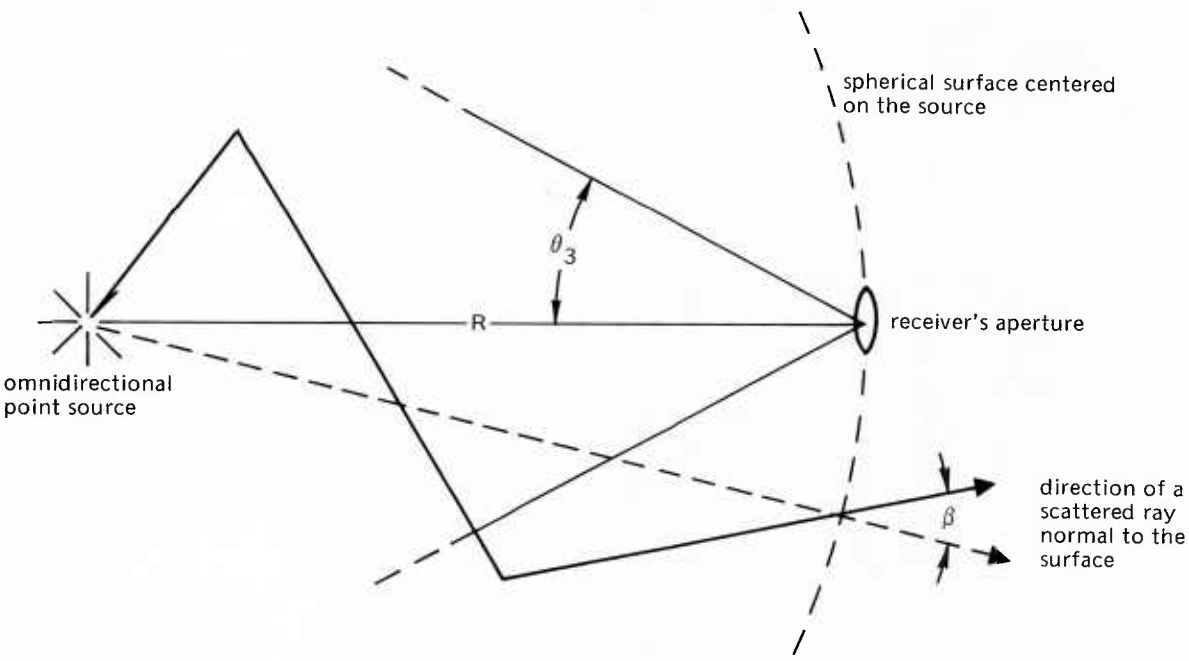

The equivalence of equations 6.4 and 6.5 for a receiver with a conical field-of-view is proven in reference 6.3. This reference also demonstrates that the functions $H(\theta_1)$ and $G(\theta_3)$ are identical because of the principle of reciprocity. Therefore, the effective attenuation coefficients c_1 and c_3 are also identical if the half-angle θ_1 of the conical beam pattern of the source is equal to the half-angle θ_3 of the conical field-of-view of the receiver, i.e., $c_1 = c_3$ if $\theta_1 = \theta_3$. This result follows immediately from equations 6.3 and 6.5. The data in figure 6.1 and table 6.1 can be used to find values for the c_3/α ratio as functions of the angle θ_3 and the s/a ratio.

6.1.2 EFFECTIVE SPECTRAL BANDWIDTHS – The spectral dependence of the basic hydrological optical properties is included in the calculation of the effective attenuation coefficients by determining the spectral variation of the s/a ratio and the regular attenuation coefficient α. (As figure 6.1 and table 6.1 illustrate, the coefficients c_1 and c_3 are functions of both the s/a ratio and α. Because the s/a ratio and α are functions of the optical wavelength λ, the coefficients c_1 and c_3 are also functions of λ. The quantity $c_2(\lambda)$ is equal to $\alpha(\lambda)$ – see section 6.1.1.2.) Figure 6.2 illustrates the spectral dependence of c_1 and c_3 for representative samples of bay water, coastal water, and deep ocean water. The $\alpha(\lambda)$ and $s(\lambda)/a(\lambda)$ ratio data, used in obtaining these curves, is listed in tables 6.2 and 6.3, respectively. Once the spectral dependence of c_1 and c_3 is determined, two approaches can be used to include this information in the system performance analysis. For optical systems with narrowband sources, such as lasers, a separate calculation should be made for each major spectral line, and the results summed to yield the total system response. For systems with broadband sources, the spectral information should be condensed to an effective spectral bandwidth, $\Delta\lambda = \lambda_2 - \lambda_1$, and a wavelength λ_0 where the transmission of light is maximum.

For signal or image-forming light, $\lambda_0(S)$ is obtained by determining the minimum of $\beta_1(\lambda) = c_1(\lambda) + \alpha(\lambda)$; for the noise or nonimage-forming light, $\lambda_0(N)$ is obtained by finding the minimum of $\beta_2(\lambda) = c_1(\lambda) + c_3(\lambda)$. The effective spectral bandwidth of image-forming light is defined so that

$$\exp[-R\{\beta_1(\lambda_1(S)) - \beta_1(\lambda_0(S))\}] = \exp[-R\{\beta_1(\lambda_2(S)) - \beta_1(\lambda_0(S))\}] = 0.5. \tag{6.6}$$

Similarly, the effective spectral bandwidth of backscattered light is defined so that

$$\exp[-R\{\beta_2(\lambda_1(N)) - \beta_2(\lambda_0(N))\}] = \exp[-R\{\beta_2(\lambda_2(N)) - \beta_2(\lambda_0(N))\}] = 0.5. \tag{6.7}$$

The bandwidths, $\Delta\lambda = \lambda_2 - \lambda_1$, are found by choosing a particular range and solving either equation 6.6 or 6.7 for λ_1 and λ_2. The range R should correspond to the distance between the target and the receiver for the effective spectral bandwidth of light reflected from the target; $R = r_0$ for the backscattered light bandwidth. The parameter r_0 is defined in

section 6.2.1. For the convenience of the user, tables 6.4 and 6.5 present a list of the parameters λ_0, λ_1, and λ_2 for image-forming and backscattered light, respectively.

The effective bandwidth approximation implies that

$$c_1(\lambda) = \begin{cases} c_1(\lambda_0(R)), & \lambda_1(R) \leqslant \lambda \leqslant \lambda_2(R) \\ \infty & \text{otherwise} \end{cases} \tag{6.8}$$

and

$$c_3(\lambda) = \begin{cases} c_3(\lambda_0(r_0)), & \lambda_1(r_0) \leqslant \lambda \leqslant \lambda_2(r_0) \\ \infty & \text{otherwise} \end{cases} \tag{6.9}$$

This approximation permits equations which require integration over spectral variables to be simplified to a single algebraic term.

6.2 CONVENTIONAL IMAGING SYSTEMS

Three sets of equations for evaluating the performance of conventional imaging systems are developed in this section. These equations are the result of coupling the light-propagation model (described in section 6.1) to idealized, analytical representations of a light source, target, and television receiver. The general characteristics of conventional imaging systems are presented in section 3. Conventional systems differ from extended-range imaging systems because they do not use special components to reduce the backscattered light in the image. The effects of backscatter can be reduced in conventional imaging systems by using large source-receiver separations and narrow source beams and receiver fields-of-view.

The first set of equations is used to calculate the signal and noise photocurrents generated by the receiver. The signal photocurrent is due to the image-forming light reflected from the target, and the noise photocurrent is due to nonimage-forming backscattered light. This set of equations is valid for conventional, wide bandwidth light sources, such as an incandescent lamp or a mercury-vapor (Hg) arc lamp, and includes the parameters which describe the spectral characteristics of these light sources. The second set of equations, which is similar to the first set except that the equations are written for lasers or other narrow bandwidth sources of light, contains the parameters which describe the amount of radiant power produced by the laser at each of its spectral lines. The different parameters for the two sets of equations are chosen to correspond to the data which is most available for the different types of sources. To facilitate hand calculations, the logarithm is taken of both sets to obtain complementary sets of decibel equations which are similar to the "sonar equation" of underwater acoustics. These equations and their decibel counterparts are simplifications and approximations of the third set of equations. This final set is derived in reference 6.1, and computer programs have been developed for their solution.

The light source is represented in these system performance equations by the specification of its beam pattern and spectral characteristics. The spectral characteristics of the 3400 °K

tungsten incandescent, mercury (Hg) arc, thallium-iodide-doped mercury (TlI Hg) arc, and xenon arc light sources are in figure 6.3 and table 6.6 Table 6.6 also includes the major spectral lines of the argon, xenon, and neodymium yttrium-aluminum-garnet (YAG) lasers. The beam pattern of the source is reduced to an "equivalent" conical beam pattern. If $J(\theta_1, \phi)$ is the actual radiant intensity of the source (the amount of power per unit solid angle emitted in the direction specified by the polar angle θ and the azimuthal angle ϕ with respect to the optical axis of the source), then the half-angle θ_1 of the "equivalent" conical beam pattern is given by

$$\theta_1 = \cos^{-1}\left\{1 - \frac{1}{2\pi J(0, \phi)} \int_0^{2\pi} \int_0^{\pi} J(\theta, \phi) \sin\theta \, d\theta \, d\phi\right\}. \tag{6.10}$$

When the beam pattern has a sharply defined edge, a good approximation for θ_1 is the half-power angle, i.e., if $J(\theta_{1/2}) = 1/2\, J(0)$, then $\theta_1 = \theta_{1/2}$.

The target is represented by the specification of its inherent contrast which is defined as

$$C_0 = \frac{\rho_2 - \rho_1}{\rho_2}, \tag{6.11}$$

where ρ_2 is the reflectance of the brighter gray level and ρ_1 corresponds to the darker level.

The television receiver is represented by the specification of its field-of-view and depth-of-field, the f/ and transmission coefficient of its optics, its spectral response, and its signal response curves. The signal response curves provide the relationship of the photocurrent level, image contrast, and noise-limited resolution for the various types of television cameras which might be used in conventional underwater imaging systems. Signal response curves are shown in figure 6.4. Included are the vidicon coupled to three image intensifiers (I^3-V); secondary electron conduction with and without a coupled image intensifier (I-SEC and SEC, respectively); the image orithicon (IO); the image isocon with and without a coupled image intensifier (III and II, respectively); and silicon-electron-bombardment-induced-response television camera systems (SEBIR). These curves were calculated by F. A. Rosell (ref. 6.5). (The signal response curves for the nonintensified vidicon were not included because of the lag characteristic of this tube. By the time that image irradiance, or photoelectron current, is increased to make the lag acceptable for imaging scenes in motion, the full-resolving capability of the vidicon is realized (ref. 6.5). The designer should use the method described in section 6.4.3 to estimate the performance of systems using nonintensified vidicons.) The spectral sensitivities of the Type II (antimony trisulfide) and Type V (silicon diode) photoconductors and the S-20 (multialkali) photocathode are in figure 6.5 and table 6.7. The Type II and Type V photoconductors are used in vidicon camera tubes, and the S-20 photocathode should be used in image intensifiers and the SEC, IO, II, and SEBIR camera tubes in underwater television systems.

6.2.1 SYSTEM GEOMETRY – To obtain simple equations for the system performance analysis, the symmetrical geometry in figure 6.6 is used to describe the conventional and extended-range imaging systems. The first two sets of signal- and noise-current equations correspond to this simplified geometry. The major restrictions imposed by this geometry are the limitation of image information to the center of the receiver's field-of-view and the use of only one light source. Considerable variation in image contrast and signal level across the receiver's field-of-view can occur in underwater imaging systems (see ref. 6.1).

6.2.1.1 Definition and Units of the Geometrical Parameters

d: source-receiver separation (m).

R: perpendicular distance from the source-receiver plane to the target element (m).

ζ_1: distance from the source to the target element (m),

$$\zeta_1 = R/\cos(\delta_s). \tag{6.12}$$

ζ_2: distance from the target element to the receiver (m),

$$\zeta_1 = R/\cos(\delta_R) = \zeta_2. \tag{6.13}$$

θ_1: half-angle of the "equivalent" conical beam pattern of the source (deg).

θ_3: half-angle of the receiver's field-of-view (deg).

δ_s: orientation angle of the optical axis of the source (deg),

$$\delta_s = \tan^{-1}\left(\frac{d}{2R}\right). \tag{6.14}$$

δ_R: orientation angle of the optical axis of the receiver (deg),

$$\delta_R = -\tan^{-1}\left(\frac{d}{2R}\right). \tag{6.15}$$

r_0: perpendicular distance from the source-receiver plane to the backscatter volume (m),

$$r_0 = \frac{d}{\left(\frac{d}{2R}\right) + \tan(\delta_s + \theta_1)}. \tag{6.16}$$

The dependence of the ratio r_0/R on the ratio d/R is illustrated in figure 6.7 for different values of θ_1.

6.2.1.2 General Geometry – A more general geometry, which permits the calculation of image information across the field-of-view, is shown in figure 6.8. The third set of signal- and noise-current equations corresponds to this geometry, which also permits systems with more than one light source to be evaluated. In this system, the signal and noise photocurrents produced by the receiver for each light source are added to obtain the total signal and noise photocurrents. The coupling of the independent variables in these equations, however,

makes the separation of these input variables into a "sonar type" decibel equation impossible.

6.2.2 SIGNAL-CURRENT EQUATIONS – The signal photocurrent is given by

$$i_s = A_0 \int_{400}^{700} h_s(\lambda)\, S(\lambda)\, d\lambda\,, \tag{6.17}$$

where $h_s(\lambda)$ is the spectral density of the signal irradiance in the image ($W/m^2 \cdot nm$); A_0 is the image format area (m^2); and $S(\lambda)$ is the sensitivity (A/W) of the television camera tube.

6.2.2.1 Signal-Equation Set 1 – The effective bandwidth approximation for conventional broadband sources reduces equation 6.17 to

$$i_s = A_0\, \tilde{h}_s(\mathrm{CON})\, \left[G(\lambda_2(S)) - G(\lambda_1(S)) \right]. \tag{6.18}$$

For the simplified geometry, the function $\tilde{h}_s(\mathrm{CON})$* is given by

$$\tilde{h}_s(\mathrm{CON}) = \rho_2 \cdot w \cdot (\tau/f/^2) \cdot \frac{4\pi}{2\pi(1-\cos\theta_1)} \cdot \frac{9}{256\pi R^2} \cdot \exp(-\alpha g_1 R), \tag{6.19}$$

where

ρ_2 is the reflectance of the brighter gray level in the target,

w is the electrical input power to the source (W),

τ is the transmission coefficient of the receiver's optics,

f/ is the f number of the receiver's optics,

θ_1 is the half-angle of the "equivalent" conical beam pattern of the source, see equation 6.10 (deg),

$\alpha = \alpha(\lambda_0)$ is the total attenuation coefficient (ln/m),

$$g_1 = \left\{ 1 + c_1/\alpha \right\}/\cos(\delta_s),\ ^{**} \tag{6.20}$$

and

R is the perpendicular distance from the source-receiver plane to the target element (m).

**The symbol CON refers to the conventional imaging system. The symbols PD, RG, and VS (used later in this section) refer to the polarization-discrimination, range-gating, and volume-scanning imaging systems, respectively.*

***Values for c_1/α are in table 6.1 for various values of θ_1 and the s/a ratio at $\lambda = \lambda_0(S)$. Table 6.3 furnishes values for the s/a ratio for different wavelengths.*

The function $G(\lambda)$ is given by

$$G(\lambda) = \int_{400}^{\lambda} E(\lambda)\, S(\lambda)\, d\lambda, \tag{6.21}$$

where

$E(\lambda)\, d\lambda$ is the amount of radiant output power in the bandwidth $d\lambda$ per watt of input electrical power to the source (see table 6.6)

and

$S(\lambda)$ is the sensitivity of the television camera tube (A/W) (see table 6.7).

Table 6.8 is a compilation of $G(\lambda)$ for the 12 combinations of the four conventional light sources – incandescent, mercury arc, thallium-iodide-doped mercury arc, and xenon arc – and the three types of photosensitive surfaces used in camera tubes – S-20 photocathode and Type II and Type V photoconductors.

Taking the logarithm of equation 6.19 and multiplying the resulting terms by 10 converts this equation into the decibel format:

$$H_s\,(CON) = TR + W + L + D + R_1 + R_2 - 19.51, \tag{6.22}$$

where

$$H_s(CON) = 10 \log (\tilde{h}_s\,(CON)), \tag{6.23}$$

$$TR = 10 \log (\rho_2), \tag{6.24}$$

$$W = 10 \log (w), \tag{6.25}$$

$$L = 10 \log (\tau/f/^2), \tag{6.26}$$

$$D = 10 \log \left(\frac{4\pi}{2\pi\,(1-\cos\theta_1)} \right),^{*} \tag{6.27}$$

$$R_1 = 10 \log \left(\frac{1}{R^2} \right) = -20 \log R, \tag{6.28}$$

and

$$R_2 = 10 \log (\exp(-\alpha R g_1)) = -4.34(\alpha g_1 R). \tag{6.29}$$

**The variation of D with θ_1 is shown in figure 6.9.*

6.2.2.2 Signal-Equation Set 2 – Equation 6.17 can be reduced to a sum over spectral lines for laser-illumination sources:

$$i_s = A_0 \sum_{i=1}^{N} h'_s (CON, \lambda_i) S(\lambda_i). \tag{6.30}$$

The signal irradiance at $\lambda = \lambda_i$ for the simplified geometry is given by

$$h'_s (CON, \lambda_i) = \rho_2 \cdot w_R \cdot (\tau/f/^2) \cdot \frac{4\pi}{2\pi(1-\cos\theta_1)} \cdot \frac{9}{256\pi R^2} \cdot \exp(-\alpha g_1 R), \tag{6.31}$$

where $w_R(\lambda_i)$ is the average radiant output power produced by the laser source at the wavelength λ_i. Relative values of $w_R(\lambda_i)$ are given in table 6.6 for common laser sources. The corresponding decibel equation is given by

$$H'_s(\lambda_i) = TR + WR + L + D + R_1 + R_2 - 19.51, \tag{6.32}$$

where

$$WR = 10 \log (w_R(\lambda_i)). \tag{6.33}$$

The other parameters have been previously defined, and can be found in the glossary (section 6.5.1).

6.2.2.3 Signal-Equation Set 3 – For the general geometry, the spectral density of the signal irradiance is given by

$$h_s(\lambda) = \frac{9\tau\rho_2 J(\theta) e^{-[c_1(\lambda)\zeta_1 + c_2(\lambda)\zeta_2]} \cos(\delta_s + \theta) \cos^4(\psi)}{64 f/^2 \zeta_1^2}. \tag{6.34}$$

The geometrical factors – ζ_1, ζ_2, ψ, δ_s, and θ – are indicated in figure 6.8.

6.2.3 NOISE-CURRENT EQUATIONS – The noise photocurrent due to backscattered light is given by

$$i_n = A_0 \int_{400}^{700} h_n(\lambda) S(\lambda) d\lambda, \tag{6.35}$$

where $h_n(\lambda)$ is the spectral density of the noise irradiance in the image.

6.2.3.1 Noise-Equation Set 1 – The effective bandwidth approximation for conventional broadband source reduces equation 6.35 to

$$i_n = A_0 \tilde{h}_n (CON) [G(\lambda_2(N)) - G(\lambda_1(N))]. \tag{6.36}$$

The function $\tilde{h}_n$ (CON) for the simplified geometry is given by

$$\tilde{h}_n\,(\mathrm{CON}) = \eta s \cdot w \cdot (\tau/f/^2) \cdot \frac{4\pi}{2\pi(1-\cos\theta_1)} \cdot \frac{9}{512\pi} \cdot$$

$$\left[\frac{1}{r_0} E_2\,(\alpha g_3 r_0) - \frac{1}{R} E_2\,(\alpha g_3 R) \right], \tag{6.37}$$

where

$s = s\,(\lambda_0(N))$ is a scattering coefficient for seawater (ln/m),

η is the fraction of s which represents the light scattered into the back hemisphere, i.e.,

$$\eta = \frac{2\pi}{s} \int_{\pi/2}^{\pi} \sigma(\theta) \sin\theta d\theta, \tag{6.38}$$

w is the electrical input power to the source (W),

τ is the transmission coefficient of the receiver's optics,

f/ is the receiver's f number,

θ_1 is the half-angle of the "equivalent" conical beam pattern (deg),

r_0 is the distance from the receiver to the volume that is common to both the beam pattern of the source and the field-of-view of the receiver (see fig. 6.6), (m),

R is the distance from the receiver to the target (m),

$\alpha = \alpha\,(\lambda_0)$ is a total attenuation coefficient for seawater (ln/m),

$$g_3 = \frac{1}{\cos(\delta_s)} \left\{ \frac{c_1}{\alpha} + \frac{c_3}{\alpha} \right\}^{*}, \tag{6.39}$$

$\delta_s = \tan^{-1}(d/2R)$ (d is the source-receiver separation),

and

$$E_2(x) = \int_1^{\infty} \frac{e^{-xt}}{t^2} dt \tag{6.40}$$

is the exponential integral of order 2.**

Values for c_1/α and c_3/α are in table 6.1 for various values of θ_1 and θ_3 and the s/a ratio at $\lambda = \lambda_0$. Table 6.3 furnishes values for the s/a ratio for different wavelengths.

***Values for $E_2(x)$ are compiled in table 6.9.*

The decibel equation corresponding to equation 6.37 is given by

$$H_n\,(CON) = BS + W + L + D + R_3 - 22.51, \tag{6.41}$$

where

$$H_n\,(CON) = 10 \log (\widetilde{h}_n\,(CON)), \tag{6.42}$$

$$BS = 10 \log (\eta s). \tag{6.43}$$

and

$$R_3 = 10 \log \left\{ \frac{1}{r_0} E_2\,(\alpha g_3 r_0) - \frac{1}{R} E_2\,(\alpha g_3 R) \right\}. \tag{6.44}$$

The other parameters have been defined previously, and can be found in the glossary (section 6.5.1).

6.2.3.2 Noise-Equation Set 2 – Equation 6.35 can be reduced to a sum over spectral lines for laser-illumination sources:

$$i_n = A_0 \sum_{i=1}^{N} h'_n\,(CON, \lambda_i)\, S\,(\lambda_i). \tag{6.45}$$

For the simplified geometry in figure 6.6, the approximate image irradiance caused by back-scatter is given by

$$h'_n\,(CON, \lambda_i) = \eta s \cdot w_R \cdot \tau / f/^2 \cdot \frac{4\pi}{2\pi\,(1\text{-}\cos\theta_1)} \cdot \frac{9}{512\pi} \cdot$$

$$\left\{ \frac{1}{r_0} E_2\,(\alpha g_3 r_0) - \frac{1}{R} E_2\,(\alpha g_3 R) \right\}. \tag{6.46}$$

Again, $w_R(\lambda_i)$ is the average radiant output power produced by the laser source at the wavelength λ_i. The corresponding decibel equation is given by

$$H'_n\,(CON) = BS + WR + L + D + R_3 - 22.51. \tag{6.47}$$

6.2.3.3 Noise-Equation Set 3 – For the general geometry, the spectral density of the noise irradiance is given by

$$h_n(\lambda) = \frac{9\pi \cos^4(\psi)\,\tau}{64\, f/^2 \cos(\delta_R + \psi)} \int_{r_0}^{R} \frac{\sigma\,(\pi\text{-}\gamma)\, J(\theta)\, e^{-(c_1\zeta_1 + c_3\zeta_2)}\, dr}{\zeta_1^{\,2}}. \tag{6.48}$$

The geometrical factors – $\zeta_1, \zeta_2, \psi, \delta_R, \theta, \gamma, r_0$, and R – are illustrated in figures 6.8 and 6.10.

6.2.3.4 Approximations – Several approximations were made in the evaluation of the noise-current equations.

To simplify the integral in equation 6.48 to obtain equations 6.37 and 6.46, the approximation,

$$\zeta_1 \cong \zeta_2 = r/\cos(\delta_R), \tag{6.49}$$

was required. Evaluation of the geometry in figure 6.10 indicates that

$$\zeta_1 = \zeta_2 \left\{1 + \left(\frac{d}{\zeta_2}\right)^2 \left(\frac{R-r}{R}\right)\right\}^{1/2} \tag{6.50}$$

and

$$\zeta_2\,(\min) = \frac{r_0}{\cos(\delta_R)} = r_0 \left(1 + \frac{d^2}{4R^2}\right)^{1/2}. \tag{6.51}$$

Thus, for the approximation in equation 6.49 and resulting simplification of equation 6.48 to be valid,

$$d \leqslant \frac{r_0}{2} \quad \text{or} \quad d \leqslant R\,(1\text{-}2\tan(\delta_s + \theta_1)). \tag{6.52}$$

The use of the effective attenuation coefficient c_3 requires a fundamental approximation because c_3 describes the attenuation of the total light flux from a point source which is accepted through the field-of-view of the receiver. Thus, when c_3 is used to calculate the light flux incident on the entrance pupil of the receiver, not all of the light is focused at the image of the point source. Figure 6.11 illustrates the situation when the "point source" is an infinitesimal volume element of seawater which contributes to the backscattered light. The rays of backscattered light from dV, which undergo additional scatterings, will be focused at different points in the image. By considering the region surrounding dV, however, an argument can be made that light scattered out of the image of dV is compensated for by light which is scattered out of the image of the surrounding region and into the image of dV, i.e., the probability that ray A_2 will be scattered near point P in the direction of ray A_1 is nearly the same as the probability that ray A_1 will be scattered near point P in the direction of ray A_2. The probabilities would be exactly the same if the volumes dV_1 and dV_2 were equally illuminated. Because the region surrounding dV is not generally uniformly illuminated, a certain degree of error is introduced by assuming exact compensation. The magnitude of this error is difficult to estimate analytically, and experimental measurements should be performed to test the validity of this approximation.

Another approximation involves the use of the coefficient c_1 to calculate the light flux incident on the backscatter volume element or the target resolution element. This approximation occurs because all incident light rays do not arrive from the same direction. For this approximation to yield negligible error, the target should be Lambertian and the volume scattering function should be nearly isotropic for 90 deg $\leqslant \theta \leqslant$ 180 deg. Most volume

scattering functions for seawater appear to satisfy this requirement (ref. 6.6). This nearly isotropic behavior of the volume scattering function for backscattered light was assumed in the simplification of the integral in equation 6.48 to obtain equations 6.37 and 6.46. The volume scattering function was assumed to be equal to

$$\sigma(\theta) = \eta \frac{s}{2\pi}, \; 90 \text{ deg} \leqslant \theta \leqslant 180 \text{ deg}, \tag{6.53}$$

where η is defined by equation 6.38 and s is the scattering coefficient.

For systems which have a narrow source beam pattern, the most questionable approximation is the use of the half-angle θ_1 of the "equivalent" conical beam pattern in equation 6.16 to determine r_0, the lower limit of the integral in equation 6.48. The scattering of light by seawater significantly spreads the narrow geometrical beam pattern. Although the divergence of the beam pattern can be determined by the Monte Carlo simulation, it is difficult to include this information in the simple equations used for the system performance analysis.

6.3 EXTENDED-RANGE IMAGING SYSTEMS

Three sets of equations are developed in this section for evaluating the performance of each of the three general classes of extended-range imaging systems – polarization discrimination, range gating, and volume scanning. These equations are the result of coupling the light-propagation model (described in section 6.1) to idealized, analytical representations of a light source, target, television camera, and the specialized equipment used for reducing the amount of received backscattered light. Signal and noise photocurrents are calculated in each set of equations. The first set of equations is valid for conventional, wide bandwidth light sources, and the second set is written for lasers or narrow bandwidth light sources. To facilitate hand calculations, the logarithm is taken of both sets of equations to obtain complementary sets of decibel equations which are similar to the "sonar equation" of underwater acoustics. These first two sets of equations are simplifications and approximations of the third set of equations. This final set of more complex equations is derived in reference 6.1, and computer programs have been developed for their solution.

6.3.1 POLARIZATION DISCRIMINATION – The polarization-discrimination system uses the polarization differences between backscattered light and light reflected from a diffuse target to enhance underwater visibility. When a polarized light source is used, much of the backscattered light will retain its polarization and can be blocked with a polarization analyzer placed in front of the receiver. Light reflected from the target is generally depolarized.

The analytical models for the light source, target, and television camera for the polarization-discrimination system are the same as the models described for the conventional imaging system in section 6.2. The polarizer placed on the source and the analyzer placed on the receiver are modeled by the efficiency factors e_1 and e_2. The geometry for the polarization-discrimination system is illustrated in figure 6.6.

6.3.1.1 Signal-Current Equations – The signal photocurrent for a polarization-discrimination system has the same form as equation 6.17,

$$i_s = A_0 \int_{400}^{700} h_s(\lambda)\, S(\lambda)\, d\lambda \,. \tag{6.17}$$

The effective bandwidth approximation reduces equation 6.17 to

$$i_s = A_0\, \tilde{h}_s(PD)\, [G(\lambda_2(S)) - G(\lambda_1(S))] \,. \tag{6.54}$$

For the simplified geometry in figure 6.6, the function $\tilde{h}_s(PD)$ is given by

$$\tilde{h}_s(PD) = e_1\, e_2\, (1 - \psi_s) \cdot \rho_2 \cdot w \cdot (\tau/f/^2) \cdot \frac{4\pi}{2\pi(1-\cos\theta_1)} \cdot \frac{9}{256\,\pi R^2} \cdot \exp(-\alpha g_1 R) \,, \tag{6.55}$$

where

e_1 is the ratio of the radiant power transmitted by the polarizer to the incident radiant power in the source beam,

e_2 is the ratio of the radiant power transmitted by the analyzer to the power of the incident unpolarized light (the analyzer is adjusted to block the polarized backscattered light),

$$\psi_s = w_p/w_t \tag{6.56}$$

is the polarization coefficient of the light reflected from the target (w_p is the polarized, reflected power which is incident on the analyzer, and w_t is the total reflected power which is incident on the analyzer),

and

the other parameters – ρ_2, w, τ, f/, θ_1, R, $\alpha(\lambda_0)$, and $g_1(\lambda_0)$ – are as defined for equation 6.19.

Taking the logarithm of equation 6.55 and multiplying the resulting terms by 10 converts this equation to the decibel format:

$$H_s(PD) = EPS + TR + W + L + D + R_1 + R_2 - 19.51 \,, \tag{6.57}$$

where

$$H_s(PD) = 10 \log(\tilde{h}_s(PD)), \tag{6.58}$$

$$EPS = 10 \log(e_1\, e_2\, (1 - \psi_s)) \,, \tag{6.59}$$

and

TR, W, L, D, R_1, and R_2, previously defined, can be found in the glossary (section 6.5.1).

Equation 6.17 is reduced to a sum over spectral lines for laser-illumination sources:

$$i_s = A_0 \sum_{i=1}^{N} h'_s (PD, \lambda_i) S(\lambda_i) . \tag{6.60}$$

The image irradiance for the simplified geometry is given by

$$h'_s (PD, \lambda_i) = e_1 e_2 (1-\psi_s) \cdot \rho_2 \cdot w_R \cdot (\tau/f/^2) \cdot \frac{4\pi}{2\pi (1-\cos\theta_1)} \cdot$$

$$\frac{9}{256\,\pi R^2} \cdot \exp(-\alpha g_1 R). \tag{6.61}$$

The corresponding decibel equation is given by

$$H'_s (PD) = EPS + TR + WR + L + D + R_1 + R_2 - 19.51 . \tag{6.62}$$

For the general geometry of figure 6.8, the spectral density of the signal irradiance is given by

$$h_s (\lambda) = \frac{9 e_1 e_2 (1-\psi_s) \tau \rho_2 J(\theta) e^{-(c_1 \zeta_1 + c_2 \zeta_2)} \cos(\delta_s + \theta) \cos^4(\psi)}{64\, f/^2 \zeta_1{}^2}. \tag{6.63}$$

With the exception of e_1, e_2, and ψ_s, the parameters are identical to those of equation 6.34.

6.3.1.2 Noise-Current Equations – The noise photocurrent due to backscattered light has the same form as equation 6.35:

$$i_n = A_0 \int_{400}^{700} h_n (\lambda) S(\lambda)\, d\lambda . \tag{6.35}$$

The effective bandwidth approximation reduces equation 6.35 to

$$i_n = A_0 \tilde{h}_n (PD) [G(\lambda_2 (N)) - G(\lambda_1 (N))] . \tag{6.64}$$

The function $\tilde{h}_n$ (PD) for the simplified geometry is given by

$$\tilde{h}_n\,(PD) = e_1\, e_2\, (1-\psi_b) \cdot \eta s \cdot w \cdot (\tau/f/^2) \cdot \frac{4\pi}{2\pi\,(1-\cos\theta_1)} \cdot \frac{9}{512\,\pi} \cdot$$

$$\left[\frac{1}{r_0} E_2\,(\alpha g_3\, r_0) - \frac{1}{R} E_2\,(\alpha g_3\, R)\right] , \qquad (6.65)$$

where

e_1 and e_2 are as defined for equation 6.55,

ψ_b is the polarization coefficient for backscattered light ,

and

the other parameters are defined as in equation 6.37.

Taking the logarithm of equation 6.56 and multiplying the resulting term by 10 converts this equation to the decibel format:

$$H_n\,(PD) = EPB + BS + W + L + D + R_3 - 22.51 , \qquad (6.66)$$

where

$$H_n\,(PD) = 10 \log (\tilde{h}_n\,(PD)) , \qquad (6.67)$$

$$EPB = 10 \log (e_1\, e_2\, (1-\psi_b)) , \qquad (6.68)$$

and

BS, W, L, D, and R_3, previously defined, are referenced in section 6.5.1.

Equation 6.35 is reduced to a sum over spectral lines for laser-illumination sources:

$$i_n = A_0 \sum_{i=1}^{N} h'_n\,(PD, \lambda_i)\, S(\lambda_i) . \qquad (6.69)$$

The function h'_n (PD, λ_i) for the simplified geometry is given by

$$h'_n\,(PD, \lambda_i) = e_1\, e_2\, (1-\psi_b) \cdot \eta\, s \cdot w_R \cdot (\tau/f/^2) \cdot \frac{4\pi}{2\pi\,(1-\cos\theta_1)} \cdot$$

$$\frac{9}{512\pi} \cdot \left[\frac{1}{r_0} E_2\,(\alpha g_3\, r_0) - \frac{1}{R} E_2\,(\alpha g_3\, R)\right] . \qquad (6.70)$$

The corresponding decibel equation is given by

$$H'_n(PD) = EPB + BS + WR + L + D + R_3 - 22.51 . \tag{6.71}$$

For the general geometry of figure 6.8, the spectral density of the noise irradiance is given by

$$h_n(\lambda) = \frac{9\, e_1\, e_2\, (1-\psi_b)\, \pi \cos^4(\psi)\, \tau}{64\, f/^2 \cos(\delta_R + \psi)} \int_{r_0}^{R} \frac{\sigma(\pi-\gamma)\, J(\theta)\, e^{-(c_1 \zeta_1 + c_3 \zeta_2)}\, dr}{\zeta_1^{\,2}} . \tag{6.72}$$

With the exception of e_1, e_2, and ψ_b, the parameters are the same as for equation 6.48.

6.3.2 RANGE GATING – In range gating the receiver rejects the backscattered light by gating out all backscattered light except that which is received during the time that the signal pulse is received from the target. The analytical models for the light source, target, and television camera for the range-gating systems are the same as the models described for the conventional imaging system in section 6.2. The electrooptical shutters used to gate the source and receiver are modeled by a square pulse of duration Δt. The geometry for the range-gating system is illustrated in figure 6.6. Pulsed lasers and conventional sources, which are shuttered using either a Pockels cell or Fabry Perot interferometer, can be used for the range-gating source.

6.3.2.1 Signal-Current Equations – The signal photocurrent for a range-gating system has the same form as equation 6.17:

$$i_s = A_0 \int_{400}^{700} h_s(\lambda)\, S(\lambda)\, d\lambda . \tag{6.17}$$

The effective bandwidth approximation reduces equation 6.17 to

$$i_s = A_0\, \tilde{h}_s(RG)\, [G(\lambda_2(S)) - G(\lambda_1(S))] . \tag{6.73}$$

For the simplified geometry in figure 6.6, the function $\tilde{h}_s(RG)$ is given by

$$\tilde{h}_s(RG) = e_3\, e_4 \cdot \rho_2 \cdot w \cdot (\tau/f/^2) \cdot \frac{4\pi}{2\pi(1-\cos\theta_1)} \cdot \frac{9}{256\,\pi R^2} \cdot \exp(-\alpha\, g_1 R) , \tag{6.74}$$

where

e_3 is the time-average transmission coefficient of the electrooptical shutter used to gate the source,

e_4 is the collection efficiency of the projection optics placed on the source to collimate the output radiation,

and

the other parameters are defined as in equation 6.19 except that τ must include the transmission characteristics of the receiver gate during its "open" condition.

The decibel equation corresponding to equation 6.74 is given by

$$H_s(RG) = ES + EC + TR + W + L + D + R_1 + R_2 - 19.51 , \tag{6.75}$$

where

$$H_s(RG) = 10 \log (\tilde{h}_s(RG)) , \tag{6.76}$$

$$ES = 10 \log e_3 , \tag{6.77}$$

$$EC = 10 \log e_4 , \tag{6.78}$$

and

TR, W, L, D, R_1, and R_2, previously defined, are referenced in section 6.5.1.

Equation 6.17 is reduced to a sum over spectral lines for laser-illumination sources:

$$i_s = A_0 \sum_{i=1}^{N} h'_s(RG, \lambda_i)\, S(\lambda_i) . \tag{6.79}$$

The image irradiance for the simplified geometry is given by

$$h'_s(RG, \lambda_i) = \rho_2 \cdot w_R \cdot (\tau/f/^2) \cdot \frac{9}{256\pi R^2} \cdot \exp(-\alpha g_1 R) . \tag{6.80}$$

The corresponding decibel equation is given by

$$H'_s(RG) = TR + WR + L + D + R_1 + R_2 - 19.51 . \tag{6.81}$$

For the general geometry in figure 6.8, the spectral density of the signal irradiance is given by

$$h_s(\lambda) = \frac{9\,\tau\, e_3 \rho_2\, J(\theta) e^{-(c_1(\lambda)\zeta_1 + c_2(\lambda)\zeta_2)} \cos(\delta_s + \theta) \cos^4(\psi)}{64\, f/^2\, \zeta_1{}^2}. \tag{6.82}$$

The parameters, except for e_3, are identical to those in equation 6.34.

6.3.2.2 Noise-Current Equations – The noise photocurrent due to backscattered light has the same form as equation 6.35:

$$i_n = A_0 \int_{400}^{700} h_n(\lambda)\, S(\lambda)\, d\lambda\,. \tag{6.35}$$

The effective bandwidth approximation reduces equation 6.35 to

$$i_n = A_0\, \widetilde{h}_n\,(RG)\ \left[G(\lambda_2(N)) - G(\lambda_1(N))\right]. \tag{6.83}$$

The function $\widetilde{h}_n$ (RG) for the simplified geometry is given by

$$\widetilde{h}_n\,(RG) = e_3 \cdot e_4 \cdot \eta s \cdot w \cdot (\tau/f/^2) \cdot \frac{4\pi}{2\pi(1\text{-}\cos\theta_1)} \cdot \frac{9}{512\pi} \cdot$$

$$\left[\frac{1}{r'_0} E_2\,(\alpha g_3 r'_0) - \frac{1}{R} E_2\,(\alpha g_3 R)\right], \tag{6.84}$$

where

$$r'_0 = \max\,(r_0,\, R - C_w \Delta\, t/2), \tag{6.85}$$

$C_w = 2.25 \times 10^8$ is the speed of light in water (m/sec),

and

the other parameters, previously defined, are referenced in section 6.5.1.

The decibel equation corresponding to equation 6.83 is given by

$$H_n(RG) = ES + EC + BS + W + L + D + R'_3 - 22.51\ , \tag{6.86}$$

where

$$H_n(RG) = 10 \log\,(\widetilde{h}_n\,(RG)), \tag{6.87}$$

$$R'_3 = 10 \log\left[\frac{1}{r'_0} E_2\,(\alpha g_3\, r'_0) - \frac{1}{R} E_2\,(\alpha g_3 R)\right], \tag{6.88}$$

and

ES, EC, BS, W, L, and D, previously defined, are referenced in section 6.5.1.

Equation 6.35 is reduced to a sum over spectral lines for laser-illumination sources:

$$i_n = A_0 \sum_{i=1}^{N} h'_n (RG, \lambda_i) S(\lambda_i) . \tag{6.89}$$

The function $h'_n (RG, \lambda_i)$ for the simplified geometry is given by

$$h'_n (RG, \lambda_i) = \eta s \cdot w_R \cdot (\tau/f/^2) \cdot \frac{4\pi}{2\pi (1-\cos\theta_1)} \cdot \frac{9}{512\pi} \cdot$$

$$\left[\frac{1}{r'_0} E_2 (\alpha g_3 r'_0) - \frac{1}{R} E_2 (\alpha g_3 R) \right] . \tag{6.90}$$

The corresponding decibel equation is given by

$$H'_n (RG) = BS + WR + L + D + R'_3 - 22.51. \tag{6.91}$$

For the general geometry in figure 6.8, the spectral density of the noise irradiance for a range-gating system is given by

$$h_n(\lambda) = \frac{9\pi \cos^4 (\psi) \tau e_3}{64 f/^2 \cos (\delta_R + \psi)} \int_{r'_0}^{R} \frac{R-r}{R-r'_0} \frac{\sigma (\pi-\gamma) J(\theta) e^{-(c_1\zeta_1 + c_3\zeta_2)} dr}{\zeta_1^{\,2}} . \tag{6.92}$$

In the simplification of equation 6.92 to obtain equations 6.84 and 6.90, the factor $R-r/R-r'_0$, in the integrand has been neglected so that the backscatter integral for the range-gating system can be expressed in terms of the exponential integral $E_2(x)$.

6.3.3 VOLUME SCANNING – The technique of volume (or synchronous) scanning allows the receiver to reject backscattered light by making the common volume of the source beam and receiver field-of-view as small as possible and as distant as possible from the receiver. This is accomplished by scanning a well collimated light source over the target. The receiver, which is usually an image-dissector tube, synchronously scans the target with a narrow differential field-of-view. The geometry for the volume-scanning system is illustrated in figure 6.12. The system forms an image by sweeping the target element in a plane that is perpendicular to the plane of the paper. Depth-of-field is an important consideration for volume scanning. As figure 6.12 indicates, the depth-of-field in front of the average viewing range is given by

$$\Delta \simeq \frac{\theta_3 R^2}{d + \theta_3 R} , \tag{6.93}$$

when θ_3 is expressed in rad.

6.3.3.1 Signal-Current Equations – The signal photocurrent for a volume-scanning system is given by

$$i_s = \int_{400}^{700} p_s(\lambda)\, S(\lambda)\, d\lambda, \tag{6.94}$$

where $p_s(\lambda)$ is the spectral density of the power incident on the photocathode of the detector. The effective bandwidth approximation reduces equation 6.94 to

$$i_s = \tilde{p}_s(VS)\left[G(\lambda_2(S)) - G(\lambda_1(S))\right] . \tag{6.95}$$

For the geometry in figure 6.12, the function $\tilde{p}_s(VS)$ is given by

$$\tilde{p}_s(VS) = e_4 \cdot \rho_2 \cdot w \cdot \tau A_e \cdot \frac{9}{16\pi} \cdot \frac{R}{(R^2 + d^2)^{3/2}} \cdot e^{-\alpha g_2 R} , \tag{6.96}$$

where

A_e is the area of the entrance pupil of the optics for the detector,

$$g_2 = \frac{c_1}{\alpha} + \frac{(R^2 + d^2)^{1/2}}{R} \frac{c_3}{\alpha} , \tag{6.97}$$ *

and

the other parameters, previously defined, are referenced in section 6.5.1.

The decibel equation corresponding to equation 6.96 is given by

$$P_s(VS) = EC + TR + W + A + R_4 + R_5 - 7.48 , \tag{6.98}$$

where

$$P_s(VS) = 10 \log(\tilde{p}_s(VS)), \tag{6.99}$$

$$A = 10 \log(\tau A_e) , \tag{6.100}$$

$$R_4 = 10 \log\left[\frac{R}{(R^2 + d^2)^{3/2}}\right], \tag{6.101}$$

$$R_5 = 10 \log\left(e^{-\alpha g_2 R}\right) = -4.34\,(\alpha g_2 R), \tag{6.102}$$

and

EC, TR, and W, previously defined, are referenced in section 6.5.1.

**Values for c_1/α and c_3/α are found in table 6.1 for various values of θ_1 and θ_3 and the s/a ratio for $\lambda = \lambda_0$. The s/a ratios for different wavelengths are found in table 6.10.*

Equation 6.94 is reduced to a sum over spectral lines for laser-illumination sources:

$$i_s = \sum_{i=1}^{N} p'_s (VS, \lambda_i)\, S(\lambda_i) \ . \tag{6.103}$$

The incident signal power at the wavelength λ_i is given by

$$p'_s (VS,\lambda_i) = \rho_2 \cdot w_R \cdot \tau A_e \cdot \frac{9}{16\pi} \cdot \frac{R}{(R^2 + d^2)^{3/2}} \cdot \exp(-\alpha g_2 R) \ . \tag{6.104}$$

The corresponding decibel equation is given by

$$P'_s (VS) = TR + WR + A + R_4 + R_5 - 7.48 \ . \tag{6.105}$$

The spectral density of the signal power is generally given by

$$p_s(\lambda) = \rho_2\, w_R(\lambda)\, \tau A_e \frac{9}{16\pi} \frac{R}{(R^2 + d^2)^{3/2}} \exp(-\alpha g_2 R) \ . \tag{6.106}$$

6.3.3.2 Noise-Current Equations – The noise photocurrent for a volume-scanning system is given by

$$i_n = \int_{400}^{700} p_n(\lambda)\, S(\lambda)\, d\lambda \ , \tag{6.107}$$

where $p_n(\lambda)$ is the spectral density of the power incident on the photocathode of the detector. The effective bandwidth approximation reduces equation 6.107 to

$$i_n = \tilde{p}_n (VS) \left[G(\lambda_2(N)) - G(\lambda_1(N)) \right] \ . \tag{6.108}$$

For the geometry of figure 6.12, the incident function $\tilde{p}_n (VS)$ is given by

$$\tilde{p}_n (VS) = e_4 \cdot \eta s \cdot w \cdot \tau A_e \cdot \frac{9}{32\pi} \cdot \left\{ \frac{1}{r''_0} E_2 (\alpha g_2 r''_0) - \frac{1}{R} E_2 (\alpha g_2 R) \right\}, \tag{6.109}$$

where

$$r''_0 = R - \Delta \quad (\Delta \text{ is given by equation 6.93}) \tag{6.110}$$

and

the other parameters, previously defined, are referenced in section 6.5.1.

The decibel equation corresponding to equation 6.109 is given by

$$P_n (VS) = EC + BS + W + A + R''_3 - 10.48 \ , \tag{6.111}$$

where

$$P_n(VS) = 10 \log (\tilde{p}_n(VS)) \ , \tag{6.112}$$

$$R''_3 = 10 \log \left[\frac{1}{r''_0} E_2(\alpha g_2 r''_0) - \frac{1}{R} E_2(\alpha g_2 R) \right] , \tag{6.113}$$

and

EC, BS, W, and A, previously defined, are referenced in section 6.5.1.

Equation 6.107 is reduced to a sum over spectral lines for laser-illumination sources:

$$i_n = \sum_{i=1}^{N} p'_n(VS, \lambda_i) S(\lambda_i) \ . \tag{6.114}$$

The incident noise power at the wavelength λ_i is given by

$$P'_n(VS, \lambda_i) = \eta s \cdot w_R \cdot \tau A_e \cdot \frac{9}{32\pi} \cdot \left[\frac{1}{r''_0} E_2(\alpha g_2 r''_0) - \frac{1}{R} E_2(\alpha g_2 R) \right] \ . \tag{6.115}$$

The corresponding decibel equation is given by

$$P'_n(VS) = BS + WR + A + R''_3 - 10.48 \ . \tag{6.116}$$

The spectral density of the noise power is generally given by

$$p_n(\lambda) = \frac{9}{16} w_R(\lambda) \tau A_e \frac{R^{1/2}}{(R^2 + d^2)^{1/2}} \int_{R-\Delta}^{R} \frac{\sigma(\pi-\gamma) e^{-(c_1 r + c_3 \sqrt{r^2 + d^2})}}{(r^2 + d^2)} dr . \tag{6.117}$$

6.4 RELATIONSHIP OF PERCEPTION, RESOLUTION, IMAGE CONTRAST, AND PHOTOCURRENT LEVEL

The signal and noise photocurrents for various types of undersea optical viewing systems are used to determine their imaging capabilities. Image contrast, noise-limited resolution,* and photocurrent level are related by the display signal-to-noise ratio of the system (ref. 6.7). This relationship is described for an ideal photon-limited receiver and for real receivers in sections 6.4.1 and 6.4.2, respectively. The signal-response curves (fig. 6.4) for the various receivers are a result of this analysis. The noise-limited resolution of the system can

Noise-limited resolution is the maximum resolution that the system can achieve; it does not include the degradation of image quality due to small-angle scattering and the limitations of the receiver's optics. The point spread function of the combined seawater-receiver optics system must be determined to specify the actual resolution which is present in the display. Under most operating conditions, the degradation of image quality due to small-angle scattering is of minor importance when compared with the other sources of image degradation which are included in the performance analysis described in this section.

be calculated from the signal and noise currents by using these curves. Table 6.10 summarizes the perception capabilities of human observers as a function of the limiting resolution per minimum dimension of the target (ref. 6.8). This data, when combined with the resolution information from the signal-response curves, determines the basic performance of the viewing system.

If only an approximate estimate of system performance is needed by the designer, the information in section 6.4.3 can be used to relate the signal current to an equivalent faceplate illuminance level in footcandles (fc) for a standard 2854 °K incandescent source.

6.4.1 IDEAL RECEIVER – For a photoelectron-noise-limited receiver, the display signal-to-noise ratio is given by (ref. 6.7)

$$SNR_D = \frac{(\dot{n}_2 - \dot{n}_1)\, t}{\left[(\dot{n}_2 + \dot{n}_1)\, t\right]^{1/2}} , \tag{6.118}$$

where $\dot{n}_2$ is the photoelectron rate from a bright area of the image; $\dot{n}_1$ is the photoelectron rate from an adjacent dark area; and t is the sampling or integration time of the human eye. The image contrast is defined by

$$C = \frac{i_2 - i_1}{i_2} = \frac{i_s\,(1-\rho_1/\rho_2)}{i_s + i_n} , \tag{6.119}$$

where

$$i_2 = i_s + i_n \tag{6.120}$$

and

$$i_1 = \frac{\rho_1}{\rho_2}\, i_s + i_n . \tag{6.121}$$

The reflectances ρ_2 and ρ_1 correspond to adjacent bright and dark resolution elements on the target. If N is the number of resolution elements (number of television lines) which can be fitted into a picture height and the picture has a 4 by 3 aspect ratio, the display signal-to-noise ratio can be written as

$$SNR_D = \frac{C}{(2-C)^{1/2}}\, \frac{1}{N} \left[\frac{i_2 t}{(4/3)\, e}\right]^{1/2} \tag{6.122}$$

For a resolution element to be detected by a human observer, SNR_D must exceed some threshold value K. For isolated disks, the value of K has been estimated to be approximately four, while K = 1.2 is sufficient for a bar pattern (ref. 6.7). The limiting resolution* of the receiver is obtained when SNR_D reaches its threshold value K. Using K = 4, the limiting resolution is

Limiting resolution is defined as the number of lines per picture height at which an element subtending one line has a 50 percent probability of detection (ref. 6.7).

$$N_L = \frac{1}{4} \frac{C}{(2-C)^{1/2}} \left[\frac{i_2 t}{(4/3)\, e} \right]^{1/2} . \tag{6.123}$$

Equation 6.123 is plotted in figure 6.13 for seven different contrast values and t = 0.2 sec.

6.4.2 REAL RECEIVERS – Internal noise sources in real receivers degrade the display signal-to-noise ratio so that its value is substantially less than that given by equation 6.122. The principal noises are the thermionic background current of the input photocathode, the fluctuation noise associated with various gain-producing mechanisms within the sensor, and the preamplifier noise. These various noises are normally statistically independent, and they can, therefore, be added in quadrature. In addition to these noise sources, the image is degraded in television camera tubes by the finite apertures of the electron optics, by the fiber-optic image-transfer plates when the camera tube is coupled to an image intensifier, and by the electron scanning beam (ref. 6.7).

For real receivers, SNR_D can be written as

$$SNR_D = \frac{(0.75t)^{1/2}}{N} \frac{C\, i_2\, R_{sq}(N)}{e^{1/2} \left[(2-C)\, i_2 + 2i_3 + 2i_4 \ldots \right]^{1/2}} , \tag{6.124}$$

where $R_{sq}(N)$ is the receiver's square-wave response, and $i_3, i_4, \ldots$, are the various mean-square noise currents referred to the input photosensitive surface. Rosell (ref. 6.5) has evaluated equation 6.124 for a variety of television cameras and image intensifiers. The curves in figure 6.4 are the results of their analysis.

6.4.3 EQUIVALENT FACEPLATE ILLUMINANCE – Often a designer is only interested in an approximate estimate of system performance. This estimate can be obtained by converting the signal and noise currents i_s and i_n into an equivalent faceplate illuminance level (fc) for a standard 2854 °K incandescent source. The typical specifications provided by manufacturers for television camera tubes usually state a faceplate illuminance range for normal operation. The equivalent illuminance is given by

$$E_s = \frac{i_s}{K_i A_0} \tag{6.125}$$

and

$$E_n = \frac{i_n}{K_i A_0} , \tag{6.126}$$

where A_0 is the image format area (m^2), and K_i is a conversion factor between current density and illuminance ($A/m^2 fc$). Specifically,

$$K_i = \frac{j_i}{E} , \tag{6.127}$$

where

$$j_i = \int S_i(\lambda)\, H(\lambda)\, d\lambda \tag{6.128}$$

and

$$E = \frac{680}{10.8} \int V(\lambda)\, H(\lambda)\, d\lambda \ . \tag{6.129}$$

$S_i(\lambda)$ is the sensitivity (A/W) of the *ith* photosensitive surface, $V(\lambda)$ is the photopic luminosity function, and $H(\lambda)$ is the spectral density of irradiance produced by a 2854 °K incandescent source. Values of K_i are compiled in table 6.11.

6.5 SYSTEM PERFORMANCE PROCEDURE

This section describes a method for organizing the previously presented equations, tables, and graphs into a systematic procedure for evaluating viewing system performance. Figure 6.14 is a block diagram which indicates the major steps required for system evaluation. The designer must first identify the problem to be solved, e.g., the calculation of the increase in viewing range provided by a sophisticated and expensive extended-range system when compared with a conventional system in a particular type of seawater. The procedure used to evaluate the performance of candidate designs depends upon which system tradeoffs are important to the designer. In the determination of input parameters, some variables will be assigned fixed values, while a set of values for other parameters must be selected so that the variation of system performance with these parameters can be determined. Once the problem is defined, the procedure normally involves the evaluation of a series of equations which provides the variation of image contrast and limiting resolution with range for each combination of input parameters.

Section 6.5.1 is a glossary of system performance analysis. Section 6.5.2 summarizes the steps which must be taken to use the procedure described in figure 6.14. A complete set of work sheets for performing the calculations according to this procedure is provided in appendix A, and appendix B furnishes numerical examples of the calculations.

6.5.1 GLOSSARY FOR THE SYSTEM PERFORMANCE ANALYSIS

6.5.1.1 Light-Source Characteristics

$E(\lambda)d\lambda$: spectral efficiency of source (radiant output power in the bandwidth $d\lambda$ per watt of input electrical power), see figure 6.3 and table 6.6 (W/W).

w : electrical input power (W).

$w_R(\lambda_i)$: average radiant output power at the wavelength λ_i (W).

$J(\theta,\phi)$: radiant intensity of the light source (W/sr).

θ_1 : half-angle of the equivalent conical beam pattern (deg).

$\theta_{1/2}$: half-power angle of the beam pattern, i.e., $J(\theta_{1/2}) = 1/2\ J(0)$ (deg).

6.5.1.2 Receiver Characteristics

A_0 : image format area on the photosensitive surface (m^2).

A_e : area of the entrance pupil of the optics (m^2).

τ : transmission coefficient of the optics (W/W).

f/ : f number of the optics (m^2/m^2).

θ_3 : half-angle of the field-of-view (deg).

$S(\lambda)$: spectral sensitivity, see figure 6.5 and table 6.7 (A/W).

$G(\lambda)$: combined spectral response for the light source and television camera, see equation 6.21 and table 6.8 (A/W).

6.5.1.3 Extended-Range Equipment Characteristics

e_1 : ratio of the radiant power transmitted by the polarizer to the incident radiant power in the source beam (W/W).

e_2 : ratio of the radiant power transmitted by the analyzer to the radiant power of incident unpolarized light (W/W).

e_3 : average transmission coefficient of the electrooptical shutter used to gate the source in a range-gating system (W/W).

e_4 : collection efficiency of the projection optics used to collimate conventional sources for the range-gating and volume-scanning systems (W/W).

ψ_s : polarization coefficient of the light reflected from the target (W/W).

ψ_b : polarization coefficient of the backscattered light (W/W).

Δt : light pulse and receiver gate duration (sec).

Δ : depth-of-field in front of the average viewing range, see equation 6.93 (m).

6.5.1.4 Target Characteristics

ρ_1 : reflectance of a dark resolution element (W/W).

ρ_2 : reflectance of a bright resolution element (W/W).

6.5.1.5 System Geometry

d : source-receiver separation (m).

R : target range (m).

δ_S : orientation of the source, see equation 6.14 (deg).

δ_R : orientation of the receiver, see equation 6.15 (deg).

r_0 : distance from the receiver to the nearest backscatter volume for the conventional and polarization-discrimination systems, see equation 6.16 and figure 6.7 (m).

r'_0 : nearest backscatter volume distance for the range-gating system, see equation 6.85 (m).

r''_0 : nearest backscatter volume distance for the volume-scanning system, see equation 6.110 (m).

6.5.1.6 Water Characteristics

$\lambda_0(S,N)$: wavelength of maximum transmission (imaging, backscatter) (nm).

$\lambda_1(S,N)$: minimum wavelength in effective spectral bandwidth (imaging, backscatter) (nm).

$\lambda_2(S,N)$: maximum wavelength in effective spectral bandwidth (imaging, backscatter) (nm).

$\alpha(\lambda)$: total attenuation coefficient (ln/m).

$s(\lambda)$: scattering coefficient (ln/m).

$a(\lambda)$: absorption coefficient (ln/m).

$\sigma(\theta)$: volume scattering function (ln/m·sr).

η : fraction of light scattered into the back hemisphere, see equation 6.38 (W/W).

$c_1(\lambda)$: effective attenuation coefficient for illuminating light, see equation 6.2, figures 6.1 and 6.2, and tables 6.1 and 6.12 (1n/m).

$c_2(\lambda)$: effective attenuation coefficient for image-forming light ($c_2(\lambda) = \alpha(\lambda)$) (ln/m).

$c_3(\lambda)$: effective attenuation coefficient for nonimage-forming light, see equation 6.4, figures 6.1 and 6.2, and tables 6.1 and 6.12 (ln/m).

$$g_1(\lambda) = \left\{1 + c_1(\lambda)/\alpha(\lambda)\right\}/\cos(\delta_S).$$

$$g_2(\lambda) = c_1(\lambda)/\alpha(\lambda) + \left\{(R^2 + d^2)^{1/2}/R\right\}\left\{c_3(\lambda)/\alpha(\lambda)\right\}.$$

$$g_3(\lambda) = \left\{c_1(\lambda)/\alpha(\lambda) + c_3(\lambda)/\alpha(\lambda)\right\}/\cos(\delta_S).$$

6.5.1.7 Decibel Equations

Conventional Systems

$$H_s\,(CON) = TR + W + L + D + R_1 + R_2 - 19.51. \tag{6.22}$$

$$H'_s\,(CON) = TR + WR + L + D + R_1 + R_2 - 19.51. \tag{6.32}$$

$$H_n\,(CON) = BS + W + L + D + R_3 - 22.51. \tag{6.41}$$

$$H'_n\,(CON) = BS + WR + L + D + R_3 - 22.51. \tag{6.47}$$

Polarization-Discrimination Systems

$$H_s\,(PD) = EPS + TR + W + L + D + R_1 + R_2 - 19.51. \tag{6.57}$$

$$H'_s\,(PD) = EPS + TR + WR + L + D + R_1 + R_2 - 19.51. \tag{6.62}$$

$$H_n\,(PD) = EPB + BS + W + L + D + R_3 - 22.51. \tag{6.66}$$

$$H'_n\,(PD) = EPB + BS + WR + L + D + R_3 - 22.51. \tag{6.71}$$

Range-Gating Systems

$$H_s\,(RG) = ES + EC + TR + W + L + D + R_1 + R_2 - 19.51. \tag{6.75}$$

$$H'_s\,(RG) = TR + WR + L + D + R_1 + R_2 - 19.51. \tag{6.81}$$

$$H_n\,(RG) = ES + EC + BS + W + L + D + R'_3 - 22.51. \tag{6.86}$$

$$H'_n\,(RG) = BS + WR + L + D + R'_3 - 22.51. \tag{6.91}$$

Volume-Scanning Systems

$$P_s\,(VS) = EC + TR + W + A + R_4 + R_5 - 7.48. \tag{6.98}$$

$$P'_s\,(VS) = TR + WR + A + R_4 + R_5 - 7.48. \tag{6.105}$$

$$P_n\,(VS) = EC + BS + W + A + R''_3 - 10.48. \tag{6.111}$$

$$P'_n\,(VS) = BS + WR + A + R''_3 - 10.48. \tag{6.116}$$

6.5.1.8 Decibel Equation Parameters

$$TR = 10 \log \rho_2. \tag{6.24}$$

$$W = 10 \log w. \tag{6.25}$$

$$L = 10 \log (\tau/f/^2). \tag{6.26}$$

$$D = 10 \log \left\{ 4\pi/2\pi(1\text{-}\cos \theta_1) \right\}, \text{ see figure 6.9.} \tag{6.27}$$

$$R_1 = -20 \log R. \tag{6.28}$$

$$R_2 = -4.34 \left\{ \alpha(\lambda_0)\, g_1(\lambda_0)\, R \right\}. \tag{6.29}$$

$$WR = 10 \log (w_R(\lambda_i)). \tag{6.33}$$

$$BS = 10 \log (\eta s). \tag{6.43}$$

$$R_3 = 10 \log \left\{ \frac{1}{r_0} E_2(\alpha(\lambda_0)\, g_3(\lambda_0)\, r_0) - \frac{1}{R} E_2(\alpha(\lambda_0)\, g_3(\lambda_0)\, R) \right\}. \tag{6.44}$$

$$R'_3 = 10 \log \left\{ \frac{1}{r'_0} E_2(\alpha(\lambda_0)\, g_3(\lambda_0)\, r'_0) - \frac{1}{R} E_2(\alpha(\lambda_0)\, g_3(\lambda_0)\, R) \right\}. \tag{6.88}$$

$$R''_3 = 10 \log \left\{ \frac{1}{r''_0} E_2(\alpha(\lambda_0)\, g_2(\lambda_0)\, r''_0) - \frac{1}{R} E_2(\alpha(\lambda_0)\, g_2(\lambda_0)\, R) \right\}. \tag{6.113}$$

$$EPS = 10 \log \left\{ e_1 e_2 (1-\psi_s) \right\}. \tag{6.59}$$

$$EPB = 10 \log \left\{ e_1 e_2 (1-\psi_b) \right\}. \tag{6.68}$$

$$ES = 10 \log e_3. \tag{6.77}$$

$$EC = 10 \log e_4. \tag{6.78}$$

$$A = 10 \log (\tau A_e). \tag{6.100}$$

$$R_4 = 10 \log \left\{ R/(R^2 + d^2)^{3/2} \right\}. \tag{6.101}$$

$$R_5 = -4.34\, (\alpha(\lambda_0)\, g_2(\lambda_0)\, R). \tag{6.102}$$

6.5.2 COMPUTATIONAL PROCEDURE – The procedure for evaluating the performance of a specified imaging system in a particular type of water can be summarized by the following steps.

Describe the Problem – Identify the type of system (conventional, polarization discrimination, range-gating, or volume scanning). Identify the type of source (conventional or laser). Identify the type of water (bay, coastal, or deep). Identify the ranges of input parameters required to evaluate the desired system tradeoffs. (At least three different target ranges are required to determine the contrast- and power-limited ranges of the system using interpolation and extrapolation procedures.)

Determine input parameters – The work sheets contained in appendix A provide a convenient format for compiling the input parameters required for a calculation. The first set of work sheets is for a system which utilizes a conventional light source, and the assumption of an effective spectral bandwidth is required. The second set of work sheets is for a laser-illuminated system; calculations are made for each of the major spectral lines of the laser. (Adjacent spectral lines can often be grouped together without significant reduction in the accuracy of the calculation. For example, the six spectral lines of an argon laser can be grouped as follows: (5145 Å, 5017 Å) → (5145 Å), (4965 Å, 4880 Å, 4765 Å) → (4880 Å), and (4579 Å) → (4579 Å).) The work sheets also provide references to tables and

figures in this handbook where numerical values for the various input parameters can be determined for representative system components.

Specify the propagation characteristics of the water – A set of effective attenuation coefficients and other optical properties for bay, coastal, and deep ocean water are compiled in table 6.12. These coefficients were determined from experimental measurements of $\alpha(\lambda)$, $a(\lambda)$, and $s(\lambda)$ in these types of water (see section 2.0) and from the analysis presented in section 6.1. If the designer chooses to use his own set of optical properties for the system performance analysis, the following steps should be taken to obtain the input parameters required to fill in the work sheet.

1. Specify the spectral variation of the total attenuation coefficient $\alpha(\lambda)$ and the $s(\lambda)/a(\lambda)$ ratio. (Values for four or five different wavelengths are often sufficient to establish these spectral curves.)
2. Determine $\beta_1(\lambda) = c_1(\lambda) + \alpha(\lambda)$ and $\beta_2(\lambda) = c_1(\lambda) + c_3(\lambda)$ from the information in table 6.1.
3. Evaluate λ_0, λ_1, and λ_2 for both image-forming and backscattered light using equations 6.6 and 6.7.
4. Determine $\alpha(\lambda_0)$, $c_1(\lambda_0)/\alpha(\lambda_0)$; $c_3(\lambda_0)/\alpha(\lambda_0)$; and $s(\lambda_0)$.

Evaluate signal- and noise-photoelectron currents – The work sheets in appendix A provide a convenient format for evaluating the various equations listed in sections 6.2 and 6.3 for predicting system performance. However, a considerable amount of work is required because of the large number of input parameters. If the designer has access to a digital computer, a simple FORTRAN program can be written to evaluate these equations.

Evaluate image contrast, limiting resolution, and human-perception capabilities – The minimum size of an object which a person is capable of perceiving at range R is given by

$$x(\min) = \frac{\pi}{180}\left(\frac{4\theta}{N_L}\right)^{3} R\, n(\min).$$

The limiting resolution N_L is obtained from the signal and backscatter photocurrents and the properties of the receiver as discussed in section 6.4. The parameter n(min) is the number of line pairs required for a given quality of human perception as stated in table 6.10 (ref. 6.8).

Evaluate the equivalent faceplate illuminance of the signal and noise photocurrent using equations 6.125 and 6.126 – This step can be used to replace the previous step if the designer is only interested in an approximate estimate of system performance or if he is using a nonintensified vidicon as the receiver in his system.

6.6 REFERENCES

6.1 Naval Undersea Research and Development Center, NUC TP 273. *Comparison of Advanced Underwater Television Systems*, by S. Bryant, D. Cozen, R. Fugitt, and C. Funk. January 1971.

6.2 Morrison, Robert Eugene. *Studies on the Optical Properties of Seawater at Argus Island in the North Atlantic Ocean and in Long Island and Block Island Sounds.* Ph.D. Dissertation, New York University, New York. June 1967.

6.3 Funk, Clarence John. *Energy Propagation Constraints on Underwater Optical and Acoustical Imaging Systems.* Ph.D. Dissertation, University of California, Los Angeles. June 1972.

6.4 Scripps Institute of Oceanography, SIO Ref. 71-1. *Underwater Lighting by Submerged Lasers and Incandescent Sources*, by S. Q. Duntley. June 1971.

6.5 Rosell, F. A. "Television Camera Tube Performance Data and Calculations," *Photoelectronic Imaging Devices, Vol II.* L. M. Biberman and Sol Nudelman, editors. Plenum Press, New York. 1971.

6.6 Duntley, S. Q. "Light in the Sea," *Journal of the Optical Society of America.* Vol. 53, pp. 214-233. February 1963.

6.7 Rosell, F. A. "The Limiting Resolution of Low-Light-Level Imaging Sensors," *Photoelectronic Imaging Devices, Vol. I,* L. M. Biberman and Sol Nudelman, editors. Plenum Press, New York. 1971.

6.8 Institute for Defense Analysis Study S254. "Analytical Description of Night Vision Devices," by J. Johnson. *Proceedings of the Seminar on Direct-Viewing Electro-Optical Aids to Night Vision,* L. M. Biberman, editor. October 1966.

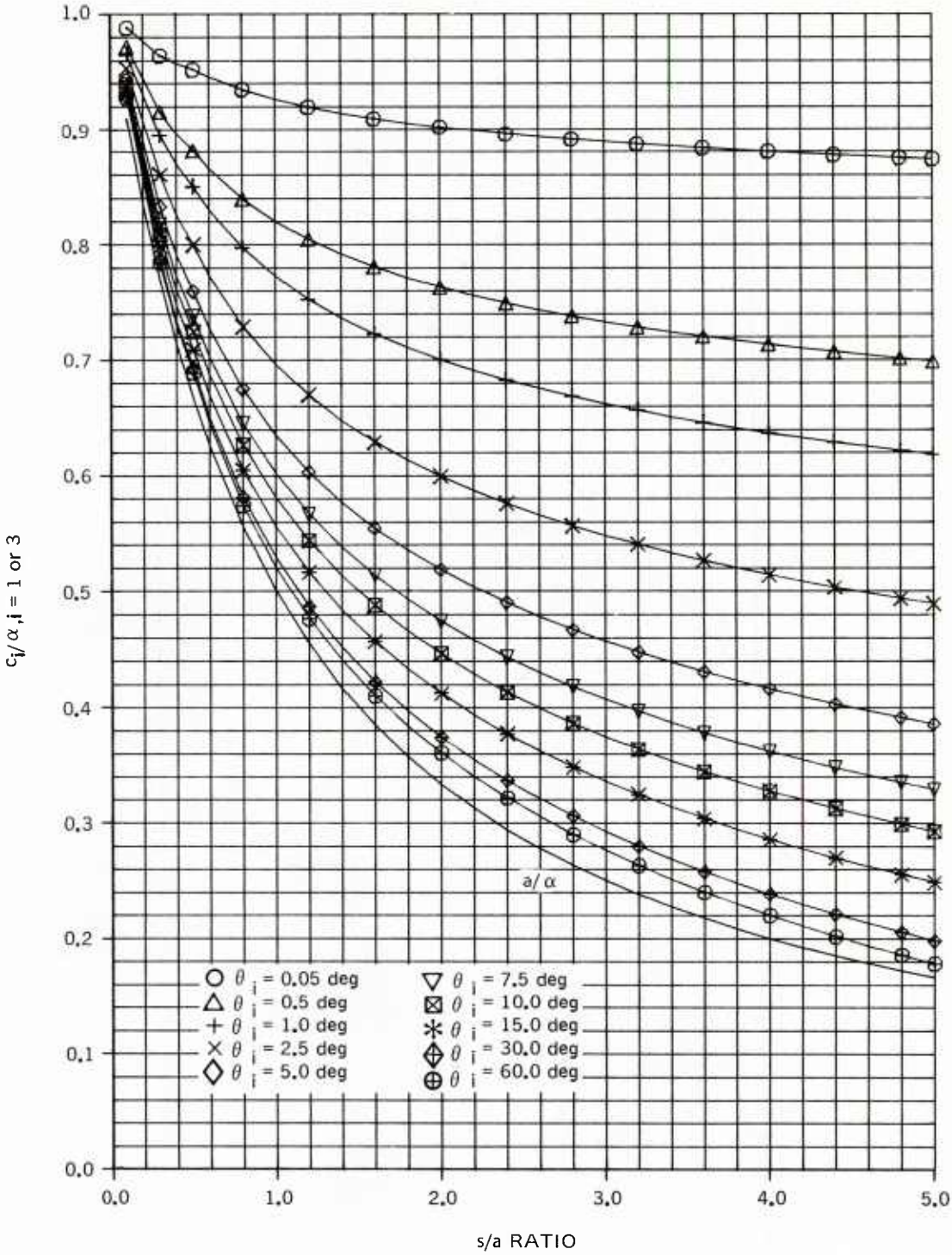

Figure 6.1. Variation of c_i/α with θ_i, i = 1 or 3, and the s/a ratio (Morrison volume scattering function, conical beam pattern or field-of-view).

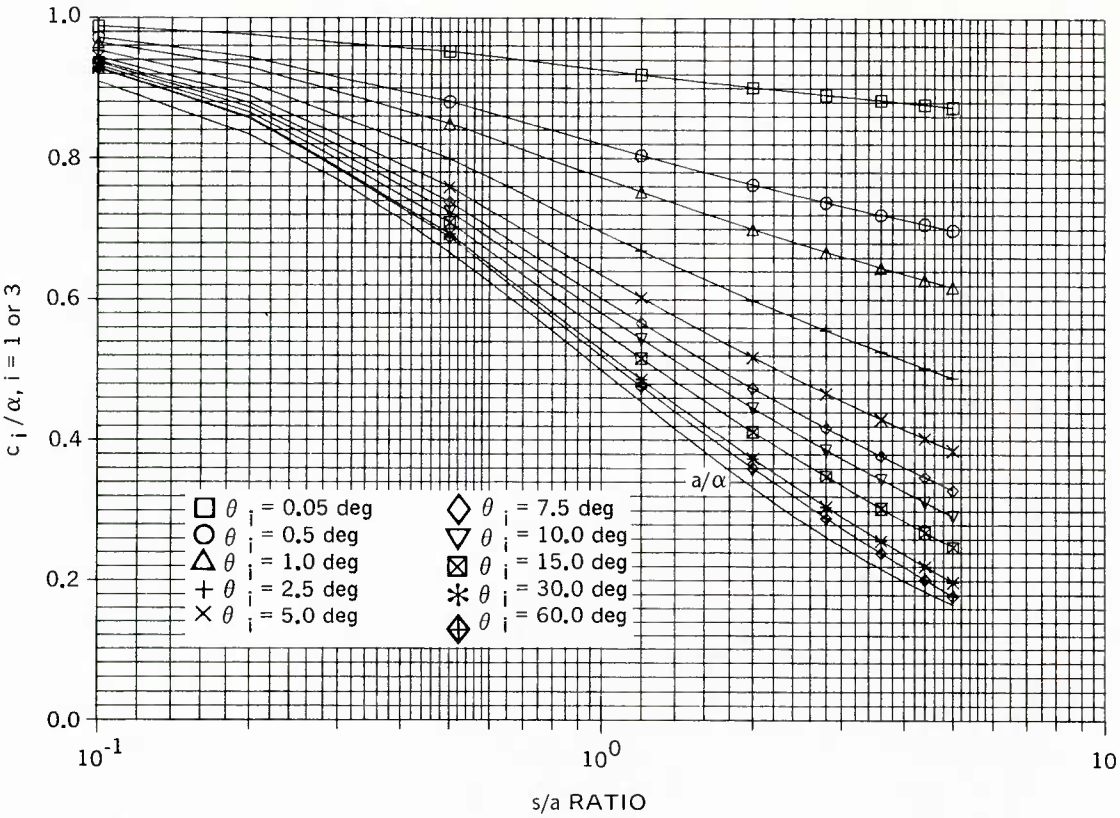

Figure 6.1. (Continued)

Part A. Bay water.

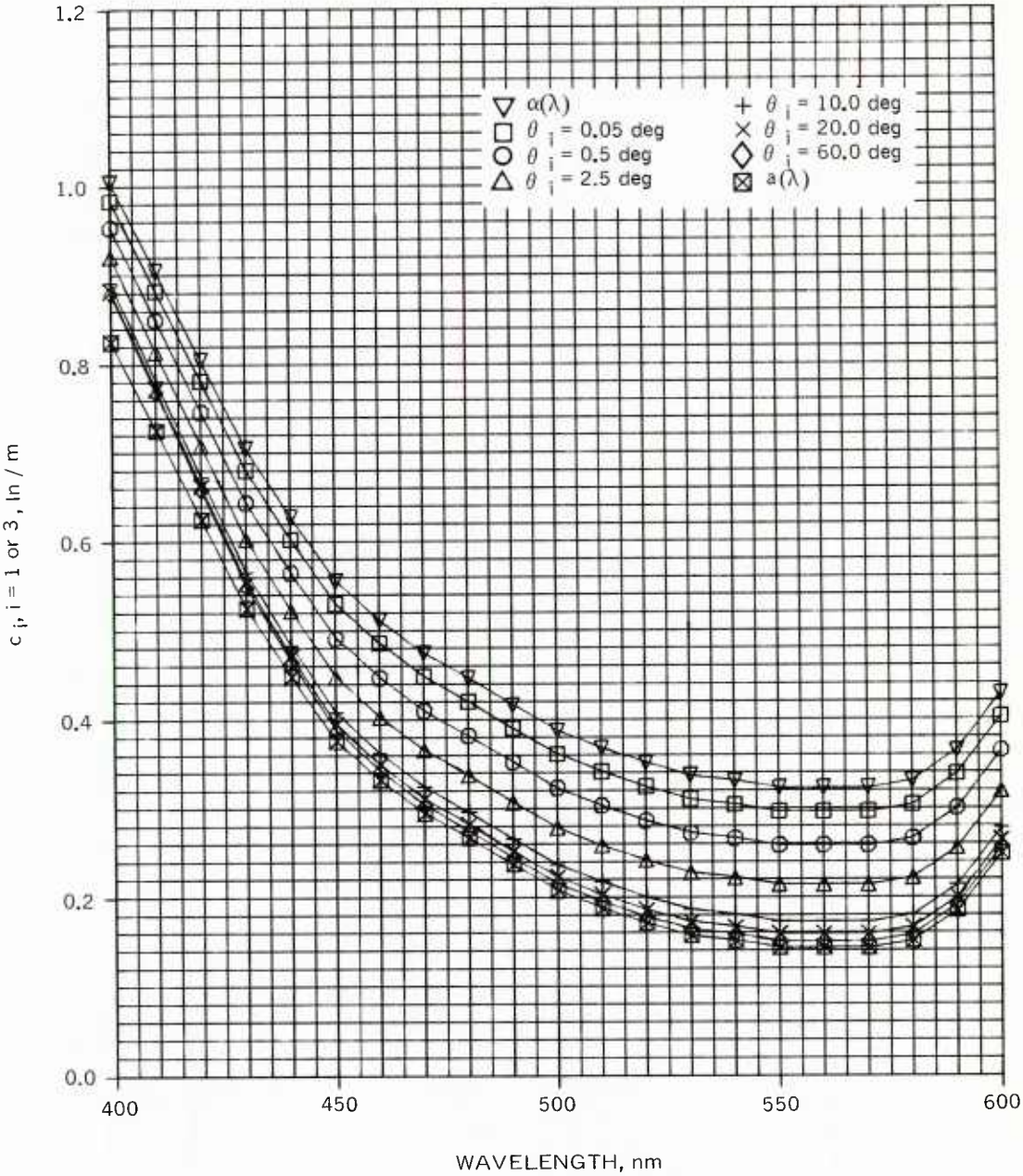

Figure 6.2. Spectral variation of c_i, i = 1 or 3.

Part B. Coastal water.

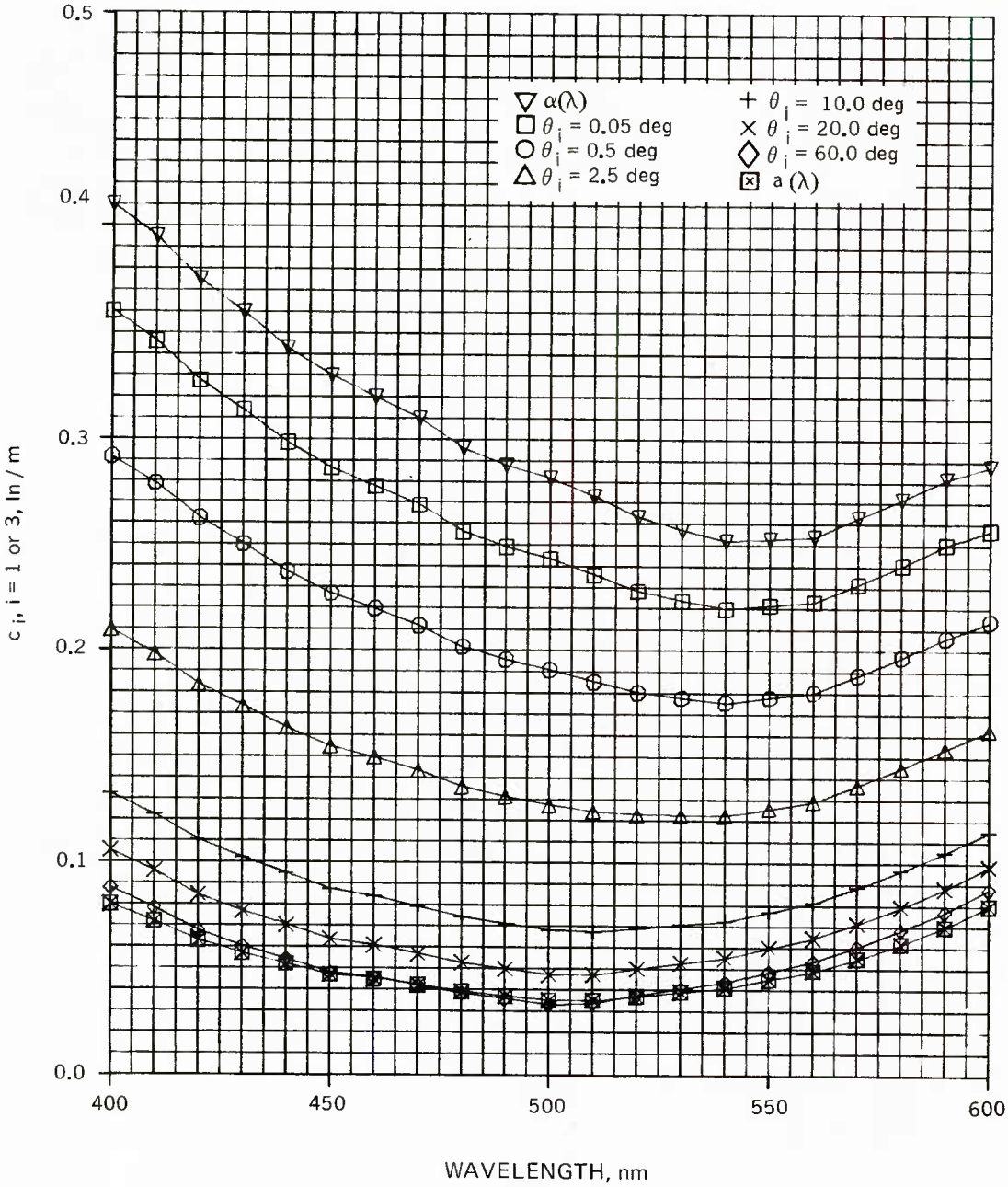

Figure 6.2. (Continued)

Part C. Deep ocean water.

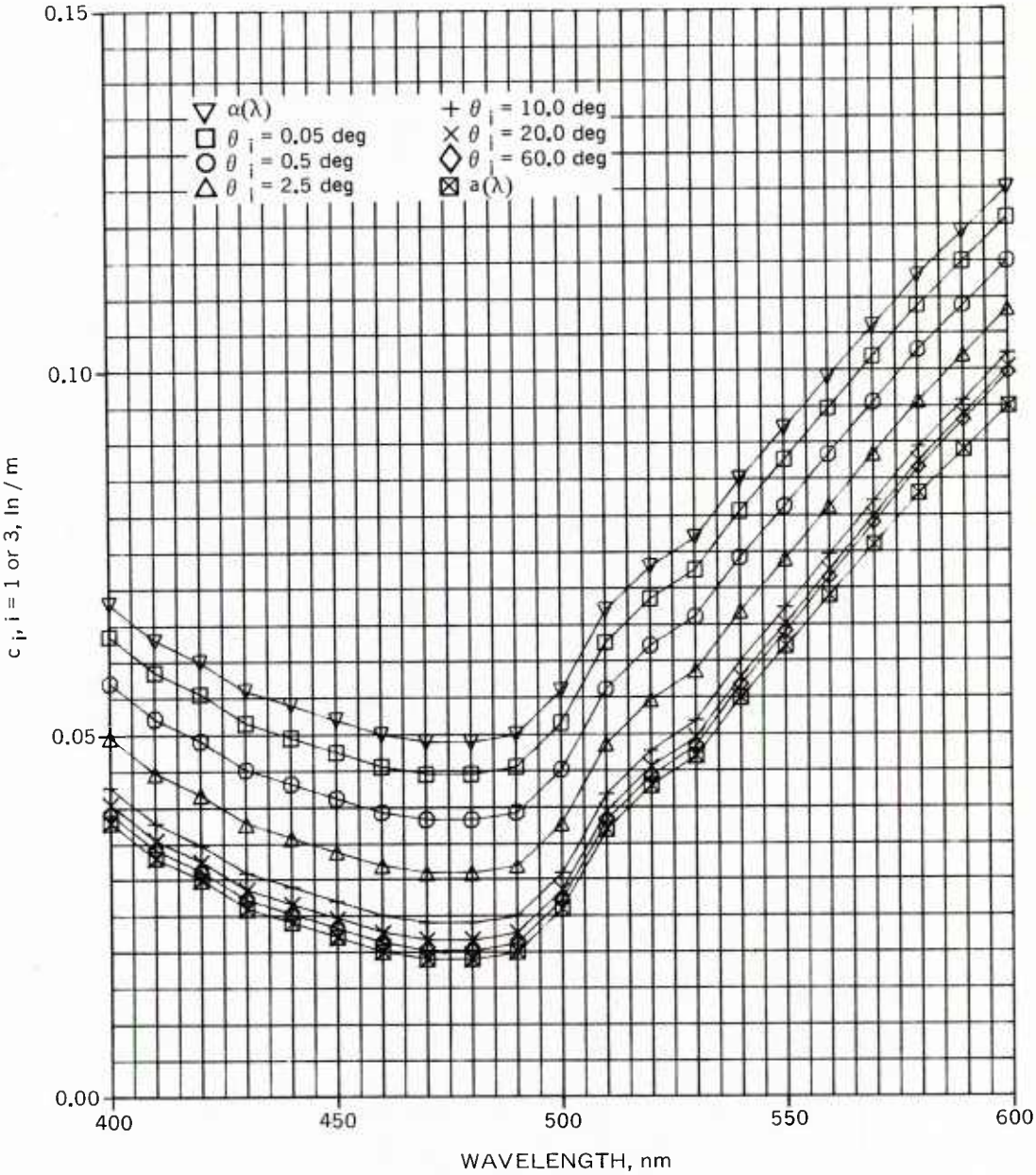

Figure 6.2. (Continued)

Part A. Radiant output power.

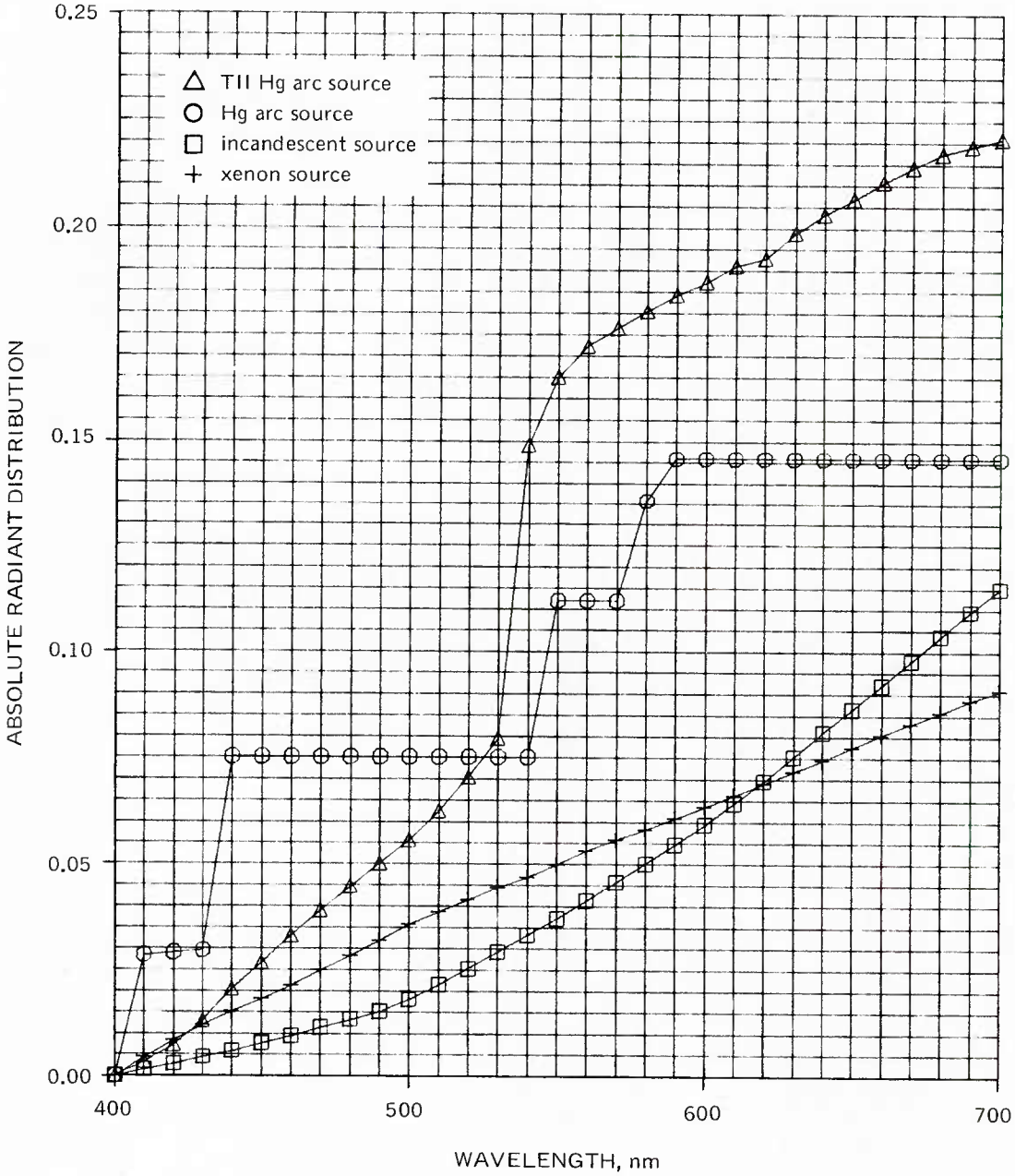

Figure 6.3. Spectral characteristics of conventional light sources.

Part B. Radiant efficiency.

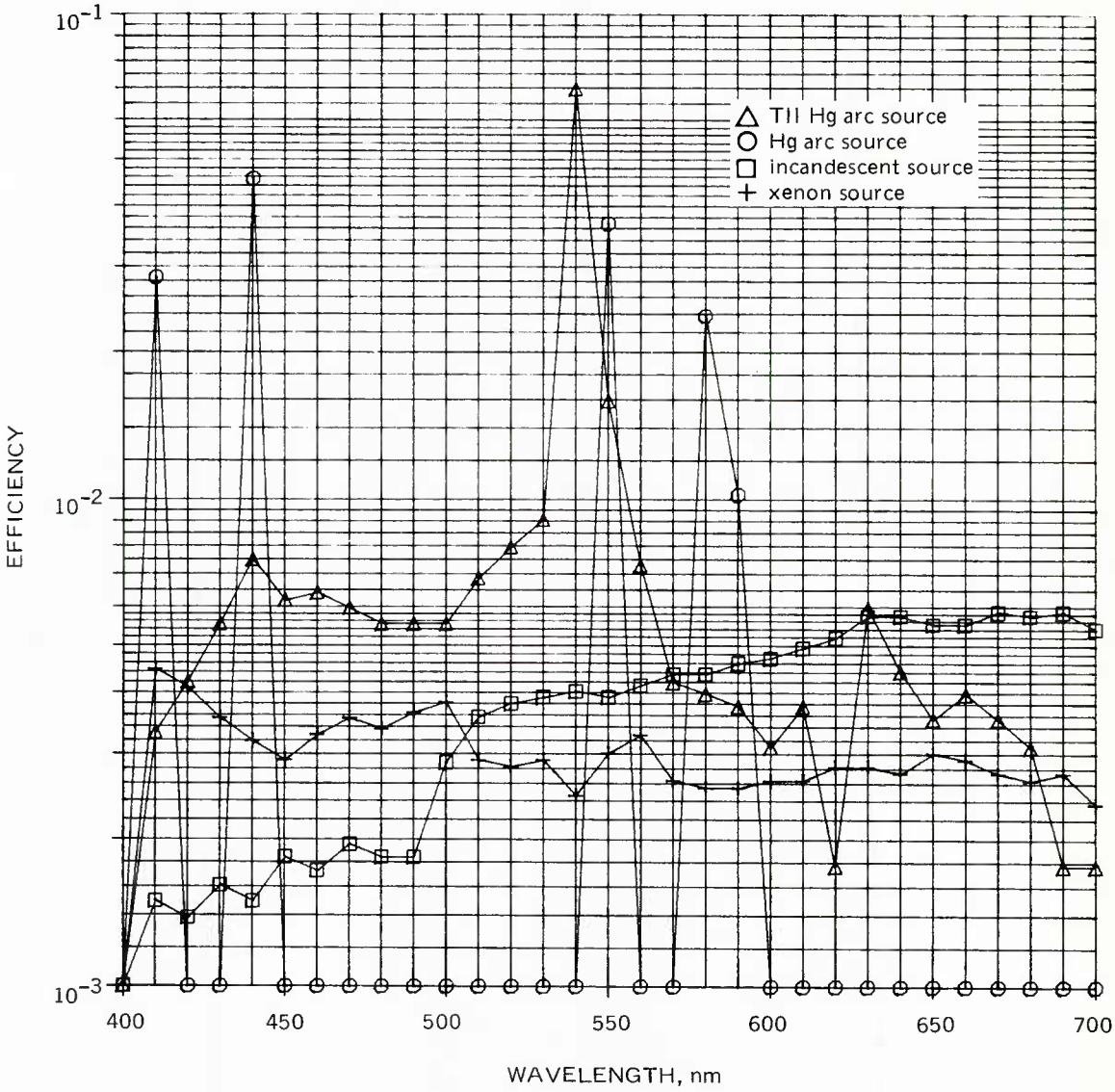

Figure 6.3. (Continued)

Part A. Triple-intensifier vidicons.

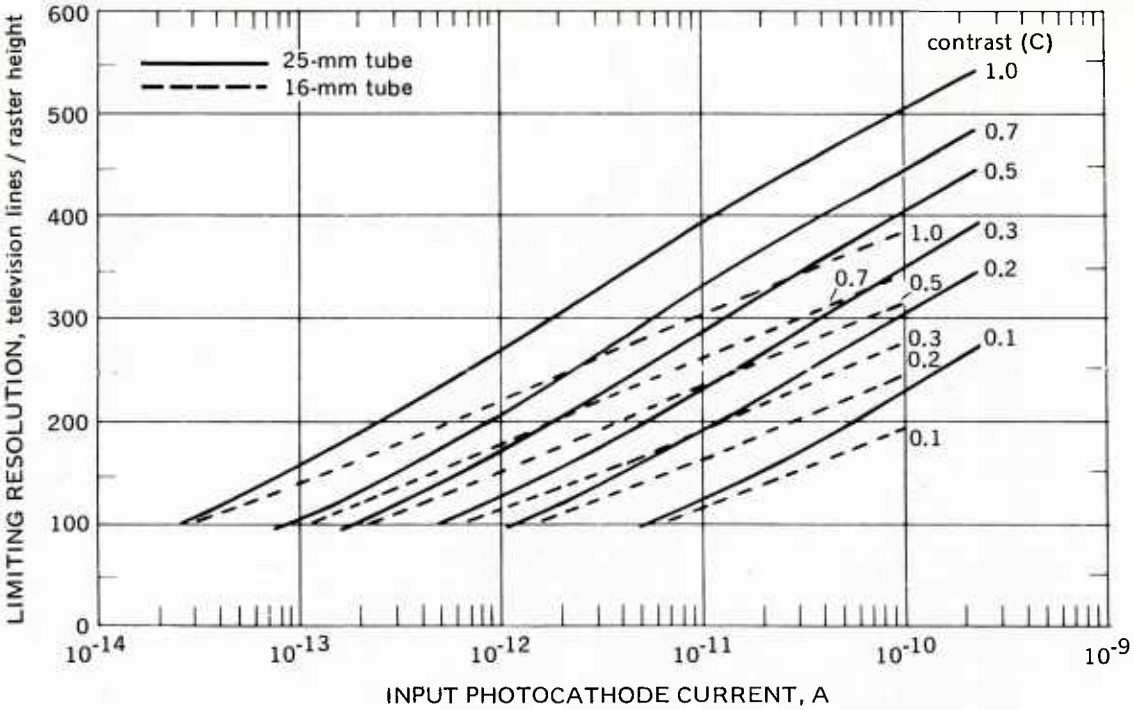

Figure 6.4. Receiver-signal-response curves.

Part B. SEC and intensifier SEC (Westinghouse WX31381).

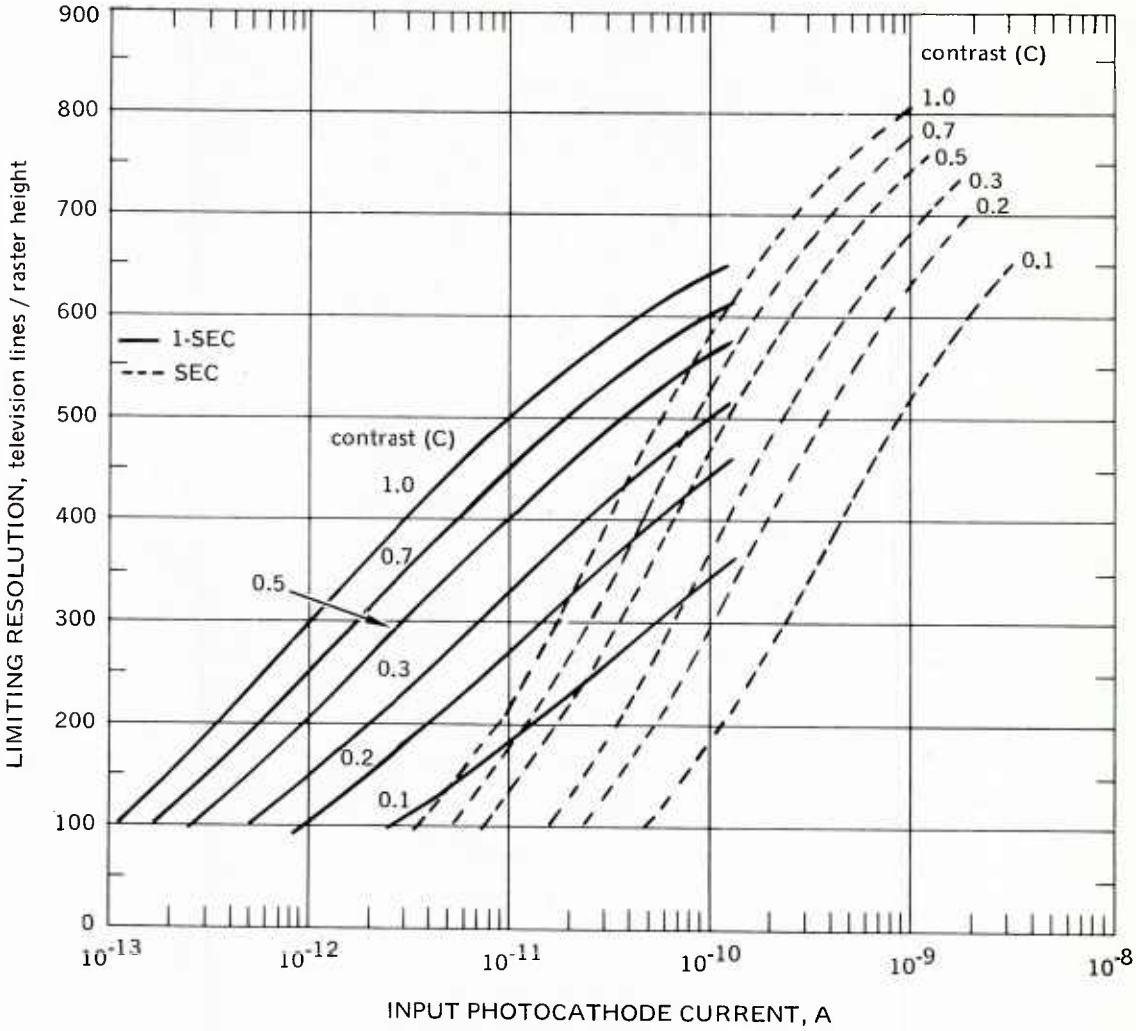

Figure 6.4. (Continued)

Part C. Image orthicon (3-in., thin-film target).

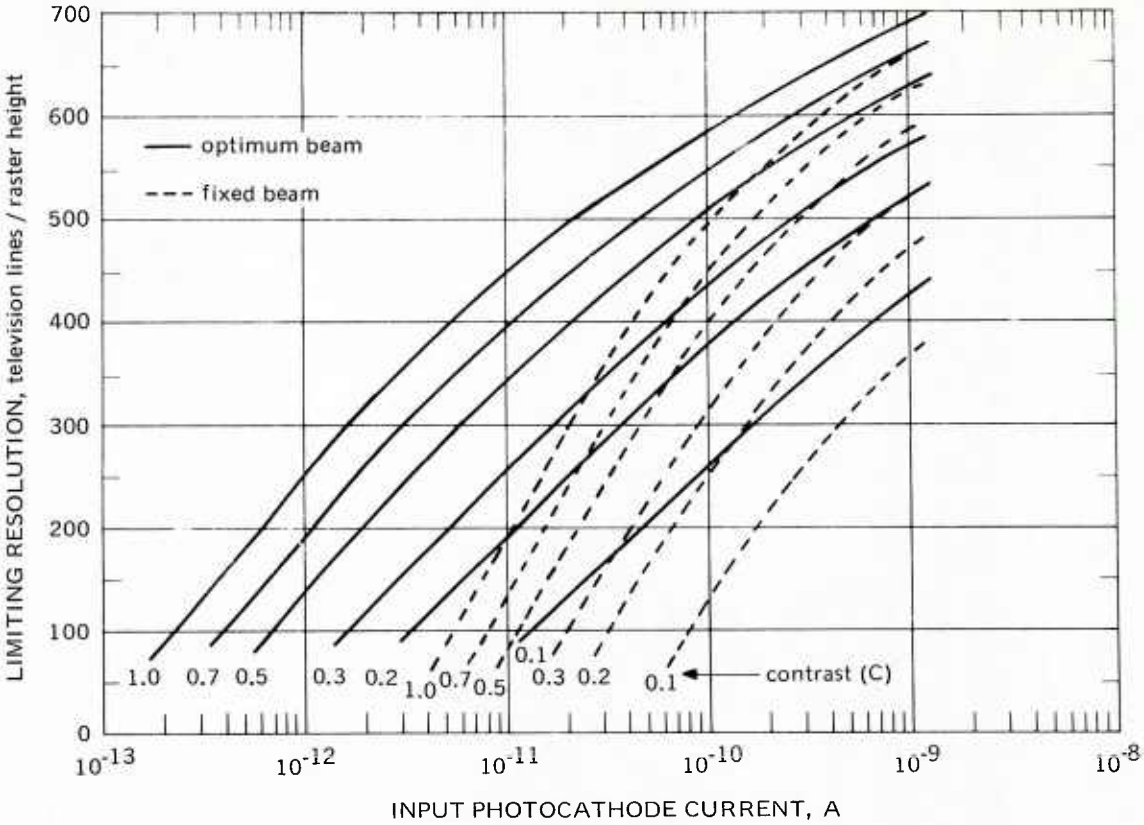

Figure 6.4. (Continued)

Part D. Image isocon (RCA C21095).

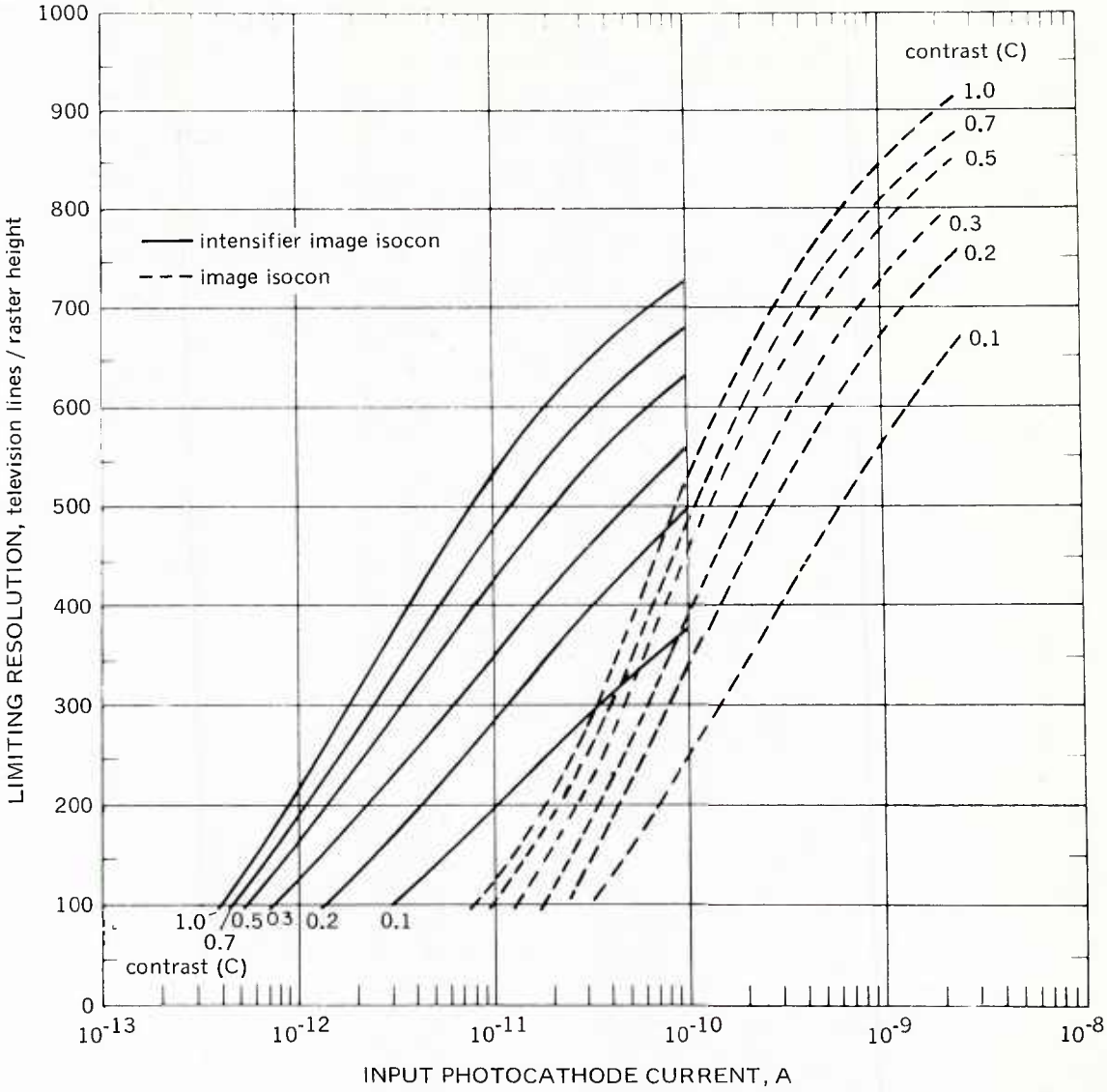

Figure 6.4. (Continued)

Part E. SIT or SEBIR.

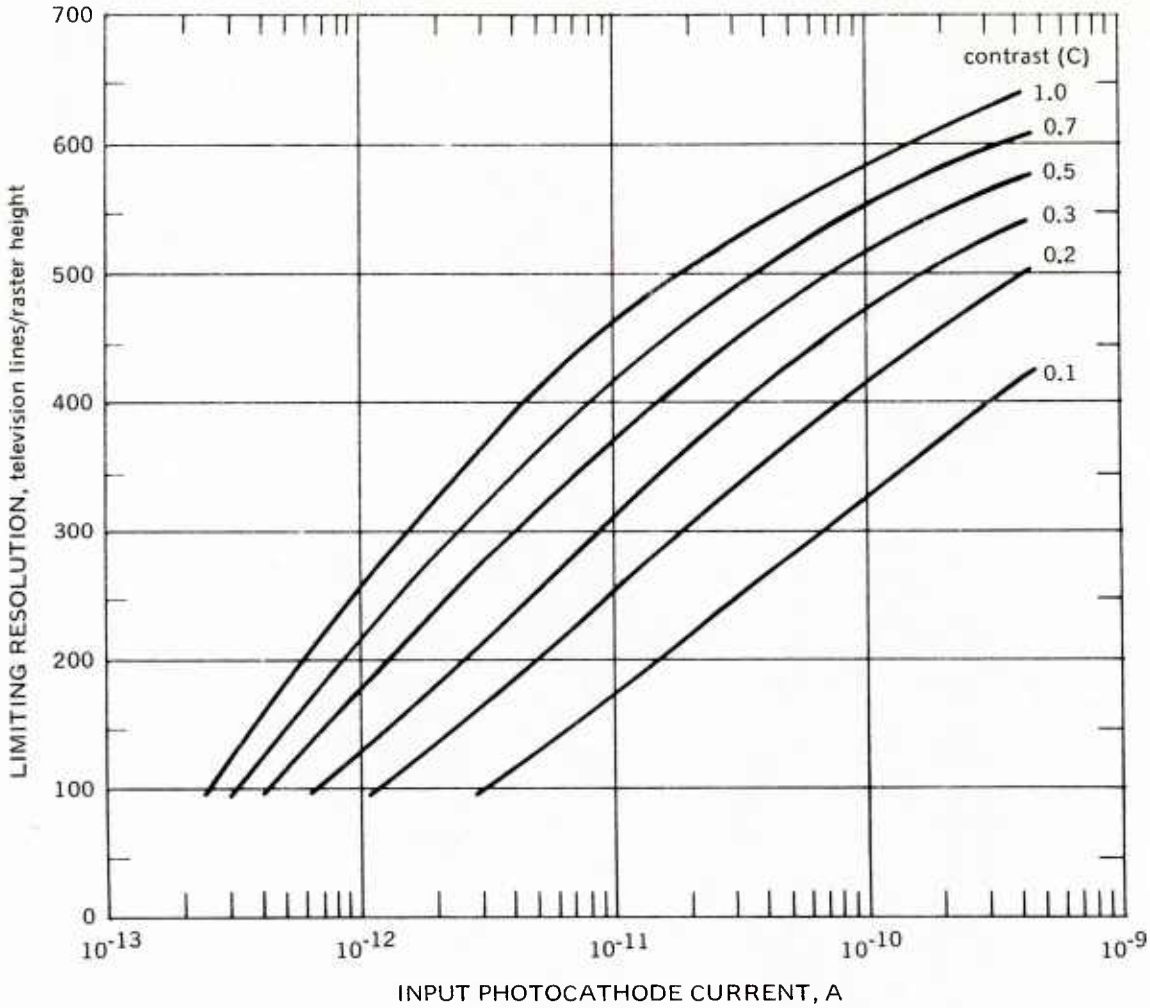

Figure 6.4. (Continued)

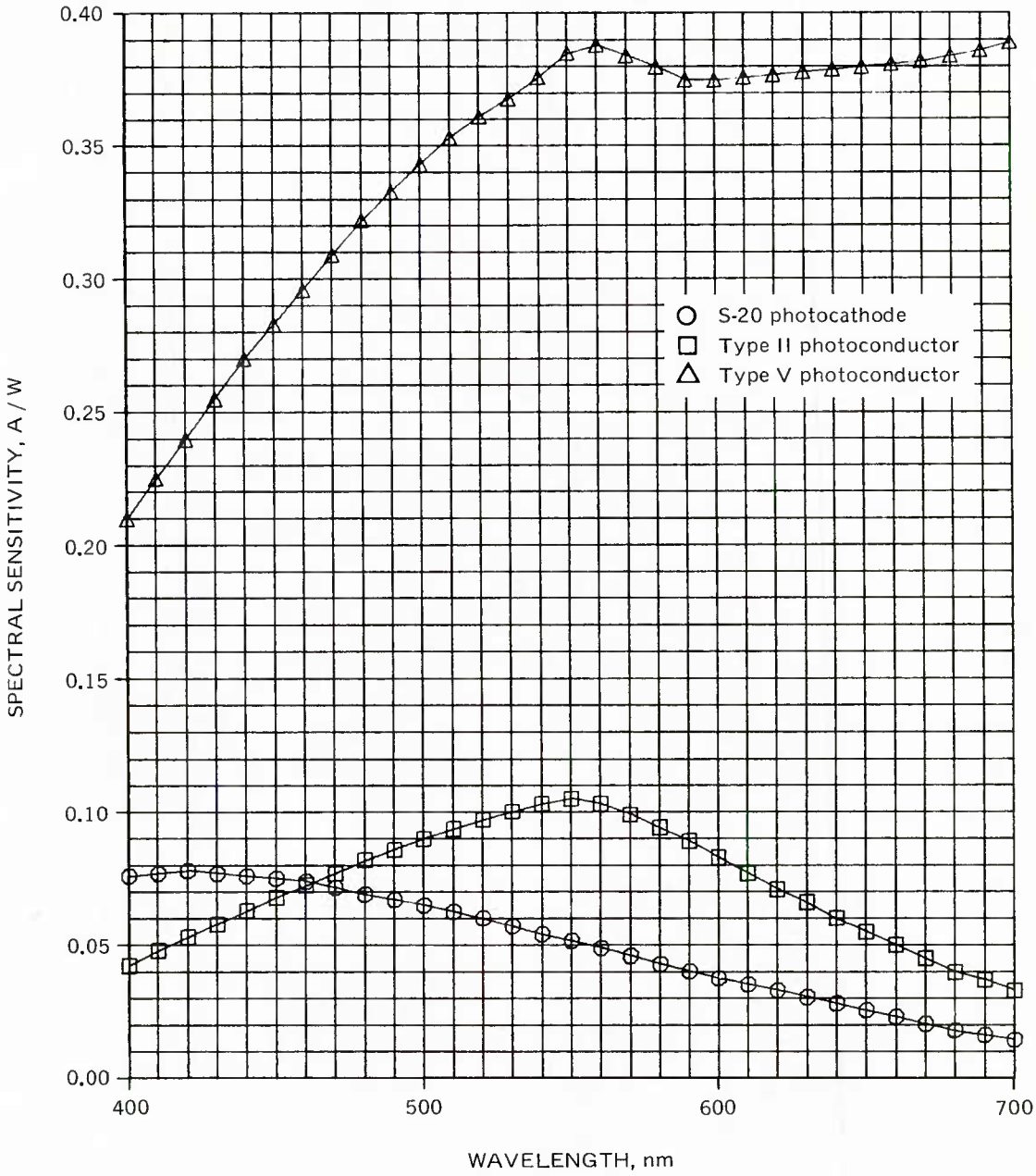

Figure 6.5. Spectral responses of photosensitive surfaces.

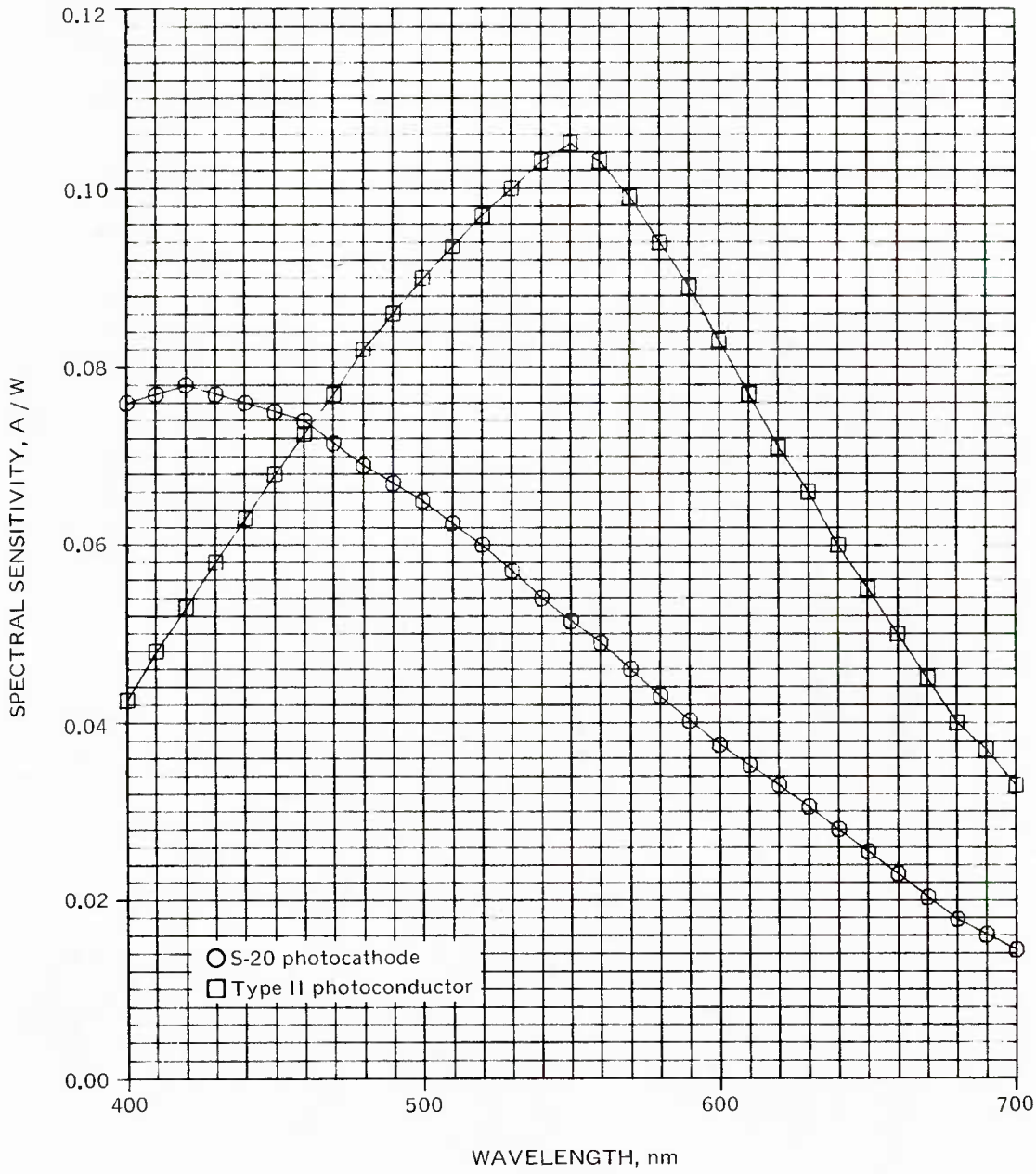

Figure 6.5. (Continued)

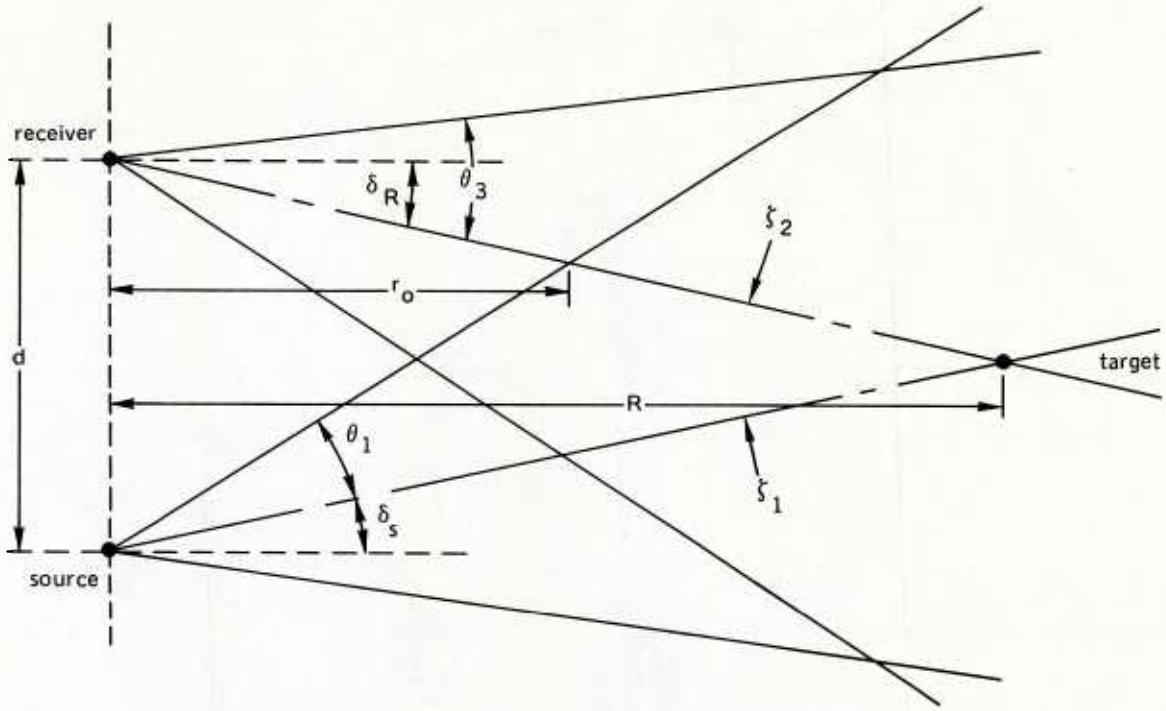

Figure 6.6. Simplified geometry for conventional and extended-range imaging systems.

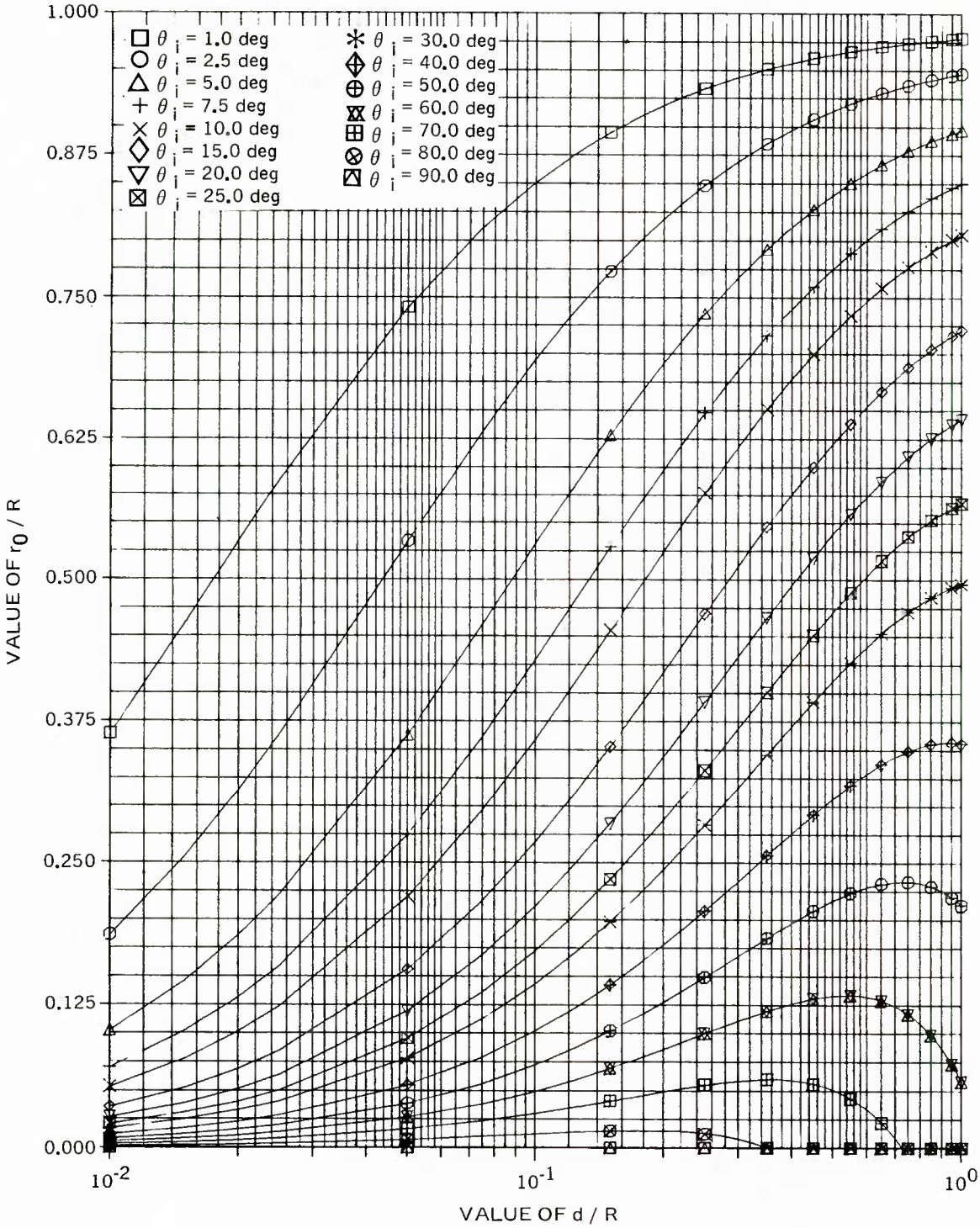

Figure 6.7. Variation of r_0/R with θ_1 and d/R.

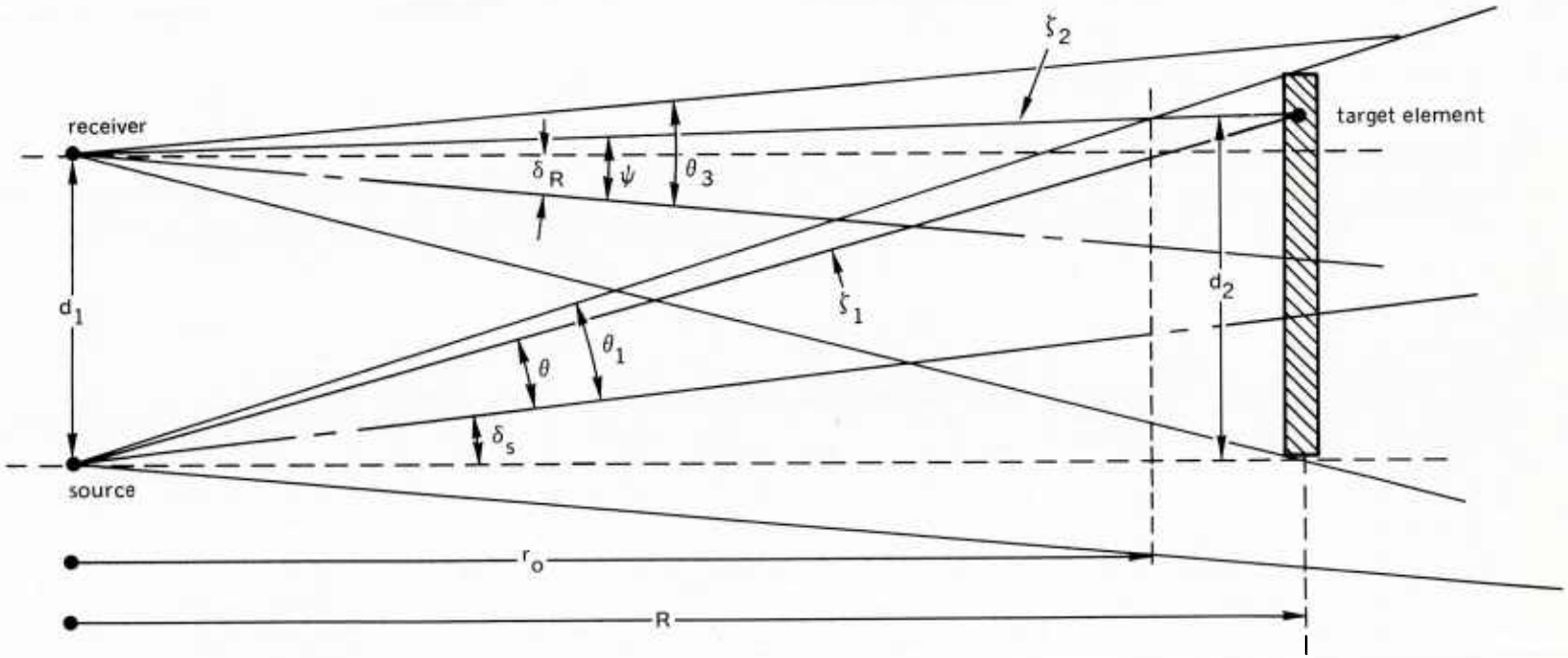

Figure 6.8. General geometry for undersea viewing systems.

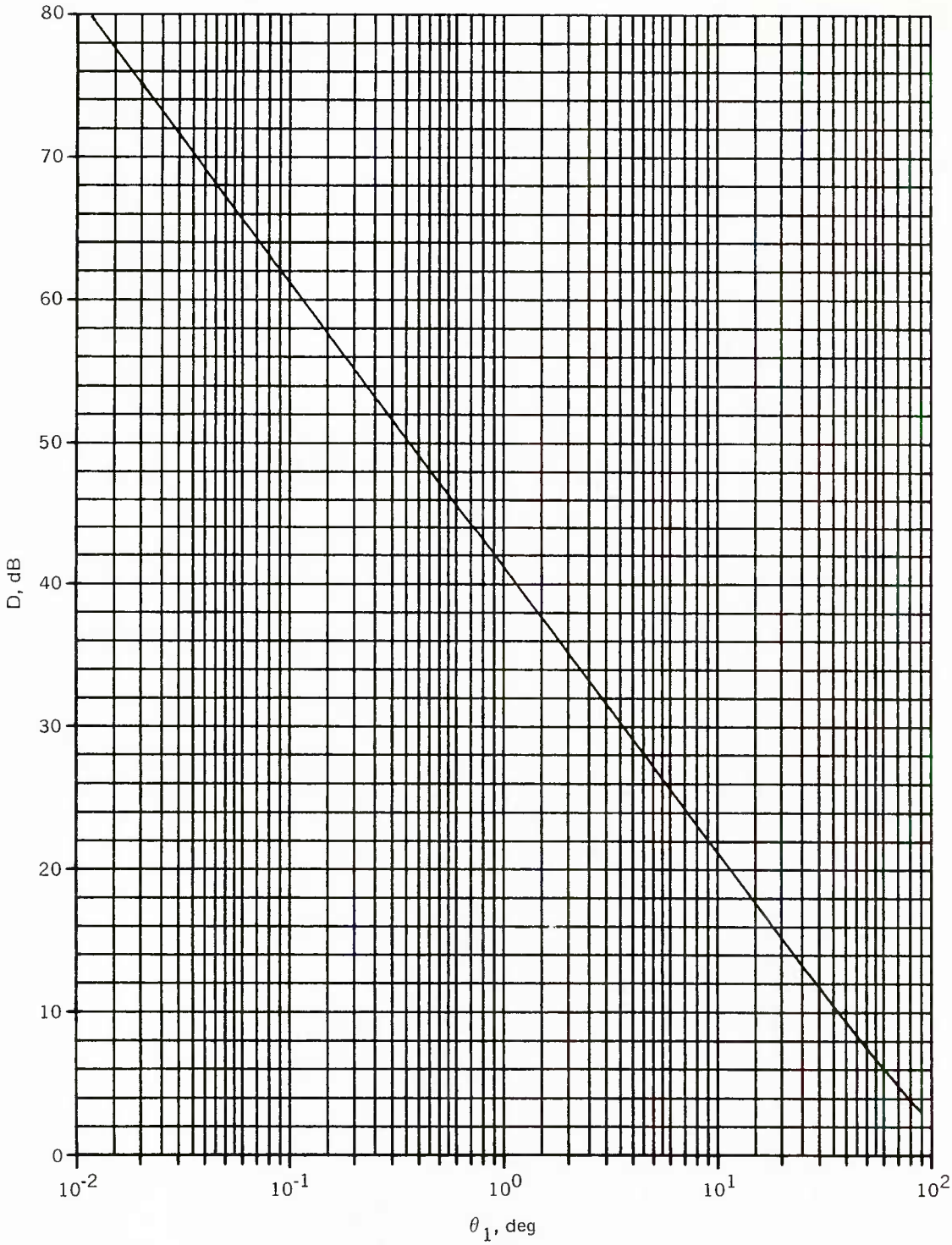

Figure 6.9. Variation of D with θ_1.

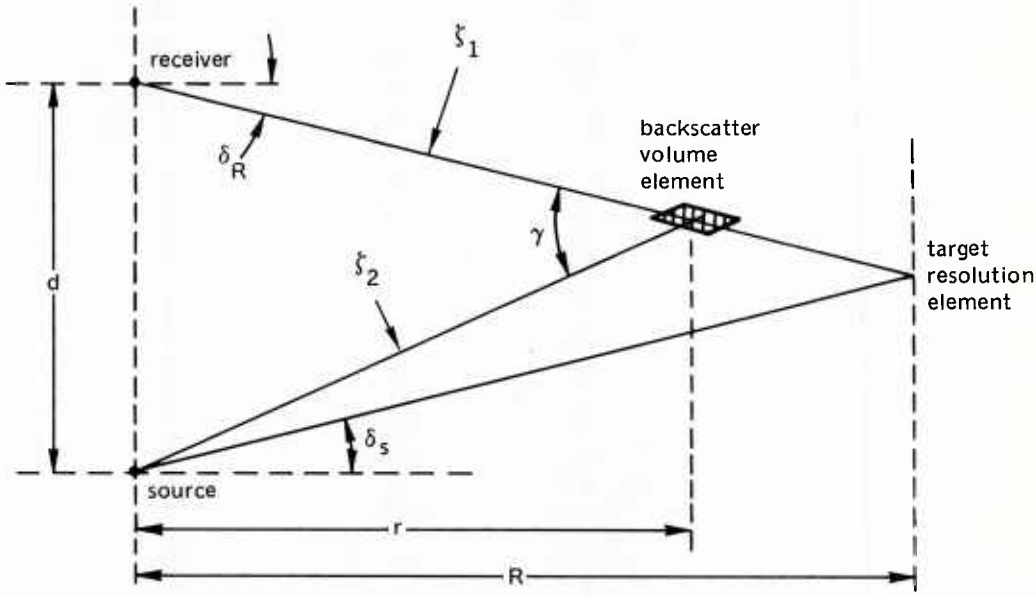

Figure 6.10. Geometry for the calculation of the backscattered light.

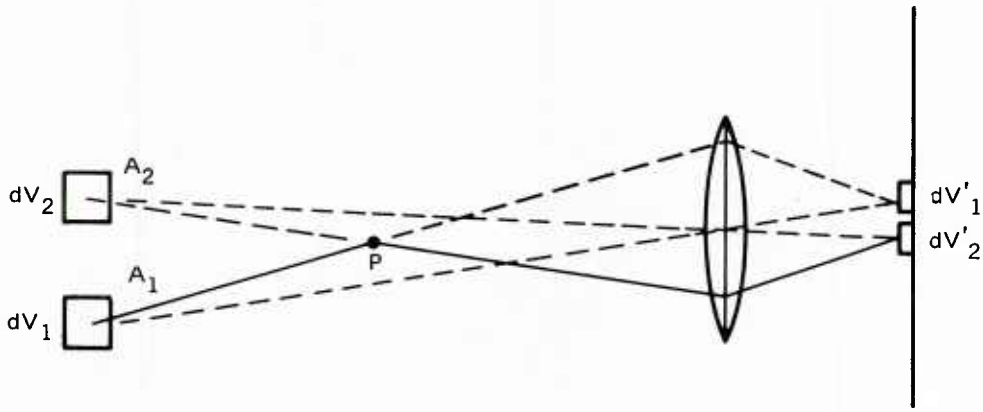

Figure 6.11. Compensating backscattered rays of light.

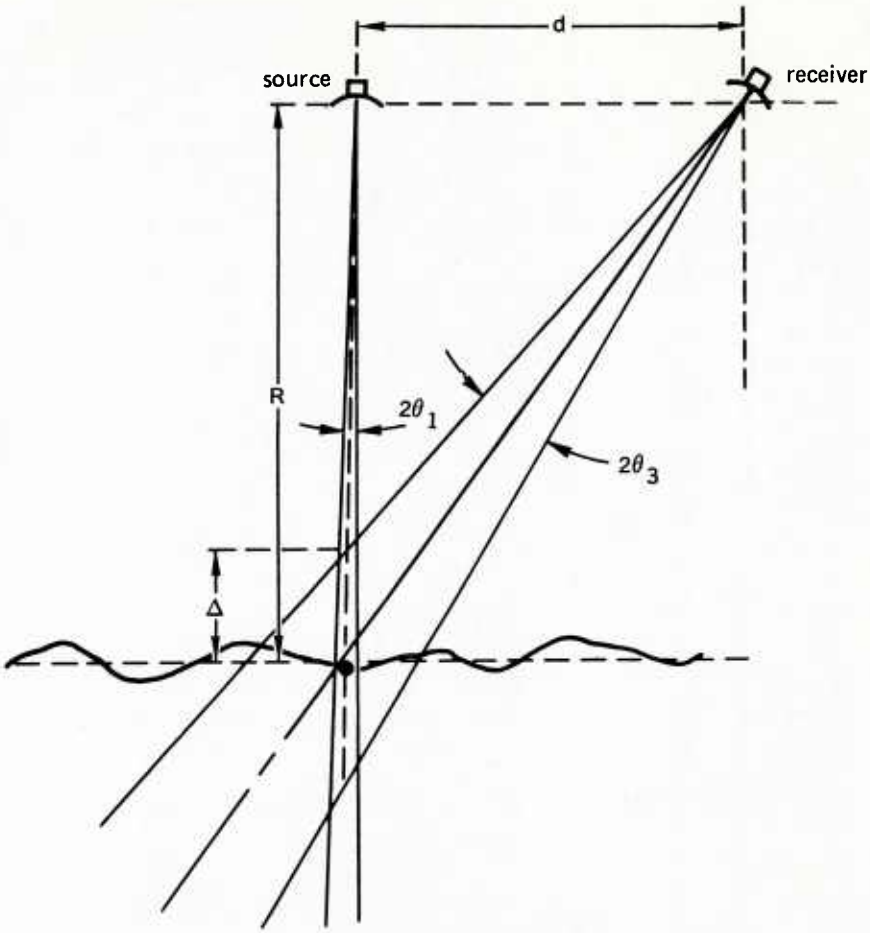

Figure 6.12. Geometry for the volume-scanning imaging system.

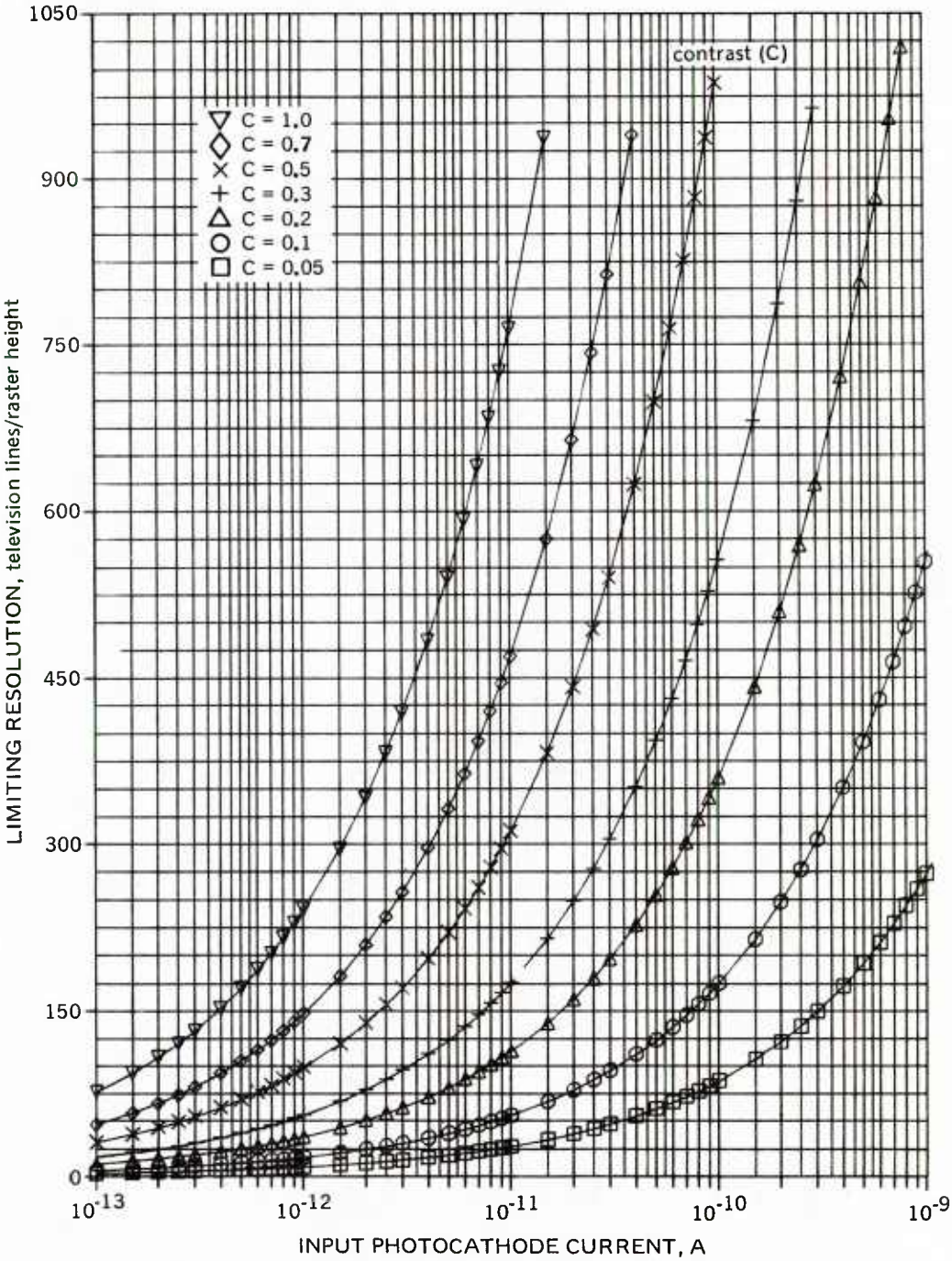

Figure 6.13. Signal-response curves for an ideal photon-noise-limited receiver.

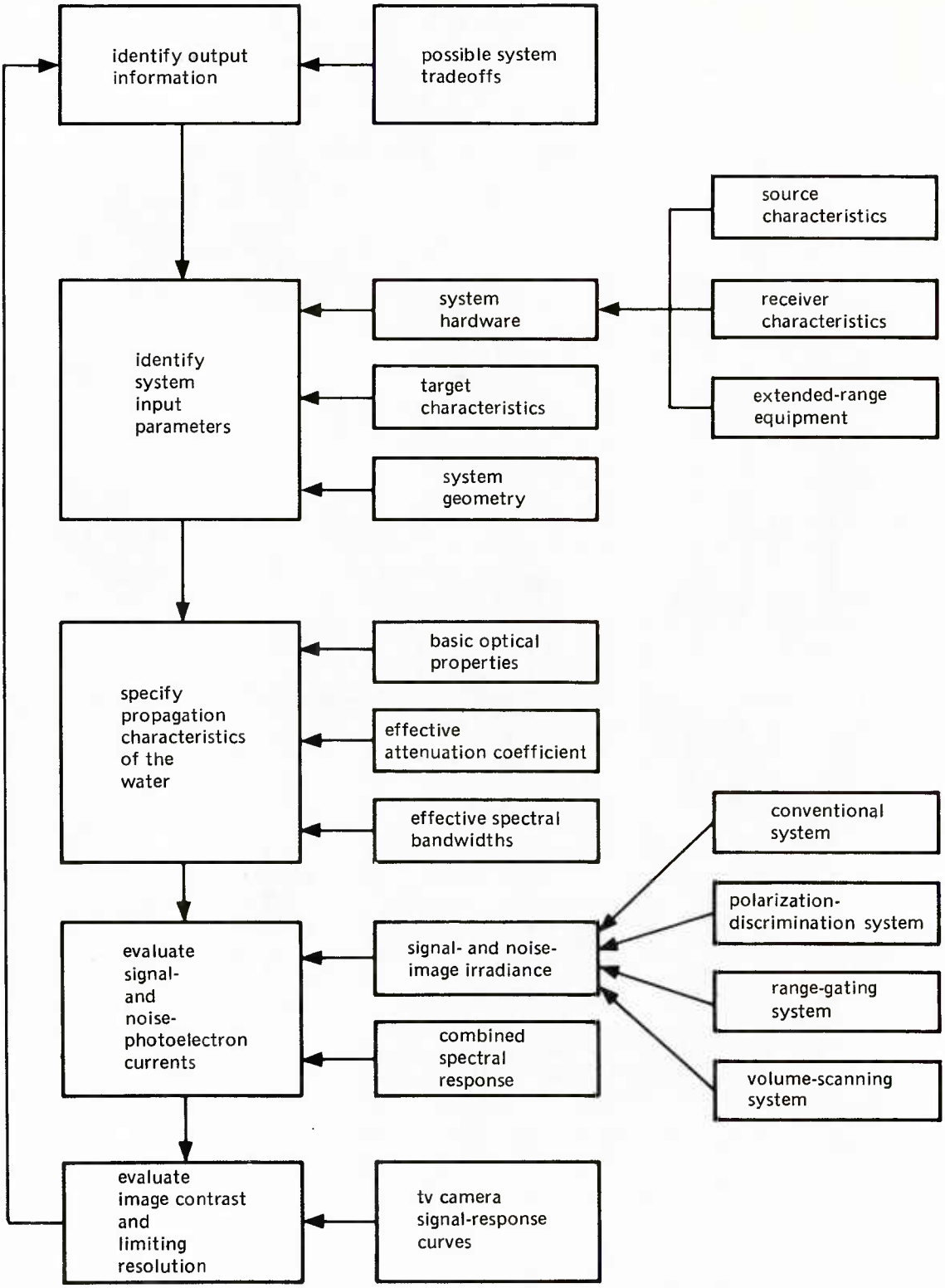

Figure 6.14. Procedure for evaluating underwater viewing system performance.

Table 6.1. Variation of c_i/α with θ_i, i = 1 or 3, and the s/a Ratio. (Morrison Volume Scattering Function, Conical Beam Pattern or Field-Of-View).

s/a	Value of θ_i						
	.05	.50	1.00	2.50	5.00	7.50	10.00
.10	.988	.972	.965	.953	.944	.939	.936
.20	.976	.944	.930	.907	.889	.879	.873
.30	.964	.916	.894	.860	.833	.818	.809
.40	.957	.896	.869	.826	.792	.773	.762
.50	.952	.881	.850	.800	.760	.738	.725
.60	.945	.865	.829	.772	.727	.702	.687
.80	.935	.839	.797	.729	.675	.645	.627
1.00	.926	.820	.772	.696	.635	.602	.581
1.20	.920	.804	.753	.670	.603	.567	.544
1.40	.914	.792	.736	.648	.577	.538	.514
1.60	.909	.781	.723	.629	.555	.514	.488
1.80	.905	.771	.711	.613	.535	.493	.466
2.00	.902	.763	.700	.599	.519	.474	.446
2.20	.899	.756	.691	.587	.504	.458	.429
2.40	.896	.749	.683	.576	.490	.443	.413
2.60	.893	.744	.675	.566	.478	.430	.399
2.80	.891	.738	.668	.557	.467	.418	.387
3.00	.889	.733	.662	.548	.457	.407	.375
3.20	.887	.729	.656	.540	.448	.397	.364
3.40	.885	.724	.651	.533	.439	.387	.354
3.60	.883	.721	.646	.526	.431	.378	.345
3.80	.881	.717	.641	.520	.423	.370	.336
4.00	.880	.713	.637	.514	.416	.362	.328
4.20	.878	.710	.633	.509	.410	.355	.320
4.40	.877	.707	.629	.503	.403	.348	.313
4.60	.876	.704	.625	.498	.397	.342	.306
4.80	.875	.701	.621	.494	.391	.335	.299
5.00	.873	.699	.618	.489	.386	.329	.293

Table 6.1. (Continued)

	Value of θ_i						
	15.0	20.0	30.0	45.0	60.0	90.0	*
.10	.933	.931	.929	.928	.928	.928	.909
.20	.866	.862	.858	.857	.856	.856	.833
.30	.798	.793	.787	.785	.784	.784	.769
.40	.748	.741	.734	.731	.731	.729	.714
.50	.709	.701	.693	.690	.689	.688	.667
.60	.669	.659	.650	.645	.644	.643	.625
.80	.605	.593	.581	.576	.574	.572	.556
1.00	.556	.542	.529	.522	.520	.518	.500
1.20	.517	.502	.487	.479	.477	.474	.455
1.40	.484	.468	.452	.443	.441	.438	.417
1.60	.457	.440	.422	.413	.410	.408	.385
1.80	.433	.415	.397	.387	.384	.381	.357
2.00	.412	.393	.375	.364	.361	.358	.333
2.20	.394	.374	.355	.344	.340	.337	.312
2.40	.377	.357	.337	.326	.322	.319	.294
2.60	.363	.342	.321	.309	.305	.302	.278
2.80	.349	.328	.306	.294	.290	.287	.263
3.00	.336	.315	.293	.280	.276	.273	.250
3.20	.325	.303	.280	.268	.263	.260	.238
3.40	.314	.292	.269	.256	.251	.248	.227
3.60	.304	.281	.258	.245	.240	.237	.217
3.80	.295	.272	.248	.234	.230	.226	.208
4.00	.286	.263	.238	.225	.220	.216	.200
4.20	.278	.254	.230	.216	.211	.207	.192
4.40	.270	.246	.221	.207	.202	.198	.185
4.60	.263	.238	.213	.199	.194	.190	.179
4.80	.256	.231	.206	.191	.186	.182	.172
5.00	.249	.224	.198	.184	.179	.175	.167

* a/α ratio which corresponds to specified s/α ratio.

Table 6.2. Spectral Variation of the Total Attenuation Coefficient for Light in Seawater (ln/m).

Lambda	Distilled Water	Deep Ocean Water	Coastal Water	Bay Water
400.	.430E-01	.680E-01	.410E 00	.100E 01
410.	.400E-01	.630E-01	.395E 00	.905E 00
420.	.350E-01	.600E-01	.375E 00	.805E 00
430.	.300E-01	.560E-01	.360E 00	.705E 00
440.	.210E-01	.540E-01	.343E 00	.628E 00
450.	.190E-01	.520E-01	.330E 00	.556E 00
460.	.180E-01	.500E-01	.320E 00	.512E 00
470.	.180E-01	.490E-01	.310E 00	.475E 00
480.	.200E-01	.490E-01	.296E 00	.447E 00
490.	.250E-01	.500E-01	.288E 00	.417E 00
500.	.360E-01	.560E-01	.282E 00	.388E 00
510.	.380E-01	.670E-01	.273E 00	.368E 00
520.	.400E-01	.730E-01	.263E 00	.351E 00
530.	.440E-01	.770E-01	.257E 00	.337E 00
540.	.530E-01	.850E-01	.252E 00	.331E 00
550.	.690E-01	.920E-01	.253E 00	.323E 00
560.	.800E-01	.990E-01	.254E 00	.323E 00
570.	.880E-01	.106E 00	.263E 00	.323E 00
580.	.100E 00	.113E 00	.272E 00	.331E 00
590.	.122E 00	.119E 00	.282E 00	.365E 00
600.	.186E 00	.125E 00	.288E 00	.429E 00

(Note: 1.00E-01 = 1.00×10^{-1}.)

Table 6.3. Spectral Variation of the s/a Ratio for Light in Seawater.

Lambda	Distilled Water	Deep Ocean Water	Coastal Water	Bay Water
400.	.132E 00	.789E 00	.412E 01	.218E 00
410.	.128E 00	.909E 00	.449E 01	.248E 00
420.	.132E 00	.100E 01	.495E 01	.288E 00
430.	.140E 00	.115E 01	.532E 01	.343E 00
440.	.196E 00	.125E 01	.560E 01	.402E 00
450.	.191E 00	.136E 01	.602E 01	.479E 00
460.	.183E 00	.150E 01	.611E 01	.542E 00
470.	.164E 00	.158E 01	.638E 01	.610E 00
480.	.131E 00	.158E 01	.659E 01	.674E 00
490.	.927E-01	.150E 01	.678E 01	.759E 00
500.	.576E-01	.115E 01	.706E 01	.865E 00
510.	.500E-01	.811E 00	.680E 01	.957E 00
520.	.436E-01	.698E 00	.611E 01	.105E 01
530.	.365E-01	.638E 00	.559E 01	.115E 01
540.	.281E-01	.545E 00	.515E 01	.119E 01
550.	.197E-01	.484E 00	.462E 01	.126E 01
560.	.156E-01	.435E 00	.418E 01	.126E 01
570.	.132E-01	.395E 00	.378E 01	.126E 01
580.	.107E-01	.361E 00	.339E 01	.119E 01
590.	.810E-02	.337E 00	.303E 01	.973E 00
600.	.503E-02	.316E 00	.260E 01	.723E 00

(Note: 1.00 E + 01 = $1.00 \times 10^{+1}$.)

Table 6.4. Effective Spectral Bandwidths for Image-Forming Light for Different Ranges (m) and Beam Patterns.

Bay water (α (560) = 0.323 1n/m).

	λ_0 = 560 $\theta_1 < 5$ deg		λ_0 = 560 5 deg $\leqslant \theta_1 \leqslant$ 20 deg		λ_0 = 560 20 deg $< \theta_1$	
Range	λ_1	λ_2	λ_1	λ_2	λ_1	λ_2
2	460	600	460	600	460	600
4	490	600	490	600	490	600
6	500	590	500	590	500	590
8	510	590	510	590	510	590
10	510	590	520	590	520	590

Coastal water (α (540) = 0.252 1n/m).

	λ_0 = 540 $\theta_1 < 5$ deg		λ_0 = 540 5 deg $\leqslant \theta_1 \leqslant$ 20 deg		λ_0 = 540 20 deg $< \theta_1$	
Range	λ_1	λ_2	λ_1	λ_2	λ_1	λ_2
5	440	600	430	600	420	600
10	480	590	470	590	460	590
15	490	580	480	580	480	580
20	500	580	490	580	485	570
25	510	570	500	570	490	570

Deep ocean water (α(475) = 0.049 1n/m).

	λ_0 = 475 $\theta_1 < 5$ deg		λ_0 = 475 5 deg $\leqslant \theta_1 \leqslant$ 20 deg		λ_0 = 475 20 deg $< \theta_1$	
Range	λ_1	λ_2	λ_1	λ_2	λ_1	λ_2
10	400	540	400	540	400	540
20	400	510	400	510	400	510
30	420	500	420	500	420	500
40	420	500	430	500	430	500
50	430	500	430	500	430	500

Table 6.5. Effective Spectral Bandwidths for Backscattered Light for Different Ranges (m) and Beam Patterns.

Bay water (α (560) = 0.323 1n/m).

Range	λ_0 = 560 $\theta_1 < 5$ deg		λ_0 = 560 5 deg $\leqslant \theta_1 \leqslant$ 20 deg		λ_0 = 560 20 deg $< \theta_1$	
	λ_1	λ_2	λ_1	λ_2	λ_1	λ_2
2	460	600	460	600	460	600
4	490	600	490	600	490	600
6	500	590	500	590	500	590
8	510	590	510	590	510	590
10	520	590	520	590	520	590

Coastal water (α (540) = 0.252 1n/m).

Range	λ_0 = 540 $\theta_1 < 5$ deg		λ_0 = 510 5 deg $\leqslant \theta_1 \leqslant$ 20 deg		λ_0 = 500 20 deg $< \theta_1$	
	λ_1	λ_2	λ_1	λ_2	λ_1	λ_2
5	410	600	400	600	400	600
10	450	590	430	590	420	580
15	470	580	450	570	440	560
20	480	570	460	570	450	550
25	480	570	470	560	450	550

Deep ocean water (α (475) = 0.049 1n/m).

Range	λ_0 = 475 $\theta_1 < 5$ deg		λ_0 = 475 5 deg $\leqslant \theta_1 \leqslant$ 20 deg		λ_0 = 475 20 deg $< \theta_1$	
	λ_1	λ_2	λ_1	λ_2	λ_1	λ_2
10	400	540	400	540	400	540
20	400	510	400	510	400	510
30	420	500	420	500	420	500
40	430	500	430	500	430	500
50	430	500	430	500	430	500

Table 6.6. Spectral Characteristics of Conventional and Laser Light Sources.

Wavelength λ_2	Radiant Output Power*			
	Incandescent Source	Hg Arc Source	TlI Hg Arc Source	Xenon Arc Source
400.	0.00E-01	0.00E-01	0.00E-01	0.00E-01
410.	1.49E-03	2.85E-02	3.31E-03	4.46E-03
420.	2.87E-03	2.91E-02	7.51E-03	8.55E-03
430.	4.48E-03	2.96E-02	1.30E-02	1.21E-02
440.	5.98E-03	7.52E-02	2.06E-02	1.53E-02
450.	7.82E-03	7.52E-02	2.67E-02	1.82E-02
460.	9.54E-03	7.52E-02	3.31E-02	2.15E-02
470.	1.15E-02	7.52E-02	3.91E-02	2.50E-02
480.	1.33E-02	7.52E-02	4.46E-02	2.84E-02
490.	1.52E-02	7.52E-02	5.02E-02	3.20E-02
500.	1.81E-02	7.52E-02	5.57E-02	3.59E-02
510.	2.16E-02	7.52E-02	6.25E-02	3.88E-02
520.	2.54E-02	7.52E-02	7.05E-02	4.16E-02
530.	2.93E-02	7.52E-02	7.96E-02	4.45E-02
540.	3.33E-02	7.52E-02	1.49E-01	4.70E-02
550.	3.73E-02	1.12E-01	1.65E-01	5.00E-02
560.	4.14E-02	1.12E-01	1.72E-01	5.32E-02
570.	4.58E-02	1.12E-01	1.77E-01	5.59E-02
580.	5.01E-02	1.36E-01	1.81E-01	5.84E-02
590.	5.47E-02	1.46E-01	1.84E-01	6.10E-02
600.	5.95E-02	1.46E-01	1.87E-01	6.36E-02
610.	6.44E-02	1.46E-01	1.91E-01	6.62E-02
620.	6.96E-02	1.46E-01	1.93E-01	6.91E-02
630.	7.53E-02	1.46E-01	1.99E-01	7.19E-02
640.	8.11E-02	1.46E-01	2.03E-01	7.46E-02
650.	8.66E-02	1.46E-01	2.07E-01	7.76E-02
660.	9.21E-02	1.46E-01	2.11E-01	8.05E-02
670.	9.80E-02	1.46E-01	2.14E-01	8.33E-02
680.	1.04E-01	1.46E-01	2.17E-01	8.59E-02
690.	1.10E-01	1.46E-01	2.19E-01	8.86E-02
700.	1.15E-01	1.46E-01	2.21E-01	9.10E-02

* Power emitted in the wavelength interval $(400,\lambda_2)$ per watt of input electrical power. (Note: 1.00 E-01 = 1.00×10^{-1}.)

Table 6.6. (Continued)

Wavelength λ_2	Radiant Efficiency of Sources*			
	Incandescent Source	Hg Arc Source	TII Hg Arc Source	Xenon Arc Source
400.	0.00E-01	0.00E-01	0.00E-01	0.00E-01
410.	1.49E-03	2.85E-02	3.31E-03	4.46E-03
420.	1.38E-03	5.84E-04	4.20E-03	4.09E-03
430.	1.61E-03	5.84E-04	5.53E-03	3.55E-03
440.	1.50E-03	4.56E-02	7.51E-03	3.19E-03
450.	1.84E-03	0.00E-01	6.19E-03	2.91E-03
460.	1.73E-03	0.00E-01	6.41E-03	3.28E-03
470.	1.96E-03	0.00E-01	5.97E-03	3.55E-03
480.	1.84E-03	0.00E-01	5.52E-03	3.37E-03
490.	1.84E-03	0.00E-01	5.53E-03	3.64E-03
500.	2.87E-03	0.00E-01	5.52E-03	3.82E-03
510.	3.56E-03	0.00E-01	6.85E-03	2.91E-03
520.	3.79E-03	0.00E-01	7.96E-03	2.82E-03
530.	3.91E-03	0.00E-01	9.06E-03	2.91E-03
540.	4.02E-03	0.00E-01	6.96E-02	2.46E-03
550.	3.91E-03	3.68E-02	1.59E-02	3.00E-03
560.	4.14E-03	0.00E-01	7.29E-03	3.28E-03
570.	4.37E-03	0.00E-01	4.20E-03	2.64E-03
580.	4.37E-03	2.38E-02	3.98E-03	2.55E-03
590.	4.60E-03	1.02E-02	3.76E-03	2.55E-03
600.	4.72E-03	0.00E-01	3.09E-03	2.64E-03
610.	4.95E-03	0.00E-01	3.76E-03	2.64E-03
620.	5.17E-03	0.00E-01	1.77E-03	2.82E-03
630.	5.75E-03	0.00E-01	5.97E-03	2.82E-03
640.	5.75E-03	0.00E-01	4.42E-03	2.73E-03
650.	5.52E-03	0.00E-01	3.54E-03	3.00E-03
660.	5.52E-03	0.00E-01	3.98E-03	2.91E-03
670.	5.87E-03	0.00E-01	3.54E-03	2.73E-03
680.	5.75E-03	0.00E-01	3.09E-03	2.64E-03
690.	5.86E-03	0.00E-01	1.77E-03	2.73E-03
700.	5.41E-03	0.00E-01	1.77E-03	2.37E-03

*Power emitted in a 10-nm-wavelength interval per watt of input electrical power.

Table 6.6. (Continued)

Laser	Relative Radiant Output Power per Spectral Line		
	λ_i, nm	Fraction of Maximum Output	Percent of Total Output
		$w_R(\lambda_i)/w_R$ (514.5 nm)	
Argon ion	514.5	1.00	33
	501.7	0.15	5
	496.5	0.25	8
	488.0	1.00	33
	476.5	0.40	13
	457.9	0.20	7
		$w_R(\lambda_i)/w_R$ (535.3 nm)	
Xenon ion	495.4	0.86	17
	500.8	0.83	17
	515.9	0.47	9
	526.0	0.89	18
	535.3	1.00	20
	539.6	0.94	19
		$w_R(\lambda_i)/w_R$ (532.4 nm)	
Neodymium YAG (doubled)	532.4	1.00	100

Table 6.7. Spectral Responses of Photosensitive Surfaces.

Wavelength	Type II Photo-conductor	S-20 Photo-cathode	Type V Photoconductor
400.	.0425	.0760	.2100
410.	.0480	.0770	.2250
420.	.0530	.0780	.2400
430.	.0580	.0770	.2550
440.	.0630	.0760	.2700
450.	.0680	.0750	.2830
460.	.0725	.0740	.2960
470.	.0770	.0715	.3090
480.	.0820	.0690	.3220
490.	.0860	.0670	.3330
500.	.0900	.0650	.3430
510.	.0935	.0625	.3530
520.	.0970	.0600	.3610
530.	.1000	.0570	.3680
540.	.1030	.0540	.3760
550.	.1050	.0515	.3850
560.	.1030	.0490	.3880
570.	.0990	.0460	.3840
580.	.0940	.0430	.3800
590.	.0890	.0402	.3750
600.	.0830	.0375	.3750
610.	.0770	.0352	.3760
620.	.0710	.0330	.3770
630.	.0660	.0305	.3780
640.	.0600	.0280	.3790
650.	.0550	.0255	.3800
660.	.0500	.0230	.3810
670.	.0450	.0204	.3820
680.	.0400	.0178	.3840
690.	.0370	.0161	.3860
700.	.0330	.0144	.3890

Table 6.8. Combined Spectral Characteristics of Light Sources and Receivers.

S-20 Photocathode (Multialkali).

Wavelength	Incandescent Source	Hg Arc Source	TII Hg Arc Source	Xenon Arc Source
400.	0.00E-01	0.00E-01	0.00E-01	0.00E-01
410.	1.15E-04	2.19E-03	2.55E-04	3.43E-04
420.	2.23E-04	2.24E-03	5.83E-04	6.63E-04
430.	3.47E-04	2.28E-03	1.01E-03	9.36E-04
440.	4.60E-04	5.74E-03	1.58E-03	1.18E-03
450.	5.98E-04	5.74E-03	2.04E-03	1.40E-03
460.	7.26E-04	5.74E-03	2.52E-03	1.64E-03
470.	8.66E-04	5.74E-03	2.94E-03	1.89E-03
480.	9.93E-04	5.74E-03	3.33E-03	2.12E-03
490.	1.12E-03	5.74E-03	3.70E-03	2.37E-03
500.	1.30E-03	5.74E-03	4.05E-03	2.62E-03
510.	1.53E-03	5.74E-03	4.48E-03	2.80E-03
520.	1.75E-03	5.74E-03	4.96E-03	2.97E-03
530.	1.98E-03	5.74E-03	5.48E-03	3.13E-03
540.	2.19E-03	5.74E-03	9.24E-03	3.27E-03
550.	2.39E-03	7.64E-03	1.01E-02	3.42E-03
560.	2.60E-03	7.64E-03	1.04E-02	3.58E-03
570.	2.80E-03	7.64E-03	1.06E-02	3.70E-03
580.	2.99E-03	8.66E-03	1.08E-02	3.81E-03
590.	3.17E-03	9.07E-03	1.09E-02	3.92E-03
600.	3.35E-03	9.07E-03	1.10E-02	4.01E-03
610.	3.52E-03	9.07E-03	1.12E-02	4.11E-03
620.	3.69E-03	9.07E-03	1.12E-02	4.20E-03
630.	3.87E-03	9.07E-03	1.14E-02	4.29E-03
640.	4.03E-03	9.07E-03	1.15E-02	4.36E-03
650.	4.17E-03	9.07E-03	1.16E-02	4.44E-03
660.	4.30E-03	9.07E-03	1.17E-02	4.51E-03
670.	4.42E-03	9.07E-03	1.18E-02	4.56E-03
680.	4.52E-03	9.07E-03	1.18E-02	4.61E-03
690.	4.61E-03	9.07E-03	1.19E-02	4.65E-03
700.	4.69E-03	9.07E-03	1.19E-02	4.69E-03

(Note: 1.00 E-01 = 1.00×10^{-1}.)

Table 6.8. (Continued)

Type II Photoconductor (Antimony Trisulfide).

Wavelength	Incandescent Source	Hg Arc Source	TII Hg Arc Source	Xenon Arc Source
400.	0.00E-01	0.00E-01	0.00E-01	0.00E-01
410.	7.18E-05	1.37E-03	1.59E-04	2.14E-04
420.	1.45E-04	1.40E-03	3.82E-04	4.31E-04
430.	2.38E-04	1.43E-03	7.02E-04	6.37E-04
440.	3.32E-04	4.30E-03	1.18E-03	8.38E-04
450.	4.58E-04	4.30E-03	1.60E-03	1.04E-03
460.	5.83E-04	4.30E-03	2.06E-03	1.27E-03
470.	7.33E-04	4.30E-03	2.52E-03	1.55E-03
480.	8.84E-04	4.30E-03	2.97E-03	1.82E-03
490.	1.04E-03	4.30E-03	3.45E-03	2.14E-03
500.	1.30E-03	4.30E-03	3.95E-03	2.48E-03
510.	1.63E-03	4.30E-03	4.59E-03	2.75E-03
520.	2.00E-03	4.30E-03	5.36E-03	3.03E-03
530.	2.39E-03	4.30E-03	6.26E-03	3.32E-03
540.	2.81E-03	4.30E-03	1.34E-02	3.57E-03
550.	3.22E-03	8.16E-03	1.51E-02	3.88E-03
560.	3.65E-03	8.16E-03	1.59E-02	4.22E-03
570.	4.08E-03	8.16E-03	1.63E-02	4.48E-03
580.	4.49E-03	1.04E-02	1.66E-02	4.72E-03
590.	4.90E-03	1.13E-02	1.70E-02	4.95E-03
600.	5.29E-03	1.13E-02	1.72E-02	5.17E-03
610.	5.67E-03	1.13E-02	1.75E-02	5.37E-03
620.	6.04E-03	1.13E-02	1.77E-02	5.57E-03
630.	6.42E-03	1.13E-02	1.80E-02	5.76E-03
640.	6.76E-03	1.13E-02	1.83E-02	5.92E-03
650.	7.07E-03	1.13E-02	1.85E-02	6.09E-03
660.	7.34E-03	1.13E-02	1.87E-02	6.23E-03
670.	7.61E-03	1.13E-02	1.89E-02	6.36E-03
680.	7.84E-03	1.13E-02	1.90E-02	6.46E-03
690.	8.05E-03	1.13E-02	1.91E-02	6.56E-03
700.	8.23E-03	1.13E-02	1.91E-02	6.64E-03

(Note: 1.00E-01 = 1.00×10^{-1}.)

Table 6.8. (Continued)

Type V Photoconductor (Silicon Diode).

Wavelength	Incandescent Source	Hg Arc Source	TII Hg Arc Source	Xenon Arc Source
400.	0.00E-01	0.00E-01	0.00E-01	0.00E-01
410.	3.36E-04	6.41E-03	7.46E-04	1.00E-03
420.	6.68E-04	6.55E-03	1.75E-03	1.99E-03
430.	1.08E-03	6.69E-03	3.16E-03	2.89E-03
440.	1.48E-03	1.90E-02	5.19E-03	3.75E-03
450.	2.00E-03	1.90E-02	6.94E-03	4.58E-03
460.	2.51E-03	1.90E-02	8.84E-03	5.54E-03
470.	3.12E-03	1.90E-02	1.07E-02	6.64E-03
480.	3.71E-03	1.90E-02	1.25E-02	7.73E-03
490.	4.32E-03	1.90E-02	1.43E-02	8.94E-03
500.	5.31E-03	1.90E-02	1.62E-02	1.02E-02
510.	6.57E-03	1.90E-02	1.86E-02	1.13E-02
520.	7.94E-03	1.90E-02	2.15E-02	1.23E-02
530.	9.38E-03	1.90E-02	2.48E-02	1.34E-02
540.	1.09E-02	1.90E-02	5.10E-02	1.43E-02
550.	1.24E-02	3.32E-02	5.71E-02	1.54E-02
560.	1.40E-02	3.32E-02	6.00E-02	1.67E-02
570.	1.57E-02	3.32E-02	6.16E-02	1.77E-02
580.	1.73E-02	4.22E-02	6.31E-02	1.87E-02
590.	1.91E-02	4.60E-02	6.45E-02	1.97E-02
600.	2.08E-02	4.60E-02	6.56E-02	2.06E-02
610.	2.27E-02	4.60E-02	6.71E-02	2.16E-02
620.	2.46E-02	4.60E-02	6.77E-02	2.27E-02
630.	2.68E-02	4.60E-02	7.00E-02	2.38E-02
640.	2.90E-02	4.60E-02	7.17E-02	2.48E-02
650.	3.11E-02	4.60E-02	7.30E-02	2.59E-02
660.	3.32E-02	4.60E-02	7.45E-02	2.71E-02
670.	3.54E-02	4.60E-02	7.59E-02	2.81E-02
680.	3.76E-02	4.60E-02	7.71E-02	2.91E-02
690.	3.99E-02	4.60E-02	7.77E-02	3.02E-02
700.	4.20E-02	4.60E-02	7.84E-02	3.11E-02

(Note: 1.00E-01 = 1.00×10^{-1}.)

Table 6.9. Values of E_2 (x).

x	0	1	2	3	4	5
.0	.1000E 01	.9680E 00	.9371E 00	.9072E 00	.8782E 00	.8501E 00
.1	.7227E 00	.7062E 00	.6902E 00	.6745E 00	.6591E 00	.6442E 00
.2	.5742E 00	.5627E 00	.5514E 00	.5404E 00	.5296E 00	.5190E 00
.3	.4691E 00	.4605E 00	.4520E 00	.4436E 00	.4354E 00	.4274E 00
.4	.3894E 00	.3826E 00	.3759E 00	.3694E 00	.3629E 00	.3566E 00
.5	.3266E 00	.3212E 00	.3158E 00	.3106E 00	.3054E 00	.3003E 00
.6	.2762E 00	.2717E 00	.2674E 00	.2631E 00	.2589E 00	.2547E 00
.7	.2350E 00	.2313E 00	.2277E 00	.2242E 00	.2207E 00	.2172E 00
.8	.2009E 00	.1978E 00	.1948E 00	.1919E 00	.1890E 00	.1861E 00
.9	.1724E 00	.1699E 00	.1673E 00	.1649E 00	.1624E 00	.1600E 00

x	5	6	7	8	9	10
.0	.8501E 00	.8229E 00	.7966E 00	.7712E 00	.7465E 00	.7227E 00
.1	.6442E 00	.6295E 00	.6152E 00	.6012E 00	.5875E 00	.5742E 00
.2	.5190E 00	.5086E 00	.4984E 00	.4885E 00	.4787E 00	.4691E 00
.3	.4274E 00	.4195E 00	.4118E 00	.4042E 00	.3967E 00	.3894E 00
.4	.3566E 00	.3504E 00	.3443E 00	.3383E 00	.3324E 00	.3266E 00
.5	.3003E 00	.2953E 00	.2904E 00	.2856E 00	.2808E 00	.2762E 00
.6	.2547E 00	.2506E 00	.2466E 00	.2427E 00	.2388E 00	.2350E 00
.7	.2172E 00	.2139E 00	.2105E 00	.2073E 00	.2040E 00	.2009E 00
.8	.1861E 00	.1833E 00	.1805E 00	.1778E 00	.1751E 00	.1724E 00
.9	.1600E 00	.1576E 00	.1553E 00	.1530E 00	.1507E 00	.1485E 00

Table 6.9. (Continued)

x	0	1	2	3	4	5
1.0	.1485E 00	.1463E 00	.1442E 00	.1421E 00	.1401E 00	.1380E 00
1.1	.1283E 00	.1265E 00	.1246E 00	.1229E 00	.1211E 00	.1194E 00
1.2	.1111E 00	.1095E 00	.1080E 00	.1065E 00	.1050E 00	.1035E 00
1.3	.9644E-01	.9511E-01	.9379E-01	.9249E-01	.9121E-01	.8995E-01
1.4	.8389E-01	.8274E-01	.8161E-01	.8049E-01	.7939E-01	.7831E-01
1.5	.7310E-01	.7211E-01	.7114E-01	.7018E-01	.6923E-01	.6829E-01
1.6	.6380E-01	.6295E-01	.6211E-01	.6128E-01	.6046E-01	.5965E-01
1.7	.5577E-01	.5503E-01	.5430E-01	.5358E-01	.5288E-01	.5218E-01
1.8	.4881E-01	.4817E-01	.4754E-01	.4692E-01	.4630E-01	.4570E-01
1.9	.4278E-01	.4222E-01	.4168E-01	.4113E-01	.4060E-01	.4007E-01

x	5	6	7	8	9	10
1.0	.1380E 00	.1360E 00	.1340E 00	.1321E 00	.1302E 00	.1283E 00
1.1	.1194E 00	.1177E 00	.1160E 00	.1143E 00	.1127E 00	.1111E 00
1.2	.1035E 00	.1021E 00	.1006E 00	.9921E-01	.9782E-01	.9644E-01
1.3	.8995E-01	.8870E-01	.8747E-01	.8626E-01	.8507E-01	.8389E-01
1.4	.7831E-01	.7724E-01	.7618E-01	.7514E-01	.7411E-01	.7310E-01
1.5	.6829E-01	.6737E-01	.6646E-01	.6556E-01	.6468E-01	.6380E-01
1.6	.5965E-01	.5885E-01	.5807E-01	.5729E-01	.5652E-01	.5577E-01
1.7	.5218E-01	.5149E-01	.5080E-01	.5013E-01	.4947E-01	.4881E-01
1.8	.4570E-01	.4510E-01	.4451E-01	.4392E-01	.4335E-01	.4278E-01
1.9	.4007E-01	.3955E-01	.3904E-01	.3853E-01	.3803E-01	.3754E-01

Table 6.9. (Continued)

x	0	1	2	3	4	5
2.0	.3754E-01	.3705E-01	.3657E-01	.3610E-01	.3564E-01	.3518E-01
2.1	.3297E-01	.3253E-01	.3213E-01	.3172E-01	.3131E-01	.3091E-01
2.2	.2898E-01	.2862E-01	.2825E-01	.2789E-01	.2754E-01	.2719E-01
2.3	.2550E-01	.2518E-01	.2487E-01	.2455E-01	.2424E-01	.2394E-01
2.4	.2246E-01	.2218E-01	.2190E-01	.2163E-01	.2136E-01	.2109E-01
2.5	.1980E-01	.1955E-01	.1931E-01	.1907E-01	.1883E-01	.1859E-01
2.6	.1746E-01	.1725E-01	.1703E-01	.1682E-01	.1661E-01	.1641E-01
2.7	.1541E-01	.1522E-01	.1504E-01	.1485E-01	.1467E-01	.1449E-01
2.8	.1362E-01	.1345E-01	.1328E-01	.1312E-01	.1296E-01	.1280E-01
2.9	.1203E-01	.1189E-01	.1174E-01	.1160E-01	.1146E-01	.1132E-01

x	5	6	7	8	9	10
2.0	.3518E-01	.3472E-01	.3428E-01	.3383E-01	.3340E-01	.3297E-01
2.1	.3091E-01	.3052E-01	.3013E-01	.2974E-01	.2936E-01	.2898E-01
2.2	.2719E-01	.2684E-01	.2650E-01	.2617E-01	.2583E-01	.2550E-01
2.3	.2394E-01	.2363E-01	.2333E-01	.2304E-01	.2275E-01	.2246E-01
2.4	.2109E-01	.2082E-01	.2056E-01	.2030E-01	.2005E-01	.1980E-01
2.5	.1859E-01	.1836E-01	.1813E-01	.1791E-01	.1768E-01	.1746E-01
2.6	.1641E-01	.1620E-01	.1600E-01	.1580E-01	.1561E-01	.1541E-01
2.7	.1449E-01	.1431E-01	.1413E-01	.1396E-01	.1379E-01	.1362E-01
2.8	.1280E-01	.1264E-01	.1249E-01	.1233E-01	.1218E-01	.1203E-01
2.9	.1132E-01	.1118E-01	.1104E-01	.1091E-01	.1077E-01	.1064E-01

Table 6.9. (Continued)

x	0	1	2	3	4	5
3.0	.1064E-01	.1051E-01	.1039E-01	.1026E-01	.1013E-01	.1001E-01
3.1	.9417E-02	.9303E-02	.9190E-02	.9079E-02	.8969E-02	.8860E-02
3.2	.8337E-02	.8236E-02	.8137E-02	.8039E-02	.7942E-02	.7846E-02
3.3	.7384E-02	.7296E-02	.7208E-02	.7122E-02	.7036E-02	.6952E-02
3.4	.6544E-02	.6466E-02	.6388E-02	.6312E-02	.6236E-02	.6162E-02
3.5	.5802E-02	.5733E-02	.5665E-02	.5597E-02	.5530E-02	.5464E-02
3.6	.5146E-02	.5085E-02	.5025E-02	.4965E-02	.4906E-02	.4848E-02
3.7	.4567E-02	.4513E-02	.4459E-02	.4406E-02	.4354E-02	.4303E-02
3.8	.4054E-02	.4006E-02	.3959E-02	.3912E-02	.3866E-02	.3820E-02
3.9	.3600E-02	.3558E-02	.3516E-02	.3475E-02	.3434E-02	.3393E-02

x	5	6	7	8	9	10
3.0	.1001E-01	.9889E-02	.9769E-02	.9650E-02	.9533E-02	.9417E-02
3.1	.8860E-02	.8753E-02	.8647E-02	.8542E-02	.8439E-02	.8337E-02
3.2	.7846E-02	.7752E-02	.7658E-02	.7566E-02	.7475E-02	.7385E-02
3.3	.6952E-02	.6868E-02	.6786E-02	.6704E-02	.6624E-02	.6544E-02
3.4	.6162E-02	.6088E-02	.6015E-02	.5943E-02	.5872E-02	.5802E-02
3.5	.5464E-02	.5399E-02	.5335E-02	.5271E-02	.5208E-02	.5146E-02
3.6	.4848E-02	.4790E-02	.4733E-02	.4677E-02	.4622E-02	.4567E-02
3.7	.4303E-02	.4252E-02	.4201E-02	.4152E-02	.4102E-02	.4054E-02
3.8	.3820E-02	.3775E-02	.3731E-02	.3687E-02	.3643E-02	.3600E-02
3.9	.3393E-02	.3353E-02	.3314E-02	.3275E-02	.3236E-02	.3198E-02

Table 6.9. (Continued)

x	0	1	2	3	4	5
4.0	.3198E-02	.3161E-02	.3124E-02	.3087E-02	.3051E-02	.3015E-02
4.1	.2842E-02	.2809E-02	.2776E-02	.2744E-02	.2712E-02	.2680E-02
4.2	.2527E-02	.2497E-02	.2468E-02	.2439E-02	.2411E-02	.2383E-02
4.3	.2247E-02	.2221E-02	.2195E-02	.2170E-02	.2144E-02	.2119E-02
4.4	.1999E-02	.1976E-02	.1953E-02	.1930E-02	.1908E-02	.1886E-02
4.5	.1779E-02	.1758E-02	.1738E-02	.1718E-02	.1698E-02	.1678E-02
4.6	.1583E-02	.1565E-02	.1547E-02	.1529E-02	.1511E-02	.1494E-02
4.7	.1410E-02	.1393E-02	.1377E-02	.1361E-02	.1346E-02	.1330E-02
4.8	.1255E-02	.1241E-02	.1227E-02	.1213E-02	.1199E-02	.1185E-02
4.9	.1118E-02	.1106E-02	.1093E-02	.1080E-02	.1068E-02	.1056E-02

x	5	6	7	8	9	10
4.0	.3015E-02	.2980E-02	.2945E-02	.2910E-02	.2876E-02	.2842E-02
4.1	.2680E-02	.2649E-02	.2618E-02	.2587E-02	.2557E-02	.2527E-02
4.2	.2383E-02	.2355E-02	.2328E-02	.2300E-02	.2274E-02	.2247E-02
4.3	.2119E-02	.2095E-02	.2070E-02	.2046E-02	.2022E-02	.1999E-02
4.4	.1886E-02	.1864E-02	.1842E-02	.1821E-02	.1800E-02	.1779E-02
4.5	.1678E-02	.1659E-02	.1640E-02	.1621E-02	.1602E-02	.1583E-02
4.6	.1494E-02	.1477E-02	.1460E-02	.1443E-02	.1426E-02	.1410E-02
4.7	.1330E-02	.1315E-02	.1300E-02	.1285E-02	.1270E-02	.1255E-02
4.8	.1185E-02	.1171E-02	.1158E-02	.1144E-02	.1131E-02	.1118E-02
4.9	.1056E-02	.1044E-02	.1032E-02	.1020E-02	.1008E-02	.9965E-03

Table 6.9. (Continued)

x	0	1	2	3	4	5
5.0	.9965E-03	.9851E-03	.9738E-03	.9626E-03	.9516E-03	.9407E-03
5.1	.8881E-03	.8780E-03	.8680E-03	.8580E-03	.8483E-03	.8386E-03
5.2	.7917E-03	.7827E-03	.7738E-03	.7650E-03	.7563E-03	.7476E-03
5.3	.7060E-03	.6980E-03	.6900E-03	.6822E-03	.6744E-03	.6667E-03
5.4	.6296E-03	.6225E-03	.6154E-03	.6084E-03	.6015E-03	.5947E-03
5.5	.5617E-03	.5553E-03	.5490E-03	.5428E-03	.5366E-03	.5306E-03
5.6	.5012E-03	.4955E-03	.4899E-03	.4843E-03	.4789E-03	.4734E-03
5.7	.4473E-03	.4422E-03	.4372E-03	.4323E-03	.4274E-03	.4226E-03
5.8	.3992E-03	.3947E-03	.3903E-03	.3859E-03	.3815E-03	.3772E-03
5.9	.3564E-03	.3524E-03	.3484E-03	.3445E-03	.3406E-03	.3368E-03

x	5	6	7	8	9	10
5.0	.9407E-03	.9300E-03	.9193E-03	.9088E-03	.8984E-03	.8881E-03
5.1	.8386E-03	.8290E-03	.8195E-03	.8102E-03	.8009E-03	.7918E-03
5.2	.7476E-03	.7391E-03	.7307E-03	.7224E-03	.7141E-03	.7060E-03
5.3	.6667E-03	.6591E-03	.6516E-03	.6442E-03	.6369E-03	.6297E-03
5.4	.5947E-03	.5879E-03	.5813E-03	.5747E-03	.5681E-03	.5617E-03
5.5	.5306E-03	.5245E-03	.5186E-03	.5127E-03	.5069E-03	.5012E-03
5.6	.4734E-03	.4681E-03	.4628E-03	.4576E-03	.4524E-03	.4473E-03
5.7	.4226E-03	.4178E-03	.4131E-03	.4084E-03	.4038E-03	.3992E-03
5.8	.3772E-03	.3730E-03	.3688E-03	.3646E-03	.3605E-03	.3564E-03
5.9	.3368E-03	.3330E-03	.3293E-03	.3256E-03	.3219E-03	.3183E-03

Table 6.9. (Continued)

x	0	1	2	3	4	5
6.0	.3183E-03	.3147E-03	.3111E-03	.3076E-03	.3042E-03	.3008E-03
6.1	.2842E-03	.2811E-03	.2779E-03	.2748E-03	.2717E-03	.2686E-03
6.2	.2539E-03	.2511E-03	.2482E-03	.2455E-03	.2427E-03	.2400E-03
6.3	.2268E-03	.2243E-03	.2218E-03	.2193E-03	.2169E-03	.2144E-03
6.4	.2027E-03	.2004E-03	.1982E-03	.1960E-03	.1938E-03	.1916E-03
6.5	.1811E-03	.1791E-03	.1771E-03	.1751E-03	.1732E-03	.1713E-03
6.6	.1619E-03	.1601E-03	.1583E-03	.1566E-03	.1548E-03	.1531E-03
6.7	.1448E-03	.1431E-03	.1415E-03	.1400E-03	.1384E-03	.1369E-03
6.8	.1294E-03	.1280E-03	.1266E-03	.1252E-03	.1238E-03	.1224E-03
6.9	.1157E-03	.1145E-03	.1132E-03	.1119E-03	.1107E-03	.1095E-03

x	5	6	7	8	9	10
6.0	.3008E-03	.2974E-03	.2940E-03	.2907E-03	.2875E-03	.2842E-03
6.1	.2686E-03	.2656E-03	.2626E-03	.2597E-03	.2568E-03	.2539E-03
6.2	.2400E-03	.2373E-03	.2346E-03	.2320E-03	.2294E-03	.2268E-03
6.3	.2144E-03	.2120E-03	.2097E-03	.2073E-03	.2050E-03	.2027E-03
6.4	.1916E-03	.1895E-03	.1874E-03	.1853E-03	.1832E-03	.1811E-03
6.5	.1713E-03	.1694E-03	.1675E-03	.1656E-03	.1637E-03	.1619E-03
6.6	.1531E-03	.1514E-03	.1497E-03	.1480E-03	.1464E-03	.1448E-03
6.7	.1369E-03	.1354E-03	.1338E-03	.1324E-03	.1309E-03	.1294E-03
6.8	.1224E-03	.1210E-03	.1197E-03	.1184E-03	.1170E-03	.1157E-03
6.9	.1095E-03	.1082E-03	.1070E-03	.1058E-03	.1047E-03	.1035E-03

Table 6.9. (Continued)

x	0	1	2	3	4	5
7.0	.1035E-03	.1024E-03	.1012E-03	.1001E-03	.9900E-04	.9790E-04
7.1	.9259E-04	.9156E-04	.9055E-04	.8955E-04	.8856E-04	.8758E-04
7.2	.8283E-04	.8192E-04	.8101E-04	.8012E-04	.7923E-04	.7835E-04
7.3	.7411E-04	.7330E-04	.7249E-04	.7169E-04	.7089E-04	.7011E-04
7.4	.6632E-04	.6559E-04	.6486E-04	.6415E-04	.6344E-04	.6274E-04
7.5	.5935E-04	.5870E-04	.5805E-04	.5741E-04	.5678E-04	.5615E-04
7.6	.5313E-04	.5254E-04	.5196E-04	.5139E-04	.5083E-04	.5027E-04
7.7	.4756E-04	.4703E-04	.4652E-04	.4601E-04	.4550E-04	.4500E-04
7.8	.4258E-04	.4211E-04	.4165E-04	.4119E-04	.4074E-04	.4029E-04
7.9	.3812E-04	.3770E-04	.3729E-04	.3688E-04	.3648E-04	.3608E-04

x	5	6	7	8	9	10
7.0	.9790E-04	.9681E-04	.9574E-04	.9468E-04	.9363E-04	.9259E-04
7.1	.8758E-04	.8661E-04	.8565E-04	.8470E-04	.8376E-04	.8283E-04
7.2	.7835E-04	.7749E-04	.7663E-04	.7578E-04	.7494E-04	.7412E-04
7.3	.7011E-04	.6933E-04	.6857E-04	.6781E-04	.6706E-04	.6632E-04
7.4	.6274E-04	.6205E-04	.6136E-04	.6069E-04	.6002E-04	.5935E-04
7.5	.5615E-04	.5554E-04	.5492E-04	.5432E-04	.5372E-04	.5313E-04
7.6	.5027E-04	.4971E-04	.4916E-04	.4862E-04	.4809E-04	.4756E-04
7.7	.4500E-04	.4450E-04	.4401E-04	.4353E-04	.4305E-04	.4258E-04
7.8	.4029E-04	.3985E-04	.3941E-04	.3898E-04	.3855E-04	.3812E-04
7.9	.3608E-04	.3568E-04	.3529E-04	.3490E-04	.3452E-04	.3414E-04

Table 6.9. (Continued)

x	0	1	2	3	4	5
8.0	.3414E-04	.3376E-04	.3339E-04	.3303E-04	.3266E-04	.3231E-04
8.1	.3057E-04	.3024E-04	.2991E-04	.2958E-04	.2926E-04	.2894E-04
8.2	.2738E-04	.2708E-04	.2679E-04	.2650E-04	.2621E-04	.2592E-04
8.3	.2453E-04	.2426E-04	.2400E-04	.2373E-04	.2347E-04	.2322E-04
8.4	.2198E-04	.2174E-04	.2150E-04	.2126E-04	.2103E-04	.2080E-04
8.5	.1969E-04	.1947E-04	.1926E-04	.1905E-04	.1884E-04	.1864E-04
8.6	.1764E-04	.1745E-04	.1726E-04	.1707E-04	.1689E-04	.1670E-04
8.7	.1581E-04	.1564E-04	.1547E-04	.1530E-04	.1513E-04	.1497E-04
8.8	.1417E-04	.1401E-04	.1386E-04	.1371E-04	.1356E-04	.1341E-04
8.9	.1270E-04	.1256E-04	.1242E-04	.1229E-04	.1216E-04	.1202E-04

x	5	6	7	8	9	10
8.0	.3231E-04	.3195E-04	.3160E-04	.3126E-04	.3091E-04	.3057E-04
8.1	.2894E-04	.2862E-04	.2830E-04	.2799E-04	.2769E-04	.2738E-04
8.2	.2592E-04	.2563E-04	.2535E-04	.2508E-04	.2480E-04	.2453E-04
8.3	.2322E-04	.2296E-04	.2271E-04	.2246E-04	.2222E-04	.2198E-04
8.4	.2080E-04	.2057E-04	.2035E-04	.2013E-04	.1991E-04	.1969E-04
8.5	.1864E-04	.1843E-04	.1823E-04	.1803E-04	.1784E-04	.1764E-04
8.6	.1670E-04	.1652E-04	.1634E-04	.1616E-04	.1598E-04	.1581E-04
8.7	.1497E-04	.1480E-04	.1464E-04	.1448E-04	.1433E-04	.1417E-04
8.8	.1341E-04	.1327E-04	.1312E-04	.1298E-04	.1284E-04	.1270E-04
8.9	.1202E-04	.1189E-04	.1176E-04	.1164E-04	.1151E-04	.1138E-04

Table 6.9. (Continued)

x	0	1	2	3	4	5
9.0	.1138E-04	.1126E-04	.1114E-04	.1102E-04	.1090E-04	.1078E-04
9.1	.1021E-04	.1009E-04	.9985E-05	.9876E-05	.9769E-05	.9663E-05
9.2	.9149E-05	.9050E-05	.8952E-05	.8855E-05	.8759E-05	.8664E-05
9.3	.8203E-05	.8115E-05	.8027E-05	.7940E-05	.7853E-05	.7768E-05
9.4	.7356E-05	.7276E-05	.7198E-05	.7120E-05	.7042E-05	.6966E-05
9.5	.6597E-05	.6525E-05	.6455E-05	.6385E-05	.6315E-05	.6247E-05
9.6	.5916E-05	.5852E-05	.5789E-05	.5726E-05	.5664E-05	.5603E-05
9.7	.5306E-05	.5249E-05	.5192E-05	.5136E-05	.5080E-05	.5026E-05
9.8	.4760E-05	.4708E-05	.4657E-05	.4607E-05	.4557E-05	.4508E-05
9.9	.4270E-05	.4224E-05	.4178E-05	.4133E-05	.4088E-05	.4044E-05

x	5	6	7	8	9	10
9.0	.1078E-04	.1066E-04	.1055E-04	.1043E-04	.1032E-04	.1021E-04
9.1	.9663E-05	.9558E-05	.9454E-05	.9352E-05	.9250E-05	.9150E-05
9.2	.8664E-05	.8570E-05	.8477E-05	.8385E-05	.8294E-05	.8204E-05
9.3	.7768E-05	.7684E-05	.7601E-05	.7518E-05	.7437E-05	.7356E-05
9.4	.6966E-05	.6891E-05	.6816E-05	.6742E-05	.6669E-05	.6597E-05
9.5	.6247E-05	.6179E-05	.6113E-05	.6046E-05	.5981E-05	.5916E-05
9.6	.5603E-05	.5542E-05	.5482E-05	.5423E-05	.5364E-05	.5306E-05
9.7	.5026E-05	.4971E-05	.4917E-05	.4864E-05	.4812E-05	.4760E-05
9.8	.4508E-05	.4459E-05	.4411E-05	.4363E-05	.4316E-05	.4270E-05
9.9	.4044E-05	.4000E-05	.3957E-05	.3914E-05	.3872E-05	.3830E-05

Table 6.9. (Continued)

x	0	1	2	3	4	5
10.0	.3830E-05	.3789E-05	.3748E-05	.3708E-05	.3668E-05	.3628E-05
10.1	.3437E-05	.3400E-05	.3363E-05	.3327E-05	.3291E-05	.3255E-05
10.2	.3083E-05	.3050E-05	.3017E-05	.2985E-05	.2953E-05	.2921E-05
10.3	.2767E-05	.2737E-05	.2708E-05	.2678E-05	.2650E-05	.2621E-05
10.4	.2483E-05	.2456E-05	.2430E-05	.2404E-05	.2378E-05	.2352E-05
10.5	.2228E-05	.2204E-05	.2181E-05	.2157E-05	.2134E-05	.2111E-05
10.6	.2000E-05	.1978E-05	.1957E-05	.1936E-05	.1915E-05	.1895E-05
10.7	.1795E-05	.1776E-05	.1757E-05	.1738E-05	.1719E-05	.1701E-05
10.8	.1611E-05	.1594E-05	.1577E-05	.1560E-05	.1543E-05	.1527E-05
10.9	.1446E-05	.1431E-05	.1415E-05	.1400E-05	.1385E-05	.1370E-05

x	5	6	7	8	9	10
10.0	.3628E-05	.3589E-05	.3550E-05	.3512E-05	.3474E-05	.3437E-05
10.1	.3255E-05	.3220E-05	.3185E-05	.3151E-05	.3117E-05	.3083E-05
10.2	.2921E-05	.2889E-05	.2858E-05	.2827E-05	.2797E-05	.2767E-05
10.3	.2621E-05	.2593E-05	.2565E-05	.2537E-05	.2510E-05	.2483E-05
10.4	.2352E-05	.2327E-05	.2302E-05	.2277E-05	.2253E-05	.2228E-05
10.5	.2111E-05	.2088E-05	.2066E-05	.2044E-05	.2022E-05	.2000E-05
10.6	.1895E-05	.1874E-05	.1854E-05	.1834E-05	.1814E-05	.1795E-05
10.7	.1701E-05	.1682E-05	.1664E-05	.1646E-05	.1629E-05	.1611E-05
10.8	.1527E-05	.1510E-05	.1494E-05	.1478E-05	.1462E-05	.1446E-05
10.9	.1370E-05	.1356E-05	.1341E-05	.1327E-05	.1312E-05	.1298E-05

Table 6.9. (Continued)

x	0	1	2	3	4	5
11.0	.1298E-05	.1285E-05	.1271E-05	.1257E-05	.1244E-05	.1230E-05
11.1	.1166E-05	.1153E-05	.1141E-05	.1129E-05	.1117E-05	.1105E-05
11.2	.1047E-05	.1035E-05	.1024E-05	.1013E-05	.1003E-05	.9918E-06
11.3	.9398E-06	.9297E-06	.9198E-06	.9099E-06	.9002E-06	.8906E-06
11.4	.8439E-06	.8349E-06	.8259E-06	.8171E-06	.8084E-06	.7997E-06
11.5	.7578E-06	.7497E-06	.7417E-06	.7338E-06	.7259E-06	.7182E-06
11.6	.6806E-06	.6733E-06	.6661E-06	.6590E-06	.6519E-06	.6450E-06
11.7	.6112E-06	.6047E-06	.5982E-06	.5918E-06	.5855E-06	.5793E-06
11.8	.5490E-06	.5431E-06	.5373E-06	.5316E-06	.5259E-06	.5203E-06
11.9	.4931E-06	.4878E-06	.4826E-06	.4775E-06	.4724E-06	.4673E-06

x	5	6	7	8	9	10
11.0	.1230E-05	.1217E-05	.1204E-05	.1191E-05	.1178E-05	.1166E-05
11.1	.1105E-05	.1093E-05	.1081E-05	.1069E-05	.1058E-05	.1047E-05
11.2	.9918E-06	.9812E-06	.9706E-06	.9602E-06	.9500E-06	.9398E-06
11.3	.8906E-06	.8810E-06	.8716E-06	.8623E-06	.8530E-06	.8439E-06
11.4	.7997E-06	.7912E-06	.7827E-06	.7743E-06	.7660E-06	.7578E-06
11.5	.7182E-06	.7105E-06	.7029E-06	.6954E-06	.6879E-06	.6806E-06
11.6	.6450E-06	.6381E-06	.6312E-06	.6245E-06	.6178E-06	.6112E-06
11.7	.5793E-06	.5731E-06	.5670E-06	.5609E-06	.5549E-06	.5490E-06
11.8	.5203E-06	.5147E-06	.5092E-06	.5038E-06	.4984E-06	.4931E-06
11.9	.4673E-06	.4623E-06	.4574E-06	.4525E-06	.4477E-06	.4429E-06

Table 6.9. (Continued)

x	0	1	2	3	4	5
12.0	.4429E-06	.4382E-06	.4335E-06	.4289E-06	.4243E-06	.4198E-06
12.1	.3979E-06	.3936E-06	.3895E-06	.3853E-06	.3812E-06	.3771E-06
12.2	.3574E-06	.3536E-06	.3499E-06	.3461E-06	.3425E-06	.3388E-06
12.3	.3211E-06	.3177E-06	.3143E-06	.3110E-06	.3077E-06	.3044E-06
12.4	.2885E-06	.2855E-06	.2824E-06	.2794E-06	.2764E-06	.2735E-06
12.5	.2592E-06	.2565E-06	.2537E-06	.2510E-06	.2484E-06	.2457E-06
12.6	.2329E-06	.2305E-06	.2280E-06	.2256E-06	.2232E-06	.2208E-06
12.7	.2093E-06	.2071E-06	.2049E-06	.2027E-06	.2005E-06	.1984E-06
12.8	.1881E-06	.1861E-06	.1841E-06	.1822E-06	.1802E-06	.1783E-06
12.9	.1690E-06	.1672E-06	.1655E-06	.1637E-06	.1620E-06	.1602E-06

x	5	6	7	8	9	10
12.0	.4198E-06	.4153E-06	.4109E-06	.4065E-06	.4022E-06	.3979E-06
12.1	.3771E-06	.3731E-06	.3691E-06	.3652E-06	.3613E-06	.3575E-06
12.2	.3388E-06	.3352E-06	.3316E-06	.3281E-06	.3246E-06	.3211E-06
12.3	.3044E-06	.3012E-06	.2979E-06	.2948E-06	.2916E-06	.2885E-06
12.4	.2735E-06	.2706E-06	.2677E-06	.2648E-06	.2620E-06	.2592E-06
12.5	.2457E-06	.2431E-06	.2405E-06	.2380E-06	.2354E-06	.2329E-06
12.6	.2208E-06	.2185E-06	.2161E-06	.2138E-06	.2116E-06	.2093E-06
12.7	.1984E-06	.1963E-06	.1942E-06	.1921E-06	.1901E-06	.1881E-06
12.8	.1783E-06	.1764E-06	.1745E-06	.1727E-06	.1708E-06	.1690E-06
12.9	.1602E-06	.1585E-06	.1569E-06	.1552E-06	.1535E-06	.1519E-06

Table 6.9. (Continued)

x	0	1	2	3	4	5
13.0	.1519E-06	.1503E-06	.1487E-06	.1471E-06	.1456E-06	.1440E-06
13.1	.1365E-06	.1351E-06	.1336E-06	.1322E-06	.1308E-06	.1294E-06
13.2	.1227E-06	.1214E-06	.1201E-06	.1188E-06	.1176E-06	.1163E-06
13.3	.1103E-06	.1091E-06	.1080E-06	.1068E-06	.1057E-06	.1046E-06
13.4	.9915E-07	.9810E-07	.9706E-07	.9603E-07	.9501E-07	.9400E-07
13.5	.8912E-07	.8818E-07	.8724E-07	.8632E-07	.8540E-07	.8450E-07
13.6	.8011E-07	.7927E-07	.7843E-07	.7760E-07	.7678E-07	.7596E-07
13.7	.7202E-07	.7126E-07	.7051E-07	.6976E-07	.6902E-07	.6829E-07
13.8	.6475E-07	.6407E-07	.6339E-07	.6272E-07	.6205E-07	.6140E-07
13.9	.5822E-07	.5760E-07	.5699E-07	.5639E-07	.5579E-07	.5520E-07

x	5	6	7	8	9	10
13.0	.1440E-06	.1425E-06	.1410E-06	.1395E-06	.1380E-06	.1365E-06
13.1	.1294E-06	.1281E-06	.1267E-06	.1254E-06	.1240E-06	.1227E-06
13.2	.1163E-06	.1151E-06	.1139E-06	.1127E-06	.1115E-06	.1103E-06
13.3	.1046E-06	.1035E-06	.1024E-06	.1013E-06	.1002E-06	.9915E-07
13.4	.9400E-07	.9300E-07	.9202E-07	.9104E-07	.9008E-07	.8912E-07
13.5	.8450E-07	.8360E-07	.8272E-07	.8184E-07	.8097E-07	.8012E-07
13.6	.7596E-07	.7516E-07	.7436E-07	.7357E-07	.7279E-07	.7202E-07
13.7	.6829E-07	.6757E-07	.6685E-07	.6615E-07	.6545E-07	.6475E-07
13.8	.6140E-07	.6075E-07	.6011E-07	.5947E-07	.5884E-07	.5822E-07
13.9	.5520E-07	.5462E-07	.5404E-07	.5347E-07	.5290E-07	.5234E-07

Table 6.9. (Continued)

x	0	1	2	3	4	5
14.0	.5234E-07	.5179E-07	.5124E-07	.5070E-07	.5016E-07	.4963E-07
14.1	.4707E-07	.4657E-07	.4607E-07	.4559E-07	.4510E-07	.4463E-07
14.2	.4232E-07	.4187E-07	.4143E-07	.4099E-07	.4056E-07	.4013E-07
14.3	.3805E-07	.3765E-07	.3725E-07	.3686E-07	.3647E-07	.3609E-07
14.4	.3422E-07	.3386E-07	.3350E-07	.3315E-07	.3280E-07	.3245E-07
14.5	.3077E-07	.3045E-07	.3013E-07	.2981E-07	.2949E-07	.2918E-07
14.6	.2768E-07	.2738E-07	.2709E-07	.2681E-07	.2653E-07	.2625E-07
14.7	.2489E-07	.2463E-07	.2437E-07	.2411E-07	.2386E-07	.2360E-07
14.8	.2238E-07	.2215E-07	.2192E-07	.2168E-07	.2146E-07	.2123E-07
14.9	.2013E-07	.1992E-07	.1971E-07	.1950E-07	.1930E-07	.1910E-07

x	5	6	7	8	9	10
14.0	.4963E-07	.4911E-07	.4859E-07	.4808E-07	.4757E-07	.4707E-07
14.1	.4463E-07	.4416E-07	.4369E-07	.4323E-07	.4277E-07	.4232E-07
14.2	.4013E-07	.3970E-07	.3928E-07	.3887E-07	.3846E-07	.3805E-07
14.3	.3609E-07	.3570E-07	.3533E-07	.3495E-07	.3459E-07	.3422E-07
14.4	.3245E-07	.3211E-07	.3177E-07	.3143E-07	.3110E-07	.3077E-07
14.5	.2918E-07	.2887E-07	.2857E-07	.2827E-07	.2797E-07	.2768E-07
14.6	.2625E-07	.2597E-07	.2570E-07	.2542E-07	.2516E-07	.2489E-07
14.7	.2360E-07	.2336E-07	.2311E-07	.2286E-07	.2262E-07	.2239E-07
14.8	.2123E-07	.2101E-07	.2078E-07	.2057E-07	.2035E-07	.2013E-07
14.9	.1910E-07	.1889E-07	.1869E-07	.1850E-07	.1830E-07	.1811E-07

Table 6.9. (Continued)

x	0	1	2	3	4	5
15.0	.1811E-07	.1792E-07	.1773E-07	.1754E-07	.1736E-07	.1717E-07
15.1	.1629E-07	.1612E-07	.1595E-07	.1578E-07	.1561E-07	.1545E-07
15.2	.1465E-07	.1450E-07	.1435E-07	.1419E-07	.1404E-07	.1390E-07
15.3	.1318E-07	.1304E-07	.1290E-07	.1277E-07	.1263E-07	.1250E-07
15.4	.1186E-07	.1173E-07	.1161E-07	.1149E-07	.1137E-07	.1125E-07
15.5	.1067E-07	.1055E-07	.1044E-07	.1033E-07	.1022E-07	.1012E-07
15.6	.9596E-08	.9495E-08	.9395E-08	.9296E-08	.9199E-08	.9102E-08
15.7	.8633E-08	.8542E-08	.8453E-08	.8364E-08	.8276E-08	.8189E-08
15.8	.7767E-08	.7686E-08	.7605E-08	.7525E-08	.7446E-08	.7368E-08
15.9	.6988E-08	.6915E-08	.6842E-08	.6770E-08	.6699E-08	.6629E-08

x	5	6	7	8	9	10
15.0	.1717E-07	.1699E-07	.1681E-07	.1664E-07	.1646E-07	.1629E-07
15.1	.1545E-07	.1529E-07	.1513E-07	.1497E-07	.1481E-07	.1465E-07
15.2	.1390E-07	.1375E-07	.1361E-07	.1346E-07	.1332E-07	.1318E-07
15.3	.1250E-07	.1237E-07	.1224E-07	.1211E-07	.1198E-07	.1186E-07
15.4	.1125E-07	.1113E-07	.1101E-07	.1089E-07	.1078E-07	.1067E-07
15.5	.1012E-07	.1001E-07	.9905E-08	.9801E-08	.9698E-08	.9596E-08
15.6	.9102E-08	.9006E-08	.8912E-08	.8818E-08	.8725E-08	.8633E-08
15.7	.8189E-08	.8103E-08	.8018E-08	.7933E-08	.7850E-08	.7768E-08
15.8	.7368E-08	.7290E-08	.7213E-08	.7137E-08	.7063E-08	.6988E-08
15.9	.6629E-08	.6559E-08	.6490E-08	.6422E-08	.6354E-08	.6287E-08

Table 6.9. (Continued)

x	0	1	2	3	4	5
16.0	.6287E-08	.6221E-08	.6156E-08	.6091E-08	.6027E-08	.5964E-08
16.1	.5658E-08	.5598E-08	.5540E-08	.5481E-08	.5424E-08	.5367E-08
16.2	.5091E-08	.5038E-08	.4985E-08	.4932E-08	.4880E-08	.4829E-08
16.3	.4581E-08	.4533E-08	.4485E-08	.4438E-08	.4392E-08	.4346E-08
16.4	.4122E-08	.4079E-08	.4036E-08	.3994E-08	.3952E-08	.3910E-08
16.5	.3710E-08	.3671E-08	.3632E-08	.3594E-08	.3556E-08	.3519E-08
16.6	.3338E-08	.3303E-08	.3269E-08	.3235E-08	.3201E-08	.3167E-08
16.7	.3004E-08	.2973E-08	.2942E-08	.2911E-08	.2880E-08	.2850E-08
16.8	.2704E-08	.2675E-08	.2647E-08	.2620E-08	.2592E-08	.2565E-08
16.9	.2433E-08	.2408E-08	.2383E-08	.2358E-08	.2333E-08	.2309E-08

x	5	6	7	8	9	10
16.0	.5964E-08	.5902E-08	.5840E-08	.5778E-08	.5718E-08	.5658E-08
16.1	.5367E-08	.5310E-08	.5255E-08	.5199E-08	.5145E-08	.5091E-08
16.2	.4829E-08	.4779E-08	.4728E-08	.4679E-08	.4630E-08	.4581E-08
16.3	.4346E-08	.4300E-08	.4255E-08	.4210E-08	.4166E-08	.4122E-08
16.4	.3910E-08	.3869E-08	.3829E-08	.3789E-08	.3749E-08	.3710E-08
16.5	.3519E-08	.3482E-08	.3446E-08	.3410E-08	.3374E-08	.3339E-08
16.6	.3167E-08	.3134E-08	.3101E-08	.3068E-08	.3036E-08	.3004E-08
16.7	.2850E-08	.2820E-08	.2791E-08	.2761E-08	.2733E-08	.2704E-08
16.8	.2565E-08	.2538E-08	.2512E-08	.2485E-08	.2459E-08	.2434E-08
16.9	.2309E-08	.2284E-08	.2260E-08	.2237E-08	.2213E-08	.2190E-08

Table 6.9. (Continued)

x	0	1	2	3	4	5
17.0	.2190E-08	.2167E-08	.2145E-08	.2122E-08	.2100E-08	.2078E-08
17.1	.1971E-08	.1951E-08	.1930E-08	.1910E-08	.1890E-08	.1870E-08
17.2	.1774E-08	.1756E-08	.1737E-08	.1719E-08	.1701E-08	.1683E-08
17.3	.1597E-08	.1580E-08	.1564E-08	.1547E-08	.1531E-08	.1515E-08
17.4	.1438E-08	.1422E-08	.1408E-08	.1393E-08	.1378E-08	.1364E-08
17.5	.1294E-08	.1280E-08	.1267E-08	.1254E-08	.1241E-08	.1228E-08
17.6	.1165E-08	.1153E-08	.1141E-08	.1129E-08	.1117E-08	.1105E-08
17.7	.1049E-08	.1038E-08	.1027E-08	.1016E-08	.1005E-08	.9949E-09
17.8	.9440E-09	.9341E-09	.9243E-09	.9147E-09	.9051E-09	.8957E-09
17.9	.8498E-09	.8409E-09	.8321E-09	.8234E-09	.8148E-09	.8063E-09

x	5	6	7	8	9	10
17.0	.2078E-08	.2056E-08	.2035E-08	.2013E-08	.1992E-08	.1971E-08
17.1	.1870E-08	.1851E-08	.1831E-08	.1812E-08	.1793E-08	.1774E-08
17.2	.1683E-08	.1666E-08	.1648E-08	.1631E-08	.1614E-08	.1597E-08
17.3	.1515E-08	.1499E-08	.1484E-08	.1468E-08	.1453E-08	.1438E-08
17.4	.1364E-08	.1350E-08	.1335E-08	.1322E-08	.1308E-08	.1294E-08
17.5	.1228E-08	.1215E-08	.1202E-08	.1190E-08	.1177E-08	.1165E-08
17.6	.1105E-08	.1094E-08	.1082E-08	.1071E-08	.1060E-08	.1049E-08
17.7	.9949E-09	.9845E-09	.9742E-09	.9640E-09	.9540E-09	.9440E-09
17.8	.8957E-09	.8863E-09	.8770E-09	.8678E-09	.8588E-09	.8498E-09
17.9	.8063E-09	.7979E-09	.7895E-09	.7813E-09	.7731E-09	.7651E-09

Table 6.9. (Continued)

x	0	1	2	3	4	5
18.0	.7650E-09	.7571E-09	.7492E-09	.7413E-09	.7336E-09	.7259E-09
18.1	.6888E-09	.6816E-09	.6745E-09	.6675E-09	.6605E-09	.6536E-09
18.2	.6201E-09	.6136E-09	.6072E-09	.6009E-09	.5946E-09	.5884E-09
18.3	.5583E-09	.5525E-09	.5467E-09	.5410E-09	.5354E-09	.5298E-09
18.4	.5027E-09	.4975E-09	.4923E-09	.4871E-09	.4820E-09	.4770E-09
18.5	.4526E-09	.4479E-09	.4432E-09	.4386E-09	.4340E-09	.4295E-09
18.6	.4076E-09	.4033E-09	.3991E-09	.3949E-09	.3908E-09	.3867E-09
18.7	.3670E-09	.3631E-09	.3594E-09	.3556E-09	.3519E-09	.3482E-09
18.8	.3304E-09	.3270E-09	.3236E-09	.3202E-09	.3169E-09	.3136E-09
18.9	.2975E-09	.2944E-09	.2914E-09	.2883E-09	.2853E-09	.2824E-09

x	5	6	7	8	9	10
18.0	.7259E-09	.7184E-09	.7109E-09	.7034E-09	.6961E-09	.6888E-09
18.1	.6536E-09	.6468E-09	.6400E-09	.6333E-09	.6267E-09	.6201E-09
18.2	.5884E-09	.5823E-09	.5762E-09	.5702E-09	.5642E-09	.5583E-09
18.3	.5298E-09	.5243E-09	.5188E-09	.5134E-09	.5080E-09	.5027E-09
18.4	.4770E-09	.4720E-09	.4671E-09	.4622E-09	.4574E-09	.4526E-09
18.5	.4295E-09	.4250E-09	.4206E-09	.4162E-09	.4119E-09	.4076E-09
18.6	.3867E-09	.3827E-09	.3787E-09	.3748E-09	.3708E-09	.3670E-09
18.7	.3482E-09	.3446E-09	.3410E-09	.3375E-09	.3339E-09	.3304E-09
18.8	.3136E-09	.3103E-09	.3071E-09	.3039E-09	.3007E-09	.2976E-09
18.9	.2824E-09	.2794E-09	.2765E-09	.2736E-09	.2708E-09	.2679E-09

Table 6.9. (Continued)

x	0	1	2	3	4	5
19.0	.2679E-09	.2651E-09	.2624E-09	.2596E-09	.2569E-09	.2543E-09
19.1	.2413E-09	.2388E-09	.2363E-09	.2338E-09	.2314E-09	.2290E-09
19.2	.2173E-09	.2150E-09	.2128E-09	.2106E-09	.2084E-09	.2062E-09
19.3	.1957E-09	.1936E-09	.1916E-09	.1896E-09	.1876E-09	.1857E-09
19.4	.1762E-09	.1744E-09	.1726E-09	.1708E-09	.1690E-09	.1672E-09
19.5	.1587E-09	.1570E-09	.1554E-09	.1538E-09	.1522E-09	.1506E-09
19.6	.1429E-09	.1414E-09	.1400E-09	.1385E-09	.1371E-09	.1356E-09
19.7	.1287E-09	.1274E-09	.1261E-09	.1248E-09	.1235E-09	.1222E-09
19.8	.1159E-09	.1147E-09	.1135E-09	.1124E-09	.1112E-09	.1100E-09
19.9	.1044E-09	.1033E-09	.1023E-09	.1012E-09	.1001E-09	.9910E-10

x	5	6	7	8	9	10
19.0	.2543E-09	.2516E-09	.2490E-09	.2464E-09	.2438E-09	.2413E-09
19.1	.2290E-09	.2266E-09	.2242E-09	.2219E-09	.2196E-09	.2173E-09
19.2	.2062E-09	.2041E-09	.2019E-09	.1998E-09	.1977E-09	.1957E-09
19.3	.1857E-09	.1838E-09	.1818E-09	.1800E-09	.1781E-09	.1762E-09
19.4	.1672E-09	.1655E-09	.1638E-09	.1621E-09	.1604E-09	.1587E-09
19.5	.1506E-09	.1490E-09	.1475E-09	.1460E-09	.1444E-09	.1429E-09
19.6	.1356E-09	.1342E-09	.1328E-09	.1315E-09	.1301E-09	.1287E-09
19.7	.1222E-09	.1209E-09	.1196E-09	.1184E-09	.1172E-09	.1159E-09
19.8	.1100E-09	.1089E-09	.1078E-09	.1066E-09	.1055E-09	.1044E-09
19.9	.9910E-10	.9807E-10	.9705E-10	.9604E-10	.9504E-10	.9405E-10

Table 6.10. Line Resolution Requirements for Varying Degrees of Perception.

Task	Line Resolution per Minimum Dimension of Target
Detection	1.0 ± 0.25 line pairs
Orientation	1.4 ± 0.35 line pairs
Recognition	4.0 ± 0.8 line pairs
Identification	6.4 ± 1.5 line pairs

Table 6.11. Conversion Factors Between Current Density and Image Illuminance.

Photosensitive Surface	Value of K_i
S-20 photocathode (multialkali)	1.893×10^{-3}
Type II photoconductor (antimony trisulfide)	3.826×10^{-3}
Type V (photoconductor (silicon diode array)	4.894×10^{-2}

Table 6.12. Selected Effective Attenuation Coefficients for Bay, Coastal, and Deep Ocean Water.

Parameter	Bay Water	Costal Water	Deep Ocean Water
Image-forming light			
$\lambda_0(S)$ (nm)	560	540	475
$\alpha(\lambda_0(S))$ (ln/m)	0.323	0.252	0.049
s/a	1.26	5.15	1.58
Backscattered light*			
$\lambda_0(N)$ (nm)	560	510	475
$\alpha(\lambda_0(N))$ (ln/m)	0.323	0.273	0.049
$s(\lambda_0(N))$ (ln/m)	0.180	0.238	0.030
s/a	1.26	6.80	1.58

c_i/α, i = 1 or 3

θ_i	Bay Water	Costal Water		Deep Ocean Water
		$\lambda_0(S) = 540$	$\lambda_0(N) = 510$	
0.05	0.92	0.87	0.87	0.91
0.50	0.80	0.69	0.68	0.78
1.00	0.75	0.62	0.59	0.72
2.50	0.67	0.49	0.45	0.63
5.00	0.60	0.38	0.34	0.55
7.50	0.57	0.33	0.28	0.51
10.00	0.54	0.29	0.25	0.49
20.00	0.50	0.22	0.18	0.44
30.00	0.48	0.20	0.15	0.42
90.00	0.47	0.17	0.14	0.41

*As indicated in table 6.5, the value of λ_0 (N) depends upon the angle θ_1. This dependence, however, is valid only for the particular set of measurements chosen to represent coastal water. The procedure for including this dependence in the analysis is sufficiently complex that the additional information which would be obtained does not justify it for most calculations.

NUC-TP-303

SECTION 7

ANALYTIC EXPRESSIONS†

by

A. Gordon

This section presents simple analytic expressions which allow the system performance analysis, described in section 6, to be significantly extended. Formulas are presented which allow the reader to calculate the effective attenuation coefficients for any water for which $\sigma(\theta)$ and the s/a ratio are known. By using an analytic approximation to the beam-spread function, allowed beam geometries are extended to both nonconical and conical beams with hot spots. Finally, expressions for the water's modulation transfer function, with which the user can calculate the loss in resolution that results from multiple forward scattering, are discussed.

7.1 ANALYTIC EFFECTIVE ATTENUATION COEFFICIENTS

The success of the system performance equations, presented in section 6 and detailed in appendices A and B, results from the simple and valid description of underwater multiple scattering in terms of the effective attenuation coefficient (EAC). For any water, its $\sigma(\theta)$ and s/a ratio uniquely determine the EACs c_1 or c_3 for every source or receiver angle, respectively (section 6.1.1). However, system performance equations (sections 6.2 and 6.3) are limited, since no analytic form for c_1 or c_3 is specified. All values for these coefficients were derived by Monte Carlo methods from Morrison's scattering function (ref. 7.1), which has a mean scattering angle of approximately 4 deg. For other types of water with different mean scattering angles, the values of the EAC will differ from those in figure 6.1. The effect of different scattering cross sections is shown in table 7.1. It can be seen that, even with the s/a ratio and θ specified, the effective attenuation coefficient still

Table 7.1. Effective attenuation coefficients as a function of cross section.

Cross Section	Mean Scattering Angle, θ, deg (s/a = 3.56)	EAC, c_1/α or c_3/α (θ_i = 1 deg)	Relative Irradiance (α R = 10)
Coastal, Southern California*	2.15	0.58	1.00
Morrison**	4.0	0.65	0.50
Visibility Laboratory*	7.3	0.77	0.15
Visibility Laboratory*	19.0	0.90	0.04

*Reference 7.2 (pages 53, 67, and 75).
**Reference 7.1.

†Reviewed by C. Funk.

depends quite strongly on the detailed shape of $\sigma(\theta)$ The resultant values of c_1 can lead to values of on-axis irradiance which differ by as much as a factor of 20, depending upon the scattering cross section used.

This section presents the procedures required to calculate the correct EAC for the $\sigma(\theta)$ most appropriate to the user's particular problem.

7.1.1 Derivation of the Effective Attenuation Coefficient

According to equation 6.2, the EAC for illuminating light c_1 is defined according to the equality

$$h(0,R) = J \exp(-c_1(\theta_1) R)/R^2 \quad , \tag{6.2}$$

where $h(0,R)$ is the on-axis irradiance (power/area) at a distance R from a uniform conical beam of half-angle θ_1 and radiant intensity (power/solid angle) J. By the principle of reciprocity (section 6.1.1.3), this equation also describes the EAC for backscattered light c_3 ($\theta_3 = \theta_1$).

Reference 7.3 shows that the factor

$$\exp(-c_1(\theta_1) R) \tag{7.1}$$

also represents the fraction of flux, i.e., power, emitted by a unidirectional point source (UPS) which passes through a circular aperture of half-angle θ_1 located a distance R from the source plane. By considering in detail the problem of flux through an aperture we will be able to derive an expression for $c_1(\theta_1)$.

The geometry needed for calculating the flux through an aperture with a UPS located at x = 0 is in figure 7.1. Water extends from x = 0 to x = R; a circular aperture, at x = R, subtends a half-angle θ at x = 0. The initial flux is W. It is desired to calculate the flux F_W which actually reaches the aperture, i.e., that power of W which is neither absorbed in the water nor scattered outside the aperture.

In deriving the usual exponential decay of the flux, multiple scattering effects are neglected and any photon which is scattered or absorbed is considered removed from the beam. According to figure 7.1, the differential loss of flux dF_W is given in terms of the scattering coefficient s and the absorption coefficient a as

$$dF_W = -F_W a dx - F_W s dx = -F_W \alpha \, dx \quad , \tag{7.2}$$

where α is the attenuation coefficient. Integrating equation 7.2 and remembering that F = W when x = 0, we obtain

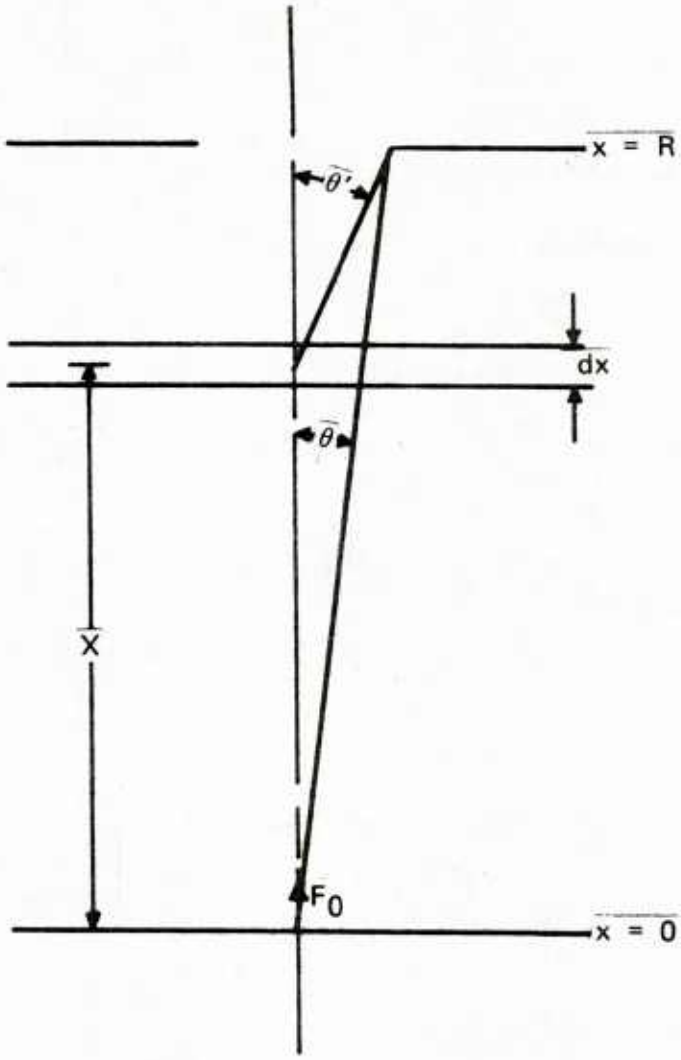

Figure 7.1. Geometry for derivation of flux through an aperture.

$$F_W = W \exp(-\alpha R) \ . \tag{7.3}$$

Equation 7.3, the standard result obtained by any single scattering model, is a good approximation as long as the aperture angle θ is small, i.e., as long as one is concerned with the on-axis flux. However, for any finite aperture there is a probability that scattered photons will enter the aperture. Thus the assumption that all scattered flux is lost to the beam must be modified. A straightforward modification, made in this paper, is to retain the flux scattered within the aperture. In figure 7.1, this corresponds to the retention of flux scattered within a cone of half-angle θ'. Expressed symbolically,

$$dF_W = -F_W a dx - F_W s \left(1 - \int_0^{\theta'} p(\psi)\, d\Omega \right) dx \ , \tag{7.4}$$

where $p(\psi)$ is the normalized scattering cross section, i.e.,

$$p(\theta) = (\sigma(\psi))/s \tag{7.5}$$

and

$$\theta' = \arctan(\tan\theta/(1-x/R)) \ . \tag{7.6}$$

Integrating equation 7.4 between the limits x = 0 and x = R,

$$\int_{F_o}^{F} dF_W/F_W = -\alpha \int_0^R dx + sR \int_0^1 \int_0^{\theta'} p(\psi)\, d\Omega\, dt \ , \tag{7.7}$$

where

$$t = x/R \ . \tag{7.8}$$

Performing the indicated integration in equation 7.7 provides the formula for the flux entering the aperture:

$$F_W = W \exp \left\{ -\alpha R + sR \int_0^1 \int_0^{\theta'} p(\psi)\, d\Omega\, dt \right\} \ . \tag{7.9}$$

Comparison of equation 7.9 with equation 7.1 provides the EAC $c_i(\theta_i)$ (i = 1 or 3):

$$c_i(\theta_i) = \alpha \left(1 - s/\alpha \int_0^1 \left[\int_0^{\theta_i'(t)} p(\psi)\, d\Omega \right] dt \right) , \tag{7.10}$$

where

$$\theta_i'(t) = \arctan[\tan\theta_i/(1-t)] \ . \tag{7.11}$$

Equation 7.10 is the final result for the EAC. It applies to forward scattering (i = 1) as well as to backscattering (i = 3) by equating θ_i with the source's half-angle (θ_1) or the receiver's half-angle (θ_3), respectively.

The above derivation of $c_i(\theta_i)$ is essentially based on a generalization of single scattering theory to encompass finite apertures. Equation 7.10 can also be derived by examining particular approximations to multiple scattering theory. Reference 7.3 presents this derivation by approximating the nth-order scattering integrals which occur in the natural solution for the transfer of radiance in the sea. This reference also presents the explicit form of all higher order scattering integrals.

A simplified form of equation 7.10 was published in reference 7.3. To obtain this simplified form, it was assumed that all scattering was concentrated at a plane located midway between the source and target plane. Referring to figure 7.1, this approximation means that the integral over x is dropped in favor of the assumption that the flux is to be distributed as if all the scattering had occurred at x = R/2. Making this additional approximation, we obtain

$$c_i'(\theta_i) = \alpha \left(1 - s/\alpha \int_0^{\theta_i''} p(\psi)\, d\Omega \right) \tag{7.12}$$

with

$$\theta'' = \arctan(2 \tan \theta_i) \ . \tag{7.13}$$

Comparing equations 7.12 and 7.10 reveals that equation 7.12 represents a computational savings as the integral over t has disappeared. The cost of this savings is the reduced accuracy of $c_i'(\theta_i)$ as compared with $c_i(\theta_i)$. Reference 7.4 exhaustively compares the relative accuracy of these two forms of the analytic EAC. These comparisons indicate that the fluxes calculated from either $c_i(\theta_i)$ or $c_i'(\theta_i)$ generally agree for short ranges and extreme values of θ_i, i.e., $\theta_i \approx 0°$ or $\theta_i > 60°$. However, for longer ranges and intermediate values of θ_i, the two EACs lead to values for the flux through an aperture (or on-axis irradiance) which can differ by as much as 50 percent at a range of 10 attenuation lengths. When compared with Monte Carlo calculations, $c_i(\theta_i)$ provides better agreement for all θ and R. This is to be expected since $c_i(\theta_i)$ is functionally the correct form (it is exact at small R), while $c_i'(\theta_i)$ is not. Because $c_i(\theta)$ provides very close agreement to Monte Carlo calculations and is, as will be shown in section 7.1.3, simple to compute, $c_i'(\theta_i)$ will not be further considered; rather, the region of validity and usage of $c_i(\theta_i)$ will be examined.

7.1.2 Region of Validity of Analytic EAC

According to equation 7.10, the analytic EAC $c_i(\theta_i)$ is independent of R, a desirable property as $c_i(\theta_i)$ can be calculated once and used at a large number of different distances. The range independence of $c_i(\theta_i)$ would imply that the flux through an aperture, equation 7.1, is represented by a straight line for every value of θ_i when plotted as a function of range on semilogarithmic paper. As seen in appendix C (fig. C.3), this type of plot, computed by Monte Carlo methods, results in a family of curves which are nearly, but not quite, straight

lines. It is therefore important to delineate the range of validity for our expression, equation 7.10, for $c_i(\theta_i)$.

As previously mentioned, equation 7.10 is exact at angles for which the small-angle approximation holds, i.e., $\theta \cong \sin\theta$, and at distances that are small compared to a scattering length, i.e., $sR \ll 1$. This occurs because the integral appearing in the exponential is the exact single scattering result (in the small-angle approximation) and single scattering is all that is important at small distances. Although the small-angle approximation was used in equation 7.10, the equation is valid at large angles because underwater scattering cross sections are highly peaked in the forward direction. This makes the contributions from large angles to the innermost integral in equation 7.10 small when compared to the small-angle contributions. Thus, predictions based on $c_i(\theta_i)$ are accurate at small ranges for any value of θ.

Figures 7.2 and 7.3 show values of flux through the aperture derived from experiments, Monte Carlo calculations, and equation 7.10. The agreement between our calculations and Monte Carlo values is all but perfect at small ranges, even to 4 attenuation lengths. Also, equation 7.10 shows that $c_i(\theta_i)$ approaches α as θ_i approaches 0 and that $c_i(\theta_i)$ approaches a as θ_i tends toward $\pi/2$. This behavior, also shown in figures 7.2 and 7.3, corresponds to the intuitive idea that a narrow beam is attenuated according to α, while a wide beam is attenuated according to a.

From previous considerations, equation 7.10 is known to be valid at small R. What is left to answer is at what range, as a function of θ_i and the s/a ratio, does equation 7.10 become inaccurate. Extensive comparisons were made between it and the Monte Carlo results. The measure of accuracy was taken to be R(20%) – the range at which the flux through the aperture predicted from equation 7.10 begins to differ from that predicted by exact Monte Carlo methods by as much as 20 percent.

Figure 7.4 shows R(20%) as a function of θ_i for three different $\sigma(\theta)$s. For $\theta_i \leqslant 2.5°$, R(20%) is between 6 and 9 attenuation lengths, i.e., $c_i(\theta_i)$ as defined by equation 7.10 is valid from 6 to 9 attenuation lengths when θ_i is less than 2.5 deg. For $\theta_i > 6.3°$, the agreement is even better since R(20%) is 10 attenuation lengths or larger. Thus, except for the very smallest angles ($\theta < 1°$), we see that the EAC given by equation 7.10 is valid out to and beyond the maximum ranges achievable by the best underwater viewing systems.

Figure 7.4 also shows data points for three different $\sigma(\theta)$s with different mean scattering angles. From the figure, we see that R(20%) is relatively insensitive to the particular $\sigma(\theta)$ chosen and that the range of validity described for $c_i(\theta_i)$ will accurately describe any $\sigma(\theta)$. Each point on figure 7.4 was computed from an average of three $c_i(\theta_i)$s, which were in turn computed for s/a ratios of 1.48, 2.28, and 3.56. The possible dependence of the region of validity of $c_i(\theta_i)$ on the s/a ratio is in figure 7.5 for a cross section with a mean scattering angle of 4.68 deg. Evidently, R(20%) is nearly independent at the s/a ratio so that figure 7.4 serves adequately to delimit the range of validity of $c_i(\theta_i)$ for the entire spectrum of $\sigma(\theta)$s and s/a ratios most likely to be found in the ocean environment.

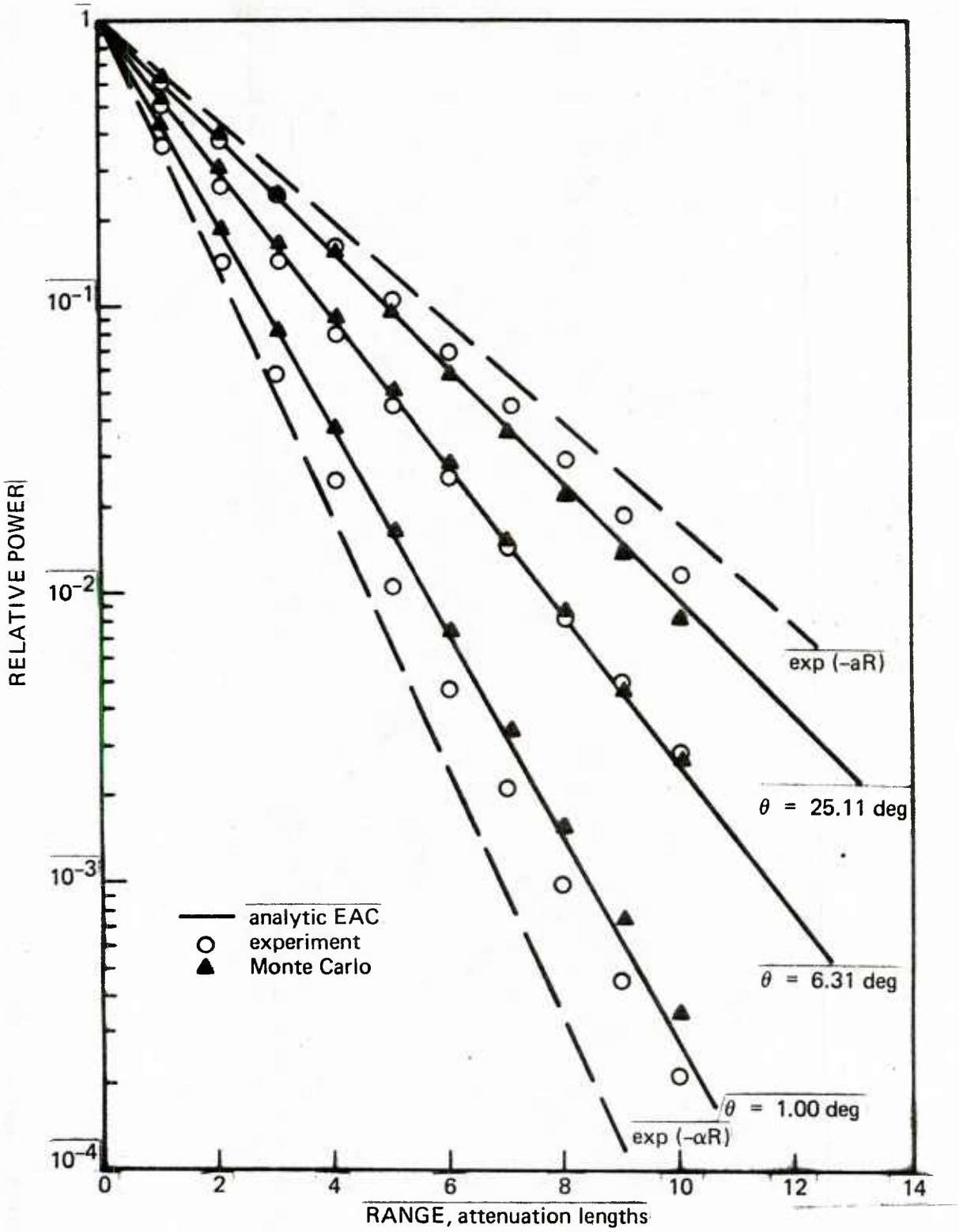

Figure 7.2. Flux through an aperture; s/a = 1.48.

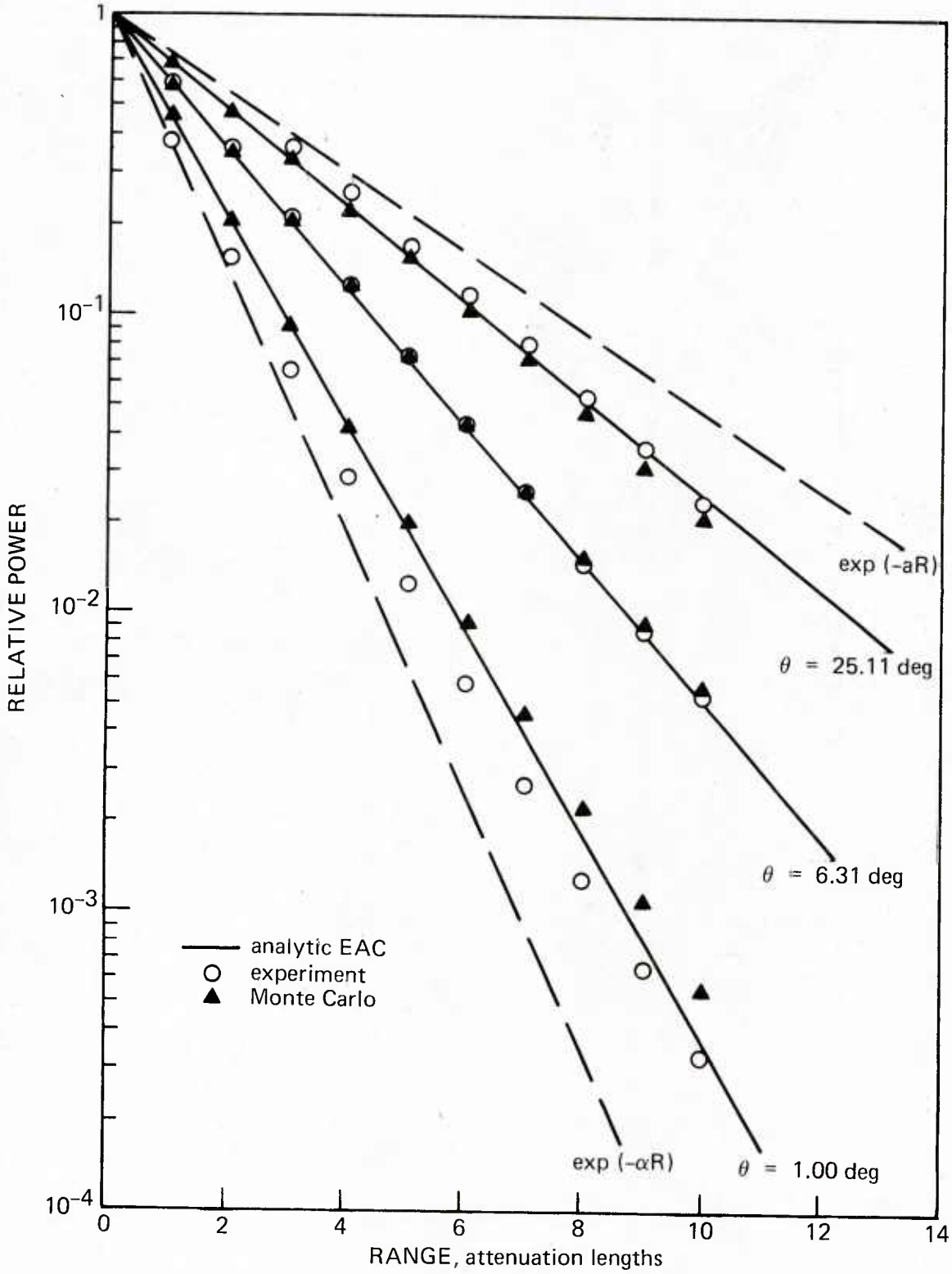

Figure 7.3. Flux through an aperture; s/a = 2.28.

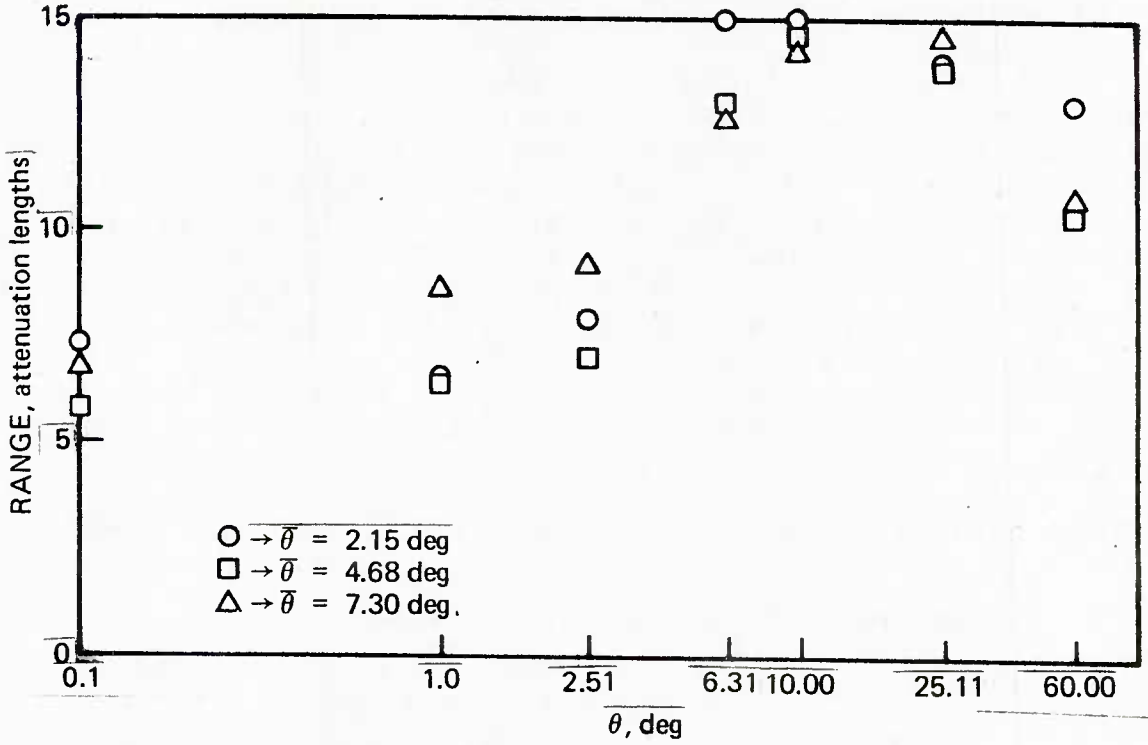

Figure 7.4. Region of validity of analytic EAC as a function of mean scattering angle.

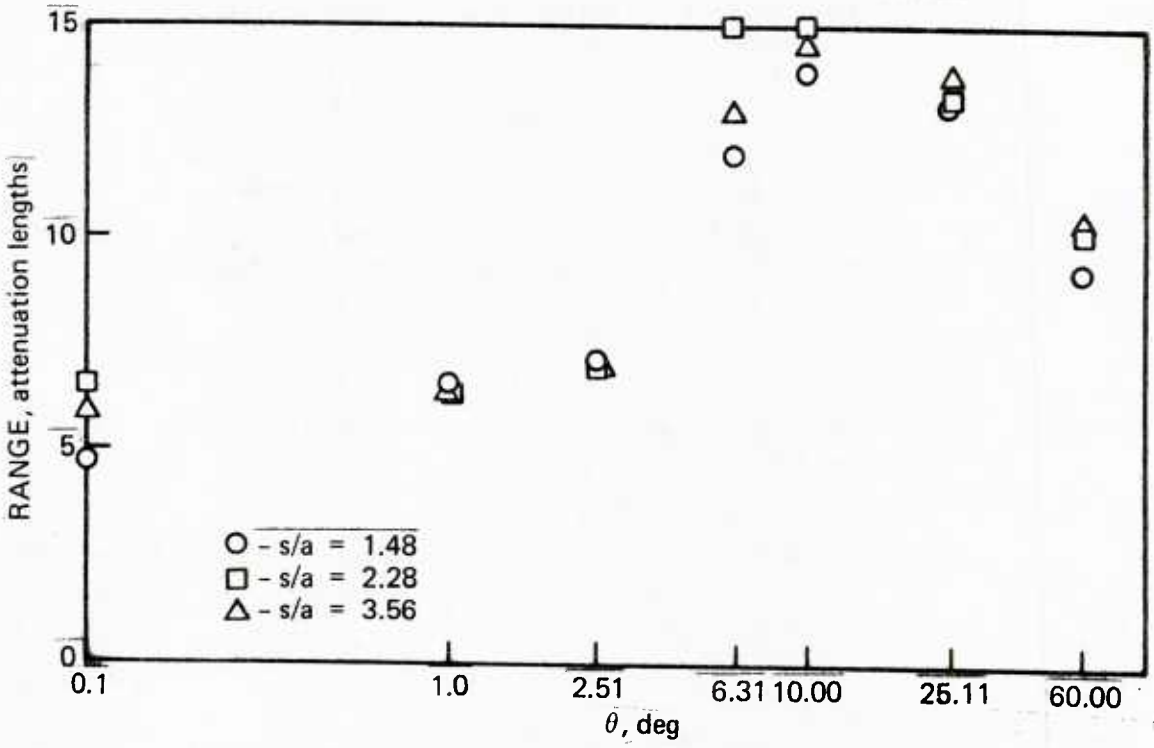

Figure 7.5. Region of validity of analytic EAC as a function of s/a ratio.

7.1.3 Use of the Analytic EAC

The analytic EAC is used exactly as the EACs in table 6.12, except that analytic EACs must be calculated by the user according to the specific cross section used, $\sigma(\theta)$. Equation 7.10 also requires a knowledge of the correct s/a ratio (or equivalently the correct s/a ratio at the wavelengths of maximum transmission for signal and backscattered light, $\lambda_0(S)$ and $\lambda_0(N)$, respectively). These quantities can be obtained either from the wavelength-dependent functions $s(\lambda)$, $a(\lambda)$, and $\alpha(\lambda)$ for the particular water which the reader wishes to simulate or, if the reader has only $\sigma(\theta)$, the spectral characteristics given in table 6.2 for the appropriate water, i.e., bay, coastal, or deep, can be used.

Procedures for modifying the methods in sections 4 through 6 (the Performance Analysis Worksheets, PAW) will be discussed in the rest of this section. These procedures will permit the reader to use a specific $\sigma(\theta)$ to calculate the appropriate analytic EAC.

7.1.3.1 Calculation of $c_i(\theta_i)/\alpha$ if $p(\theta)$ and any two of $\alpha(\lambda)$, $a(\lambda)$, and $s(\lambda)$ are known

1. Specify basic optical properties (section 4 of PAW).
   a. Determine the wavelength of maximum transmission for signal light $\lambda_0(S)$, which can be considered the minimum value of $\alpha(\lambda)$.*
   b. Determine the wavelength of maximum transmission for backscattered light $\lambda_0(N)$, which can be considered the minimum value of $a(\lambda)$.*
   c. Evaluate the ratios $s/\alpha(\lambda_0(S))$ and $s/\alpha(\lambda_0(N))$. The s/α ratios are related to the s/a ratios by

$$(s/\alpha(\lambda)) = (s/a(\lambda))(1/(s/a(\lambda) + 1)) \quad , \tag{7.14}$$

   where s/a is determined from the reader's water characteristics.*
   d. Evaluate $s/\alpha(\lambda_i)$. The reader's water characteristics for $s(\lambda)$ and $\alpha(\lambda)$ are evaluated at each of the laser's primary spectral wavelengths, and their ratio is calculated.**
   e. Evaluate $\alpha(\lambda_0(S))$, $\alpha(\lambda_0(N))$, and $s(\lambda_0(N))$. The reader uses the appropriate water characteristics.*
   f. Evaluate $\alpha(\lambda_i)$ and $s(\lambda_i)$. The reader uses water characteristics for all primary laser lines.**
   g. Evaluate η. Use $p(\theta)$ and equation 6.38.
   h. Evaluate ψ_b. The quantity, which must be measured for each case, varies between 0.2 and 0.7. (ψ_b was introduced in section 2.2.)

**Perform this step for conventional sources only.*
***Perform this step for laser sources only.*

2. Specify effective attenuation coefficients (section 5 of PAW).

   a. Evaluate $c_1/\alpha\,(\lambda_0(S))$. Use equation 7.10 with $s/\alpha\,(\lambda_0(S))$ and $\theta_i = \theta_1$, the source angle.*

   b. Evaluate $c_1/\alpha\,(\lambda_0(N))$. Use equation 7.10 with $s/\alpha\,(\lambda_0(N))$ and $\theta_i = \theta_1$, the source angle.*

   c. Evaluate $c_3/\alpha\,(\lambda_0(N))$. Use equation 7.10 with $s/\alpha\,(\lambda_0(N))$ and $\theta_i = \theta_3$, the receiver angle.*

   d. Evaluate $c_1/\alpha\,(\lambda_i)$ and $c_3/\alpha\,(\lambda_i)$. Evaluate the integral in equation 7.10 for $\theta_i = \theta_1$ and $\theta_i = \theta_3$. Then evaluate each $c/\alpha\,(\lambda_i)$ by inserting the corresponding $s/\alpha\,(\lambda_i)$ in equation 7.10.**

3. Specify effective spectral bandwidths (section 5 of PAW). Use equation 6.6 with $\beta_1(\lambda) = \alpha(\lambda)\,(1 + c_1/\alpha\,(\lambda_0(S)))$ to evaluate $\lambda_1(S)$ and $\lambda_2(S)$. Then use equation 6.7 with $\beta_2(\lambda) = a(\lambda) \times (\alpha/a\,(\lambda_0(N))\,(c_1/\alpha\,(\lambda_0(N)) + c_3/\alpha\,(\lambda_0(N))))$ to evaluate $\lambda_1(N)$ and $\lambda_2(N)$.*

7.1.3.2 Calculation of $c_i(\theta_i)$ when only $p(\theta)$ is known.

1. Specify basic optical properties (section 4 of PAW).

   a. Obtain all quantities except η as indicated in section 4 of PAW.

   b. Evaluate η. Use $p(\theta)$ and equation 6.38.

   c. Obtain $s/\alpha\,(\lambda_0(S))$ and $s/\alpha\,(\lambda_0(N))$ from the respective s/α ratios using equation 7.14.

2. Specify effective attenuation coefficients (section 5 of PAW). The c_i are calculated exactly as in part 2 of section 7.1.3.1.

3. Specify effective spectral bandwidths (section 6 of PAW). Calculate as indicated in section 7.1.3.1, except use the spectral dependence of $a(\lambda)$ and $\alpha(\lambda)$ as in figure 6.2.

7.1.3.3 Example of use of analytic effective attenuation coefficients. As an example we will obtain the analytic EACs and spectral bandwidths for the conventional system analyzed in appendix B. However, the water will have a scattering function whose shape most resembles Petzold's (ref. 7.2, table 7.2) rather than Morrison's, which is used as the basis for the calculation in appendix B. Since all the independent information available is $p(\theta)$, this calculation is an example of the type discussed in section 7.1.3.2. We will see that all that is really necessary for the calculation (and consequently all that is in table 7.2) is $P(\theta)$, the distribution function, where

$$P(\theta) = \int_0^{2\pi} \int_0^{\theta} p(t) \sin t \, dt \, d\phi \; . \tag{7.15}$$

Perform this step for conventional sources only.
***Perform this step for laser sources only.*

Table 7.2. Petzold's cross section.

θ, deg	$\sigma(\theta)$, m^{-1}		$P(\theta)$	
0.100	1.79	10^{-2}	4.38	10^{-3}
0.126	1.60		6.11	
0.158	1.39		8.52	
0.199	1.17		1.18	10^{-2}
0.251	9.64	10^{1}	1.61	
0.316	7.87		2.17	
0.398	6.32		2.89	
0.501	5.05		3.80	
0.631	4.08		4.95	
0.794	3.31		6.44	
1.00	2.64		8.34	
1.26	2.07		1.07	10^{-1}
1.58	1.60		1.37	
2.00	1.26		1.73	
2.51	9.70	10^{0}	2.17	
3.16	7.20		2.71	
3.98	5.15		3.33	
5.01	3.54		4.02	
6.31	2.37		4.76	
7.94	1.52		5.52	
10.0	9.18	10^{-1}	6.28	
15.0	3.27		7.43	
20.0	1.65		8.13	
25.0	8.64	10^{-2}	8.59	
30.0	5.25		8.90	
35.0	3.19		9.12	
40.0	2.13		9.28	
45.0	1.55		9.40	
50.0	1.13		9.50	
55.0	8.12	10^{-3}	9.58	
60.0	6.08		9.63	
65.0	4.75		9.68	
70.0	3.76		9.72	
75.0	2.99		9.75	
80.0	2.46		9.78	
85.0	2.07		9.80	
90.0	1.82		9.82	

Table 7.3. Evaluation of integral for EAC.

t	θ', deg	$P(\theta')$
0.05	10.51	0.6399
0.15	11.72	0.6677
0.25	13.23	0.7025
0.35	15.18	0.7458
0.45	17.78	0.7822
0.55	21.40	0.8260
0.65	26.74	0.8695
0.75	35.20	0.9125
0.85	49.61	0.9490
0.95	74.17	0.9748
		$\Sigma P(\theta') = 8.070$

Note: $\Sigma P(\theta)(\Delta t) = 0.807$.

The final part of this calculation is to determine the effective spectral bandwidths. Substituting the expression for $\beta_1(\lambda)$, given in step 3 of section 7.1.3.1, into equation 6.6, we obtain

$$0.5 = \exp\left[-R\left(\beta_1(\lambda_1(S)) - \beta_1(\lambda_0(S))\right)\right]$$

$$= \exp\left[-R\left(1 + c_1/\alpha(\lambda_0(S))\right)\left(\alpha(\lambda_1(S)) - \alpha(\lambda_0(S))\right)\right] \quad . \tag{7.23}$$

Using R = 20 m, $\alpha(\lambda_0(S)) = 0.252$ m (as given in appendix B), and the value just calculated for $c_1/\alpha(\lambda_0(S))$, we obtain

$$0.5 = \exp\left[-(20)(1 + 0.32)\left(\alpha(\lambda_1(S)) - 0.252\right)\right] \quad . \tag{7.24}$$

Solving this equation we have $\alpha[\lambda_1(S)] = 0.278$. From figure 6.2 this corresponds to $\lambda_1(S) = 505$ nm. Since equation 6.6 is symmetric in $\beta[\lambda_1(S)]$ and $\beta[\lambda_2(S)]$, we have $\alpha[\lambda_2(S)] = 0.278$ or $\lambda_2(S) = 585$ nm. $\lambda_1(N)$ and $\lambda_2(N)$ are obtained in the same manner,

From step 4 of appendix B we have $s/a\ (\lambda_0(S)) = 5.15$ and $s/a\ (\lambda_0(N)) = 6.80$. Using equation 7.14 we obtain $s/\alpha\ (\lambda_0(S)) = 0.837$ and $s/\alpha\ (\lambda_0(N)) = 0.872$. From the definition of η (eq. 6.38), table 7.2, and the definition of $p(\theta)$ (eq. 7.15), we have

$$\eta = P\,(180°) - P\,(90°) = 1 - 0.982 = 0.018\ . \tag{7.16}$$

We now proceed to evaluate the three EACs – $c_1/\alpha\ (\lambda_0(S))$, $c_1/\alpha\ (\lambda_0(N))$, and $c_3/\alpha\ (\lambda_0(N))$ – as required in step 5 of appendix B. Since the source and receiver half-angles are each equal to 10 deg, $c_1/\alpha\ (\lambda_0(N)) = c_3/\alpha\ (\lambda_0(N))$. We now rewrite equation 7.10 with the outer integral written as a sum (for computational purposes) and the inner integral in terms of $P(\theta)$:

$$c_i(\theta_i,\lambda) = \alpha\,(\lambda)\ \ (1 - s/\alpha\,(\lambda) \sum_t P(\theta_i{}')\,(\Delta t)) \tag{7.17}$$

with

$$\theta_i{}' = \text{arc tan}\,(\tan\theta_i/1 - t)\ . \tag{7.18}$$

The sum in equation 7.17 can be evaluated with sufficient accuracy with $\Delta t = 0.1$. Since the source and receiver angles are each equal to 10 deg, equation 7.18 becomes

$$\theta'_{1,3} = \text{arc tan}\,(\tan 10°/1 - t) = \text{arc tan}\,(0.1763/1-t)\ . \tag{7.19}$$

The procedure is now to find $\theta'_{1,3}$ for t taking on values between 0.05 and 0.95 in increments of 0.1. The corresponding $P(\theta'_{1,3})$ is found by entering $\theta'_{1,3}$ into table 7.2 and interpolating for the $P(\theta'_{1,3})$. The sum is evaluated by summing the 10 values of $P(\theta'_{1,3})$ and multiplying by $\Delta t = 0.1$. This calculation is detailed in table 7.3, resulting in a value of 0.81. Thus

$$c_i/\alpha\,(\lambda) = 1 - 0.81\ s/\alpha\,(\lambda)\ . \tag{7.20}$$

For the s/α ratios calculated above, we obtain

$$c_1/\alpha\,(\lambda(S)) = 1 - (0.81)\,(0.837) = 0.32 \tag{7.21}$$

and

$$c_1/\alpha\,(\lambda(N)) = c_3/\alpha\,(\lambda(N)) = 1 - (0.81)\,(0.872) = 0.29\ . \tag{7.22}$$

These values are slightly larger than those in appendix B, since Petzold's cross section has a larger mean scattering angle which causes any given beam to lose a greater fraction of its flux because of scattering.

except that equation 6.7, β_2 (see step 3 of section 7.1.3.1), and r_0 (see step 7 of appendix B) are used.

7.2 BEAM-SPREAD FUNCTION

If only the on-axis propagation of conical beams is considered, the EACs are sufficient to describe the propagation of light. However, if information related to off-axis irradiance or the on-axis performance of nonconical beams is required, the previous analysis is too limited. By introducing the concept of the beam-spread function, the analysis can be extended to encompass more general beam geometries.

Referring to figure 7.1, the beam-spread function (BSF) is equivalent to $h_B(\theta,R)$, the irradiance distribution, on the plane x = R due to a unidirection point source (UPS) of unit strength, i.e., W = 1, at x = 0. Readers familiar with linear systems theory will recognize $h_B(\theta,R)$ as the impulse response function for the system, which in the present case is the seawater bounded by the planes x = 0 and x = R. The utility of the impulse response is a result of the beam's radiance pattern convolved with the impulse response function yielding the beam's irradiance pattern. Another useful property for the BSF is that, aside from scale factors, it is the impulse response function for received light (ref. 7.5), i.e., the point-spread function (PSF). The PSF is the irradiance distribution $h_B(\theta,R)$ on the receiver's image plane caused by an omnidirectional point source located a distance R from the receiver. The Fourier transform of $h_B(\theta,R)$, the modulation transfer function (MTF), yields information on contrast degradation caused by small-angle multiple scattering (see section 7.4).

Since the BSF is important to understanding underwater light propagation, we will derive a simple analytic approximation to the BSF, indicate its region of validity, and give examples of its use as an adjunct to the PAW.

7.2.1 Derivation of the Beam-Spread Function

As defined above, $h_B(\theta,R)$, the beam-spread function, is the target plane's irradiance resulting from a UPS of unit strength. In section 7.1.1, we derived the analytic EAC by considering the flux through an aperture of half-angle θ resulting from such a source.

Since irradiance is defined as the flux per unit area, we can write

$$dF = h_B(\theta,R)\, dA \tag{7.25}$$

and obtain $h_B(\theta,R)$ by evaluating dF/dA. Using azimuthal symmetry, we have

$$dA = 2\pi\,(R\theta)\, d(R\theta) = 2\pi\, R^2\theta\, d\theta \ . \tag{7.26}$$

Thus

$$h_B(\theta,R) = (1/2\,\pi\,R^2\theta)\,dF/d\theta\ . \tag{7.27}$$

Using equations 7.9 and 7.11 with W = 1 in equation 7.27 yields for the derivative

$$dF/d\theta = \exp(-c_1(\theta)R)\left\{2\pi\,sR\int_0^1 (\partial/\partial\theta)\int_0^{\tan^{-1}(\theta/1-t)} p(\psi)\sin\psi\,d\psi\,dt\right\}, \tag{7.28}$$

where we have used the small-angle approximation for θ, i.e., $\sin\theta \approx \theta$. The derivative in equation 7.28 can be computed using Leibnitz's rule:

$$\partial/\partial\lambda \int_{u(\lambda)}^{v(\lambda)} f(x,\lambda)\,dx = \int_{u(\lambda)}^{v(\lambda)} \partial/\partial\lambda\, f(x,\lambda)\,dx$$

$$+ f(v,\lambda)\,\partial v/\partial\lambda - f(u,\lambda)\,\partial v/\partial\lambda\ . \tag{7.29}$$

If equation 7.29 is applied to equation 7.28, the derivative with respect to θ becomes

$$dF/d\theta = \exp(-c_1(\theta)R)\left\{2\pi\,sR\int_0^1 p\left(\tan^{-1}\frac{\theta}{1-t}\right)\sin\left(\tan^{-1}\frac{\theta}{1-t}\right)\right.$$

$$\left.(1/(1+(\theta/1-t)^2))\,(1/(1-t))\,dt\right\}\ . \tag{7.30}$$

Using the substitution

$$u = \tan^{-1}\frac{\theta}{1-t}\ , \tag{7.31}$$

equation 7.30 reduces to

$$dF/d\theta = \exp(-c_1(\theta)R)\left\{2\pi\,sR\int_\theta^{\pi/2} p(u)\cos u\,du\right\}\ . \tag{7.32}$$

Substituting this result for the derivative in equation 7.26 results in the final expression for the beam-spread function:

$$h_B(\theta,R) = sF/R\theta \int_{\theta}^{\pi/2} p(u) \cos u \, du \ , \tag{7.33}$$

where F is given in equation 7.9.

Equation 7.33 exhibits the following limiting forms for extreme values of R and θ:

$$\theta \to \pi/2 \text{ or } R \to \infty \Rightarrow h_B(\theta,R) \to 0$$

$$\theta \to 0 \text{ or } R \to 0 \Rightarrow h_B(\theta,R) \to \infty \ . \tag{7.34}$$

These limits appear reasonable, except for the singularity at R = 0. However, even this is correct: at short distances the scattering probability is proportional to R, but the area available for scattering, which appears in the denominator, increases with R^2.

7.2.2 Region of Validity of the Beam-Spread Function

We expect the region of validity for $h_B(\theta,R)$ (equation 7.33) to be no greater than that for F (eq. 7.9), since both were derived under identical assumptions. In fact, the region of validity should be considerably less than that for F, since $h_B(\theta,R)$ is proportional to the derivative of an approximate quantity which is generally less accurate than the quantity itself. Because $h_B(\theta,R)$ is a derivative it cannot be directly compared with the corresponding Monte Carlo result to delimit its region of validity. Because Monte Carlo results are statistical in nature, it would be prohibitive to obtain accurate derivatives of the data necessary for the evaluation of a Monte Carlo $h_B(\theta, R)$, making the existence of an approximate analytic form of $h_B(\theta,R)$ more valuable.

Since an equivalent Monte Carlo result is unavailable, $h_B(\theta,R)$'s region of validity will be ascertained by direct comparison with experimental data. Duntley (ref. 7.6) measured $h_B(\theta,R)$ by determining the irradiance produced at a distance R and angle θ caused by a laser beam which was allowed to propagate through water characterized by Petzold's cross section (table 7.2). Although a laser beam is not a perfectly collimated UPS, its divergence is small enough so that at all angles greater than the laser's divergence angle the laser acts effectively like a UPS.

For comparison with experimental results, equation 7.33 was evaluated by Simpson's Rule, a three-point integration routine. To obtain appropriate values of the integrand, Petzold's data for p (u) were interpolated according to a three-point Aitken fit. There were no real convergence problems, although p (u) rises rapidly near $\theta = 0$. Any appropriate standard computer library software can be applied to the evaluation of equation 7.33.

Both the experimental and theoretical values of $h_B(\theta, R)$ were compared over a wide range of θ and R values and at three different s/a ratios. The results of these calculations are shown in figures 7.6 through 7.8. The heavily shaded area represents that region of R and θ where the theoretical and experimental results agree within 20 percent, while the lightly shaded areas show agreement within 40 percent. The regions of agreement are complexly shaped, and their domains vary as a function of s/a ratios. However, inspection reveals that for $2 \leqslant R \leqslant 10$ attenuation lengths and $1° \leqslant \theta \leqslant 20°$, the agreement is almost always better than 20 percent. This region probably represents the domain for which equation 7.33 can be applied in practice.

Figures 7.9 and 7.10 show the kind of agreement expected within the domain of validity. Note that the agreement is maintained over four orders of magnitude as θ increases from 1 to 50 deg. The experimentally observed broadening of $h_B(\theta, R)$ as R is increased, i.e., from figure 7.9 to 7.10, is also reflected in the theoretical curves.

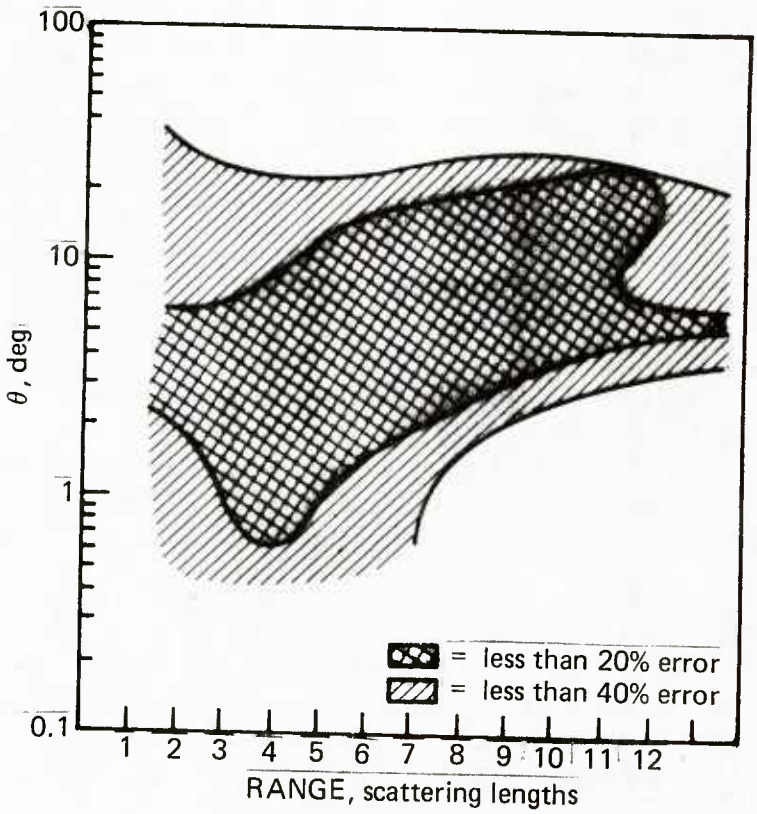

Figure 7.6. Region of validity of $h_B(\theta, R)$ for s/a = 4.88.

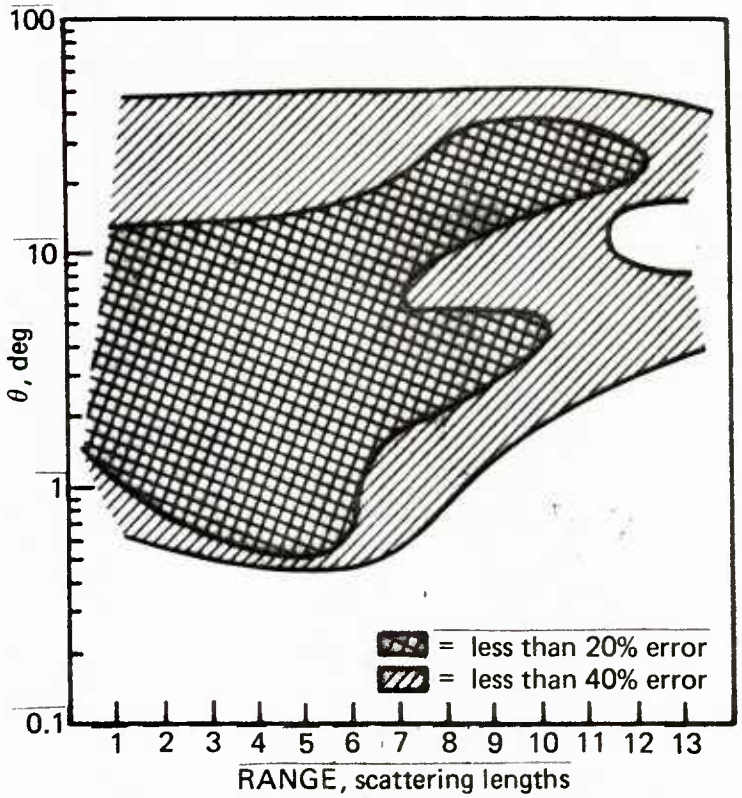

Figure 7.7. Region of validity of $h_B(\theta,R)$ for s/a = 3.00.

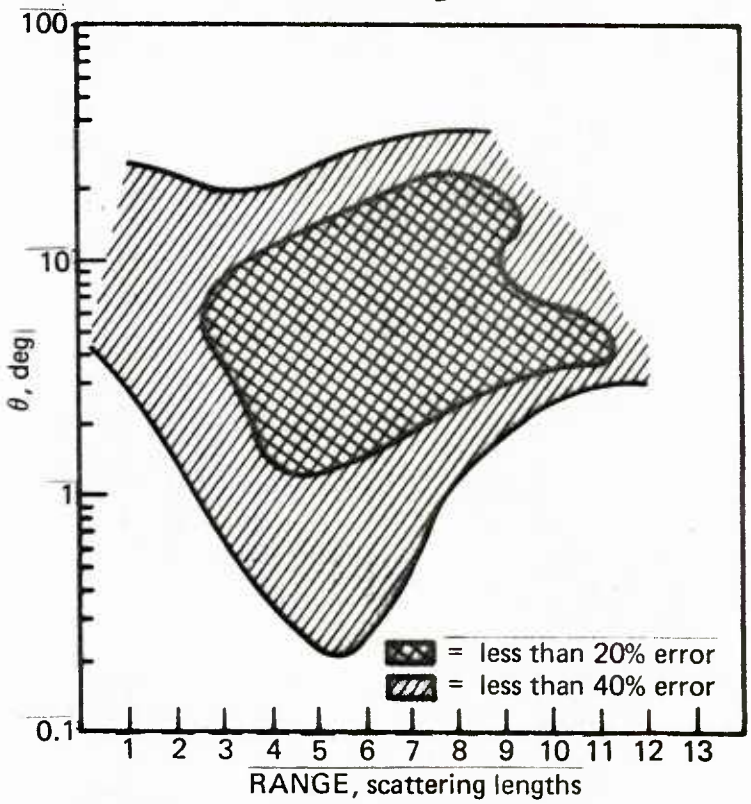

Figure 7.8. Region of validity of $h_B(\theta,R)$ for s/a = 2.29.

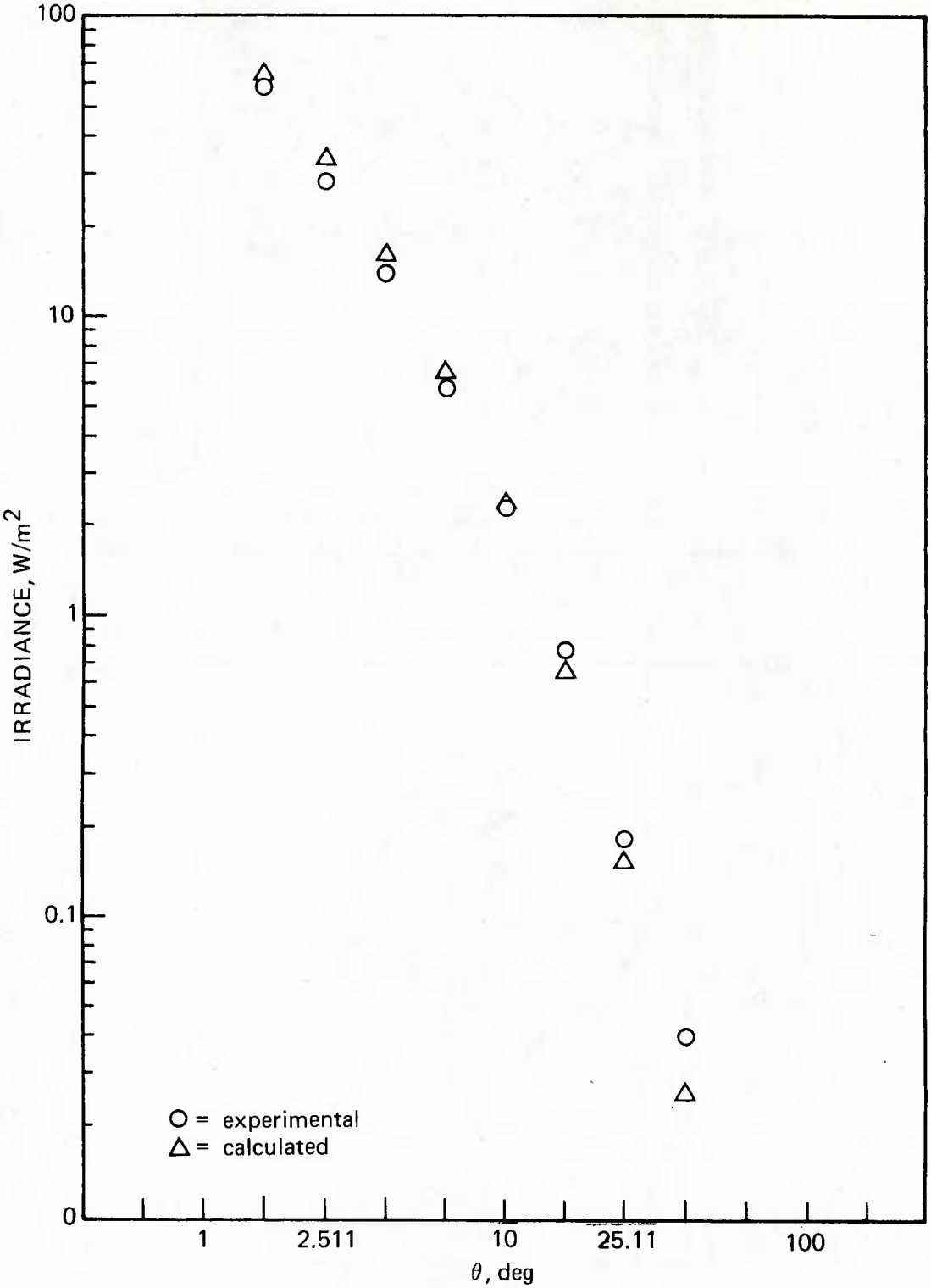

Figure 7.9. Comparison of calculated and experimental values of $h_B(\theta,R)$ for $\alpha R = 2.12$.

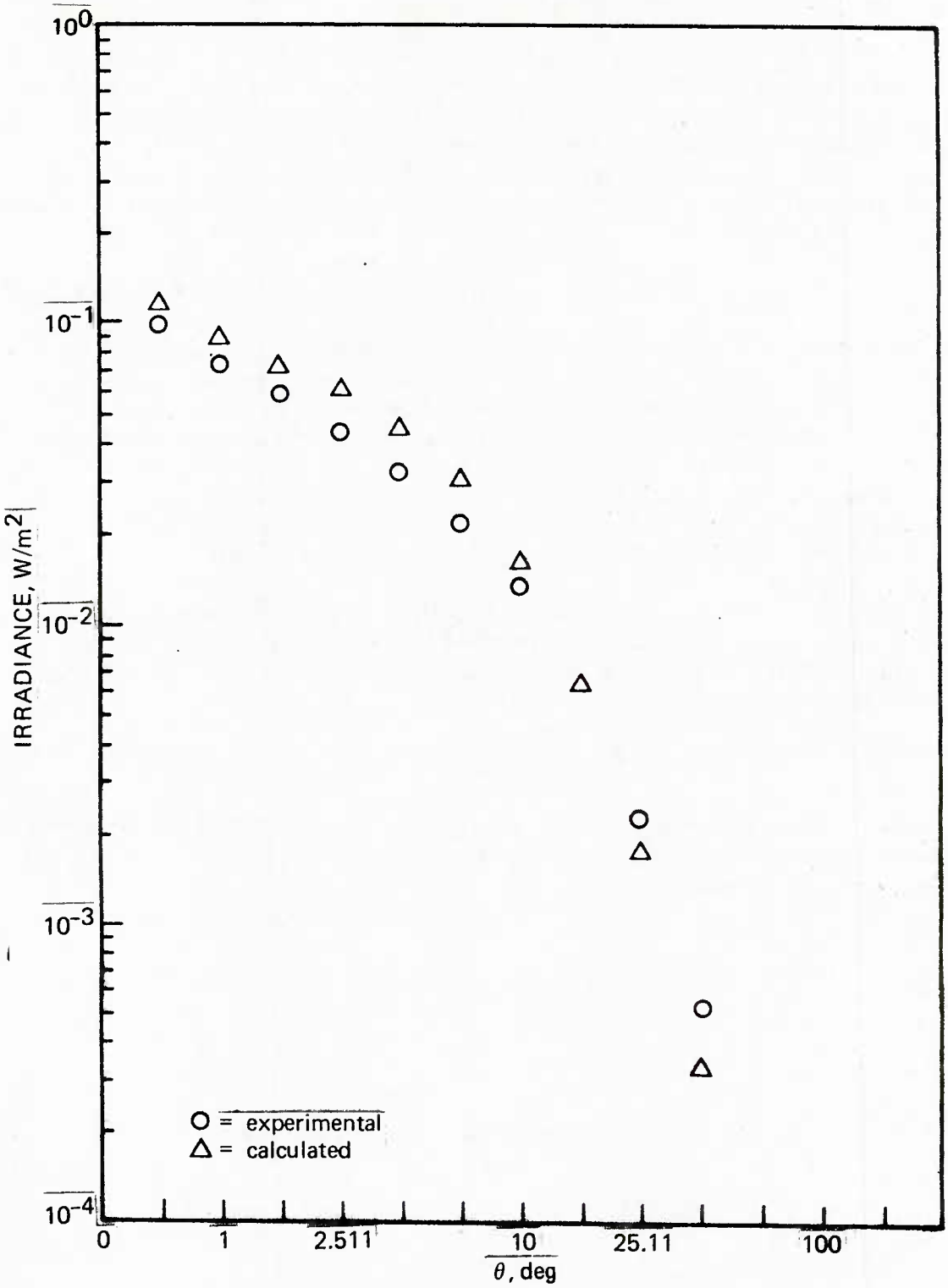

Figure 7.10. Comparison of calculated and experimental values of $h_B(\theta,R)$ for $\alpha R = 8.94$.

7.2.3 Use of the Beam-Spread Function

The utility of the beam-spread function results from the fact that the medium's response to a source of arbitrary radiant intensity $J(\theta,\phi)$ can be expressed in terms of the beam-spread function $h_B(\theta,R)$ and $J(\theta,\phi)$ alone. The resulting expression is in the form of a convolution which generally must be evaluated for each direction of the source beam. However, when the radiant intensity exhibits enough symmetry, or even better when only the on-axis irradiance need be calculated (as in the PAW), the required convolutions reduce to much simpler calculations.

Specific examples of the use of $h_B(\theta,R)$ are given in the following sections.

7.2.3.1 General form of the off-axis irradiance. Although the analysis covered in the PAW requires only the evaluation of on-axis irradiance, there are some special system geometries which require a knowledge of off-axis irradiance. One such system is that which uses "glow field illumination," which is obtained when the source beam is moved away from the target until the target is illuminated only by scattered light. Such an illumination scheme increases the distance r_0, the perpendicular distance from the source receiver plane to the backscatter volume. This reduces the backscatter at the expense of some signal current, yielding a net increase in image contrast.

A source of radiant intensity can be considered as being the summation of a number of pencil beams, $J_i(\theta_i,\phi_i)$, each with a strength of $J(\theta_i,\phi_i)\sin\theta_i\, d\theta_i\, d\phi_i$. According to the definition of the BSF, the irradiance in a direction θ_j,ϕ_j, caused by the beams pointing in the direction θ_i,ϕ_i, is given by

$$h(\theta_j,\phi_j,R) = h_B(\theta_{ij},R)\, J(\theta_i,\phi_i)\sin\theta_i\, d\theta_i\, d\phi_i \ , \tag{7.35}$$

where θ_{ij} is the angle between the directions (θ_j,ϕ_j) and (θ_i,ϕ_i). The total off-axis intensity $h(\theta_1,\phi_1,R)$ in the direction (θ_1,ϕ_1) at range R resulting from the entire beam $J(\theta_2,\phi_2)$ is thus given by the convolution integral

$$h(\theta_1,\phi_1,R) = \int_0^{2\pi}\int_0^{\pi} h_B(\theta_{12},R)\, J(\theta_2,\phi_2)\sin\theta_2\, d\theta_2\, d\phi_2 \ , \tag{7.36}$$

with

$$\theta_{12} = \arccos\left\{\sin\theta_1\cos\phi_1\sin\theta_2\cos\phi_2 + \sin\theta_1\sin\phi_1\sin\theta_2\sin\phi_2 + \cos\theta_1\cos\theta_2\right\} . \tag{7.37}$$

$h_B(\theta,R)$ is given by equation 7.33.

Although equation 7.36 provides the necessary formalism for calculating the off-axis irradiance resulting from an arbitrary beam, the indicated integration must be generally performed by numerical methods. Two special but useful applications, in which the required number of integrations is greatly reduced, will now be considered.

7.2.3.2 **On-axis irradiance of the general azimuthally symmetric beam.** The worksheets require the assumption of a conical beam, i.e., a beam whose radiant intensity is constant out to some angle and zero beyond. However, this is not generally a realistic model for actual sources. In this section, we will derive an expression for the on-axis irradiance of a more general type of source which has a radiant intensity $J(\theta)$, which is azimuthally symmetric but a nontrivial function of θ. The necessary correction to the computational procedure of the PAW will also be given.

For the case of on-axis irradiance caused by an azimuthally symmetric beam, equation 7.36 reduces to

$$h(0,R) = 2\pi \int h_B(\theta,R)\, J(\theta)\, \theta\, d\theta \quad , \tag{7.38}$$

where $h(\theta,R)$ is the resultant on-axis irradiance and the small-angle approximation is used as in the derivation of $h_B(\theta,R)$. Remembering that

$$h_B(\theta,R) = (1/2\,\pi\, R^2\, \theta)\,(dF/d\theta) \tag{7.39}$$

we have, after inserting equation 7.39 into equation 7.38 and integrating in by parts,

$$h(0,R) = (1/R^2) \left\{ J(\theta)\, F \Big|_0^{\pi/2} - \int_0^{\pi/2} J'F\, d\theta \right\} , \tag{7.40}$$

where F is given by equation 7.9. We can discard the first term of equation 7.40 if we require that $J(\theta)$ will vanish for large θ and take $J'(\theta)$ to be the right-hand derivative in the vicinity of $\theta = 0$. Equation 7.40 then simplifies to

$$h(0,R) = -(1/R^2) \int_0^{\pi/2} J'F\, d\theta \quad , \tag{7.41}$$

which is the desired formula for the on-axis irradiance of an azimuthally symmetric beam. Note that the final formula involves only the function F rather than $h_B(\theta,R)$, which means that it will have the larger range of validity for the function F (section 7.1.2) and be relatively simple to compute.

To incorporate equation 7.41 into the worksheets, a correction factor K must be defined:

$$K = 10 \log \left[h(0,R) / F_W / \Omega_c R^2 \right] \quad . \tag{7.42}$$

The term $F_W/\Omega_c R^2$ is the on-axis irradiance caused by the equivalent conical beam (section 6.10), and Ω_c is the beam's solid angle – $\Omega_c = 2\pi\,(1-\cos\theta_1) \approx \pi\,\theta_1{}^2$, with θ_1 defined according to equation 6.10.

To use the worksheets with a nonconical azimuthally symmetric beam h(0,R) is evaluated according to equation 7.41, and equation 7.42 is used to determine K. K is then added to the decibel terms appearing in the first line of step 7C of the worksheet.

A simple expression results for K in the case of Gaussian beams. The radiant intensity $J(\theta)$ of a Gaussian beam having a total power W and a 1/e width of θ_0 can be expressed, in the small-angle approximation, as

$$J(\theta) = W/\pi\,\theta_0^2 \exp\left[-(\theta/\theta_0)^2\right] \quad . \tag{7.43}$$

Using the results of equations 7.41 and 7.42 we obtain the correction factor

$$K = 10 \log \left[2/\theta_0^2 \int_0^{\pi/2} \exp\left[-(\theta/\theta_0)^2 - (c_1(\theta) - c_1(\theta_0))\, R/\cos\delta_s\right] \theta\, d\theta \right] , \tag{7.44}$$

where δ_s is defined in equation 6.14.

7.2.3.3 **On-axis irradiance of a beam containing hot spots.** In the design of light sources, attempts are usually made to provide a beam whose radiant intensity is both azimuthally symmetric and a slowly varying function of the polar angle θ. However, because of imperfections in the source components, misalignment, or subsequent rough handling, the resultant radiant intensity can depart from the ideal, resulting in a pattern with regions of high radiant intensity known as hot spots. If for all i the ith hot spot centered at θ_i has an angular extent $\Delta\,\theta_i$, so that $\Delta\,\theta_i \ll \theta_i$, then each hot spot can be considered a UPS and present formalism can be used to calculate the on-axis irradiance.

Let W_i be the power in the ith hot spot centered at θ_i. The on-axis irradiance h(0,R) is then given by

$$h(0,R) = h_s(0,R) + \sum_i W_i h_B(\theta i, R) \quad , \tag{7.45}$$

where

$$h_s(0,R) = -(1/R^2) \int_0^{\pi/2} J_s'(\theta)\, F\, d\theta \quad . \tag{7.46}$$

$J_s(\theta)$ is the radiant intensity in the symmetric portion of the beam. As in the previous section an appropriate correction factor K can be defined and added to the decibel terms in the first line of step 7C of the worksheets. The form of this term for a beam containing hot spots is

$$K = 10 \log \left[h(0,R) / \left(F_W / \Omega_c R^2 \right) \right] \tag{7.47}$$

with h(0,R) given by equation 7.45 and the remaining terms in the logarithm defined in section 7.2.3.1. When $\cos \delta_s$ departs substantially from unity, R should be replaced by $R/\cos \delta_s$ where it occurs in equation 7.47.

7.3 MODULATION TRANSFER FUNCTION

The worksheets yield the final degradations in image contrast caused by backscatter. In systems not well designed to eliminate backscatter, in water where the s/a ratio is low, or when the resolution of small objects is not required, the major cause of contrast degradation is backscatter and the results of the worksheets can be used for accurate prediction of image contrast. However, where the system is designed to minimize backscatter, where water has a large s/a ratio, or where the resolution of small objects is required, another source of contrast degradation becomes important. This degradation is caused by small-angle forward scattering of the imaging light as it returns from the target to the receiver. To describe its effects, the modulation transfer function (MTF) will be discussed.

7.3.1 Functional Form of MTF

The MTF, M(f,R), is mathematically defined as the Fourier transform of the point-spread function (PSF). Its physical significance arises from the fact that $M(f_0,R)$ is the ratio of the image to the object contrast of a sinusoidal bar chart of spatial frequency f_0. For more complicated targets $M(f_0,R)$ is the ratio of the f_0th component of the image's transform to the same component of the object's transform.

Because of the reciprocity relationship between the PSF and BSF, an expression for the MTF can be obtained by calculating the Fourier transform of $h_B(\theta,R)$ (equation 7.33). However, it must be remembered that while the derived $h_B(\theta,R)$ is simple in form and has a useful range of validity, these properties are not necessarily valid for its Fourier transform. An expression for the MTF which is relatively simple in form (refs. 7.7 and 7.8) is

$$\mathrm{MTF}\,(\psi,R) = \exp\left[-(D(\psi) - a)\, R\right] \quad , \tag{7.48}$$

where

$$D(\psi) = \alpha - 2\pi s \int_0^1 \int_0^{\pi/2} J_0(2\pi\theta\psi t)\, p(\theta)\, \theta\, d\theta\, dt \ . \tag{7.49}$$

In the above equation, J_0 is the 0th-order Bessel function of the first kind, while (ψ), the angular frequency in cycles/radians, is related to the spatial frequency f. It is expressed in cycles/meters by

$$\psi = fR \ . \tag{7.50}$$

Although the evaluation of the double integral in equation 7.49 is nontrivial, the advantage of Wells' formalism is that since $D(\psi)$ is independent of R the MTF at any range can be easily obtained using equation 7.48.

7.3.2 System Performance Analysis Using MTF

The following procedure details a method whereby the MTF can be used to estimate the effects of contrast degradation caused by multiple small-angle scattering of the imaging beam.

1. Obtain the critical spatial frequency f_c. f_c is of the order of $1/\Delta x$, where Δx is the desired resolution.

2. Calculate the critical radian frequency ψ_c from

$$\psi_c = f_c R \ . \tag{7.51}$$

3. Calculate $M(\psi_c, R)$ using equations 7.48 and 7.49. $p(\theta)$ corresponds to the reader's water characteristics.

4. Calculate $C_f = C_0\, M(\psi_c, R)$, where C_0 is the contrast of the object. C_f represents the contrast of the degraded image, with respect to C_0, which is caused by multiple small-angle scattering.

5. Perform the analysis in the PAW by obtaining C_1, the image contrast in the presence of backscatter (refer to PAW, step 8).

The minimum of C_f, C_1 will govern the contrast expected in the actual television image.

As an example of these procedures we will examine the contrast degradation of a standard, three-bar, 100-percent, contrast target that is 1 m wide and has a 2-m separation between the bar's centers. C_f will be calculated for this target at ranges of R = 20 and 40 m in water described by $\alpha = 0.145$, a = 0.033, and D (ψ) is as computed in ref. 7.7.

The fundamental spacing Δx between the objects of the bar chart is the bar-to-bar spacing, i.e., $\Delta x = 2$ m. Therefore, $f_c = 0.5$ m, and for the 20- and 40-m range ψ_c equals 10 and 20 cycles/rad, respectively. From figure 11 of reference 7.7 we find that $D(10) = 0.10$ and $D(20) = 0.12$. Therefore, the MTFs at these ranges are

$$M(\psi_c = 10, R=20) = \exp\,[-(D(10) - 0.033)\,(20)] = 0.26$$

$$M(\psi_c = 20, R=40) = \exp\,[-(D(20) - 0.033)\,(40)] = 0.03\,. \qquad (7.52)$$

Thus the image contrast caused by multiple small-angle scattering C_f equals 26 percent at 20 m (2.9 attenuation lengths) and 3 percent at 40 m (5.8 attenuation lengths). This contrast reduction can be traced to the large s/a ratio (s/a = 3.4) of the water from which $D(\psi)$ was computed.

It should be noted that equation 7.48 has not been completely verified experimentally. Some authorities maintain that underwater resolution is better than predicted by the MTF. Thus, until more data are available, the contrast reduction predicted by this formula should be considered as an upper bound.

7.4 REFERENCES

7.1 Morrison, Robert Eugene. Studies on the Optical Properties of Seawater at Argus Island in the North Atlantic Ocean and in Long Island and Block Island Sounds. Ph.D. Dissertation, New York University, New York. June 1967.

7.2 Scripps Institution of Oceanography, SIO Reference 72-78. Volume Scattering Functions for Selected Ocean Waters, by Theodore J. Petzold. October 1972.

7.3 Naval Undersea Center, NUC TP 371. Underwater Multiple Scattering of Light for System Designers, by A. Gordon and M. R. Knittel. November 1973.

7.4 Naval Undersea Center, NUC TN 1159. Underwater Multiple Scattering of Light for System Designers, by A. Gordon. August 1973.

7.5 Levin, I. M. "Observation of Objects Illuminated by a Narrow Light Beam in a Scattering Medium," Izvestia-Atmospheric and Ocean Physics, vol. 5, no. 1, pp. 62-76. 1969.

7.6 Scripps Institution of Oceanography, SIO Reference SIO 71-1. Underwater Lighting by Submerged Lasers and Incandescent Sources, by S. Q. Duntley. June 1971.

7.7 North Atlantic Treaty Organization, AGARD Report LS-61. Optics of the Sea, Article 3.4, by W. H. Wells. August 1973.

7.8 Wells, W. H. "Loss of Resolution in Water as a Result of Multiple Small-Angle Scattering," Journal of the Optical Society of America, vol. 59, no. 6, pp. 686-691. June 1969.

APPENDIX A. PERFORMANCE ANALYSIS WORKSHEETS

This appendix contains two sets of worksheets that are designed to facilitate hand calculations of the performance analysis described in section 6. The first set of worksheets is for the computation of the performance data for systems that use conventional light sources. The second set of worksheets is for systems that use lasers, i.e., for sources whose outputs are concentrated at several distinct wavelengths.

Each set of worksheets is divided into six columns. The first column identifies the step to be performed. These steps were established by the performance analysis developed in section 6; a block diagram of the analysis is presented in figure 6.14. The second column identifies the term to be evaluated at a given point in the analysis. The third column identifies the symbol for the term; these terms and symbols are summarized in section 6.5.1. The fourth column identifies the appropriate units for the term. It is essential that these units be used to insure proper cancellation of units throughout the analysis. If the column is blank for any given term, the term is unitless. The fifth column lists figures or tables that can be used to reference the term, or the column provides an equation to evaluate the term. These references are presented for the specific lights, cameras, and water for which data is available in this handbook. (If the designer has data for a specific viewing system or for the water in which the system is to be used, this data should be inserted.) For most terms, this fifth column also identifies where the term was introduced in the handbook. The final column contains boxes in which the values for given terms should be entered. The boxes are provided for four viewing systems – conventional, polarization discrimination, range gating, and volume scanning; thus, up to four systems can be simultaneously evaluated for the same viewing range, target contrast, and water type. (If a box is shaded, it does not need to be filled in for that system.)

Because of the problems discussed in section 6.2, systems using vidicons should be evaluated by the procedure described in section 6.4.3. For the first set of worksheets, this consists of omitting step 11 and performing step 12; for the second set of worksheets, step 9 is omitted, and step 10 is performed.

Use of these worksheets is straightforward. The designer should choose the appropriate set of worksheets and systematically fill in the values. Only those boxes relevant to the systems being evaluated must be used. A set of completed worksheets is in appendix B.

SET 1. PERFORMANCE ANALYSIS WORKSHEETS FOR VIEWING SYSTEMS USING CONVENTIONAL LIGHT SOURCES

STEP	TERM	SYMBOL	UNIT	REFERENCE	VALUE: CONVENTIONAL	VALUE: POLARIZATION DISCRIMINATION	VALUE: RANGE GATING	VALUE: VOLUME SCANNING
IDENTIFY SYSTEM INPUT PARAMETERS								
1. Specify System Hardware Characteristics	Type of light source			Choices for which data is available in this handbook: incandescent, Hg-arc, TlI-doped Hg-arc, xenon-arc. (These sources are introduced in section 3.1.)				
	Electrical input power to light source	w	W	Table 3.4 (w is introduced in equation 6.19.)				
	Half-angle of the "equivalent" conical beam pattern	θ_1	deg	Table 3.4 (θ_1 is defined in equation 6.10 and figure 6.6.)				
	Type of receiver			Choices for which data is available in this handbook: intensified vidicon, image orthicon, image isocon, SEC, SEBIR. (These receivers are introduced in section 3.2.) For volume-scanning systems, assume image-dissector tubes.				
	Type of photocathode or photoconductor			Choices for which data is available in this handbook: S-20 (multialkali), Type II (antimony trisulfide), and Type V (silicon diode). (cont'd)				

STEP	TERM	SYMBOL	UNIT	REFERENCE	VALUE: CONVENTIONAL	VALUE: POLARIZATION DISCRIMINATION	VALUE: RANGE GATING	VALUE: VOLUME SCANNING
				Vidicon cameras use Types II and V photoconductors; all other receivers use the S-20 photocathode.				
	Half-angle of the receiver's field-of-view	θ_3	deg	Table 3.5 (θ_3 is introduced in figure 6.6.)				
	Transmission coefficient of the receiver's optics	τ		Table 3.5. (τ is introduced in equation 6.19. For the range-gating system, see the discussion of equation 6.74.)				
	f number of receiver's optics	f/		Table 3.5. (f/ is introduced in equation 6.19.)				
	Image format area on the photosensitive surface of the receiver	A_0	m^2	Table 3.5. (A_0 is introduced in equation 6.18.)				
	Area of the entrance pupil of the image dissector	A_e	m^2	Use specific data when available. In one proposed system, $A_e = 0.043\ m^2$ (A_e is introduced in equation 6.96.)				
	Efficiency of the polarizer	e_1		Table 4.2. (e_1 is introduced in equation 6.55.)				
	Efficiency of the analyzer	e_2		Table 4.2. (e_2 is introduced in equation 6.55.)				

STEP	TERM	SYMBOL	UNIT	REFERENCE	VALUE: CONVENTIONAL	VALUE: POLARIZATION DISCRIMINATION	VALUE: RANGE GATING	VALUE: VOLUME SCANNING
	Time-average transmission coefficient of the electrooptic shutter	e_3		Unless specific data is available, use $e_3 = 0.03$. (e_3 is introduced in equation 6.74. See section 4.4.2.3 for derivation of the value.)				
	Collection efficiency of the projection optics placed on the source to collimate the output radiation	e_4		Use specific data when available; e_4 is generally < 0.20. The narrower the beam required, the smaller e_4 becomes. (e_4 is defined in equation 4.5.)				
	Duration of the source and receiver gates	Δt	sec	Use specific data when available. A useful average is 20×10^{-9} sec. (Δt is introduced in section 6.3.2.)				
2. Specify Target Characteristics	Reflectance of the dark resolution element	ρ_1		When specific data is not available, select ρ_1 and ρ_2 to achieve a desired target contrast, which is defined by $\left[\frac{\rho_2 - \rho_1}{\rho_2}\right]$. ($\rho_2$ is introduced in equation 6.19.)				
	and							
	Reflectance of the bright resolution element	ρ_2						

STEP	TERM	SYMBOL	UNIT	REFERENCE	VALUE: CONVENTIONAL	VALUE: POLARIZATION DISCRIMINATION	VALUE: RANGE GATING	VALUE: VOLUME SCANNING
	Polarization coefficient of the light reflected off the dark resolution element	ψ_s(dark)		Table 4.3. (ψ_s is introduced in equation 6.56.)				
	Polarization coefficient of the light reflected off the bright resolution element	ψ_s(bright)		Table 4.3.				
3. Specify System Geometry	Source-receiver separation	d	m	(d is defined in figure 6.6.)				
	Viewing range	R	m	(R is defined in figure 6.6.)				
SPECIFY PROPAGATION CHARACTERISTICS OF THE WATER								
4. Specify Basic Optical Properties	Type of water			Choices for which data is available in this handbook: bay, coastal, deep ocean.				
	Wavelength of maximum transmission for signal light	λ_0(S)	nm	Table 6.4. (S refers to the image-forming light.) (λ_0 is introduced in section 6.1.2.)				

STEP	TERM	SYMBOL	UNIT	REFERENCE	VALUE: CONVENTIONAL	VALUE: POLARIZATION DISCRIMINATION	VALUE: RANGE GATING	VALUE: VOLUME SCANNING
	Wavelength of maximum transmission for back-scattered light	$\lambda_0(N)$	nm	Table 6.5. (N refers to the backscattered light.)				
	Scattering-to-absorption ratio	$s/a(\lambda_0(S))$		Table 6.3. (s/a is introduced in section 2.2.)				
		$s/a(\lambda_0(N))$		Table 6.3.				
	Total attenuation coefficient	$a(\lambda_0(S))$	ln/m	Table 6.2. (a is introduced in section 2.2.)				
		$a(\lambda_0(N))$	ln/m	Table 6.2.				
	Total scattering coefficient	$s(\lambda_0(N))$	ln/m	$s = \dfrac{a(\lambda_0(N))}{1+[s/a(\lambda_0(N))]^{-1}}$				
	Fractional backscatter	η		Between 0.01 and 0.05 for most water; must be measured for specific cases. (η is defined by equation 6.38.)				
	Polarization coefficient of the backscattered light	ψ_b		Must be measured for each case; varies between 0.2 and 0.7. (ψ_b is introduced in section 2.2.)				
5. Specify Effective Attenuation Coefficients		$c_1/a(\lambda_0(S))$		Table 6.12. (c_1 is introduced in section 6.1.1.1.)				
		$c_1/a(\lambda_0(N))$		Table 6.12.				
		$c_3/a(\lambda_0(N))$		Table 6.12. (c_3 is introduced in section 6.1.1.3.)				

STEP	TERM	SYMBOL	UNIT	REFERENCE	VALUE: CONVENTIONAL	VALUE: POLARIZATION DISCRIMINATION	VALUE: RANGE GATING	VALUE: VOLUME SCANNING
6. Specify Effective Spectral Bandwidths	Minimum wavelength in the effective spectral bandwidth for the signal light	$\lambda_1(S)$	nm	Table 6.4. (λ_1 is introduced in section 6.1.2.)				
	Maximum wavelength in the effective spectral bandwidth for the signal light	$\lambda_2(S)$	nm	Table 6.4. (λ_2 is introduced in section 6.1.2.)				
	Minimum wavelength in the effective spectral bandwidth for the backscattered light	$\lambda_1(N)$	nm	Table 6.5.				
	Maximum wavelength in the effective spectral bandwidth for the backscattered light	$\lambda_2(N)$	nm	Table 6.5.				
EVALUATE SIGNAL- AND NOISE-PHOTOELECTRON CURRENTS								
7. Calculate the Signal- and Noise-Image Irradiance								
A. Calculate geometric factors	Angular orientation of the source	δ_s	deg	$\delta_s = \tan^{-1}\left(\frac{d}{2R}\right)$ (δ_s is shown in figure 6.6.)				

STEP	TERM	SYMBOL	UNIT	REFERENCE	VALUE: CONVENTIONAL	VALUE: POLARIZATION DISCRIMINATION	VALUE: RANGE GATING	VALUE: VOLUME SCANNING
	Angular orientation of the receiver	δ_R	deg	$\delta_R = -\tan^{-1}\left(\frac{d}{2R}\right)$ (δ_R is shown in figure 6.6.)				
	Distance to the backscatter volume for the conventional and polarization-discrimination systems	r_0	m	$r_0 = \frac{2d}{\left(\frac{d}{R}\right) + 2\tan(\delta_s + \theta_1)}$ or use figure 6.7. (r_0 is shown in figure 6.6.)				
	Distance to the backscatter volume for the range-gating system	r'_0	m	r'_0 = maximum of (r_0, $R - 1/2\, C_w\, \Delta t$), where $C_w = 2.25 \times 10^8$ m/sec. (r'_0 is introduced in equation 6.85.)				
	Half-angle of the receiver's field-of-view and	θ_3	deg	If θ_3 is known, use it to compute Δ according to $\Delta \simeq \frac{\theta_3 R^2}{d + \theta_3 R}$				
	Depth-of-field for the volume-scanning system	Δ	m	If θ_3 is not known, establish a desired Δ and solve for θ_3. (Δ is introduced in equation 6.93.)				
	Distance to the backscatter volume for the volume-scanning system	r''_0	m	$r''_0 = R - \Delta$. (r''_0 is introduced in equation 6.110.)				

STEP	TERM	SYMBOL	UNIT	REFERENCE	VALUE: CONVENTIONAL	VALUE: POLARIZATION DISCRIMINATION	VALUE: RANGE GATING	VALUE: VOLUME SCANNING
B. Calculate decibel terms		TR	dB	$TR = 10 \log (\rho_2)$.				
		W	dB	$W = 10 \log (w)$.				
		L	dB	$L = 10 \log \left(\frac{\tau}{f/^2} \right)$				
		D	dB	$D = 10 \log \left[\frac{2}{(1 - \cos \theta_1)} \right]$				
		R_1	dB	$R_1 = -20 \log R$.				
		$g_1(\lambda_0(S))$		$g_1 = (1 + c_1/a)/\cos \delta_s$. Use $c_1/a(\lambda_0(S))$.				
		R_2	dB	$R_2 = -4.34\ [a\ g_1\ R]$. Use $a\ (\lambda_0(S))$ and $g_1\ (\lambda_0(S))$.				
		BS	dB	$BS = 10 \log (\eta s)$.				
		$g_3(\lambda_0(N))$		$g_3 = \left(\frac{c_1}{a} + \frac{c_3}{a} \right) \Big/ \cos \delta_s$. Use $c_1/a\ (\lambda_0(N))$ and $c_3/a\ (\lambda_0(N))$.				
		$g_2(\lambda_0(N))$		$g_2 = \frac{c_1}{a} + \frac{(R^2 + d^2)^{1/2}}{R} \frac{c_3}{a}$. Use $c_1/a\ (\lambda_0(N))$ and $c_3/a\ (\lambda_0(N))$.				
	Exponential backscatter integrals	$E_2[ag_3 r_0]$		Table 6.9. ($E_2(x)$ is defined in equation 6.40.) Use $a(\lambda_0(N))$ and $g_3(\lambda_0(N))$.				
		$E_2[ag_3 r'_0]$		Table 6.9. Use $a(\lambda_0(N))$ and $g_3(\lambda_0(N))$.				

STEP	TERM	SYMBOL	UNIT	REFERENCE	VALUE: CONVENTIONAL	VALUE: POLARIZATION DISCRIMINATION	VALUE: RANGE GATING	VALUE: VOLUME SCANNING
		$E_2[ag_3R]$		Table 6.9. Use $a(\lambda_0(N))$ and $g_3(\lambda_0(N))$.				
		$E_2[ag_2r''_0]$		Table 6.9. Use $a(\lambda_0(N))$ and $g_2(\lambda_0(N))$.				
		$E_2[ag_2R]$		Table 6.9. Use $a(\lambda_0(N))$ and $g_2(\lambda_0(N))$.				
		R_3	dB	$R_3 = 10 \log \left[\frac{1}{r_0} E_2(ag_3r_0) - \frac{1}{R} E_2(ag_3R)\right]$.				
		R'_3	dB	$R'_3 = 10 \log \left[\frac{1}{r'_0} E_2 \times (ag_3r'_0) - \frac{1}{R} E_2(ag_3R)\right]$.				
		R''_3	dB	$R''_3 = 10 \log \left[\frac{1}{r''_0} E_2 \times (ag_2r''_0) - \frac{1}{R} E_2(ag_2R)\right]$.				
		R_4	dB	$R_4 = 10 \log \left[R/(R^2+d^2)^{3/2}\right]$.				
		R_5	dB	$R_5 = -4.34\,(ag_2R)$. Use $a(\lambda_0(S))$ and $g_2(\lambda_0(S))$.				
		$g_2(\lambda_0(S))$		$g_2 = c_1/a + \frac{(R^2+d^2)^{1/2}}{R} \frac{c_3}{a}$. Use $c_1/a\,(\lambda_0(S))$ and $c_3/a\,(\lambda_0(S))$.				

STEP	TERM	SYMBOL	UNIT	REFERENCE	VALUE: CONVENTIONAL	VALUE: POLARIZATION DISCRIMINATION	VALUE: RANGE GATING	VALUE: VOLUME SCANNING
		EPS	dB	EPS = 10 log $\{e_1 e_2 [1 - \psi_s (\text{bright})]\}$.	▨		▨	▨
		EPB	dB	EPB = 10 log $[e_1 e_2 (1-\psi_b)]$.	▨		▨	▨
		ES	dB	ES = 10 log e_3.	▨	▨		▨
		EC	dB	EC = 10 log e_4.	▨	▨		
		A	dB	A = 10 log (τA_e).	▨	▨	▨	
C. Sum decibel terms and calculate signal- and noise-image irradiances		$H_s(CON)$	dB	$H_s(CON) = TR + W + L + D + R_1 + R_2 - 19.51$.		▨	▨	▨
	Conventional system's signal irradiance	$\tilde{h}_s(CON)$	W/m^2	$\tilde{h}_s(CON)$ = antilog $[H_s(CON)/10]$. (Introduced in equation 6.19.)		▨	▨	▨
		$H_n(CON)$	dB	$H_n(CON) = BS + W + L + D + R_3 - 22.51$.		▨	▨	▨
	Conventional system's noise irradiance	$\tilde{h}_n(CON)$	W/m^2	$\tilde{h}_n(CON)$ = antilog $[H_n(CON)/10]$. (Introduced in equation 6.37.)		▨	▨	▨
		$H_s(PD)$	dB	$H_s(PD) = EPS + TR + W + L + D + R_1 + R_2 - 19.51$.	▨		▨	▨
	Polarization-discrimination system's signal irradiance	$\tilde{h}_s(PD)$	W/m^2	$\tilde{h}_s(PD)$ = antilog $[H_s(PD)/10]$. (Introduced in equation 6.55.)	▨		▨	▨
		$H_n(PD)$	dB	$H_n(PD) = EPB + BS + W + L + D + R_3 - 22.51$.	▨		▨	▨
	Polarization-discrimination system's noise irradiance	$\tilde{h}_n(PD)$	W/m^2	$\tilde{h}_n(PD)$ = antilog $[H_n(PD)/10]$. (Introduced in equation 6.65.)	▨		▨	▨

STEP	TERM	SYMBOL	UNIT	REFERENCE	VALUE: CONVENTIONAL	VALUE: POLARIZATION DISCRIMINATION	VALUE: RANGE GATING	VALUE: VOLUME SCANNING
		$H_s(RG)$	dB	$H_s(RG) = ES + EC + TR + W + L + D + R_1 + R_2 - 19.51.$				
	Range-gating system's signal irradiance	$\tilde{h}_s(RG)$	W/m^2	$\tilde{h}_s(RG) = \text{antilog}\,[H_s(RG)/10]$. (Introduced in equation 6.74.)				
		$H_n(RG)$	dB	$H_n(RG) = ES + EC + BS + W + L + D + R'_3 - 22.51.$				
	Range-gating system's noise irradiance	$\tilde{h}_n(RG)$	W/m^2	$\tilde{h}_n(RG) = \text{antilog}\,[H_n(RG)/10]$. (Introduced in equation 6.84.)				
		$P_s(VS)$	dB	$P_s(VS) = EC + A + TR + W + R_4 + R_5 - 7.48.$				
	Volume-scanning system's signal power	$\tilde{p}_s(VS)$	W	$\tilde{p}_s(VS) = \text{antilog}\,[P_s(VS)/10]$. (Introduced in equation 6.96.)				
		$P_n(VS)$	dB	$P_n(VS) = A + EC + BS + W + R''_3 - 10.48.$				
	Volume-scanning system's noise power	$\tilde{p}_n(VS)$	W	$\tilde{p}_n(VS) = \text{antilog}\,[P_n(VS)/10]$. (Introduced in equation 6.109.)				
8. Calculate Combined Spectral Response	Combined spectral response for the light source and the camera	$G[\lambda_2(S)]$	A/W	Table 6.8. (This term is introduced in equation 6.21.)				
		$G[\lambda_1(S)]$	A/W	Table 6.8.				
		$G[\lambda_2(N)]$	A/W	Table 6.8.				
		$G[\lambda_1(N)]$	A/W	Table 6.8.				

STEP	TERM	SYMBOL	UNIT	REFERENCE	VALUE: CONVENTIONAL	VALUE: POLARIZATION DISCRIMINATION	VALUE: RANGE GATING	VALUE: VOLUME SCANNING
9. Calculate Signal- and Noise-Photoelectron Currents	Signal photo-electron current from the bright resolution element	$i_s(\rho_2)$	A	$i_s(\rho_2) = A_0\tilde{h}_s \times \{G[\lambda_2(S)] - G[\lambda_1(S)]\}$. ($i_s$ is introduced in equation 6.18.)				▨
	Signal photo-electron current from the bright resolution element	$i_s(\rho_2)$	A	$i_s(\rho_2) = \tilde{p}_s(VS) \times \{G[\lambda_2(S)] - G[\lambda_1(S)]\}$.	▨	▨	▨	
	Signal photo-electron current from the dark resolution element	$i_s(\rho_1)$	A	$i_s(\rho_1) = \left(\frac{\rho_1}{\rho_2}\right) i_s(\rho_2)$.		▨		
	Signal photo-electron current from the dark resolution element	$i_s(\rho_1)$	A	$i_s(\rho_1) = \left(\frac{\rho_1}{\rho_2}\right) \times \frac{[1 - \psi_s(\text{dark})]}{[1 - \psi_s(\text{bright})]} i_s(\rho_2)$.	▨		▨	▨
	Noise photo-electron current	i_n	A	$i_n = A_0\tilde{h}_n \times \{G[\lambda_2(N)] - G[\lambda_1(N)]\}$. ($i_n$ is introduced in equation 6.36.)				▨
	Noise photo-electron current	i_n	A	$i_n = \tilde{p}_n(VS) \times \{G[\lambda_2(N)] - G[\lambda_1(N)]\}$. ($i_n$ for VS is introduced in equation 6.108.)	▨	▨	▨	

STEP	TERM	SYMBOL	UNIT	REFERENCE	VALUE: CONVENTIONAL	VALUE: POLARIZATION DISCRIMINATION	VALUE: RANGE GATING	VALUE: VOLUME SCANNING
EVALUATE IMAGE CONTRAST AND LIMITING RESOLUTION								
10. Evaluate Image Contrast	Image contrast	C		$C = \frac{i_s(\rho_2) - i_s(\rho_1)}{i_s(\rho_2) + i_n}$. (C is introduced in equation 6.119.)				
11. Evaluate Limiting Resolution (For Systems Using Standard Vidicons, Omit This Step)	Limiting resolution	N_L	Television lines	Figure 6.4. For input photocathode current, use $[i_s(\rho_2) + i_n]$.				
	Limiting resolution	N_L	Television lines	Figure 6.13. For input photocathode current, use $[i_s(\rho_2) + i_n]$.				
12. Calculate Equivalent Faceplate Illuminance *(Optional)*	Conversion factor	K_i	$\frac{A}{m^2 fc}$	Table 6.11. (K_i is introduced in equation 6.127.)				
	Equivalent signal faceplate illuminance	E_s	fc	$E_s = \frac{i_s(\rho_2)}{K_i A_0}$. Table 3.5 relates E_s to performance thresholds. (E_s is introduced in equation 6.125.)				
	Equivalent noise faceplate illuminance	E_n	fc	$E_n = \frac{i_n}{K_i A_0}$ Table 3.5 relates E_n to performance thresholds.				

SET 2. PERFORMANCE ANALYSIS WORKSHEETS FOR VIEWING SYSTEMS USING LASERS

STEP	TERM	SYMBOL	UNIT	REFERENCE	VALUE: CONVENTIONAL	VALUE: POLARIZATION DISCRIMINATION	VALUE: RANGE GATING	VALUE: VOLUME SCANNING
IDENTIFY SYSTEM INPUT PARAMETERS								
1. Specify System Hardward Characteristics	Type of laser			Lasers are most commonly used for range-gating and volume-scanning systems. Suggested choices: range gating, pulsed xenon ion; volume scanning, CW argon ion. (These and other lasers are introduced in sections 4.3.2.1 and 4.4.2.1.)				
	Primary spectral wavelengths of the source	λ_1	nm	Table 6.6. For sources with more than six primary wavelengths, either combine wavelengths as described in section 6.5.2 or write in values on a separate sheet.				
		λ_2						
		λ_3						
		λ_4						
		λ_5						
		λ_6						
	Number of primary spectral wavelengths	N		(N is introduced in equation 6.30.)				
	Total average radiant output power	w	W	For lasers used in range-gating systems, use table 4.5. For volume-scanning lasers, see section 4.3.2.1.				

STEP	TERM	SYMBOL	UNIT	REFERENCE	VALUE: CONVENTIONAL	VALUE: POLARIZATION DISCRIMINATION	VALUE: RANGE GATING	VALUE: VOLUME SCANNING
	Fractional output at each primary wavelength	$f(\lambda_1)$		Table 6.6. Convert percentages to decimal fractions.				
		$f(\lambda_2)$						
		$f(\lambda_3)$						
		$f(\lambda_4)$						
		$f(\lambda_5)$						
		$f(\lambda_6)$						
	Average radiant output at the wavelength λ_i	$w_R(\lambda_1)$	W	$w_R(\lambda_i) = f(\lambda_i)w$.				
		$w_R(\lambda_2)$						
		$w_R(\lambda_3)$						
		$w_R(\lambda_4)$						
		$w_R(\lambda_5)$						
		$w_R(\lambda_6)$						
	Half-angle of the "equivalent" conical beam pattern	θ_1	deg	Lower limit for the volume-scanning system: 1 mrad (0.057 deg). For other systems, use the values in table 3.4. (θ_1 is introduced in equation 6.10 and in figure 6.6.)				
	Type of receiver			Choices for which data is available in this handbook: intensified vidicon, image orthicon, image isocon, SEC, SEBIR. (These receivers are introduced in section 3.2.) For volume-scanning systems, assume an image-dissector tube.				

STEP	TERM	SYMBOL	UNIT	REFERENCE	VALUE: CONVENTIONAL	VALUE: POLARIZATION DISCRIMINATION	VALUE: RANGE GATING	VALUE: VOLUME SCANNING
	Type of photocathode or photoconductor			Choices for which data is available in this handbook: S-20 (multialkali), Type II (antimony trisulfide), Type V (silicon diode). Vidicon cameras use Types II and V photoconductors; all other receivers use the S-20 photocathode.				
	Spectral response of the receiver	$S(\lambda_1)$	A/W	Table 6.7.				
		$S(\lambda_2)$						
		$S(\lambda_3)$						
		$S(\lambda_4)$						
		$S(\lambda_5)$						
		$S(\lambda_6)$						
	Half-angle of the receiver's field-of-view	θ_3	deg	Table 3.5. (θ_3 is introduced in figure 6.6.)				
	Transmission coefficient of the receiver's optics	τ		Table 3.5. (τ is introduced in equation 6.19. For a range-gating system, see discussion of equation 6.74.)				
	f number of the receiver's optics	f/		Table 3.5. (f/ is introduced in equation 6.19.)				
	Image format area on the photosensitive surface of the receiver	A_0	m^2	Table 3.5. (A_0 is introduced in equation 6.18.)				

STEP	TERM	SYMBOL	UNIT	REFERENCE	VALUE: CONVENTIONAL	VALUE: POLARIZATION DISCRIMINATION	VALUE: RANGE GATING	VALUE: VOLUME SCANNING
	Area of the entrance pupil of the image dissector	A_e	m^2	Use specific data when available. In one proposed system, $A_e = 0.043\ m^2$. (A_e is introduced in equation 6.96.)				
	Efficiency of the polarizer	e_1		Table 4.2. (e_1 is introduced in equation 6.55.)				
	Efficiency of the analyzer	e_2		Table 4.2. (e_2 is introduced in equation 6.55.)				
	Duration of the source and receiver gates	Δt	sec	Table 4.5. (Δt is introduced in section 6.3.2.)				
2. Specify Target Characteristics	Reflectance of the dark resolution element	ρ_1		When specific data is not available, select ρ_1 and ρ_2 to achieve a desired target contrast which is defined by				
	and			$\left[\frac{\rho_2 - \rho_1}{\rho_2}\right]$. ($\rho_2$ is introduced in equation 6.19.)				
	Reflectance of the bright resolution element	ρ_2						
	Polarization coefficient of the light reflected off the dark resolution element	ψ_s(dark)		Table 4.3. (ψ_s is introduced in equation 6.56.)				

STEP	TERM	SYMBOL	UNIT	REFERENCE	VALUE: CONVENTIONAL	VALUE: POLARIZATION DISCRIMINATION	VALUE: RANGE GATING	VALUE: VOLUME SCANNING
	Polarization coefficient of the light reflected off the bright resolution element	ψ_s(bright)		Table 4.3.				
3. Specify System Geometry	Source-receiver separation	d	m	(d is defined in figure 6.6.)				
	Viewing range	R	m	(R is defined in figure 6.6.)				
SPECIFY PROPAGATION CHARACTERISTICS OF THE WATER								
4. Specify Basic Optical Properties	Type of water			Choices for which data is available in this handbook: bay, coastal, deep ocean.				
	Total attenuation coefficient	$a(\lambda_1)$	ln/m	Table 6.2. (a is introduced in section 2.2.)				
		$a(\lambda_2)$						
		$a(\lambda_3)$						
		$a(\lambda_4)$						
		$a(\lambda_5)$						
		$a(\lambda_6)$						

STEP	TERM	SYMBOL	UNIT	REFERENCE	VALUE: CONVENTIONAL	VALUE: POLARIZATION DISCRIMINATION	VALUE: RANGE GATING	VALUE: VOLUME SCANNING
	Scattering-to-absorption ratio	$\frac{s}{a}(\lambda_1)$		Table 6.3. (s/a is introduced in section 2.2.)				
		$\frac{s}{a}(\lambda_2)$						
		$\frac{s}{a}(\lambda_3)$						
		$\frac{s}{a}(\lambda_4)$						
		$\frac{s}{a}(\lambda_5)$						
		$\frac{s}{a}(\lambda_6)$						
	Total scattering coefficient	$s(\lambda_1)$	ln/m	$s(\lambda_i) \doteq \frac{a(\lambda_i)}{\left\{1 + \left[\frac{s}{a}(\lambda_i)\right]^{-1}\right\}}$				
		$s(\lambda_2)$						
		$s(\lambda_3)$						
		$s(\lambda_4)$						
		$s(\lambda_5)$						
		$s(\lambda_6)$						
	Fractional backscatter	η		Between 0.01 and 0.05 for most water; must be measured for specific cases. (η is defined by equation 6.38.)				
	Polarization coefficient of the backscattered light	ψ_b		Must be measured for each case; varies between 0.2 and 0.7. (ψ_b is introduced in section 2.2.)				

STEP	TERM	SYMBOL	UNIT	REFERENCE	VALUE: CONVENTIONAL	VALUE: POLARIZATION DISCRIMINATION	VALUE: RANGE GATING	VALUE: VOLUME SCANNING
5. Specify Effective Attenuation Coefficients		$\frac{c_1}{a}(\lambda_1)$		Table 6.1. Use $\theta_i = \theta_1$. For s/a > 5.0, use figure 6.1. (c_1 is introduced in section 6.1.1.1.)				
		$\frac{c_1}{a}(\lambda_2)$						
		$\frac{c_1}{a}(\lambda_3)$						
		$\frac{c_1}{a}(\lambda_4)$						
		$\frac{c_1}{a}(\lambda_5)$						
		$\frac{c_1}{a}(\lambda_6)$						
		$\frac{c_3}{a}(\lambda_1)$		Table 6.1. Use $\theta_i = \theta_3$. θ_3 for the volume-scanning system is evaluated below. For s/a > 5.0, use figure 6.1. (c_3 is introduced in section 6.1.1.3.)				
		$\frac{c_3}{a}(\lambda_2)$						
		$\frac{c_3}{a}(\lambda_3)$						
		$\frac{c_3}{a}(\lambda_4)$						
		$\frac{c_3}{a}(\lambda_5)$						
		$\frac{c_3}{a}(\lambda_6)$						
EVALUATE SIGNAL- AND NOISE-PHOTOELECTRON CURRENTS								
6. Calculate Signal- and Noise-Image Irradiance								
A. Calculate geometric factors	Angular orientation of the source	δ_s	deg	$\delta_s = \tan^{-1}(d/2R)$. ($\delta_s$ is shown in figure 6.6.)				

STEP	TERM	SYMBOL	UNIT	REFERENCE	VALUE: CONVENTIONAL	VALUE: POLARIZATION DISCRIMINATION	VALUE: RANGE GATING	VALUE: VOLUME SCANNING
	Angular orientation of the receiver	δ_R	deg	$\delta_R = -\tan^{-1}(d/2R)$. ($\delta_R$ is shown in figure 6.6.)				
	Distance to the backscatter volume for the conventional and polarization-discrimination systems	r_0	m	$r_0 = \dfrac{2d}{\left(\frac{d}{R}\right) + 2\tan(\delta_s + \theta_1)}$ or use figure 6.7. (r_0 is shown in figure 6.6.)				
	Distance to the backscatter volume for the range-gating system	r'_0	m	r'_0 = maximum of (r_0, $R - 1/2\, C_w\, \Delta t$), where $C_w = 2.25 \times 10^8$ m/sec. (r'_0 is introduced in equation 6.85.)				
	Half-angle of the receiver's field-of-view	θ_3	deg	If θ_3 is known, use it to compute Δ according to $\Delta \simeq \dfrac{\theta_3 R^2}{d + \theta_3 R}$				
	and Depth-of-field for the volume-scanning system	Δ	m	If θ_3 is not known, establish a desired Δ and solve for θ_3. (Δ is introduced in equation 6.93.)				
	Distance to the backscatter volume for the volume-scanning system	r''_0	m	$r''_0 = R - \Delta$. (r''_0 is introduced in equation 6.110.)				

STEP	TERM	SYMBOL	UNIT	REFERENCE	VALUE: CONVENTIONAL	VALUE: POLARIZATION DISCRIMINATION	VALUE: RANGE GATING	VALUE: VOLUME SCANNING
B. Calculate decibel terms		TR	dB	$TR = 10 \log (\rho_2)$.				
		$WR(\lambda_1)$	dB	$WR(\lambda_i) = 10 \log w_R(\lambda_i)$.				
		$WR(\lambda_2)$						
		$WR(\lambda_3)$						
		$WR(\lambda_4)$						
		$WR(\lambda_5)$						
		$WR(\lambda_6)$						
		L	dB	$L = 10 \log \left[\frac{\tau}{f/2}\right]$.				
		D	dB	$D = 10 \log \left[\frac{2}{(1 - \cos\theta_1)}\right]$.				
		R_1	dB	$R_1 = -20 \log R$.				
		$g_1(\lambda_1)$		$g_1(\lambda_i) = \left[1 + \frac{c_1}{a}(\lambda_i)\right] \Big/ \cos \delta_s$.				
		$g_1(\lambda_2)$						
		$g_1(\lambda_3)$						
		$g_1(\lambda_4)$						
		$g_1(\lambda_5)$						
		$g_1(\lambda_6)$						
		$R_2(\lambda_1)$		$R_2(\lambda_i) = -4.34 \times [a(\lambda_i)\, g_1(\lambda_i)\, R]$.				
		$R_2(\lambda_2)$						
		$R_2(\lambda_3)$						
		$R_2(\lambda_4)$						
		$R_2(\lambda_5)$						
		$R_2(\lambda_6)$						

STEP	TERM	SYMBOL	UNIT	REFERENCE	VALUE: CONVENTIONAL	VALUE: POLARIZATION DISCRIMINATION	VALUE: RANGE GATING	VALUE: VOLUME SCANNING
		$BS(\lambda_1)$	dB	$BS = 10 \log [\eta s(\lambda_i)]$.				
		$BS(\lambda_2)$						
		$BS(\lambda_3)$						
		$BS(\lambda_4)$						
		$BS(\lambda_5)$						
		$BS(\lambda_6)$						
		$g_3(\lambda_1)$		$g_3(\lambda_i) = \left[\frac{c_1}{a}(\lambda_i)\right.$				
		$g_3(\lambda_2)$						
		$g_3(\lambda_3)$		$\left.+\frac{c_3'}{a}(\lambda_i)\right] \Big/ \cos\delta_s$.				
		$g_3(\lambda_4)$						
		$g_3(\lambda_5)$						
		$g_3(\lambda_6)$						
		$g_2(\lambda_1)$		$g_2(\lambda_i) = \left[\frac{c_1}{a}(\lambda_i) + \right.$				
		$g_2(\lambda_2)$						
		$g_2(\lambda_3)$		$\left.\frac{c_3}{a}(\lambda_i)\frac{(R^2+d^2)^{1/2}}{R}\right]$.				
		$g_2(\lambda_4)$						
		$g_2(\lambda_5)$						
		$g_2(\lambda_6)$						
	Exponential backscatter integrals	$E_2[ag_3r_0]_i$		$E_2[ag_3r_0]_i =$				
				$E_2[a(\lambda_i)g_3(\lambda_i)r_0]$,				
				$i = 1, N$.				
				Table 6.9.				
				[$E_2(x)$ is defined in equation 6.40.)				

STEP	TERM	SYMBOL	UNIT	REFERENCE	VALUE: CONVENTIONAL	VALUE: POLARIZATION DISCRIMINATION	VALUE: RANGE GATING	VALUE: VOLUME SCANNING
		$E_2[ag_3r'_0]_i$		$E_2[ag_3r'_0]_i =$ $E_2[a(\lambda_i)g_3(\lambda_i)r'_0]$, $i = 1, N$. Table 6.9.				
		$E_2[ag_3R]_i$		$E_2[ag_3R]_i =$ $E_2[a(\lambda_i)g_3(\lambda_i)R]$, $i = 1, N$. Table 6.9.				
		$E_2[ag_2r''_0]_i$		$E_2[ag_2r''_0]_i =$ $E_2[a(\lambda_i)g_2(\lambda_i)r''_0]$, $i = 1, N$. Table 6.9.				
		$E_2[ag_2R]_i$		$E_2[ag_2R]_i =$ $E_2[a(\lambda_i)g_2(\lambda_i)R]$, $i = 1, N$. Table 6.9.				

STEP	TERM	SYMBOL	UNIT	REFERENCE	VALUE: CONVENTIONAL	VALUE: POLARIZATION DISCRIMINATION	VALUE: RANGE GATING	VALUE: VOLUME SCANNING
		$R_3(\lambda_1)$	dB	$R_3(\lambda_i) = 10 \log \left\{ \frac{1}{r_0} \times \right.$				
		$R_3(\lambda_2)$		$E_2[a(\lambda_i)g_3(\lambda_i)r_0]$				
		$R_3(\lambda_3)$		$\left. - \frac{1}{R} E_2[a(\lambda_i)g_3(\lambda_i)R] \right\}$.				
		$R_3(\lambda_4)$						
		$R_3(\lambda_5)$						
		$R_3(\lambda_6)$						
		$R'_3(\lambda_1)$	dB	$R'_3(\lambda_i) = 10 \log \left\{ \frac{1}{r'_0} \times \right.$				
		$R'_3(\lambda_2)$		$E_2[a(\lambda_i)g_3(\lambda_i)r'_0]$				
		$R'_3(\lambda_3)$		$\left. - \frac{1}{R} E_2[a(\lambda_i)g_3(\lambda_i)R] \right\}$.				
		$R'_3(\lambda_4)$						
		$R'_3(\lambda_5)$						
		$R'_3(\lambda_6)$						
		$R''_3(\lambda_1)$	dB	$R''_3(\lambda_i) = 10 \log$				
		$R''_3(\lambda_2)$		$\left\{ \frac{1}{r''_0} E_2[a(\lambda_i)g_2(\lambda_i)r''_0] \right.$				
		$R''_3(\lambda_3)$		$\left. - \frac{1}{R} E_2[a(\lambda_i)g_2(\lambda_i)R] \right\}$.				
		$R''_3(\lambda_4)$						
		$R''_3(\lambda_5)$						
		$R''_3(\lambda_6)$						
		R_4	dB	$R_4 = 10 \log$				
				$\left[R/(R^2 + d^2)^{3/2} \right]$.				
		$R_5(\lambda_1)$	dB	$R_5(\lambda_i) = -4.34$				
		$R_5(\lambda_2)$		$[a(\lambda_i)g_2(\lambda_i)\ R]$.				
		$R_5(\lambda_3)$						
		$R_5(\lambda_4)$						
		$R_5(\lambda_5)$						
		$R_5(\lambda_6)$						

STEP	TERM	SYMBOL	UNIT	REFERENCE	VALUE: CONVENTIONAL	VALUE: POLARIZATION DISCRIMINATION	VALUE: RANGE GATING	VALUE: VOLUME SCANNING
		EPS	dB	EPS = 10 log $\{e_1 e_2 \times [1 - \psi_s(\text{bright})]\}$.				
		EPB	dB	EPB = 10 log $[e_1 e_2 (1 - \psi_b)]$.				
		A	dB	A = 10 log (τA_e) .				
C. Sum decibel terms and calculate signal- and noise-image irradiances.		$H'_s(CON)_i$	dB	$H'_s(CON)_i = TR + WR(\lambda_i) + L + D + R_1 + R_2(\lambda_i) - 19.51, i = 1, N$				
	Conventional system's signal irradiance	$\tilde{h}'_s(CON)_i$	W/m^2	$\tilde{h}'_s(CON)_i$ = antilog $[H_s(CON)_i/10]$, i = 1,N. (Introduced in equation 6.31.)				
		$H'_n(CON)_i$	dB	$H'_n(CON)_i = BS(\lambda_i) + WR(\lambda_i) + L + D + R_3(\lambda_i) - 22.51, i = 1, N.$				

STEP	TERM	SYMBOL	UNIT	REFERENCE	VALUE: CONVENTIONAL	VALUE: POLARIZATION DISCRIMINATION	VALUE: RANGE GATING	VALUE: VOLUME SCANNING
	Conventional system's noise irradiance	$\tilde{h}'_n(CON)_i$	W/m^2	$\tilde{h}'_n(CON)_i$ = antilog $[H'_n(CON)_i/10]$, $i = 1, N$. (Introduced in equation 6.46.)				
		$H'_s(PD)_i$	dB	$H'_s(PD)_i = EPS + TR + WR(\lambda_i) + L + D + R_1 + R_2(\lambda_i) - 19.51$, $i = 1, N$.				
	Polarization-discrimination system's signal irradiance	$\tilde{h}'_s(PD)_i$	W/m^2	$\tilde{h}'_s(PD)_i$ = antilog $[H'_s(PD)_i/10]$, $i = 1, N$. (Introduced in equation 6.61.)				
		$H'_n(PD)_i$	dB	$H'_n(PD)_i = EPB + BS(\lambda_i) + WR(\lambda_i) + L + D + R_3(\lambda_i) - 22.51$, $i = 1, N$.				

STEP	TERM	SYMBOL	UNIT	REFERENCE	VALUE: CONVENTIONAL	VALUE: POLARIZATION DISCRIMINATION	VALUE: RANGE GATING	VALUE: VOLUME SCANNING
	Polarization-discrimination system's noise irradiance	$\tilde{h}'_n(PD)_i$	W/m^2	$\tilde{h}'_n(PD)_i$ = antilog $[H'_n(PD)_i/10]$, i = 1, N. (Introduced in equation 6.70.)				
		$H'_s(RG)_i$	dB	$H'_s(RG)_i = TR + WR(\lambda_i) + L + D + R_1 + R_2(\lambda_i) - 19.51$, i = 1, N.				
	Range-gating system's signal irradiance	$\tilde{h}'_s(RG)_i$	W/m^2	$\tilde{h}'_s(RG)_i$ = antilog $[H'_s(RG)_i/10]$, i = 1, N. (Introduced in equation 6.80.)				
		$H'_n(RG)_i$	dB	$H'_n(RG)_i = BS(\lambda_i) + WR(\lambda_i) + L + D + R'_3(\lambda_i) - 22.51$, i = 1, N.				

STEP	TERM	SYMBOL	UNIT	REFERENCE	VALUE: CONVENTIONAL	VALUE: POLARIZATION DISCRIMINATION	VALUE: RANGE GATING	VALUE: VOLUME SCANNING
	Range-gating system's noise irradiance	$\tilde{h}'_n(RG)_i$	W/m^2	$\tilde{h}'_n(RG)_i$ = antilog $[H'_n(RG)_i/10]$, i = 1, N. (Introduced in equation 6.90.)				
		$P'_s(VS)_i$	dB	$P'_s(VS)_i = A + TR + WR(\lambda_i) + R_4 + R_5(\lambda_i) - 7.48$, i = 1, N.				
	Volume-scanning system's signal power	$\tilde{p}'_s(VS)_i$	W	$\tilde{p}'_s(VS)_i$ = antilog $[P'_s(VS)_i/10]$, i = 1, N. (Introduced in equation 6.106.)				
		$P'_n(VS)_i$	dB	$P'_n(VS)_i = A + BS(\lambda_i) + WR(\lambda_i) + R''_3(\lambda_i) - 10.48$, i = 1, N.				

STEP	TERM	SYMBOL	UNIT	REFERENCE	VALUE: CONVENTIONAL	VALUE: POLARIZATION DISCRIMINATION	VALUE: RANGE GATING	VALUE: VOLUME SCANNING
	Volume-scanning system's noise power	$\tilde{p}'_n(VS)_i$	W	$\tilde{p}'_n(VS)_i$ = antilog $[P'_s(VS)_i/10]$, i = 1, N. (Introduced in equation 6.117.)				
7. Calculate Signal- and Noise-Photoelectron Currents	Signal photoelectron current from the bright resolution element	$i_s(\rho_2)$	A	$i_s(\rho_2) = A_0 \sum_{i=1}^{N} \tilde{h}'_s(X)_i\, S(\lambda_i)$, X = CON, PD, or RG for i_s(CON, PD, or RG). (i_s is introduced in equation 6.30.)				
	Signal photoelectron current from the bright resolution element	$i_s(\rho_2)$	A	$i_s(\rho_2) = \sum_{i=1}^{N} \tilde{p}'_s(VS)_i\, S(\lambda_i)$. ($i_s$ for VS is introduced in equation 6.103.)				
	Signal photoelectron current from the dark resolution element	$i_s(\rho_1)$	A	$i_s(\rho_1) = (\rho_1/\rho_2)\, i_s(\rho_2)$.				

STEP	TERM	SYMBOL	UNIT	REFERENCE	VALUE: CONVENTIONAL	VALUE: POLARIZATION DISCRIMINATION	VALUE: RANGE GATING	VALUE: VOLUME SCANNING
	Signal photo-electron current from the dark resolution element	$i_s(\rho_1)$	A	$i_s(\rho_1) = \left(\frac{\rho_1}{\rho_2}\right)\frac{[1-\psi_s(\text{dark})]}{[1-\psi_s(\text{bright})]} i_s(\rho_2)$				
	Noise photo-electron current	i_n	A	$i_n = A_0 \sum_{i=1}^{N} \tilde{h}'_n(X)_i S(\lambda_i)$, X = CON, PD, or RG for i_n(CON, PD, or RG). (Introduced in equation 6.45.)				
	Noise photo-electron current	i_n	A	$i_n = \sum_{i=1}^{N} \tilde{p}'_n(VS)_i S(\lambda_i)$. (Introduced in equation 6.114.)				
EVALUATE IMAGE CONTRAST AND LIMITING RESOLUTION								
8. Evaluate Image Contrast	Image contrast	C		$C = \frac{i_s(\rho_2) - i_s(\rho_1)}{i_s(\rho_2) + i_n}$. (C is introduced in equation 6.119.)				
9. Evaluate the Limiting Resolution (For Systems Using Standard Vidicons, Omit This Step)	Limiting resolution	N_L	Tele-vision lines	Figure 6.4. For input photocathode current, use $[i_s(\rho_2) + i_n]$.				

STEP	TERM	SYMBOL	UNIT	REFERENCE	VALUE: CONVENTIONAL	VALUE: POLARIZATION DISCRIMINATION	VALUE: RANGE GATING	VALUE: VOLUME SCANNING
	Limiting resolution	N_L	Tele-vision lines	Figure 6.13. For input photocathode current, use $[i_s(\rho_2) + i_n]$.				
10. Calculate Equivalent Faceplate Illuminance *(Optional)*	Conversion factor	K_i	A/m^2fc	Table 6.11. (K_i is introduced in equation 6.127.)				
	Equivalent signal faceplate illuminance	E_s	fc	$E_s = \frac{i_s}{K_i A_0}$. Table 3.5 relates E_s to performance thresholds. (E_s is introduced in equation 6.125.)				
	Equivalent noise faceplate illuminance	E_n	fc	$E_n = \frac{i_n}{K_i A_0}$ Table 3.5 relates E_n to performance thresholds.				

APPENDIX B. SAMPLE CALCULATIONS

This appendix contains detailed solutions to two representative underwater imaging problems. These solutions illustrate the proper execution of the analytical resources developed in section 6, display the variety of problems tractable by the analysis, and demonstrate the applicability of the analysis to realistic viewing situations. The problems were chosen so that it was necessary to use both sets of worksheets in appendix A.*

B.1 CONVENTIONAL IMAGING SYSTEM WITH AND WITHOUT POLARIZATION DISCRIMINATION

B.1.1 PROBLEM – Consider a conventional imaging system consisting of a 200-W, thallium-iodide-doped mercury-vapor arc lamp (TlI Hg) and an SEC vidicon television camera. The system is to be operated aboard a small submersible where the source-receiver separation is limited to a maximum of 1.5 m. Because of the small source-receiver separation and the desire to achieve long search ranges, backscatter is expected to be a limiting factor. Thus, system performance will be enhanced by polarization discrimination. The desired search range is 20 m, or approximately 5 attenuation lengths in 4-m water ($a \approx 0.252$). The problem is as follows: Determine viewing range performance at 20 m with and without polarization discrimination.

The problem is further defined by the specification of all relevant hardware characteristics, target characteristics, system geometry, and water characteristics. These quantities are identified in table B.1. In practice, the designer determines the required input parameters by filling in the first few pages of the appropriate set of worksheets in appendix A. The worksheets require only those input parameters necessary for the specific system being analyzed.

B.1.2 SOLUTION – The following text is keyed step-by-step to the sample worksheets on pages B-6 through B-18.

Steps 1 through 3. Values from table B.1 are entered in the appropriate boxes in the worksheets. Note that only those boxes in the "conventional" and "polarization discrimination" columns are used; the remaining columns are ignored for this exercise.

Steps 4 through 6. The remaining values from table B.1 are entered in the appropriate boxes in the worksheets. Other values are found in the tables in the body of the handbook or by direct calculations according to instructions in the worksheets. When terms are looked up as functions of wavelength, the wavelength can be rounded off to two significant figures.

It is assumed that the reader is familiar with the terms that will be used in this appendix. These terms were defined in the worksheets in appendix A and in the text of section 6.

Special attention is called to two of the water characteristics inputs – the fractional backscatter η and the polarization coefficient ψ_b. Very little data exists for these two terms. When possible, they should be measured for the specific water in which the system is to be used. Section 2 discusses the required instrumentation. For the present exercise, $\eta = 0.02$ was chosen as a value often encountered in coastal waters, and $\psi_b = 0.7$ was chosen as an optimum value to calculate the maximum amount of visibility improvement available with polarizing filters.

Steps 7 through 9. Values are directly calculated or are found in the tables according to the instructions in the worksheets. An electronic calculator with a logarithm capability is a great convenience in performing the logarithm calculations of steps 8 and 9; however, standard logarithm tables can be used.

Steps 10 through 11. Using the values calculated in the previous steps, image contrast is calculated and the limiting resolution is determined according to the instructions in the worksheets.

Note that difficulty is encountered in determining the limiting resolution for the conventional system without polarization discrimination. The noise-photoelectron current is so large that it is off the scale of figure 6.4, and the contrast (0.02) is lower than the lowest contrast curve of figure 6.4.

Polarization discrimination, however, yields satisfactory results. The filters help in two ways: They lower the incoming light level, shifting the photoelectron level into the useful operating range of the camera, and they reject much of the backscatter, increasing the contrast to a useful level.

B.1.3 DISCUSSION – The results for the polarization-discrimination system indicate that the system will perform well at the desired viewing range of 5 attenuation lengths. This performance, however, is contingent on a polarization coefficient of 0.7.

This first problem illustrates the general procedure to be followed for determining viewing performance for a particular system, viewing geometry, water type, and target contrast. To determine system performance as a function of one or more variables, the problem must be reworked for each variable. Most of the work, however, is done the first time that the worksheets are used. Only those terms directly affected by the new variable need be changed; second and third changes to the problem can generally be performed very quickly.

B.2 RANGE-GATING SYSTEM

B.2.1 PROBLEM – Consider a range-gating imaging system consisting of a pulsed xenon laser* and a gated SEC vidicon television camera. As in the first problem, the system is to be operated aboard a small submersible where source-receiver separation is limited to a

---

**The laser discussed on page 4-18 will be used in this exercise.*

maximum of 1.5 m. The desired search range is 20 m, or approximately 5 attenuation lengths in 4-m water ($a \approx 0.252$). The problem is as follows: Determine viewing range performance at 20 m.

The problem is further defined by the specification of all relevant hardware characteristics, target characteristics, system geometry, and water characteristics. These quantities are identified in table B.2. In practice, the designer determines the required input parameters by filling in the first pages of the appropriate set of appendix A worksheets.

B.2.2 **SOLUTION** – Because the output of a pulsed xenon laser is concentrated at several distinct wavelengths, the second set of worksheets is required to solve the problem. Pages B-19 through B-37 are sample, filled-in worksheets for this problem.

The solution to this problem is straightforward; no special problems occur in filling in the worksheets. The final result, $N_L = 680$ television lines, indicates that this system should provide excellent resolution at this viewing range.

Table B.1. Input Parameters for the Evaluation of a Conventional Imaging System With and Without Polarization Discrimination.

Parameter	Description
System Hardware	
• Source	
Type	TlI Hg
Input power (w)	200 W
Beam half-angle (θ_1)	10 deg
• Receiver	
Type	SEC vidicon
Photocathode	S-20
Field-of-view half-angle (θ_3)	10 deg
Transmission coefficient (τ)	1.0
f/	1.5
Image format area (A_0)	1.2×10^{-4} m^2
• Extended-range equipment	
Polarization efficiency (e_1)	0.88
Analyzer efficiency (e_2)	0.37
Target Characteristics	
• Reflectivity of dark resolution element (ρ_1)	0.2
• Reflectivity of bright resolution element (ρ_2)	0.8
• Polarization coefficient of light reflected off dark resolution element	0.77
• Polarization coefficient of light reflected off bright resolution element	0.04
System Geometry	
• Source-receiver separation (d)	1.5 m
• Viewing range (R)	20 m
Propagation Characteristics of Water	
• Type	Coastal
• Fractional backscatter (η)	0.02
• Polarization coefficient (ψ_b)	0.7

Table B.2. Input Parameters for the Evaluation of a Range-Gating Imaging System.

Parameter	Description
System Hardware	
• Source	
Type	Pulsed xenon laser
Beam half-angle (θ_1)	5 deg
• Receiver	
Type	SEC vidicon
Photocathode	S-20
Field-of-view half-angle (θ_3)	10 deg
Transmission coefficient (τ)	1.0
f/	1.5
Image format area (A_0)	1.2×10^{-4} m^2
Target Characteristics	
• Reflectivity of dark resolution element (ρ_1)	0.2
• Reflectivity of bright resolution element (ρ_2)	0.8
System Geometry	
• Source-receiver separation (d)	1.5 m
• Viewing range (R)	20 m
Propagation Characteristics of Water	
• Type	Coastal
• Fractional backscatter (η)	0.02

SET 1. PERFORMANCE ANALYSIS WORKSHEETS FOR VIEWING SYSTEMS USING CONVENTIONAL LIGHT SOURCES

STEP	TERM	SYMBOL	UNIT	REFERENCE	VALUE: CONVENTIONAL	VALUE: POLARIZATION DISCRIMINATION	VALUE: RANGE GATING	VALUE: VOLUME SCANNING
IDENTIFY SYSTEM INPUT PARAMETERS								
1. Specify System Hardware Characteristics	Type of light source			Choices for which data is available in this handbook: incandescent, Hg-arc, TlI-doped Hg-arc, xenon-arc. (These sources are introduced in section 3.1.)	TlI	TlI		
	Electrical input power to light source	w	W	Table 3.4 (w is introduced in equation 6.19.)	200	200		
	Half-angle of the "equivalent" conical beam pattern	θ_1	deg	Table 3.4 (θ_1 is defined in equation 6.10 and figure 6.6.)	10	10		
	Type of receiver			Choices for which data is available in this handbook: intensified vidicon, image orthicon, image isocon, SEC, SEBIR. (These receivers are introduced in section 3.2.) For volume-scanning systems, assume image-dissector tubes.	SEC	SEC		
	Type of photocathode or photoconductor			Choices for which data is available in this handbook: S-20 (multialkali), Type II (antimony trisulfide), and Type V (silicon diode). (cont'd)	S-20	S-20		

STEP	TERM	SYMBOL	UNIT	REFERENCE	VALUE: CONVENTIONAL	VALUE: POLARIZATION DISCRIMINATION	VALUE: RANGE GATING	VALUE: VOLUME SCANNING
				Vidicon cameras use Types II and V photoconductors; all other receivers use the S-20 photocathode.				
	Half-angle of the receiver's field-of-view	θ_3	deg	Table 3.5 (θ_3 is introduced in figure 6.6.)	10.0	10.0		
	Transmission coefficient of the receiver's optics	τ		Table 3.5. (τ is introduced in equation 6.19. For the range-gating system, see the discussion of equation 6.74.)	1.00	1.00		
	f number of receiver's optics	f/		Table 3.5. (f/ is introduced in equation 6.19.)	1.5	1.5		
	Image format area on the photosensitive surface of the receiver	A_0	m^2	Table 3.5. (A_0 is introduced in equation 6.18.)	1.20×10^{-4}	1.20×10^{-4}		
	Area of the entrance pupil of the image dissector	A_e	m^2	Use specific data when available. In one proposed system, $A_e = 0.043\ m^2$. (A_e is introduced in equation 6.96.)				
	Efficiency of the polarizer	e_1		Table 4.2. (e_1 is introduced in equation 6.55.)		0.88		
	Efficiency of the analyzer	e_2		Table 4.2. (e_2 is introduced in equation 6.55.)		0.37		

STEP	TERM	SYMBOL	UNIT	REFERENCE	VALUE: CONVENTIONAL	VALUE: POLARIZATION DISCRIMINATION	VALUE: RANGE GATING	VALUE: VOLUME SCANNING
	Time-average transmission coefficient of the electrooptic shutter	e_3		Unless specific data is available, use $e_3 = 0.03$. (e_3 is introduced in equation 6.74. See section 4.4.2.3 for derivation of the value.)				
	Collection efficiency of the projection optics placed on the source to collimate the output radiation	e_4		Use specific data when available; e_4 is generally < 0.20. The narrower the beam required, the smaller e_4 becomes. (e_4 is defined in equation 4.5.)				
	Duration of the source and receiver gates	Δt	sec	Use specific data when available. A useful average is 20×10^{-9} sec. (Δt is introduced in section 6.3.2.)				
2. Specify Target Characteristics	Reflectance of the dark resolution element	ρ_1		When specific data is not available, select ρ_1 and ρ_2 to achieve a desired target contrast, which is defined by $\left[\frac{\rho_2 - \rho_1}{\rho_2}\right]$. ($\rho_2$ is introduced in equation 6.19.)				
	and							
	Reflectance of the bright resolution element	ρ_2						

STEP	TERM	SYMBOL	UNIT	REFERENCE	VALUE: CONVENTIONAL	VALUE: POLARIZATION DISCRIMINATION	VALUE: RANGE GATING	VALUE: VOLUME SCANNING
	Polarization coefficient of the light reflected off the dark resolution element	ψ_s(dark)		Table 4.3. (ψ_s is introduced in equation 6.56.)		0.77		
	Polarization coefficient of the light reflected off the bright resolution element	ψ_s(bright)		Table 4.3.		0.04		
3. Specify System Geometry	Source-receiver separation	d	m	(d is defined in figure 6.6.)	1.50	1.50		
	Viewing range	R	m	(R is defined in figure 6.6.)	20.0	20.0		
SPECIFY PROPAGATION CHARACTERISTICS OF THE WATER								
4. Specify Basic Optical Properties	Type of water			Choices for which data is available in this handbook: bay, coastal, deep ocean.	coastal	coastal		
	Wavelength of maximum transmission for signal light	λ_0(S)	nm	Table 6.4. (S refers to the image-forming light.) (λ_0 is introduced in section 6.1.2.)	540	540		

STEP	TERM	SYMBOL	UNIT	REFERENCE	VALUE: CONVENTIONAL	VALUE: POLARIZATION DISCRIMINATION	VALUE: RANGE GATING	VALUE: VOLUME SCANNING
	Wavelength of maximum transmission for back-scattered light	$\lambda_0(N)$	nm	Table 6.5. (N refers to the backscattered light.)	510	510		
	Scattering-to-absorption ratio	$s/a(\lambda_0(S))$		Table 6.3. (s/a is introduced in section 2.2.)	5.15	5.15		
		$s/a(\lambda_0(N))$		Table 6.3.	6.80	6.80		
	Total attenuation coefficient	$a(\lambda_0(S))$	ln/m	Table 6.2. (a is introduced in section 2.2.)	.252	.252		
		$a(\lambda_0(N))$	ln/m	Table 6.2.	.273	.273		
	Total scattering coefficient	$s(\lambda_0(N))$	ln/m	$s = \dfrac{a(\lambda_0(N))}{1+[s/a(\lambda_0(N))]^{-1}}$	.238	.238		
	Fractional backscatter	η		Between 0.01 and 0.05 for most water; must be measured for specific cases. (η is defined by equation 6.38.)	.02	.02		
	Polarization coefficient of the backscattered light	ψ_b		Must be measured for each case; varies between 0.2 and 0.7. (ψ_b is introduced in section 2.2.)		0.7		
5. Specify Effective Attenuation Coefficients		c_1/a $(\lambda_0(S))$		Table 6.12. (c_1 is introduced in section 6.1.1.1.)	.29	.29		
		c_1/a $(\lambda_0(N))$		Table 6.12.	.25	.25		
		c_3/a $(\lambda_0(N))$		Table 6.12. (c_3 is introduced in section 6.1.1.3.)	.25	.25		

STEP	TERM	SYMBOL	UNIT	REFERENCE	VALUE: CONVENTIONAL	VALUE: POLARIZATION DISCRIMINATION	VALUE: RANGE GATING	VALUE: VOLUME SCANNING
6. Specify Effective Spectral Bandwidths	Minimum wavelength in the effective spectral bandwidth for the signal light	$\lambda_1(S)$	nm	Table 6.4. (λ_1 is introduced in section 6.1.2.)	490	490		
	Maximum wavelength in the effective spectral bandwidth for the signal light	$\lambda_2(S)$	nm	Table 6.4. (λ_2 is introduced in section 6.1.2.)	580	580		
	Minimum wavelength in the effective spectral bandwidth for the backscattered light	$\lambda_1(N)$	nm	Table 6.5.	460	460		
	Maximum wavelength in the effective spectral bandwidth for the backscattered light	$\lambda_2(N)$	nm	Table 6.5.	570	570		
EVALUATE SIGNAL- AND NOISE-PHOTOELECTRON CURRENTS								
7. Calculate the Signal- and Noise-Image Irradiance								
A. Calculate geometric factors	Angular orientation of the source	δ_s	deg	$\delta_s = \tan^{-1}\left(\frac{d}{2R}\right)$. ($\delta_s$ is shown in figure 6.6.)	2.15	2.15		

STEP	TERM	SYMBOL	UNIT	REFERENCE	VALUE: CONVENTIONAL	VALUE: POLARIZATION DISCRIMINATION	VALUE: RANGE GATING	VALUE: VOLUME SCANNING
	Angular orientation of the receiver	δ_R	deg	$\delta_R = -\tan^{-1}\left(\frac{d}{2R}\right)$. ($\delta_R$ is shown in figure 6.6.)	-2.15	-2.15		
	Distance to the backscatter volume for the conventional and polarization-discrimination systems	r_0	m	$r_0 = \frac{2d}{\left(\frac{d}{R}\right) + 2\tan(\delta_s + \theta_1)}$ or use figure 6.7. (r_0 is shown in figure 6.6.)	5.93	5.93		
	Distance to the backscatter volume for the range-gating system	r'_0	m	r'_0 = maximum of (r_0, R - 1/2 C_w Δt), where $C_w = 2.25 \times 10^8$ m/sec. (r'_0 is introduced in equation 6.85.)				
	Half-angle of the receiver's field-of-view and	θ_3	deg	If θ_3 is known, use it to compute Δ according to $\Delta \simeq \frac{\theta_3 R^2}{d + \theta_3 R}$.				
	Depth-of-field for the volume-scanning system	Δ	m	If θ_3 is not known, establish a desired Δ and solve for θ_3. (Δ is introduced in equation 6.93.)				
	Distance to the backscatter volume for the volume-scanning system	r''_0	m	$r''_0 = R - \Delta$. (r''_0 is introduced in equation 6.110.)				

STEP	TERM	SYMBOL	UNIT	REFERENCE	VALUE: CONVENTIONAL	VALUE: POLARIZATION DISCRIMINATION	VALUE: RANGE GATING	VALUE: VOLUME SCANNING
B. Calculate decibel terms		TR	dB	$TR = 10 \log (\rho_2)$.	-.969	-.969		
		W	dB	$W = 10 \log (w)$.	23.01	23.01		
		L	dB	$L = 10 \log \left(\frac{\tau}{f/^2} \right)$.	-3.52	-3.52		
		D	dB	$D = 10 \log \left[\frac{2}{(1 - \cos \theta_1)} \right]$.	21.19	21.19		
		R_1	dB	$R_1 = -20 \log R$.	-26.02	-26.02		
		$g_1(\lambda_0(S))$		$g_1 = (1 + c_1/a)/\cos \delta_s$. Use $c_1/a(\lambda_0(S))$.	1.29	1.29		
		R_2	dB	$R_2 = -4.34\ [a\ g_1\ R]$. Use $a\ (\lambda_0(S))$ and $g_1\ (\lambda_0(S))$.	-28.22	-28.22		
		BS	dB	$BS = 10 \log (\eta s)$.	-23.22	-23.22		
		$g_3(\lambda_0(N))$		$g_3 = \left(\frac{c_1}{a} + \frac{c_3}{a} \right) \Big/ \cos \delta_s$. Use $c_1/a\ (\lambda_0(N))$ and $c_3/a\ (\lambda_0(N))$.	.500	.500		
		$g_2(\lambda_0(N))$		$g_2 = \frac{c_1}{a} + \frac{(R^2 + d^2)^{1/2}}{R} \frac{c_3}{a}$ Use $c_1/a\ (\lambda_0(N))$ and $c_3/a\ (\lambda_0(N))$.				
	Exponential backscatter integrals	$E_2[ag_3 r_0]$		Table 6.9. ($E_2(x)$ is defined in equation 6.40.) Use $a(\lambda_0(N))$ and $g_3(\lambda_0(N))$.	.198	.198		
		$E_2[ag_3 r'_0]$		Table 6.9. Use $a(\lambda_0(N))$ and $g_3(\lambda_0(N))$.				

STEP	TERM	SYMBOL	UNIT	REFERENCE	VALUE: CONVENTIONAL	VALUE: POLARIZATION DISCRIMINATION	VALUE: RANGE GATING	VALUE: VOLUME SCANNING
		$E_2[ag_3R]$		Table 6.9. Use $a(\lambda_0(N))$ and $g_3(\lambda_0(N))$.	.015	.015		
		$E_2[ag_2r''_0]$		Table 6.9. Use $a(\lambda_0(N))$ and $g_2(\lambda_0(N))$.				
		$E_2[ag_2R]$		Table 6.9. Use $a(\lambda_0(N))$ and $g_2(\lambda_0(N))$.				
		R_3	dB	$R_3 = 10 \log \left[\frac{1}{r_0} E_2(ag_3r_0) - \frac{1}{R} E_2(ag_3R)\right]$.	-14.86	-14.86		
		R'_3	dB	$R'_3 = 10 \log \left[\frac{1}{r'_0} E_2 \times (ag_3r'_0) - \frac{1}{R} E_2(ag_3R)\right]$.				
		R''_3	dB	$R''_3 = 10 \log \left[\frac{1}{r''_0} E_2 \times (ag_2r''_0) - \frac{1}{R} E_2(ag_2R)\right]$.				
		R_4	dB	$R_4 = 10 \log \left[R/(R^2+d^2)^{3/2}\right]$.				
		R_5	dB	$R_5 = -4.34\,(ag_2R)$. Use $a(\lambda_0(S))$ and $g_2(\lambda_0(S))$.				
		$g_2(\lambda_0(S))$		$g_2 = c_1/a + \frac{(R^2+d^2)^{1/2}}{R} \frac{c_3}{a}$. Use $c_1/a\,(\lambda_0(S))$ and $c_3/a\,(\lambda_0(S))$.				

STEP	TERM	SYMBOL	UNIT	REFERENCE	VALUE: CONVENTIONAL	VALUE: POLARIZATION DISCRIMINATION	VALUE: RANGE GATING	VALUE: VOLUME SCANNING
		EPS	dB	EPS = 10 log $\{e_1 e_2 [1 - \psi_s (\text{bright})]\}$.		-5.05		
		EPB	dB	EPB = 10 log $[e_1 e_2 (1-\psi_b)]$.		-10.10		
		ES	dB	ES = 10 log e_3.				
		EC	dB	EC = 10 log e_4.				
		A	dB	A = 10 log (τA_e).				
C. Sum decibel terms and calculate signal- and noise-image irradiances		$H_s(CON)$	dB	$H_s(CON) = TR + W + L + D + R_1 + R_2 - 19.51$.	-34.04			
	Conventional system's signal irradiance	$\tilde{h}_s(CON)$	W/m^2	$\tilde{h}_s(CON)$ = antilog $[H_s(CON)/10]$. (Introduced in equation 6.19.)	3.95×10^{-4}			
		$H_n(CON)$	dB	$H_n(CON) = BS + W + L + D + R_3 - 22.51$.	-19.91			
	Conventional system's noise irradiance	$\tilde{h}_n(CON)$	W/m^2	$\tilde{h}_n(CON)$ = antilog $[H_n(CON)/10]$. (Introduced in equation 6.37.)	1.02×10^{-2}			
		$H_s(PD)$	dB	$H_s(PD) = EPS + TR + W + L + D + R_1 + R_2 - 19.51$.		-39.09		
	Polarization-discrimination system's signal irradiance	$\tilde{h}_s(PD)$	W/m^2	$\tilde{h}_s(PD)$ = antilog $[H_s(PD)/10]$. (Introduced in equation 6.55.)		1.23×10^{-4}		
		$H_n(PD)$	dB	$H_n(PD) = EPB + BS + W + L + D + R_3 - 22.51$.		-30.01		
	Polarization-discrimination system's noise irradiance	$\tilde{h}_n(PD)$	W/m^2	$\tilde{h}_n(PD)$ = antilog $[H_n(PD)/10]$. (Introduced in equation 6.65.)		9.98×10^{-4}		

STEP	TERM	SYMBOL	UNIT	REFERENCE	VALUE: CONVENTIONAL	VALUE: POLARIZATION DISCRIMINATION	VALUE: RANGE GATING	VALUE: VOLUME SCANNING
		$H_s(RG)$	dB	$H_s(RG) = ES + EC + TR + W + L + D + R_1 + R_2 - 19.51.$				
	Range-gating system's signal irradiance	$\tilde{h}_s(RG)$	W/m^2	$\tilde{h}_s(RG) = \text{antilog}\,[H_s(RG)/10]$. (Introduced in equation 6.74.)				
		$H_n(RG)$	dB	$H_n(RG) = ES + EC + BS + W + L + D + R'_3 - 22.51.$				
	Range-gating system's noise irradiance	$\tilde{h}_n(RG)$	W/m^2	$\tilde{h}_n(RG) = \text{antilog}\,[H_n(RG)/10]$. (Introduced in equation 6.84.)				
		$P_s(VS)$	dB	$P_s(VS) = EC + A + TR + W + R_4 + R_5 - 7.48.$				
	Volume-scanning system's signal power	$\tilde{p}_s(VS)$	W	$\tilde{p}_s(VS) = \text{antilog}\,[P_s(VS)/10]$. (Introduced in equation 6.96.)				
		$P_n(VS)$	dB	$P_n(VS) = A + EC + BS + W + R''_3 - 10.48.$				
	Volume-scanning system's noise power	$\tilde{p}_n(VS)$	W	$\tilde{p}_n(VS) = \text{antilog}\,[P_n(VS)/10]$. (Introduced in equation 6.109.)				
8. Calculate Combined Spectral Response	Combined spectral response for the light source and the camera	$G[\lambda_2(S)]$	A/W	Table 6.8. (This term is introduced in equation 6.21.)	1.08×10^{-2}	1.08×10^{-2}		
		$G[\lambda_1(S)]$	A/W	Table 6.8.	3.70×10^{-3}	3.70×10^{-3}		
		$G[\lambda_2(N)]$	A/W	Table 6.8.	1.06×10^{-2}	1.06×10^{-2}		
		$G[\lambda_1(N)]$	A/W	Table 6.8.	2.52×10^{-3}	2.52×10^{-3}		

STEP	TERM	SYMBOL	UNIT	REFERENCE	VALUE: CONVENTIONAL	VALUE: POLARIZATION DISCRIMINATION	VALUE: RANGE GATING	VALUE: VOLUME SCANNING
9. Calculate Signal- and Noise-Photoelectron Currents	Signal photo-electron current from the bright resolution element	$i_s(\rho_2)$	A	$i_s(\rho_2) = A_0\tilde{h}_s \times \{G[\lambda_2(S)] - G[\lambda_1(S)]\}$. ($i_s$ is introduced in equation 6.18.)	3.37×10^{-10}	1.05×10^{-10}		
	Signal photo-electron current from the bright resolution element	$i_s(\rho_2)$	A	$i_s(\rho_2) = \tilde{p}_s(VS) \times \{G[\lambda_2(S)] - G[\lambda_1(S)]\}$.				
	Signal photo-electron current from the dark resolution element	$i_s(\rho_1)$	A	$i_s(\rho_1) = \left(\frac{\rho_1}{\rho_2}\right) i_s(\rho_2)$.	8.43×10^{-11}			
	Signal photo-electron current from the dark resolution element	$i_s(\rho_1)$	A	$i_s(\rho_1) = \left(\frac{\rho_1}{\rho_2}\right) \times \frac{[1 - \psi_s(\text{dark})]}{[1 - \psi_s(\text{bright})]} i_s(\rho_2)$.		6.29×10^{-12}		
	Noise photo-electron current	i_n	A	$i_n = A_0\tilde{h}_n \times \{G[\lambda_2(N)] - G[\lambda_1(N)]\}$. ($i_n$ is introduced in equation 6.36.)	9.89×10^{-9}	9.68×10^{-10}		
	Noise photo-electron current	i_n	A	$i_n = \tilde{p}_n(VS) \times \{G[\lambda_2(N)] - G[\lambda_1(N)]\}$. ($i_n$ for VS is introduced in equation 6.108.)				

STEP	TERM	SYMBOL	UNIT	REFERENCE	VALUE: CONVENTIONAL	VALUE: POLARIZATION DISCRIMINATION	VALUE: RANGE GATING	VALUE: VOLUME SCANNING
EVALUATE IMAGE CONTRAST AND LIMITING RESOLUTION								
10. Evaluate Image Contrast	Image contrast	C		$C = \frac{i_s(\rho_2) - i_s(\rho_1)}{i_s(\rho_2) + i_n}$. (C is introduced in equation 6.119.)	2.47×10^{-2}	9.20×10^{-2}		
11. Evaluate Limiting Resolution (For Systems Using Standard Vidicons, Omit This Step)	Limiting resolution	N_L	Television lines	Figure 6.4. For input photocathode current, use $[i_s(\rho_2) + i_n]$.	OFF SCALE	480		
	Limiting resolution	N_L	Television lines	Figure 6.13. For input photocathode current, use $[i_s(\rho_2) + i_n]$.				
12. Calculate Equivalent Faceplate Illuminance *(Optional)*	Conversion factor	K_i	$\frac{A}{m^2 fc}$	Table 6.11. (K_i is introduced in equation 6.127.)				
	Equivalent signal faceplate illuminance	E_s	fc	$E_s = \frac{i_s(\rho_2)}{K_i A_0}$. Table 3.5 relates E_s to performance thresholds. (E_s is introduced in equation 6.125.)				
	Equivalent noise faceplate illuminance	E_n	fc	$E_n = \frac{i_n}{K_i A_0}$ Table 3.5 relates E_n to performance thresholds.				

SET 2. PERFORMANCE ANALYSIS WORKSHEETS FOR VIEWING SYSTEMS USING LASERS

STEP	TERM	SYMBOL	UNIT	REFERENCE	VALUE: CONVENTIONAL	VALUE: POLARIZATION DISCRIMINATION	VALUE: RANGE GATING	VALUE: VOLUME SCANNING
IDENTIFY SYSTEM INPUT PARAMETERS								
1. Specify System Hardward Characteristics	Type of laser			Lasers are most commonly used for range-gating and volume-scanning systems. Suggested choices: range gating, pulsed xenon ion; volume scanning, CW argon ion. (These and other lasers are introduced in sections 4.3.2.1 and 4.4.2.1.)			pulsed xenon	
	Primary spectral wavelengths of the source	λ_1	nm	Table 6.6. For sources with more than six primary wavelengths, either combine wavelengths as described in section 6.5.2 or write in values on a separate sheet.			495	
		λ_2					501	
		λ_3					516	
		λ_4					526	
		λ_5					535	
		λ_6					539	
	Number of primary spectral wavelengths	N		(N is introduced in equation 6.30.)			6	
	Total average radiant output power	w	W	For lasers used in range-gating systems, use table 4.5. For volume-scanning lasers, see section 4.3.2.1.			20	

STEP	TERM	SYMBOL	UNIT	REFERENCE	VALUE: CONVENTIONAL	VALUE: POLARIZATION DISCRIMINATION	VALUE: RANGE GATING	VALUE: VOLUME SCANNING
	Fractional output at each primary wavelength	$f(\lambda_1)$		Table 6.6. Convert percentages to decimal fractions.			0.17	
		$f(\lambda_2)$					0.17	
		$f(\lambda_3)$					0.09	
		$f(\lambda_4)$					0.18	
		$f(\lambda_5)$					0.20	
		$f(\lambda_6)$					0.19	
	Average radiant output at the wavelength λ_i	$w_R(\lambda_1)$	W	$w_R(\lambda_i) = f(\lambda_i)w$.			3.4	
		$w_R(\lambda_2)$					3.4	
		$w_R(\lambda_3)$					1.8	
		$w_R(\lambda_4)$					3.6	
		$w_R(\lambda_5)$					4.0	
		$w_R(\lambda_6)$					3.8	
	Half-angle of the "equivalent" conical beam pattern	θ_1	deg	Lower limit for the volume-scanning system: 1 mrad (0.057 deg). For other systems, use the values in table 3.4. (θ_1 is introduced in equation 6.10 and in figure 6.6.)			5.00	
	Type of receiver			Choices for which data is available in this handbook: intensified vidicon, image orthicon, image isocon, SEC, SEBIR. (These receivers are introduced in section 3.2.) For volume-scanning systems, assume an image-dissector tube.			sec	

STEP	TERM	SYMBOL	UNIT	REFERENCE	VALUE: CONVENTIONAL	VALUE: POLARIZATION DISCRIMINATION	VALUE: RANGE GATING	VALUE: VOLUME SCANNING
	Type of photocathode or photoconductor			Choices for which data is available in this handbook: S-20 (multialkali), Type II (antimony trisulfide), Type V (silicon diode). Vidicon cameras use Types II and V photoconductors; all other receivers use the S-20 photocathode.			S-20	
	Spectral response of the receiver	$S(\lambda_1)$	A/W	Table 6.7.			.065	
		$S(\lambda_2)$					.065	
		$S(\lambda_3)$					.060	
		$S(\lambda_4)$					.057	
		$S(\lambda_5)$					.054	
		$S(\lambda_6)$					.054	
	Half-angle of the receiver's field-of-view	θ_3	deg	Table 3.5. (θ_3 is introduced in figure 6.6.)			10.0	
	Transmission coefficient of the receiver's optics	τ		Table 3.5. (τ is introduced in equation 6.19. For a range-gating system, see discussion of equation 6.74.)			1.00	
	f number of the receiver's optics	f/		Table 3.5. (f/ is introduced in equation 6.19.)			1.5	
	Image format area on the photosensitive surface of the receiver	A_0	m^2	Table 3.5. (A_0 is introduced in equation 6.18.)			1.20×10^{-4}	

STEP	TERM	SYMBOL	UNIT	REFERENCE	VALUE: CONVENTIONAL	VALUE: POLARIZATION DISCRIMINATION	VALUE: RANGE GATING	VALUE: VOLUME SCANNING
	Area of the entrance pupil of the image dissector	A_e	m^2	Use specific data when available. In one proposed system, $A_e = 0.043\ m^2$. (A_e is introduced in equation 6.96.)				
	Efficiency of the polarizer	e_1		Table 4.2. (e_1 is introduced in equation 6.55.)				
	Efficiency of the analyzer	e_2		Table 4.2. (e_2 is introduced in equation 6.55.)				
	Duration of the source and receiver gates	Δt	sec	Table 4.5. (Δt is introduced in section 6.3.2.)			20.0×10^{-9}	
2. Specify Target Characteristics	Reflectance of the dark resolution element	ρ_1		When specific data is not available, select ρ_1 and ρ_2 to achieve a desired target contrast which is defined by			0.20	
	and			$\left[\frac{\rho_2 - \rho_1}{\rho_2}\right]$. ($\rho_2$ is introduced in equation 6.19.)				
	Reflectance of the bright resolution element	ρ_2					0.80	
	Polarization coefficient of the light reflected off the dark resolution element	ψ_s(dark)		Table 4.3. (ψ_s is introduced in equation 6.56.)				

STEP	TERM	SYMBOL	UNIT	REFERENCE	VALUE: CONVENTIONAL	VALUE: POLARIZATION DISCRIMINATION	VALUE: RANGE GATING	VALUE: VOLUME SCANNING
	Polarization coefficient of the light reflected off the bright resolution element	ψ_s(bright)		Table 4.3.				
3. Specify System Geometry	Source-receiver separation	d	m	(d is defined in figure 6.6.)			1.50	
	Viewing range	R	m	(R is defined in figure 6.6.)			20.0	
SPECIFY PROPAGATION CHARACTERISTICS OF THE WATER								
4. Specify Basic Optical Properties	Type of water			Choices for which data is available in this handbook: bay, coastal, deep ocean.			coastal	
	Total attenuation coefficient	$a(\lambda_1)$	ln/m	Table 6.2. (a is introduced in section 2.2.)			.282	
		$a(\lambda_2)$					.282	
		$a(\lambda_3)$					.263	
		$a(\lambda_4)$					.257	
		$a(\lambda_5)$					.252	
		$a(\lambda_6)$					.252	

STEP	TERM	SYMBOL	UNIT	REFERENCE	VALUE: CONVENTIONAL	VALUE: POLARIZATION DISCRIMINATION	VALUE: RANGE GATING	VALUE: VOLUME SCANNING
	Scattering-to-absorption ratio	$\frac{s}{a}(\lambda_1)$		Table 6.3. (s/a is introduced in section 2.2.)			7.06	
		$\frac{s}{a}(\lambda_2)$					7.06	
		$\frac{s}{a}(\lambda_3)$					6.11	
		$\frac{s}{a}(\lambda_4)$					5.59	
		$\frac{s}{a}(\lambda_5)$					5.15	
		$\frac{s}{a}(\lambda_6)$					5.15	
	Total scattering coefficient	$s(\lambda_1)$	ln/m	$s(\lambda_i) = \frac{a(\lambda_i)}{\left\{1 + \left[\frac{s}{a}(\lambda_i)\right]^{-1}\right\}}$			.247	
		$s(\lambda_2)$					.247	
		$s(\lambda_3)$					.226	
		$s(\lambda_4)$					.218	
		$s(\lambda_5)$					.211	
		$s(\lambda_6)$					.211	
	Fractional backscatter	η		Between 0.01 and 0.05 for most water; must be measured for specific cases. (η is defined by equation 6.38.)			0.02	
	Polarization coefficient of the back-scattered light	ψ_b		Must be measured for each case; varies between 0.2 and 0.7. (ψ_b is introduced in section 2.2.)				

STEP	TERM	SYMBOL	UNIT	REFERENCE	VALUE: CONVENTIONAL	VALUE: POLARIZATION DISCRIMINATION	VALUE: RANGE GATING	VALUE: VOLUME SCANNING
5. Specify Effective Attenuation Coefficients		$\frac{c_1}{a}(\lambda_1)$		Table 6.1. Use $\theta_i = \theta_1$. For s/a > 5.0, use figure 6.1. (c_1 is introduced in section 6.1.1.1.)			.30	
		$\frac{c_1}{a}(\lambda_2)$					.30	
		$\frac{c_1}{a}(\lambda_3)$					.31	
		$\frac{c_1}{a}(\lambda_4)$					.32	
		$\frac{c_1}{a}(\lambda_5)$					.33	
		$\frac{c_1}{a}(\lambda_6)$					.33	
		$\frac{c_3}{a}(\lambda_1)$		Table 6.1. Use $\theta_i = \theta_3$. θ_3 for the volume-scanning system is evaluated below. For s/a > 5.0, use figure 6.1. (c_3 is introduced in section 6.1.1.3.)			.19	
		$\frac{c_3}{a}(\lambda_2)$					.19	
		$\frac{c_3}{a}(\lambda_3)$					.22	
		$\frac{c_3}{a}(\lambda_4)$					.23	
		$\frac{c_3}{a}(\lambda_5)$					.24	
		$\frac{c_3}{a}(\lambda_6)$					.24	
EVALUATE SIGNAL- AND NOISE-PHOTOELECTRON CURRENTS								
6. Calculate Signal- and Noise-Image Irradiance								
A. Calculate geometric factors	Angular orientation of the source	δ_s	deg	$\delta_s = \tan^{-1}(d/2R)$. ($\delta_s$ is shown in figure 6.6.)			2.15	

STEP	TERM	SYMBOL	UNIT	REFERENCE	VALUE: CONVENTIONAL	VALUE: POLARIZATION DISCRIMINATION	VALUE: RANGE GATING	VALUE: VOLUME SCANNING
	Angular orientation of the receiver	δ_R	deg	$\delta_R = -\tan^{-1}(d/2R)$. ($\delta_R$ is shown in figure 6.6.)			-2.15	
	Distance to the backscatter volume for the conventional and polarization-discrimination systems	r_0	m	$r_0 = \dfrac{2d}{\left(\frac{d}{R}\right) + 2\tan(\delta_s+\theta_1)}$ or use figure 6.7. (r_0 is shown in figure 6.6.)				
	Distance to the backscatter volume for the range-gating system	r'_0	m	r'_0 = maximum of (r_0, $R - 1/2\, C_w\, \Delta t$), where $C_w = 2.25 \times 10^8$ m/sec. (r'_0 is introduced in equation 6.85.)				
	Half-angle of the receiver's field-of-view	θ_3	deg	If θ_3 is known, use it to compute Δ according to $\Delta \simeq \dfrac{\theta_3 R^2}{d + \theta_3 R}$				
	and							
	Depth-of-field for the volume-scanning system	Δ	m	If θ_3 is not known, establish a desired Δ and solve for θ_3. (Δ is introduced in equation 6.93.)				
	Distance to the backscatter volume for the volume-scanning system	r''_0	m	$r''_0 = R - \Delta$. (r''_0 is introduced in equation 6.110.)				

STEP	TERM	SYMBOL	UNIT	REFERENCE	VALUE: CONVENTIONAL	VALUE: POLARIZATION DISCRIMINATION	VALUE: RANGE GATING	VALUE: VOLUME SCANNING
B. Calculate decibel terms		TR	dB	$TR = 10 \log (\rho_2)$.			-.969	
		$WR(\lambda_1)$	dB	$WR(\lambda_i) = 10 \log w_R(\lambda_i)$.			5.31	
		$WR(\lambda_2)$					5.31	
		$WR(\lambda_3)$					2.55	
		$WR(\lambda_4)$					5.56	
		$WR(\lambda_5)$					6.02	
		$WR(\lambda_6)$					5.80	
		L	dB	$L = 10 \log \left[\frac{\tau}{f/2}\right]$.			-3.52	
		D	dB	$D = 10 \log \left[\frac{2}{(1 - \cos\theta_1)}\right]$.			27.21	
		R_1	dB	$R_1 = -20 \log R$.			-26.02	
		$g_1(\lambda_1)$		$g_1(\lambda_i) = \left[1 + \frac{c_1}{a}(\lambda_i)\right] / \cos \delta_s$.			1.30	
		$g_1(\lambda_2)$					1.30	
		$g_1(\lambda_3)$					1.31	
		$g_1(\lambda_4)$					1.32	
		$g_1(\lambda_5)$					1.32	
		$g_1(\lambda_6)$					1.32	
		$R_2(\lambda_1)$		$R_2(\lambda_i) = -4.34 \times [a(\lambda_i)\, g_1(\lambda_i)\, R]$.			-31.82	
		$R_2(\lambda_2)$					-31.82	
		$R_2(\lambda_3)$					-29.91	
		$R_2(\lambda_4)$					-29.45	
		$R_2(\lambda_5)$					-28.87	
		$R_2(\lambda_6)$					-28.87	

STEP	TERM	SYMBOL	UNIT	REFERENCE	VALUE: CONVENTIONAL	VALUE: POLARIZATION DISCRIMINATION	VALUE: RANGE GATING	VALUE: VOLUME SCANNING
		$BS(\lambda_1)$	dB	$BS = 10 \log [\eta s (\lambda_i)]$.			-23.06	
		$BS(\lambda_2)$					-23.06	
		$BS(\lambda_3)$					-23.45	
		$BS(\lambda_4)$					-23.61	
		$BS(\lambda_5)$					-23.75	
		$BS(\lambda_6)$					-23.75	
		$g_3(\lambda_1)$		$g_3(\lambda_i) = \left[\frac{c_1}{a}(\lambda_i)\right.$			0.49	
		$g_3(\lambda_2)$					0.49	
		$g_3(\lambda_3)$		$\left.+\frac{c_3}{a}(\lambda_i)\right] \Big/ \cos \delta_s$.			0.53	
		$g_3(\lambda_4)$					0.55	
		$g_3(\lambda_5)$					0.56	
		$g_3(\lambda_6)$					0.56	
		$g_2(\lambda_1)$		$g_2(\lambda_i) = \left[\frac{c_1}{a}(\lambda_i) +\right.$				
		$g_2(\lambda_2)$						
		$g_2(\lambda_3)$		$\left.\frac{c_3}{a}(\lambda_i)\frac{(R^2 + d^2)^{1/2}}{R}\right]$.				
		$g_2(\lambda_4)$						
		$g_2(\lambda_5)$						
		$g_2(\lambda_6)$						
	Exponential backscatter integrals	$E_2[ag_3r_0]_i$		$E_2[ag_3r_0]_i =$				
				$E_2[a(\lambda_i)g_3(\lambda_i)r_0]$,				
				$i = 1, N$.				
				Table 6.9.				
				[$E_2(x)$ is defined in equation 6.40.)				

STEP	TERM	SYMBOL	UNIT	REFERENCE	VALUE: CONVENTIONAL	VALUE: POLARIZATION DISCRIMINATION	VALUE: RANGE GATING	VALUE: VOLUME SCANNING
		$E_2[\alpha g_3 r'_0]_i$		$E_2[\alpha g_3 r'_0]_i =$			.0211	
				$E_2[\alpha(\lambda_i) g_3(\lambda_i) r'_0]$,			.0211	
				i = 1, N.			.0206	
				Table 6.9.			.0196	
							.0198	
							.0198	
		$E_2[\alpha g_3 R]_i$		$E_2[\alpha g_3 R]_i =$			.0143	
				$E_2[\alpha(\lambda_i) g_3(\lambda_i) R]$,			.0143	
				i = 1, N.			.0138	
				Table 6.9.			.0131	
							.0133	
							.0133	
		$E_2[\alpha g_2 r''_0]_i$		$E_2[\alpha g_2 r''_0]_i =$				
				$E_2[\alpha(\lambda_i) g_2(\lambda_i) r''_0]$,				
				i = 1, N.				
				Table 6.9.				
		$E_2[\alpha g_2 R]_i$		$E_2[\alpha g_2 R]_i =$				
				$E_2[\alpha(\lambda_i) g_2(\lambda_i) R]$,				
				i = 1, N.				
				Table 6.9.				

STEP	TERM	SYMBOL	UNIT	REFERENCE	VALUE: CONVENTIONAL	VALUE: POLARIZATION DISCRIMINATION	VALUE: RANGE GATING	VALUE: VOLUME SCANNING
		$R_3(\lambda_1)$	dB	$R_3(\lambda_i) = 10 \log \left\{ \frac{1}{r_0} \times \right.$				
		$R_3(\lambda_2)$						
		$R_3(\lambda_3)$		$E_2[a(\lambda_i)g_3(\lambda_i)r_0]$				
		$R_3(\lambda_4)$		$\left. - \frac{1}{R} E_2[a(\lambda_i)g_3(\lambda_i)R] \right\}$.				
		$R_3(\lambda_5)$						
		$R_3(\lambda_6)$						
		$R'_3(\lambda_1)$	dB	$R'_3(\lambda_i) = 10 \log \left\{ \frac{1}{r'_0} \times \right.$			-33.24	
		$R'_3(\lambda_2)$					-33.24	
		$R'_3(\lambda_3)$		$E_2[a(\lambda_i)g_3(\lambda_i)r'_0]$			-33.27	
		$R'_3(\lambda_4)$		$\left. - \frac{1}{R} E_2[a(\lambda_i)g_3(\lambda_i)R] \right\}$.			-33.48	
		$R'_3(\lambda_5)$					-33.46	
		$R'_3(\lambda_6)$					-33.46	
		$R''_3(\lambda_1)$	dB	$R''_3(\lambda_i) = 10 \log$				
		$R''_3(\lambda_2)$		$\left\{ \frac{1}{r''_0} E_2[a(\lambda_i)g_2(\lambda_i)r''_0] \right.$				
		$R''_3(\lambda_3)$						
		$R''_3(\lambda_4)$		$\left. - \frac{1}{R} E_2[a(\lambda_i)g_2(\lambda_i)R] \right\}$.				
		$R''_3(\lambda_5)$						
		$R''_3(\lambda_6)$						
		R_4	dB	$R_4 = 10 \log$				
				$\left[R/(R^2 + d^2)^{3/2} \right]$.				
		$R_5(\lambda_1)$	dB	$R_5(\lambda_i) = -4.34$				
		$R_5(\lambda_2)$		$[a(\lambda_i)g_2(\lambda_i)\ R]$.				
		$R_5(\lambda_3)$						
		$R_5(\lambda_4)$						
		$R_5(\lambda_5)$						
		$R_5(\lambda_6)$						

STEP	TERM	SYMBOL	UNIT	REFERENCE	VALUE: CONVENTIONAL	VALUE: POLARIZATION DISCRIMINATION	VALUE: RANGE GATING	VALUE: VOLUME SCANNING
		EPS	dB	EPS = 10 log $\{e_1 e_2 \times [1 - \psi_s(\text{bright})]\}$.				
		EPB	dB	EPB = 10 log $[e_1 e_2 (1 - \psi_b)]$.				
		A	dB	A = 10 log (τA_e) .				
C. Sum decibel terms and calculate signal- and noise-image irradiances.		$H'_s(CON)_i$	dB	$H'_s(CON)_i = TR + WR(\lambda_i) + L + D + R_1 + R_2(\lambda_i) - 19.51, i = 1, N$				
	Conventional system's signal irradiance	$\tilde{h}'_s(CON)_i$	W/m^2	$\tilde{h}'_s(CON)_i$ = antilog $[H_s(CON)_i/10]$, i = 1,N. (Introduced in equation 6.31.)				
		$H'_n(CON)_i$	dB	$H'_n(CON)_i = BS(\lambda_i) + WR(\lambda_i) + L + D + R_3(\lambda_i) - 22.51, i = 1, N.$				

STEP	TERM	SYMBOL	UNIT	REFERENCE	VALUE: CONVENTIONAL	VALUE: POLARIZATION DISCRIMINATION	VALUE: RANGE GATING	VALUE: VOLUME SCANNING
	Conventional system's noise irradiance	$\tilde{h}'_n(CON)_i$	W/m^2	$\tilde{h}'_n(CON)_i$ = antilog $[H'_n(CON)_i/10]$, $i = 1, N$. (Introduced in equation 6.46.)				
		$H'_s(PD)_i$	dB	$H'_s(PD)_i = EPS + TR + WR(\lambda_i) + L + D + R_1 + R_2(\lambda_i) - 19.51$, $i = 1, N$.				
	Polarization-discrimination system's signal irradiance	$\tilde{h}'_s(PD)_i$	W/m^2	$\tilde{h}'_s(PD)_i$ = antilog $[H'_s(PD)_i/10]$, $i = 1, N$. (Introduced in equation 6.61.)				
		$H'_n(PD)_i$	dB	$H'_n(PD)_i = EPB + BS(\lambda_i) + WR(\lambda_i) + L + D + R_3(\lambda_i) - 22.51$, $i = 1, N$.				

STEP	TERM	SYMBOL	UNIT	REFERENCE	VALUE: CONVENTIONAL	VALUE: POLARIZATION DISCRIMINATION	VALUE: RANGE GATING	VALUE: VOLUME SCANNING
	Polarization-discrimination system's noise irradiance	$\tilde{h}'_n(PD)_i$	W/m^2	$\tilde{h}'_n(PD)_i$ = antilog $[H'_n(PD)_i/10]$, i = 1, N. (Introduced in equation 6.70.)				
		$H'_s(RG)_i$	dB	$H'_s(RG)_i = TR + WR(\lambda_i) + L + D + R_1 + R_2(\lambda_i) - 19.51$, i = 1, N.			-49.32	
							-49.32	
							-50.17	
							-46.69	
							-45.66	
							-45.88	
	Range-gating system's signal irradiance	$\tilde{h}'_s(RG)_i$	W/m^2	$\tilde{h}'_s(RG)_i$ = antilog $[H'_s(RG)_i/10]$, i = 1, N. (Introduced in equation 6.80.)			1.17×10^{-5}	
							1.17×10^{-5}	
							9.62×10^{-6}	
							2.14×10^{-5}	
							2.72×10^{-5}	
							2.58×10^{-5}	
		$H'_n(RG)_i$	dB	$H'_n(RG)_i = BS(\lambda_i) + WR(\lambda_i) + L + D + R'_3(\lambda_i) - 22.51$, i = 1, N.			-49.81	
							-49.81	
							-52.99	
							-50.35	
							-50.01	
							-50.24	

STEP	TERM	SYMBOL	UNIT	REFERENCE	VALUE: CONVENTIONAL	VALUE: POLARIZATION DISCRIMINATION	VALUE: RANGE GATING	VALUE: VOLUME SCANNING
	Range-gating system's noise irradiance	$\tilde{h}'_n(RG)_i$	W/m^2	$\tilde{h}'_n(RG)_i$ = antilog $[H'_n(RG)_i/10]$, i = 1, N. (Introduced in equation 6.90.)			1.04×10^{-5}	
							1.04×10^{-5}	
							5.02×10^{-6}	
							9.23×10^{-6}	
							9.98×10^{-6}	
							9.46×10^{-6}	
		$P'_s(VS)_i$	dB	$P'_s(VS)_i = A + TR + WR(\lambda_i) + R_4 + R_5(\lambda_i) - 7.48$, i = 1, N.				
	Volume-scanning system's signal power	$\tilde{p}'_s(VS)_i$	W	$\tilde{p}'_s(VS)_i$ = antilog $[P'_s(VS)_i/10]$, i = 1, N. (Introduced in equation 6.106.)				
		$P'_n(VS)_i$	dB	$P'_n(VS)_i = A + BS(\lambda_i) + WR(\lambda_i) + R''_3(\lambda_i) - 10.48$, i = 1, N.				

STEP	TERM	SYMBOL	UNIT	REFERENCE	VALUE: CONVENTIONAL	VALUE: POLARIZATION DISCRIMINATION	VALUE: RANGE GATING	VALUE: VOLUME SCANNING
	Volume-scanning system's noise power	$\tilde{p}'_n(VS)_i$	W	$\tilde{p}'_n(VS)_i$ = antilog $[P'_s(VS)_i/10]$, i = 1, N. (Introduced in equation 6.117.)				
7. Calculate Signal- and Noise-Photoelectron Currents	Signal photoelectron current from the bright resolution element	$i_s(\rho_2)$	A	$i_s(\rho_2) = A_0 \sum_{i=1}^{N} \tilde{h}'_s(X)_i\, S(\lambda_i)$, X = CON, PD, or RG for i_s (CON, PD, or RG). (i_s is introduced in equation 6.30.)			7.44×10^{-10}	
	Signal photoelectron current from the bright resolution element	$i_s(\rho_2)$	A	$i_s(\rho_2) = \sum_{i=1}^{N} \tilde{p}'_s(VS)_i\, S(\lambda_i)$. ($i_s$ for VS is introduced in equation 6.103.)				
	Signal photoelectron current from the dark resolution element	$i_s(\rho_1)$	A	$i_s(\rho_1) = (\rho_1/\rho_2)\, i_s(\rho_2)$.			1.86×10^{-10}	

STEP	TERM	SYMBOL	UNIT	REFERENCE	VALUE: CONVENTIONAL	VALUE: POLARIZATION DISCRIMINATION	VALUE: RANGE GATING	VALUE: VOLUME SCANNING
	Signal photo-electron current from the dark resolution element	$i_s(\rho_1)$	A	$i_s(\rho_1) = \left(\frac{\rho_1}{\rho_2}\right)\frac{[1-\psi_s(\text{dark})]}{[1-\psi_s(\text{bright})]} i_s(\rho_2)$				
	Noise photo-electron current	i_n	A	$i_n = A_0 \sum_{i=1}^{N} \tilde{h}'_n(X)_i S(\lambda_i)$, X = CON, PD, or RG for i_n(CON, PD, or RG). (Introduced in equation 6.45.)			3.90×10^{-10}	
	Noise photo-electron current	i_n	A	$i_n = \sum_{i=1}^{N} \tilde{p}'_n(VS)_i S(\lambda_i)$. (Introduced in equation 6.114.)				
EVALUATE IMAGE CONTRAST AND LIMITING RESOLUTION								
8. Evaluate Image Contrast	Image contrast	C		$C = \frac{i_s(\rho_2) - i_s(\rho_1)}{i_s(\rho_2) + i_n}$. (C is introduced in equation 6.119.)			.492	
9. Evaluate the Limiting Resolution (For Systems Using Standard Vidicons, Omit This Step)	Limiting resolution	N_L	Tele-vision lines	Figure 6.4. For input photocathode current, use $[i_s(\rho_2) + i_n]$.			680	

STEP	TERM	SYMBOL	UNIT	REFERENCE	VALUE: CONVENTIONAL	VALUE: POLARIZATION DISCRIMINATION	VALUE: RANGE GATING	VALUE: VOLUME SCANNING
	Limiting resolution	N_L	Tele-vision lines	Figure 6.13. For input photocathode current, use $[i_s(\rho_2) + i_n]$.				
10. Calculate Equivalent Faceplate Illuminance *(Optional)*	Conversion factor	K_i	A/m^2fc	Table 6.11. (K_i is introduced in equation 6.127.)				
	Equivalent signal faceplate illuminance	E_s	fc	$E_s = \frac{i_s}{K_i A_0}$. Table 3.5 relates E_s to performance thresholds. (E_s is introduced in equation 6.125.)				
	Equivalent noise faceplate illuminance	E_n	fc	$E_n = \frac{i_n}{K_i A_0}$ Table 3.5 relates E_n to performance thresholds.				

APPENDIX C. EXPERIMENTAL VALIDATION OF THE SYSTEM PERFORMANCE ANALYSIS.

		Page
C.1	Radiation Field of an Argon Laser in Artificial Seawater	C-3
C.2	Functional Form of the On-Axis Irradiance Produced by a Noncollimated Source	C-8
C.3	Polarization-Discrimination Systems Tested at Morris Dam	C-9
C.4	References	C-12

Page

Figures

C.1	Comparison of Experimental and Calculated Estimates of the Radiation Field (s/a (T) = s/a (E))	C-13
C.2	Probability Distribution Functions for Single-Scattered Light	C-18
C.3	Comparison of Experimental and Calculated Estimates of the Radiation Field (s/a (T) $\neq$ s/a (E))	C-19
C.4	Housing for Controlling the Divergence of the Beam Pattern of the Noncollimated Source (Ref. C.2)	C-24
C.5	Comparison of the On-Axis Irradiance Predicted by the Semiempirical Formula $\tilde{h}(\theta_j, R)$ and by the Effective Attenuation Coefficient Formula $h_n(\theta_j, R)$	C-25
C.6	Comparison of N(exp) and N(cal) for the Polarization-Discrimination System in Type II Water	C-28
C.7	Estimates of $R_{sq}(N)$ for the Polarization-Discrimination System in Type II Water	C-29
C.8	Comparison of N(exp) and N(cal) for the Polarization-Discrimination System in Type I, Type II, and Type III-B Waters	C-30
C.9	Estimates of $R_{sq}(N)$ for the Polarization-Discrimination System in Type I, Type II, and Type III-B Waters	C-31

Tables

C.1	Maximum Experimental Viewing Ranges (m) for the Polarization-Discrimination System Tested at Morris Dam	C-32
C.2	Maximum Viewing Ranges (m) for the Polarization-Discrimination System Predicted by the System Performance Analysis Method	C-32
C.3	Optical Properties and Corresponding Predicted Maximum Viewing Ranges for Three Assumed Types of Water	C-32

APPENDIX C. EXPERIMENTAL VALIDATION OF THE SYSTEM PERFORMANCE ANALYSIS

The credibility of the system performance analysis presented in section 6 depends on how well these calculations agree with experimental data. Comparisons of the calculated results with experimental data demand that the basic scattering and absorption properties of the water – $\alpha(\lambda)$, $a(\lambda)$, $s(\lambda)$, and $\sigma(\theta)$ – be accurately measured and that these properties remain constant during the measurement of a system's performance. Satisfaction of these requirements is difficult to achieve for *in situ* measurements. Fortunately, sufficient experimental data exists to document some of the basic equations used in the system performance analysis. In addition, comparisons* can be made between the performance of the imaging systems tested at Morris Dam (ref. C.1) and calculated predictions.

The first section of this appendix compares the calculated radiation field of a unidirectional point source (UPS)** with the experimental measurements of a radiation field produced by a well collimated, quasimonochromatic,† polarized argon laser in artificial seawater (ref. C.2). The values for the effective attenuation coefficients c_1 and c_3 can be directly determined from these experimental measurements; thus, the agreement of the calculated radiation field with the measured radiation field indicates the validity of these parameters. The equation,

$$h(R) = J \exp(-c_1 R)/R^2 , \tag{C.1}$$

is used in the development of the system performance equations to describe the irradiance produced by a noncollimated source. In the second section of this appendix, the functional form of equation C.1 is documented by experimental measurements, and, in the third section, the measured performance of the polarization-discrimination systems tested at Morris Dam is compared with calculated predictions.

C.1 RADIATION FIELD OF AN ARGON LASER IN ARTIFICIAL SEAWATER

The radiation field produced by a well collimated laser approximates the function $B(\theta_j)$ which describes the spatial distribution of radiation emitted from a true UPS. The function $B(\theta_j)$ is equal to the fraction of the total radiant power emitted by the UPS that is incident on a spherical cap centered on the axis of the source (see the diagram on page C-4).

**The spectral variations of $\alpha(\lambda)$, $a(\lambda)$, and $s(\lambda)$ were not determined. In addition, the effective attenuation coefficients which correspond to the measured volume scattering functions were not calculated. Because of these deficiencies, only approximate comparisons between experimental and calculated data are possible.*

***A unidirectional point source (UPS) emits light in only one direction.*

†The radiant output of the laser was passed through a prism, and a stop was adjusted so that only the 5145-Å line was permitted to propagate in the water.

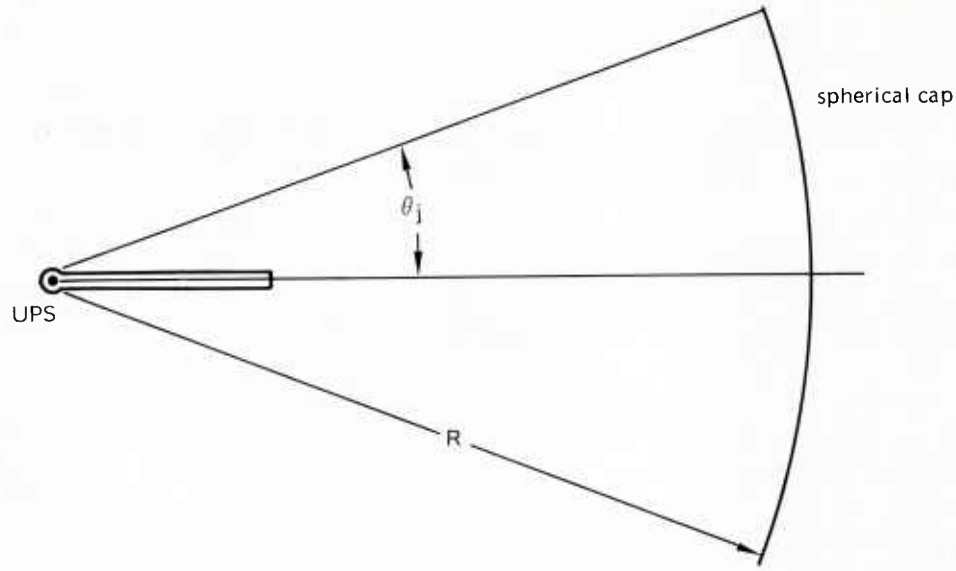

The area of the spherical cap is given by

$$A = 2\pi R^2 (1 - \cos\theta_j) , \tag{C.2}$$

where R is the distance from the source to the cap and θ_j is the angle between the axis of the source and the edge of the cap. (In addition to θ_j, the function $B(\theta_j)$ depends on the radius R and the scattering and absorption properties of the water.) The calculated estimate of $B(\theta_j)$, obtained from the Monte Carlo simulation set of n trajectories* emitted from a UPS, is given by the function $B_n(\theta_j)$. The experimental estimate** of $B(\theta_j)$ is given by the function $\widetilde{B}(\theta_j)$. This function was determined from measurements made with a spectrally filtered, CW argon ion laser in artificial seawater. (In addition to θ_j, the function $\widetilde{B}(\theta_j)$ depends the distance R, the scattering and absorption properties of the water, and the divergence, cross-sectional shape, and polarization characteristics of the laser beam.) The geometry used to measure $\widetilde{B}(\theta_j)$ is illustrated in the following diagram.

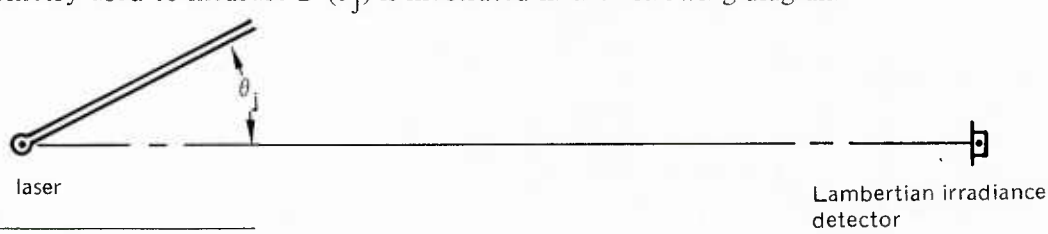

*A detailed discussion of the Monte Carlo simulation of a set of light ray trajectories is given in reference C.3. By using appropriate statistical weighting techniques to account for absorption, meaningful Monte Carlo simulations can be performed with less than 2000 trajectories.

**Tabulated values of $\widetilde{B}(\theta_j)$ were provided by S. Q. Duntley and W. H. Wilson of the Visibility Laboratory, Scripps Institute of Oceanography, University of California, San Diego. Chapter 7 of reference C.2 gives a detailed account of their experiment which produced this data. The Wilson volume scattering function, which was used to determine the probability distribution function in figure C.2, was also provided by the Visibility Laboratory. This volume scattering function was used in the Monte Carlo simulation to obtain the function $B_n(\theta_j)$.

The measured irradiance values were integrated and normalized by the total radiant power emitted by the laser to obtain $\widetilde{B}(\theta_j)$. The artificial seawater was prepared by using a series of ion-exchange and millipore filters to purify tap water. A black-absorbing dye (Nigrosin, Central Scientific Company No. 39680) and a scattering agent (Rexall Aluminox) were added to the purified tap water in carefully measured portions to simulate the optical properties of the various types of seawater.

Ideally, the discrepancy between the experimental function $\widetilde{B}(\theta_j)$ and the calculated function $B_n(\theta_j)$ should be small, and both of these functions should closely approximate the true function $B(\theta_j)$. Figure C.1 illustrates the comparison of $B_n(\theta_j)$ and $\widetilde{B}(\theta_j)$ for five different s/a ratios. The solid curves correspond to the calculated values for different values of θ_j, and the adjacent isolated points represent the tabulated experimental data. Although there is fair agreement between the calculated and experimental data, the systematic nature of the discrepancies indicates the probable existence of some underlying differences between the two sets of data.

There are several possible sources which could have caused these differences.

1. Because the polarization of the laser beam produced small asymmetries in the measured radiation field for polar angles less than 4 deg (ref. C.2), comparisons of $B_n(\theta_j)$ and $\widetilde{B}(\theta_j)$ might not be meaningful for θ_j less than 4 deg.

2. Experimental errors might have occurred in the measurement of the volume scattering function for small angles, and computational errors could have occurred in the extrapolation and integration of this data to obtain the probability distribution function used in the Monte Carlo simulation. These errors could create significant differences between $B_n(\theta_j)$ and $\widetilde{B}(\theta_j)$ for small values of θ_j.

3. Differences in the values of the acceptance angle θ_0 in the instrument used to measure the coefficients α, s, and a could cause a fundamental discrepancy between the s/a ratios which correspond to the calculated and experimental data, respectively.*

4. Experimental errors could have occurred in the measurement of $\widetilde{B}(\theta_j)$.

Of these possible sources, the third one is the easiest to analyze. (To analyze the first source, the computational model would have to be extended to include polarization effects, and to analyze the second source, a complete Monte Carlo simulation with a new volume scattering function would be required.) The acceptance angle $\theta_0(T)$ associated with the coefficients $\alpha(T)$, s(T), and a(T), which are used in the theoretical Monte Carlo simulation, is 0.1 deg (fig. C.2). Because this angle is less than the acceptance angle $\theta_0(E)$ of many transmissometers, the coefficients associated with the experimental measurements $\alpha(E)$, s(E), and a(E) are related to the coefficients used in the calculations as follows:

$$s(T) = s(E) + \Delta , \tag{C.3}$$

$$a(T) = a(E) = a , \tag{C.4}$$

Light scattered by angles less than θ_0 does not contribute to the measured values of α and s.

$$\alpha(T) = \alpha(E) + \Delta \,, \tag{C.5}$$

and

$$\Delta = 2\pi \int_{\theta_0(T)}^{\theta_0(E)} \sigma(\theta) \sin\theta \, d\theta \,. \tag{C.6}$$

(The experimental and theoretical absorption coefficients are assumed equal because the absorption coefficient was determined by the amount of Nigrosin dye added to the purified tap water; therefore, determination of the value of this coefficient did not involve either $\theta_0(E)$ or $\theta_0(T)$.) The relation of the theoretical and experimental s/a ratios follows from equations C.3 and C.4:

$$s/a(T) = s/a(E) + \Delta/a \,. \tag{C.7}$$

A simple approximation can be used to evaluate the change in $B_n(\theta_j)$ caused by small changes in the s/a ratios (ref. C.3). To first order,

$$B_n(\theta_j, s/a(T)) = B_n(\theta_j, s/a(E))\, \Gamma(s/a(E), s/a(T)) \,, \tag{C.8}$$

where

$$\Gamma(s/a(E), s/a(T)) = \exp[-D\,\alpha R \,\{\ln(s/a(T)) - \ln(s/a(E))\}] \tag{C.9}$$

and

$$D = \frac{c_1(\theta_j, s/a(T))/\alpha - c_1(\theta_j, s/a(E))/\alpha}{\ln(s/a(T)) - \ln(s/a(E))} \,. \tag{C.10}$$

To test the hypothesis that the use of a larger s/a ratio in the Monte Carlo simulation will provide a better fit of the experimental data, equation C.8 was evaluated for five different s/a ratios. The results were compared with the experimental values given by

$$\widetilde{B}(\theta_j) = \exp\left\{ \sum_{i=0}^{3} \widetilde{A}_i(\theta_j, s/a)\, R^i \right\} . \tag{C.11}$$

The coefficients $\widetilde{A}_i$ were determined from the tabulated experimental data by standard least square methods using orthogonal polynomials (ref. C.4). The average fractional discrepancy is defined by

$$\mu(\theta_j, s/a(T), s/a(E)) = \frac{1}{10} \sum_{i=1}^{10} d(\theta_j, s/a(T), s/a(E), R_i) \,, \tag{C.12}$$

where

$$d\,(\theta_j, s/a(T), s/a(E), R_i) = \frac{B_n\,(\theta_j, s/a(T), R_i) - \widetilde{B}\,(\theta_j, s/a(E), R_i)}{\widetilde{B}\,(\theta_j, s/a(E), R_i)} \tag{C.13}$$

and R_i is equal to 1, 2, . . . , 10 attenuation lengths. The sample standard deviation estimate is defined by

$$\sigma\,(\theta_j, s/a(T), s/a(E)) = \left\{ \frac{1}{9} \sum_{i=1}^{10} [d\,(\theta_j, s/a(T), s/a(E), R_i) - \mu\,(\theta_j, s/a(T), s/a(E))]^2 \right\}^{1/2} . \tag{C.14}$$

The statistics for the fractional discrepancies indicate that the differences between the calculated and experimental values for $\theta_j \geqslant 6.3$ deg first decrease and then increase as s/a (T) increases (ref. C.3). Figure C.3 illustrates the comparison of the tabulated experimental data and the values calculated using equation C.8. The s/a(T) and s/a(E) values used to obtain the curves in figure C.3 correspond as follows.

s/a(E)	s/a(T)
4.87	5.27
3.85	4.15
3.56	3.96
2.28	2.38
1.48	1.58

The differences between s/a(E) and s/a(T) can be related to $\theta_0(E)$ using equation C.6. The following values for $\theta_0(E)$ were obtained.

s/a(E)	$\theta_0(E)$, deg
4.87	0.69
3.85	0.56
3.56	0.86
2.28	0.32
1.48	0.48

For conical source beam patterns and receiver fields-of-view, the effective attenuation coefficients can be directly related to the function $B_n\,(\theta_j)$ (ref. C.3):

$$c_1\,(\theta_j) = c_3\,(\theta_j) = -\ln\,(B_n\,(\theta_j))/R\,. \tag{C.15}$$

Therefore, the effective attenuation coefficients are range independent to the extent that the curves in figures C.1 and C.3 can be approximated by straight lines. In addition, the agreement between $B_n(\theta_j, s/a\ (T))$ and $\widetilde{B}(\theta_j, s/a\ (E))$ (fig. C.3) indicates the accuracy of the calculated values of the effective attenuation coefficients if appropriate values of the s/a ratio are used. (Experimental values of the scattering coefficient s(E) should be increased by the factor Δ determined from equation C.6, and the parameters,

$$s/a(T) = s/a(E) + \Delta \tag{C.16}$$

and

$$\alpha(T) = \alpha(E) + \Delta\ , \tag{C.17}$$

determined before the values of c_1 and c_3 are obtained from figure 6.1 and table 6.1.)

C.2 FUNCTIONAL FORM OF THE ON-AXIS IRRADIANCE PRODUCED BY A NONCOLLIMATED SOURCE

In an experiment at Lake Winnipesaukee, New Hampshire, the on-axis irradiance produced by a 1000-W incandescent lamp was determined as a function of range (ref. C.2). A housing was built around the lamp (fig. C.4) to vary the divergence of the beam pattern of the source. A Wratten no. 60 gelatin filter was placed in the optical path of the irradiance detector to limit its spectral response to a narrowband (approximately 60 nm) in the green region of the spectrum. The average total attenuation coefficient for this bandwidth varied in the range $0.179 \leqslant \alpha \leqslant 0.212$ ln/ft during the experiment.

The measured irradiance at the distance R from the source was fitted by the semiempirical equation (ref. C.2):

$$\begin{aligned} h(\theta_j, R) = {} & J \exp(-\alpha R)/R^2 \\ & + J\,(2.5 - 1.5 \log(\pi/\theta_j))\,(1 + 7\,(\pi/\theta_j)^{1/2} \exp(-kR))\,k \exp(-kR)/4\pi R\ , \end{aligned} \tag{C.18}$$

where θ_j is the half-angle (rad) of the beam pattern and k is an attenuation coefficient whose value is adjusted to fit the measured data.* The first term in the equation corresponds to the irradiance produced by unscattered light, and the second term, whose functional form is based on an equation derived from diffusion theory (ref. C.2), gives the irradiance produced by the scattered radiation. Equation C.18 closely fits measured irradiance values for large and small values of R. The maximum fractional discrepancy between the measured values and equation C.18 is 0.64 and occurs at a range of 21 ft. (The fractional discrepancy is defined as the difference between the measured and experimental values divided by the experimental value.) The parameter k was assigned the value of 0.057 ln/ft.

The value of k is approximately equal to the measured value of the attenuation coefficient of scalar irradiance (ref. C.2).

The Monte Carlo simulation estimate of the on-axis irradiance which corresponds to equation C.18 is given by

$$h_n(\theta_j, R) = J \exp(-c_1 R)/R^2 , \tag{C.19}$$

where $c_1(\theta_j)$ is the effective attenuation coefficient for illuminating light. Figure C.5 illustrates the comparison of $h_n(\theta_j, R)$ and $\tilde{h}(\theta_j, R)$ for the following values of θ_j and $c_1(\theta_j)/\alpha$.

θ_j, deg	$c_1(\theta_j)/\alpha$
10	0.388
25	0.333
45	0.325

The lower solid curve in figure C.5 corresponds to the function

$$h_\alpha(R) = J \exp(-\alpha R)/R^2 , \tag{C.20}$$

and the upper curve corresponds to the function

$$h_a(R) = J \exp(-aR)/R^2 , \tag{C.21}$$

where a value of 0.284 was assumed for the a/α ratio. The close agreement between $h_n(\theta_j, R)$ and $\tilde{h}(\theta_j, R)$ indicates the validity of the functional form of the effective attenuation coefficient equation. In addition, $h_n(\theta_j, R)$ has proper asymptotic behavior for both large and small values of θ_j, while $\tilde{h}(\theta_j, R)$ gives nonphysical results for $\theta_j \leqslant 4$ deg.

C.3 POLARIZATION-DISCRIMINATION SYSTEMS TESTED AT MORRIS DAM

Two polarization-discrimination systems were tested at Morris Dam during the 1970 system comparison test program (ref. C.1). The system chosen for comparison with the system performance analysis consisted of a 1000-W incandescent source (color temperature 3400 °K) with a dichroic HGCP 21 polarizer and an SEC television camera tube with a dichroic HGCP 21 analyzer. The available experimental data, which characterizes the properties of the system components and the properties of the different types of water in which the system was tested, is listed below. (The data is from ref. C.1.) The maximum viewing ranges are compiled in table C.1.

1. Light-source characteristics

   $E(\lambda)\, d\lambda$ - 3400 °K incandescent source (table 6.6)
   $w = 1000$ W
   $\theta_1 = 15$ deg

2. Receiver characteristics

$A_0 = 3.10 \times 10^{-4}\ m^2$ (1-in. image diagonal)
$\tau = 1.0$
f/8
$\theta_3 = 12.7$ deg
$S(\lambda)$ = S-20 photocathode (table 6.7)
$G(\lambda)$ = incandescent source, S-20 photocathode (table 6.8)

3. Extended-range equipment characteristics

$e_1 = 0.230$ (dichroic HGCP 21 polarizer)
$e_2 = 0.230$ (dichroic HGCP 21 analyzer)
$\psi_s = 0.00$
$\psi_b = 0.71$

4. Target characteristics – bar chart

$\rho_1 = 0.035$ (black bar)
$\rho_2 = 0.86$ (high contrast)
$\rho_2 = 0.35$ (medium contrast)
$\rho_2 = 0.15$ (low contrast)

5. System Geometry

d = 0.343 m
R = 10, 11, . . . , 17, 18 m (clearest water, $1/\alpha$ = 5.0 m/ln)
R = 8, 9, . . . , 13, 14 m (intermediate water, $1/\alpha$ = 3.5 m/ln)
R = 2, 3, . . . , 7, 8 m (most turbid water, $1/\alpha$ = 1.0 m/ln)

6. Water Characteristics

Spectral characteristics – $\lambda_1(S), \lambda_0(S), \lambda_2(S), \lambda_1(N), \lambda_0(N), \lambda_2(N)$
(These parameters cannot be specified because the spectral variation of $\alpha(\lambda)$ and $s(\lambda)/\alpha(\lambda)$ were not measured. Therefore, the values

$\lambda_1(S) = 500$ nm
$\lambda_2(S) = 570$ nm
$\lambda_1(N) = 470$ nm
$\lambda_2(N) = 570$ nm

were assumed. The corresponding values

$\Delta G = G(570) - G(500) = 1.50 \times 10^3$
$\Delta G = G(570) - G(470) = 1.93 \times 10^3$

give the combined spectral response for the incandescent source and the S-20 photocathode.)

Values of the optical properties at $\lambda = \lambda_0$

Water Type	$\alpha(\lambda_0)$	$s(\lambda_0)$	η	s/a	c_1/α	c_3/α
I	0.200	0.010	0.018	0.05	0.96	0.96
II	0.286	0.038	0.018	0.16	0.89	0.89
III	1.000	0.660	0.018	1.94	0.43	0.43

A computer program was written to calculate the maximum viewing ranges for this system using the formulas described in section 6. The predicted maximum viewing ranges are compiled in table C.2. These maximum ranges were determined from the signal response curves for the SEC camera tube (table 6.8) and the data calculated by the computer program. (The maximum viewing ranges correspond to a calculated noise-limited resolution of 50 television lines.)

The calculated and experimental values for the maximum viewing ranges agree reasonably well for the clearest water (Type I) and the moderately turbid water (Type II). The discrepancy between the experimental and calculated values for the most turbid water (Type III) is assumed to be due to the erroneous specification of the optical properties of the water. To test this hypothesis, the predicted maximum viewing ranges were calculated for three different sets of optical properties – Type III-A; Type III-B; and Type III-C.

The optical properties which specify these new types of water and the predicted maximum viewing ranges are in table C.3. The parameters chosen for the Type III-A and the Type III-B waters both assume the same smaller value of the total attenuation coefficient $\alpha(\lambda_0)$, but different values of η, the fraction of light which is scattered into the back hemisphere. (The values of $s(\lambda_0)$ which correspond to the selected values of $\alpha(\lambda_0)$ were determined from reference C.1, and the values for the c_1/α and c_3/α ratios were obtained from table 6.1.) The values for the Type III-C water were selected to test the validity of the assumptions described in section 6.2.3.4, which are required for using the effective attenuation coefficient c_3 to calculate the backscattered irradiance in the image. The ranges predicted for the Type III-B water most nearly match the experimental values. The constant change in the values of the optical properties during the course of the system performance measurements could be a possible reason for the erroneous specification of the original set, Type III, of optical properties.

The variation of resolution in television lines with viewing range was also determined for the polarization-discrimination system (ref. C.1). To compare this experimental resolution with the calculated noise-limited resolution, the square-wave response function $R_{sq}(N)$ must be considered. As indicated in equation 6.124, the function $R_{sq}(N)$ gives the ratio of the observed or experimental resolution in television lines to the calculated noise-limited resolution given by the signal response curves. The function $R_{sq}(N)$ describes the degradation in resolution due to aberrations and finite apertures in the optical system of the receiver. In addition, for an underwater optical viewing system, the decrease in resolution due to small-angle scattering in the seawater medium must also be included in $R_{sq}(N)$.

Figure C.6 compares the calculated resolution N(cal) and the experimental resolution N(exp) for the polarization-discrimination system in Type II water. The values of N(exp) were determined according to the equation,

$$N(\exp)\,W = (3/4)\cdot(39.4)\cdot(\pi/180)\cdot(2\theta_3)\cdot R = 13.15R\,, \qquad \text{(C.22)}$$

where W is the minimum resolvable bar width measured at the target in inches. Estimates of the square-wave response function which are calculated using

$$R_{sq}(N) = \frac{N(exp)}{N(cal)} \tag{C.23}$$

are plotted in figure C.7. The functions N(exp) and N(cal) are compared in figure C.8 for Type I, Type II, and Type III-B waters, and the corresponding estimates of $R_{sq}(N)$ are plotted in figure C.9. Although the deviations in the estimates of $R_{sq}(N)$ are larger than desired, this function appears to converge to a value of 0.5 as N(cal) approaches zero. This agrees with the data in table 6.10 which indicates that about two lines (1.00 ± 0.25 line pairs) are required to detect the minimum dimension of a target element. According to equation C.22, N(exp) is the number of target elements of minimum size which can be placed across the vertical field-of-view of the receiver. Because two lines (one line pair) are required to detect a resolution element (target object of minimum size), the value of N(cal) should be approximately twice the value of N(exp).

C.4 REFERENCES

C.1 Naval Undersea Research and Development Center, NUC TP 273. *Comparison of Advanced Underwater Television Systems,* by S. B. Bryant, D. Cozen, R. Fugitt, and C. Funk. San Diego, California. January 1972.

C.2 Scripps Institute of Oceanography, SIO Ref. 71-1. *Underwater Lighting by Submerged Lasers and Incandescent Source,* by S. Q. Duntley. San Diego, California. June 1971.

C.3 Funk, Clarence J. *Energy Propagation Constraints on Underwater Optical and Acoustical Imaging Systems.* Ph.D. Dissertation, University of California, Los Angeles, California. June 1972.

C.4 Forsythe, George E. "Generation and Use of Orthogonal Polynomials for Data-Fitting with a Digital Computer," *J. Soc. Indust. Appl. Math.* Vol. 15, pp. 74-88. June 1957.

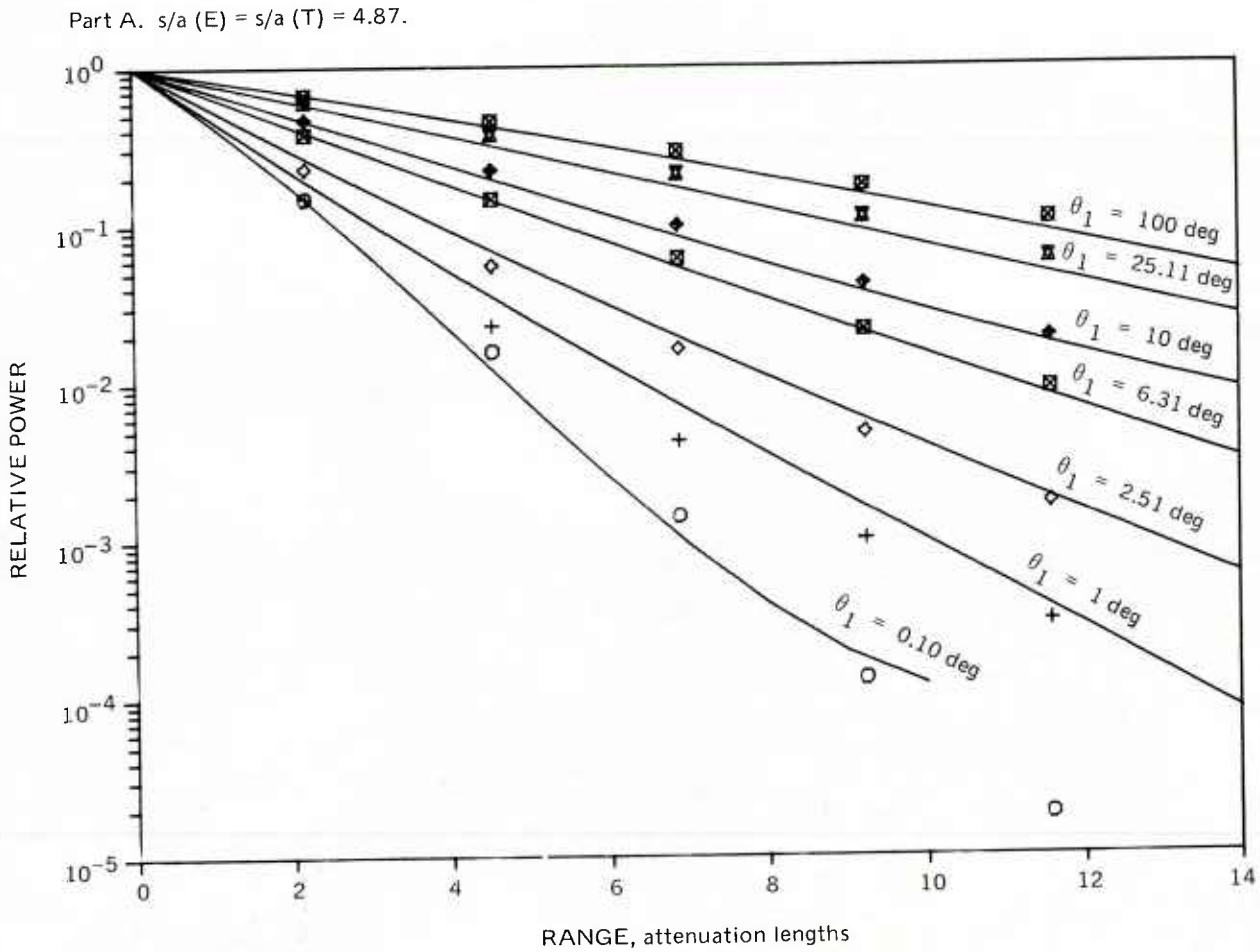

Figure C.1. Comparison of experimental and calculated estimates of the radiation field (s/a (T) = s/a (E)).

Part B. s/a (E) = s/a (T) = 3.85.

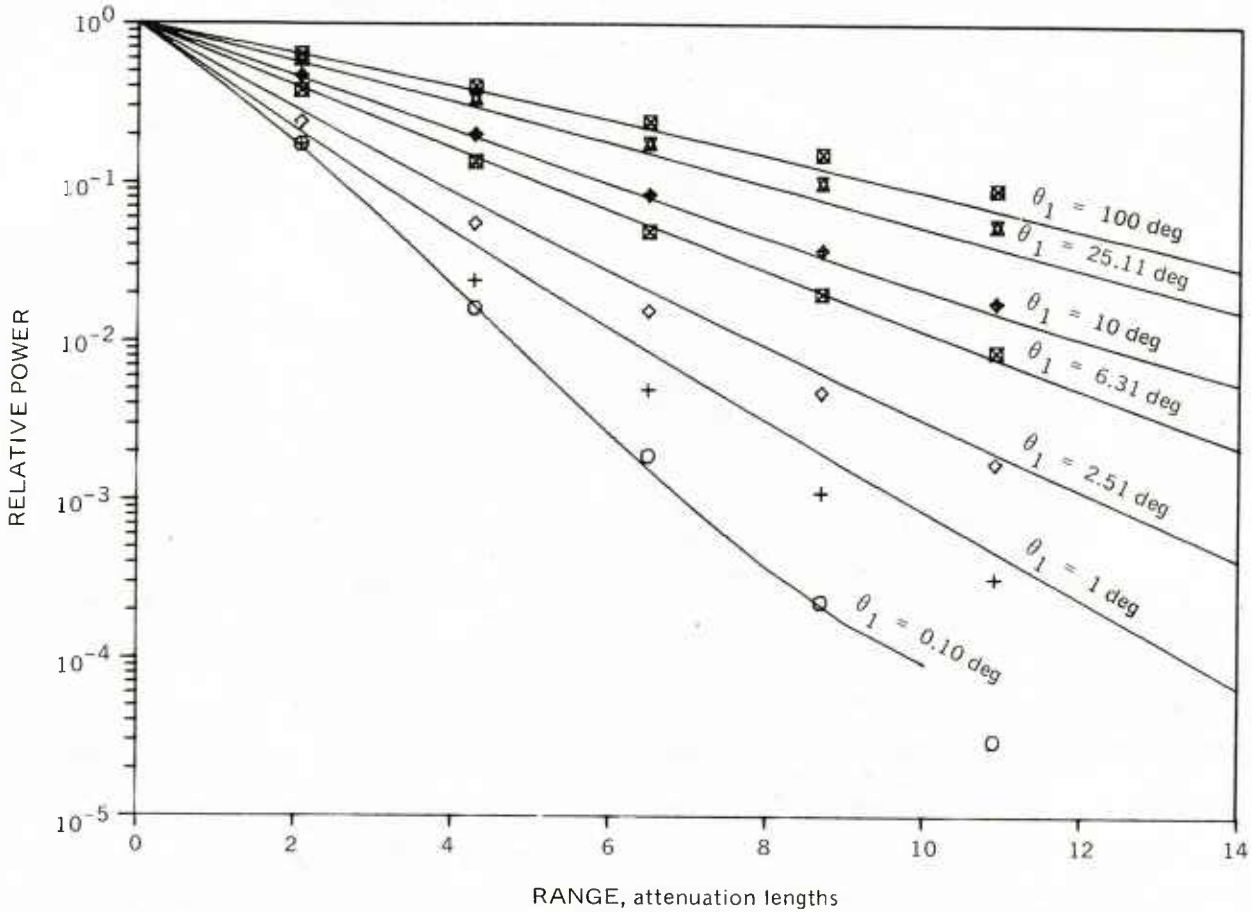

Figure C.1. (Continued).

Part C. s/a (E) = s/a (T) = 3.56.

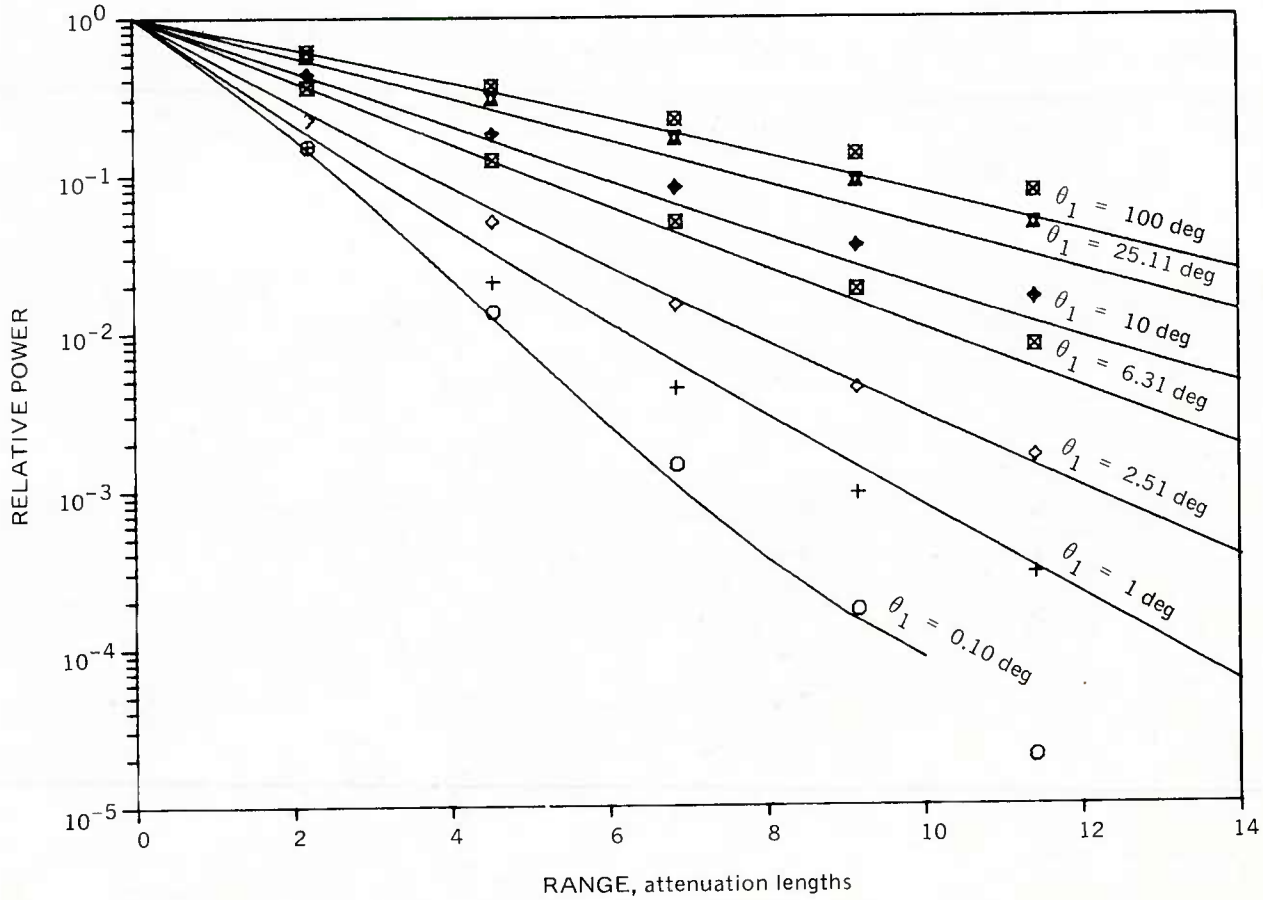

Figure C.1. (Continued).

Part D. s/a (E) = s/a (T) = 2.28.

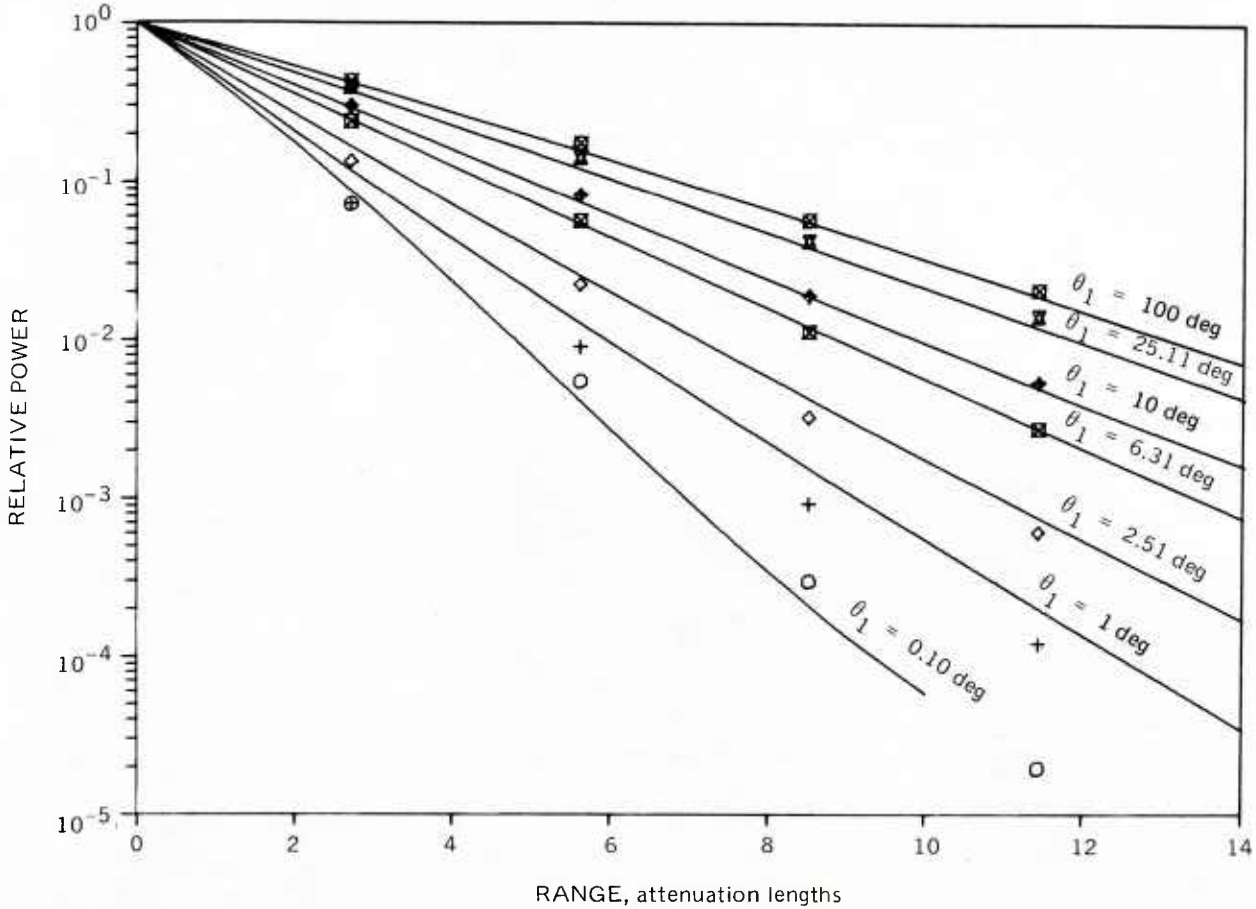

Figure C.1. (Continued).

Part E. s/a (E) = s/a (T) = 1.48.

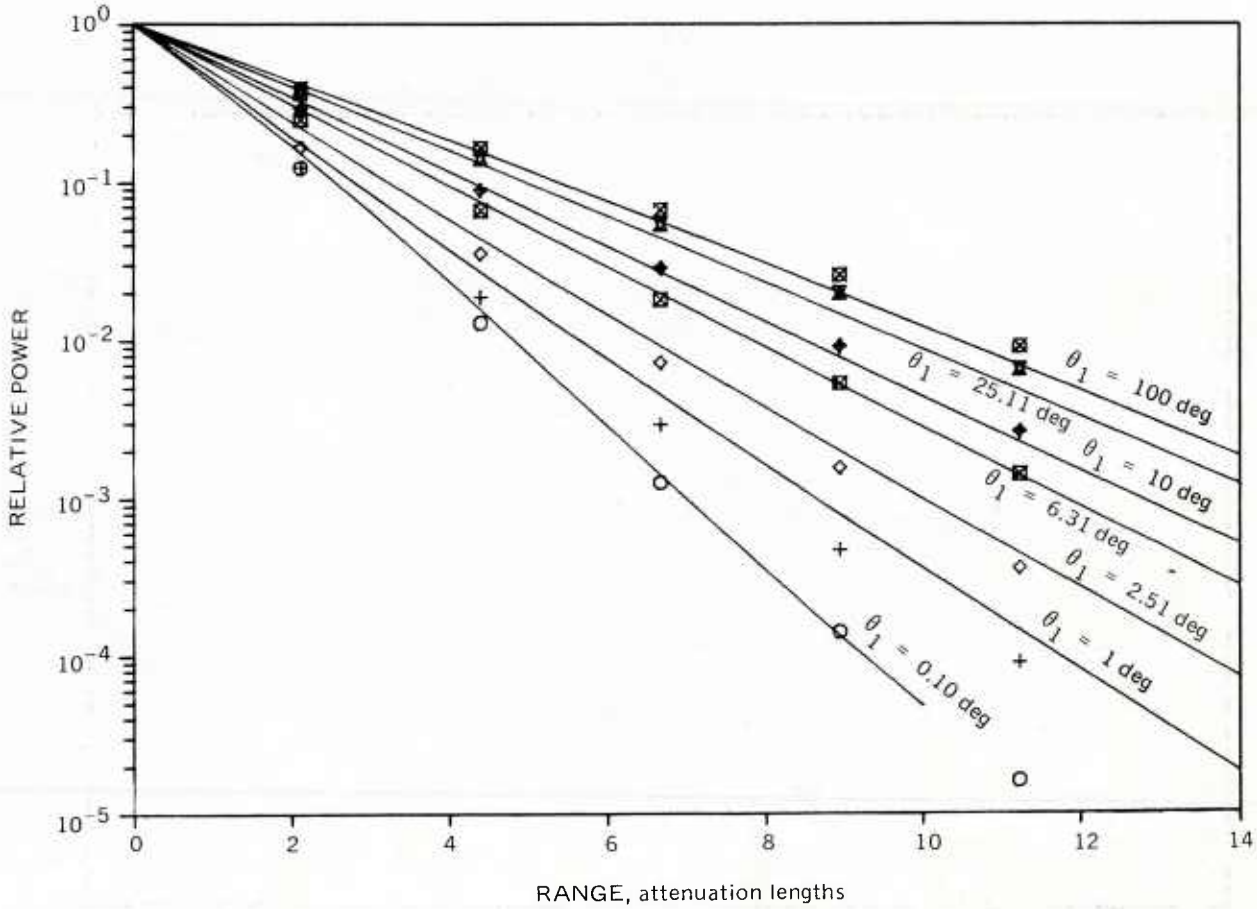

Figure C.1. (Continued).

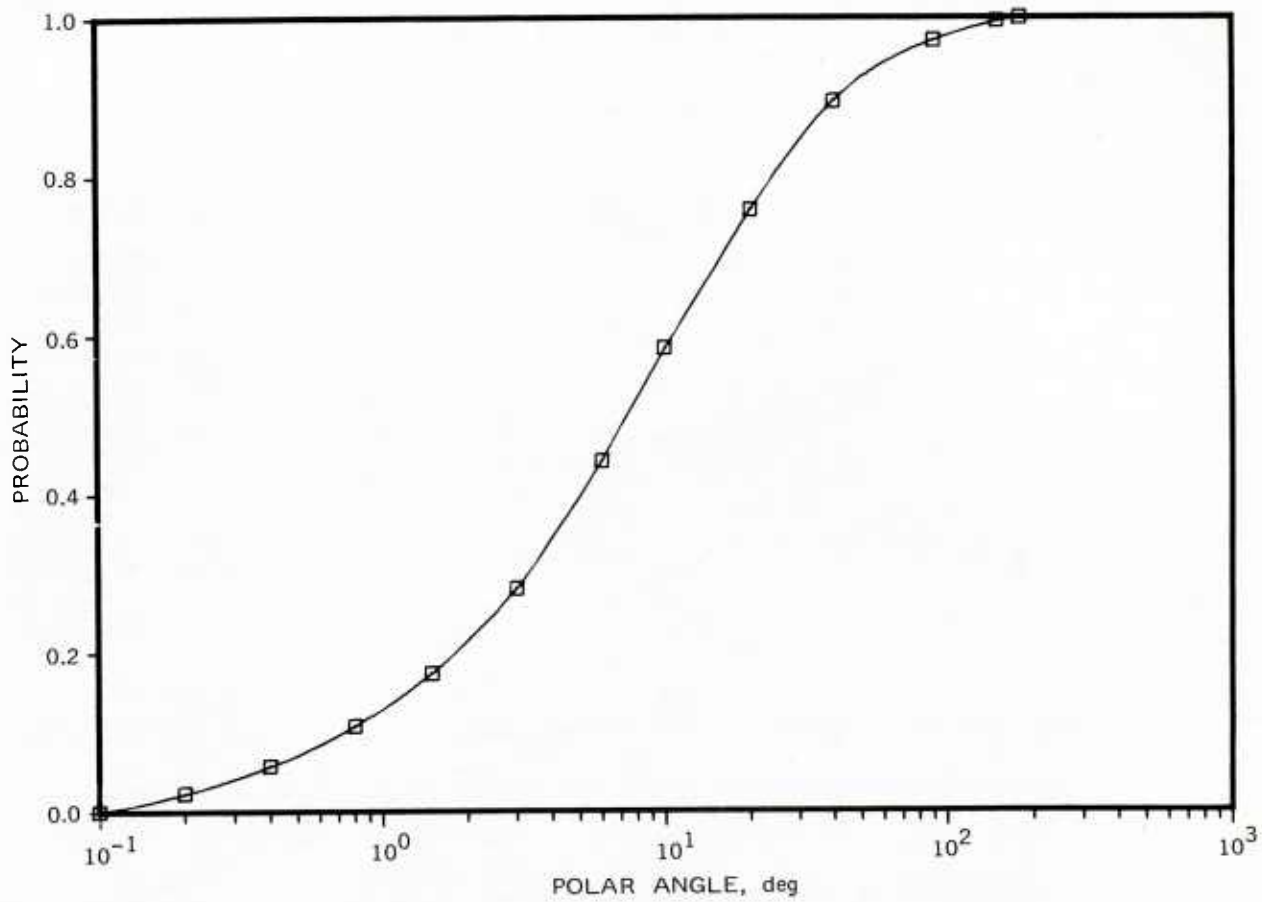

Figure C.2. Probability distribution functions for single-scattered light.

Part A. s/a(E) = 4.87, s/a(T) = 5.27.

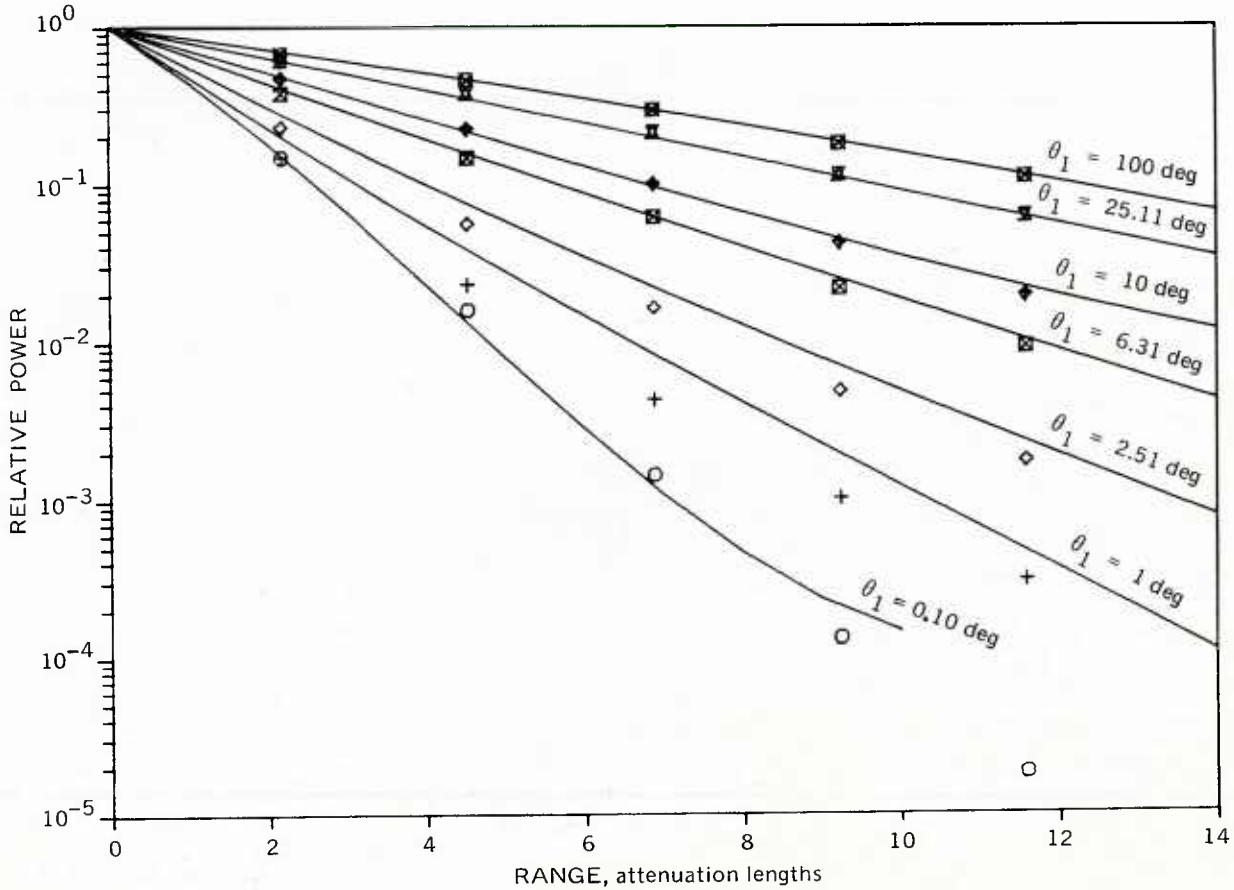

Figure C.3. Comparison of experimental and calculated estimates of the radiation field (s/a (T) ≠ s/a (E)).

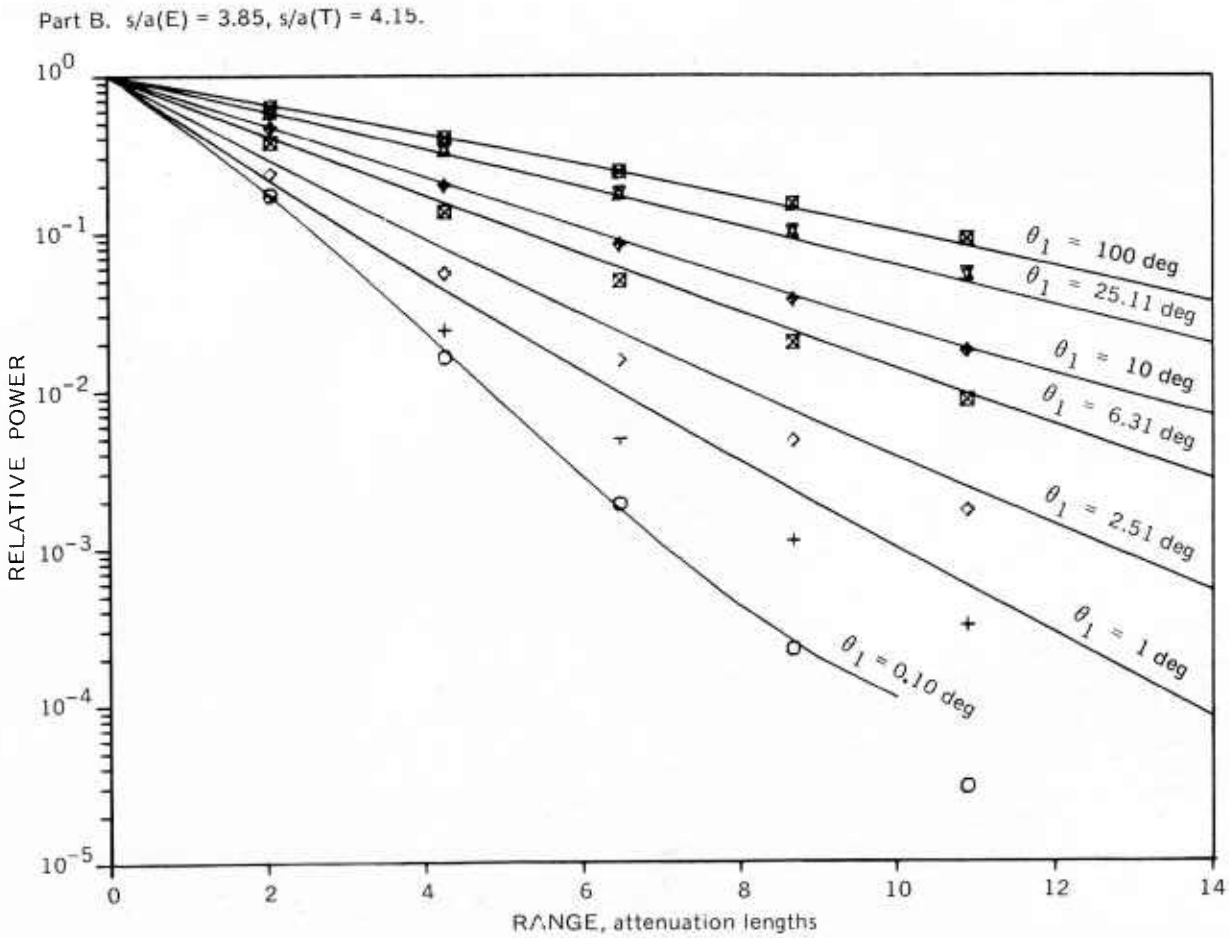

Figure C.3. (Continued).

Part C. s/a(E) = 3.56, s/a(T) = 3.96.

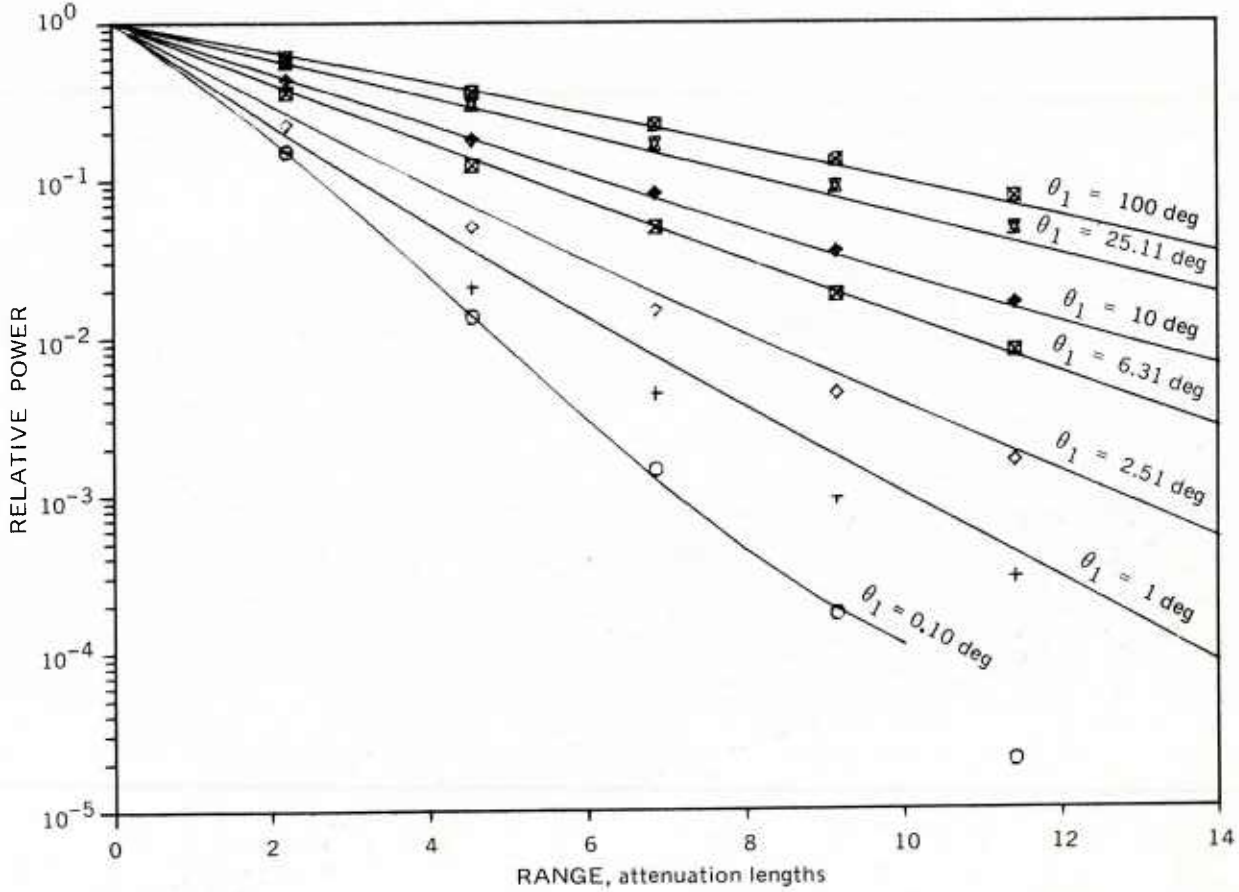

Figure C.3. (Continued).

Part D. s/a(E) = 2.28, s/a(T) = 2.38.

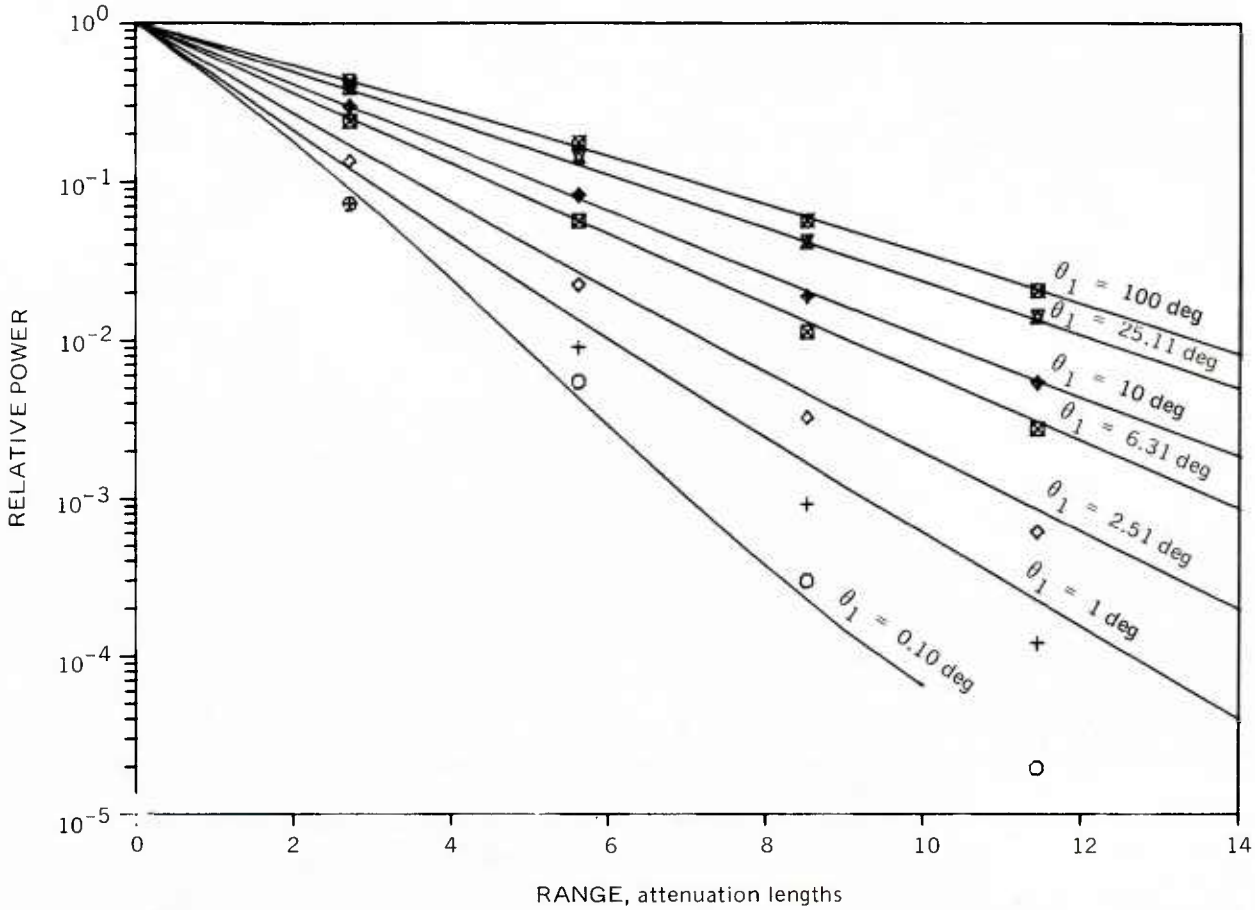

Figure C.3. (Continued).

Part E. s/a(E) = 1.48, s/a(T) = 1.58.

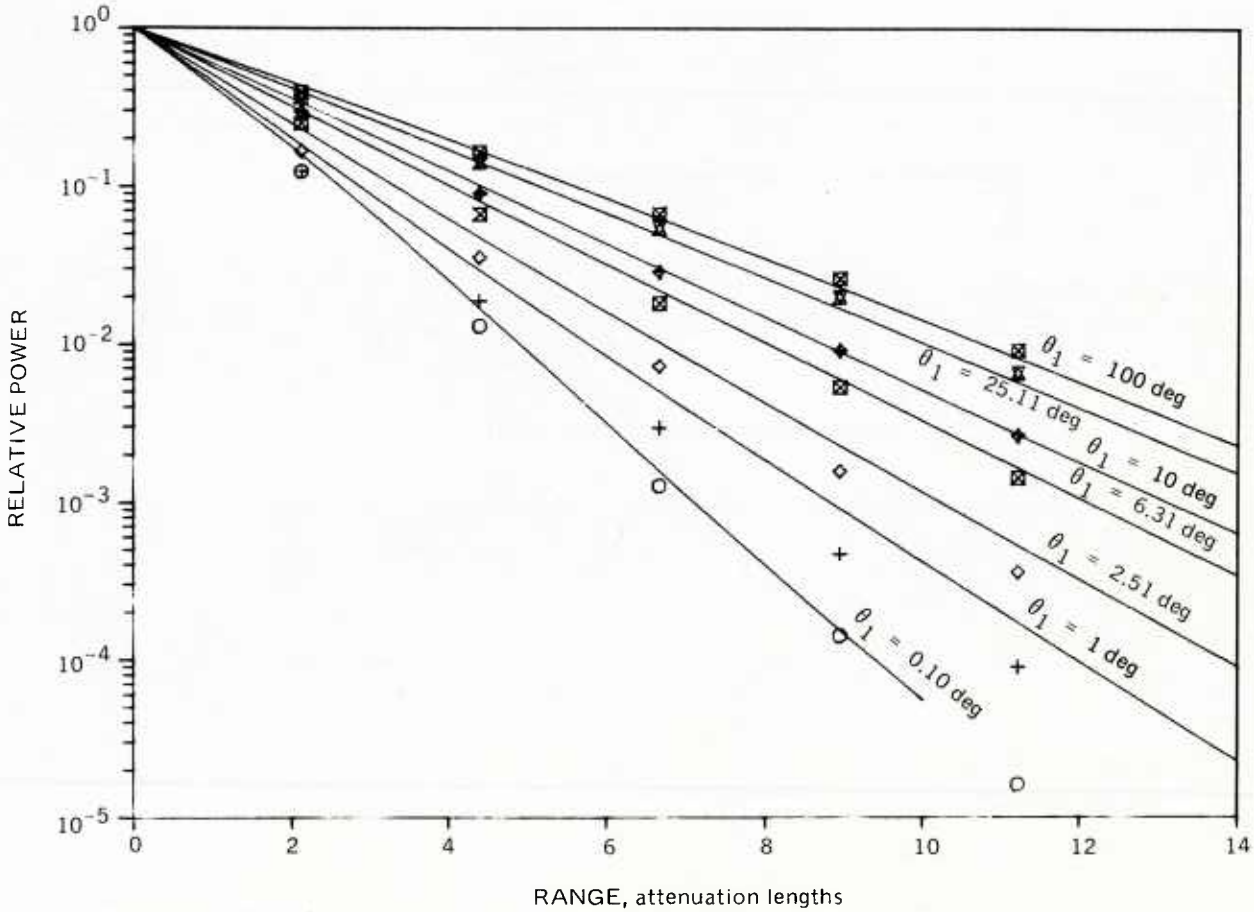

Figure C.3. (Continued).

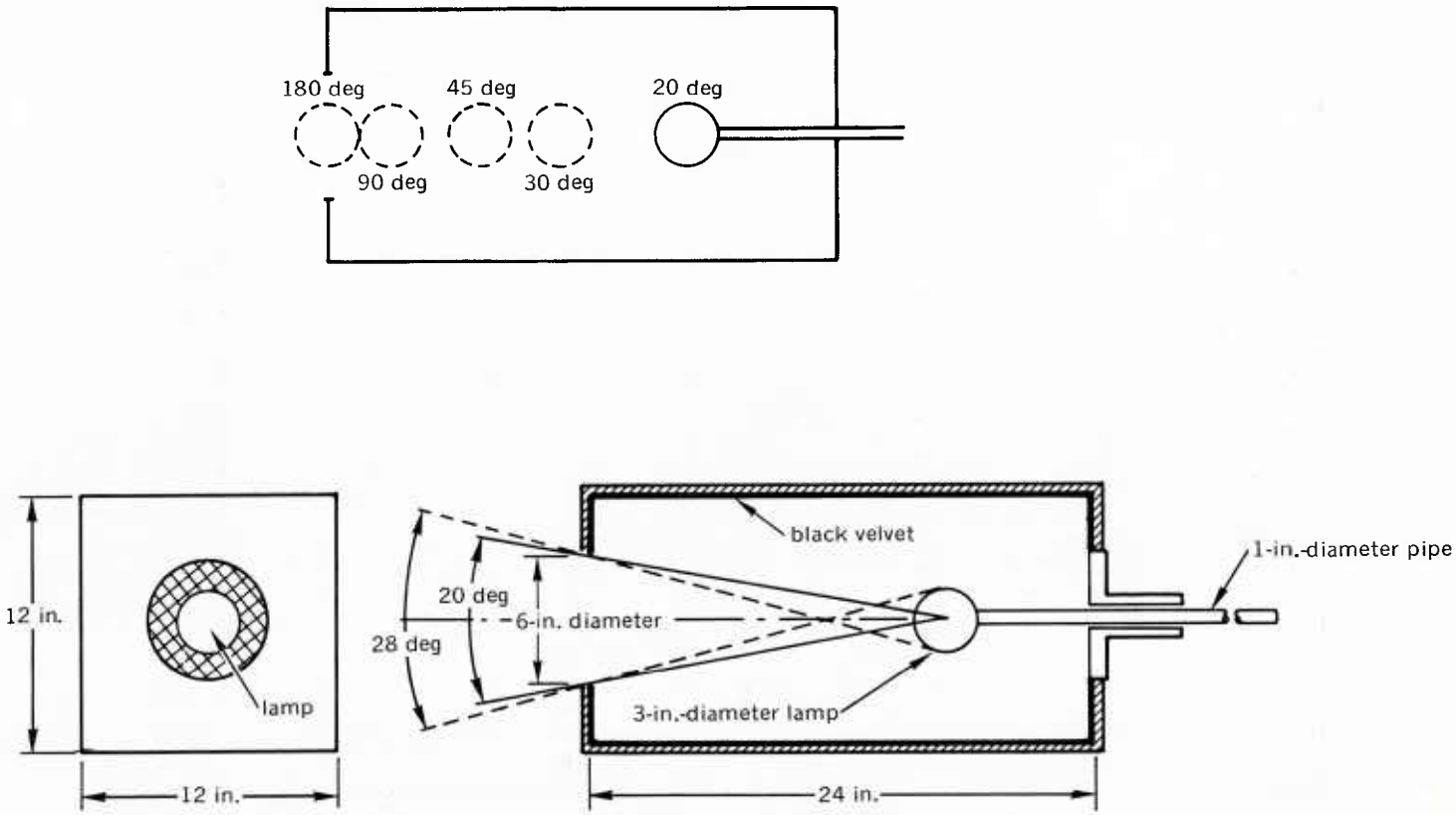

Figure C.4. Housing for controlling the divergence of the beam pattern of the noncollimated source (ref. C.2).

Part A. θ_j = 10 deg.

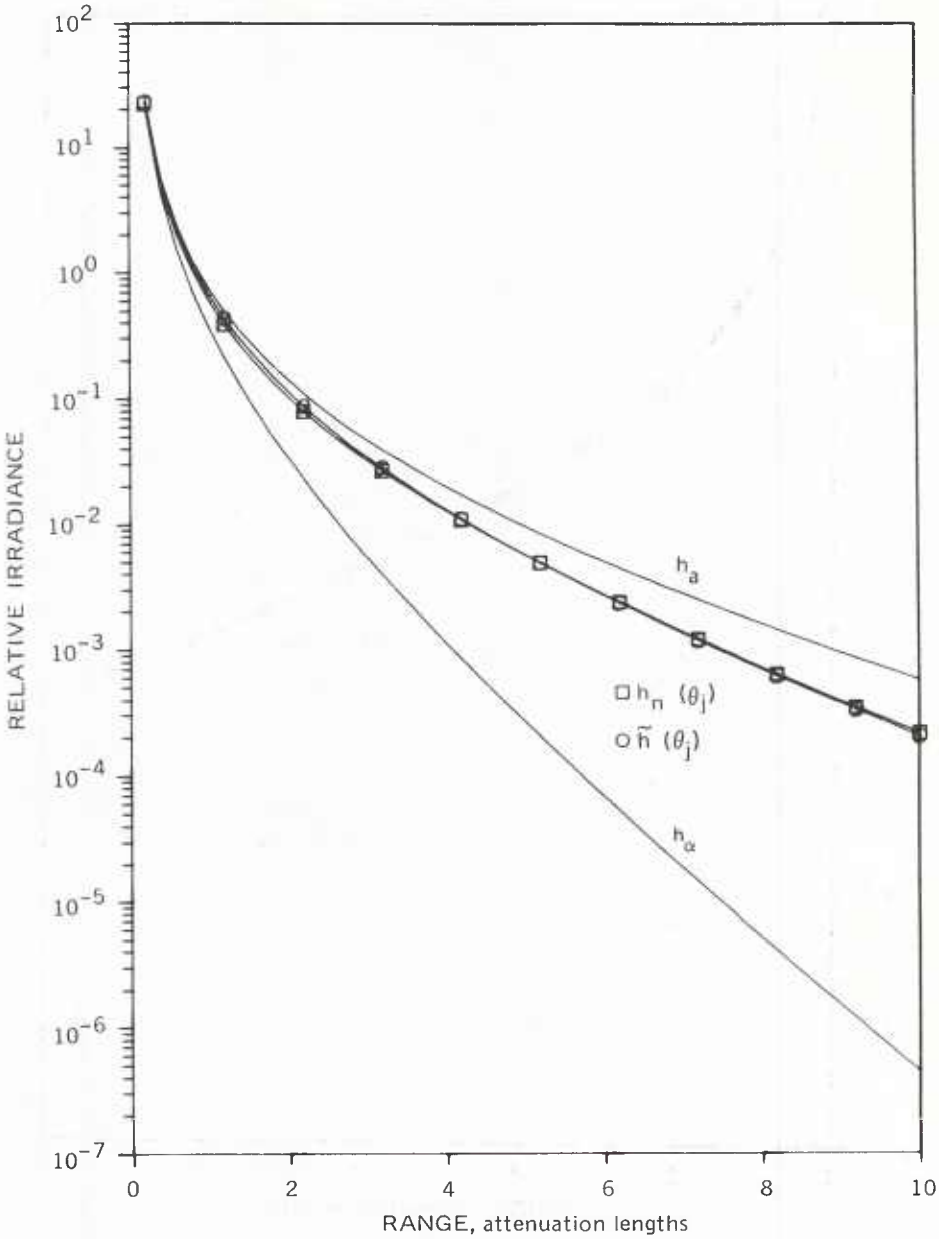

Figure C.5. (Continued).

Part B. θ_j = 25 deg.

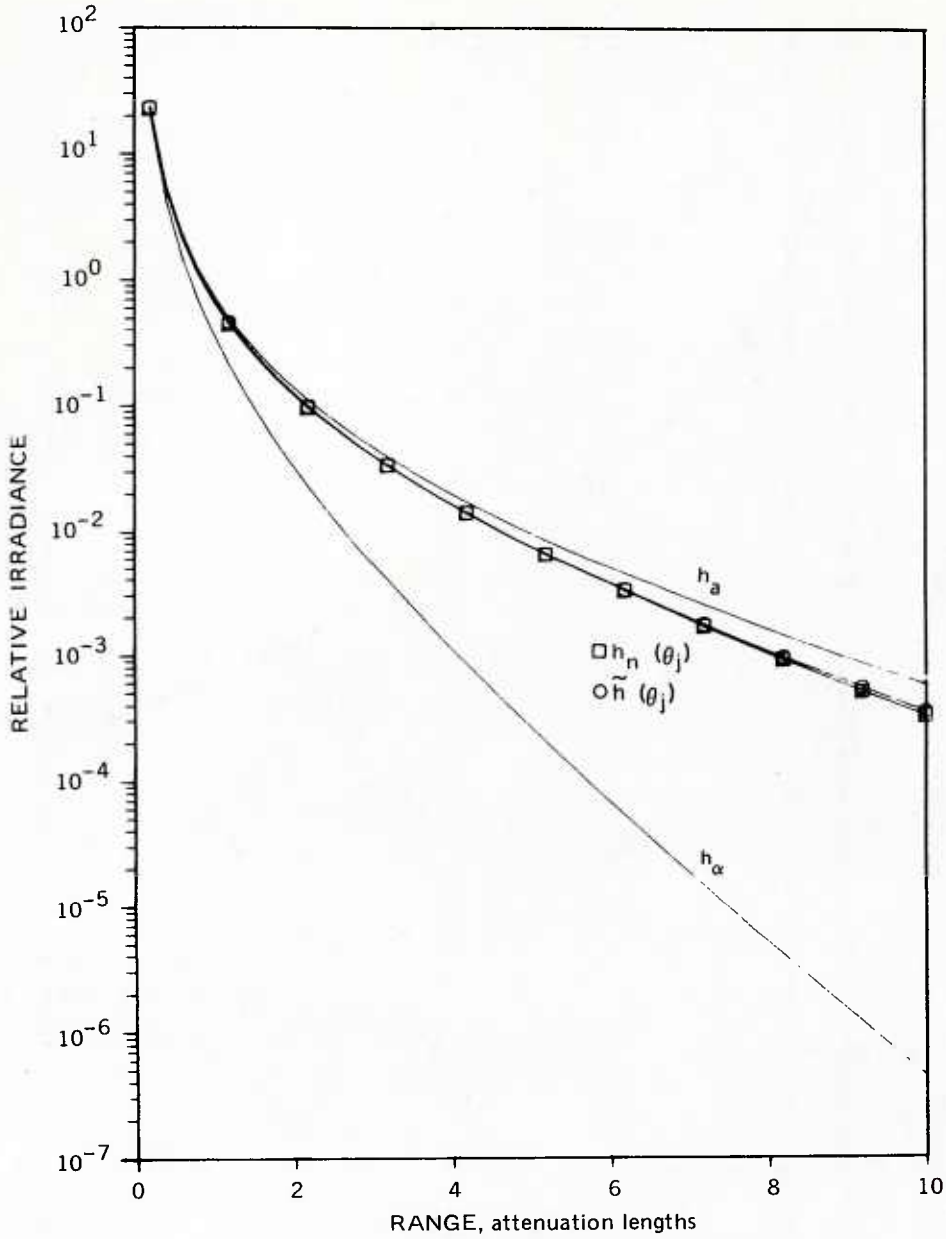

Figure C.5. (Continued).

Part C. θ_j = 45 deg.

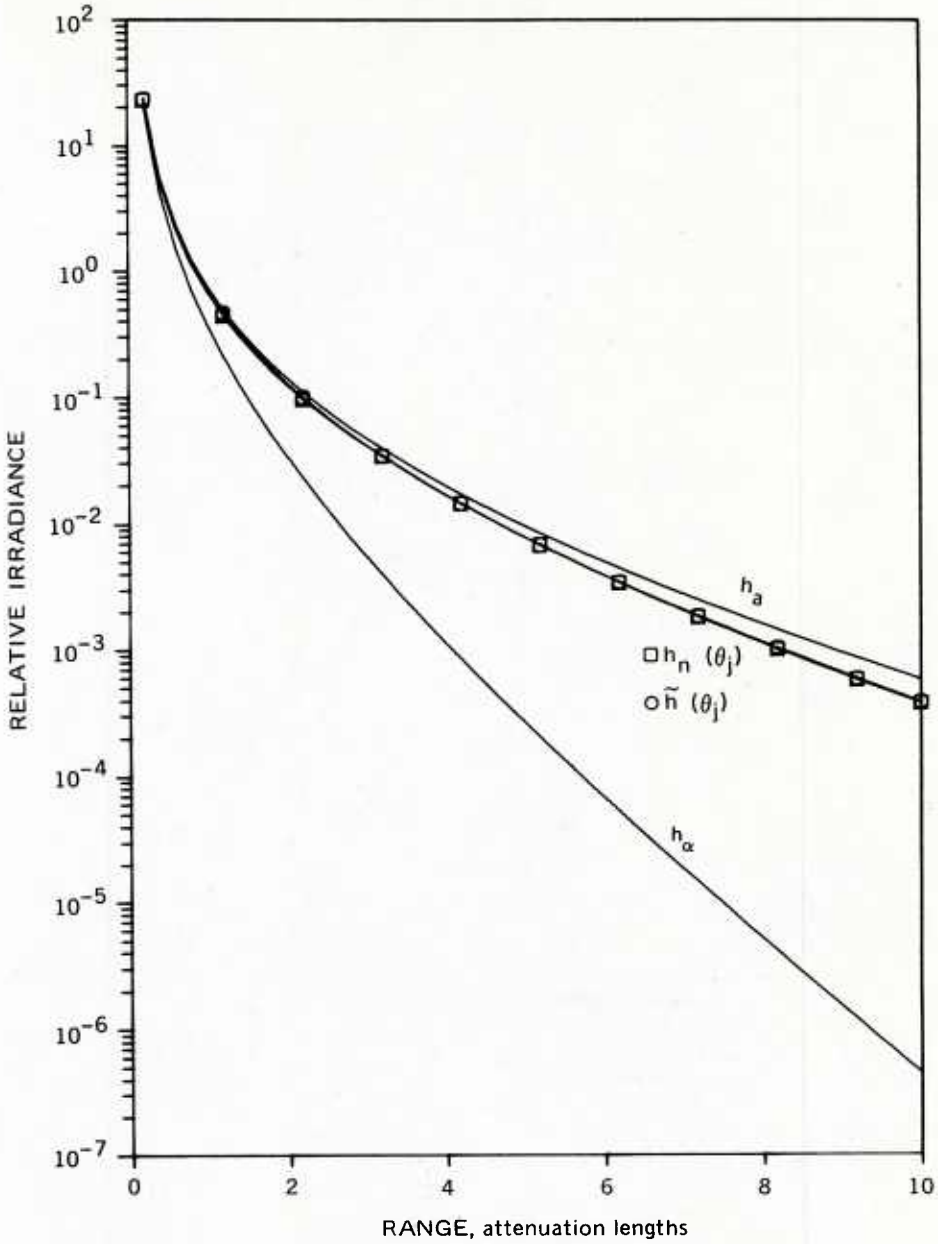

Figure C.5. Comparison of the on-axis irradiance predicted by the semiempirical formula $\tilde{h}(\theta_j, R)$ and by the effective attenuation coefficient formula $h_n(\theta_j, R)$.

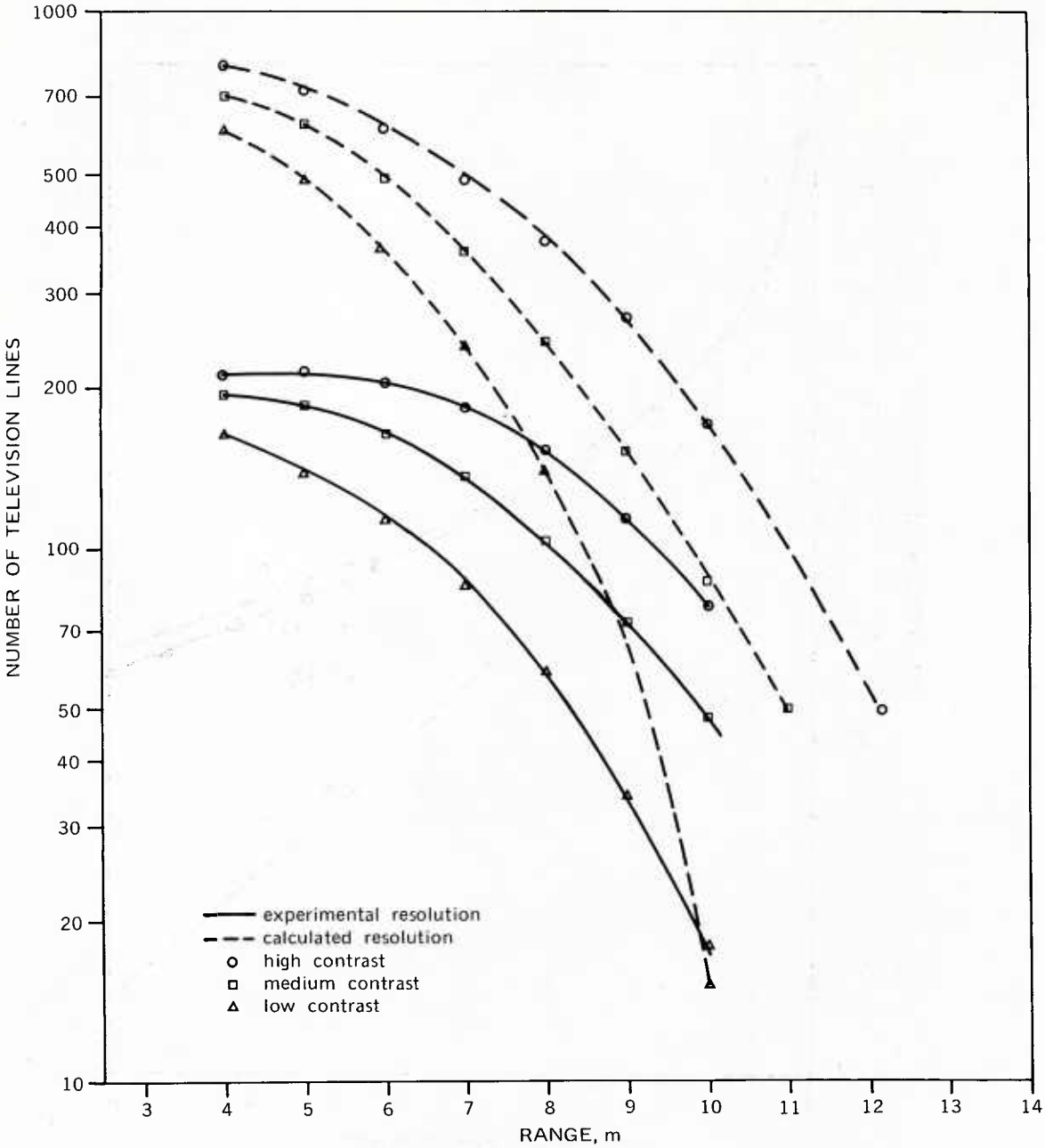

Figure C.6. Comparison of N(exp) and N(cal) for the polarization-discrimination system in Type II water.

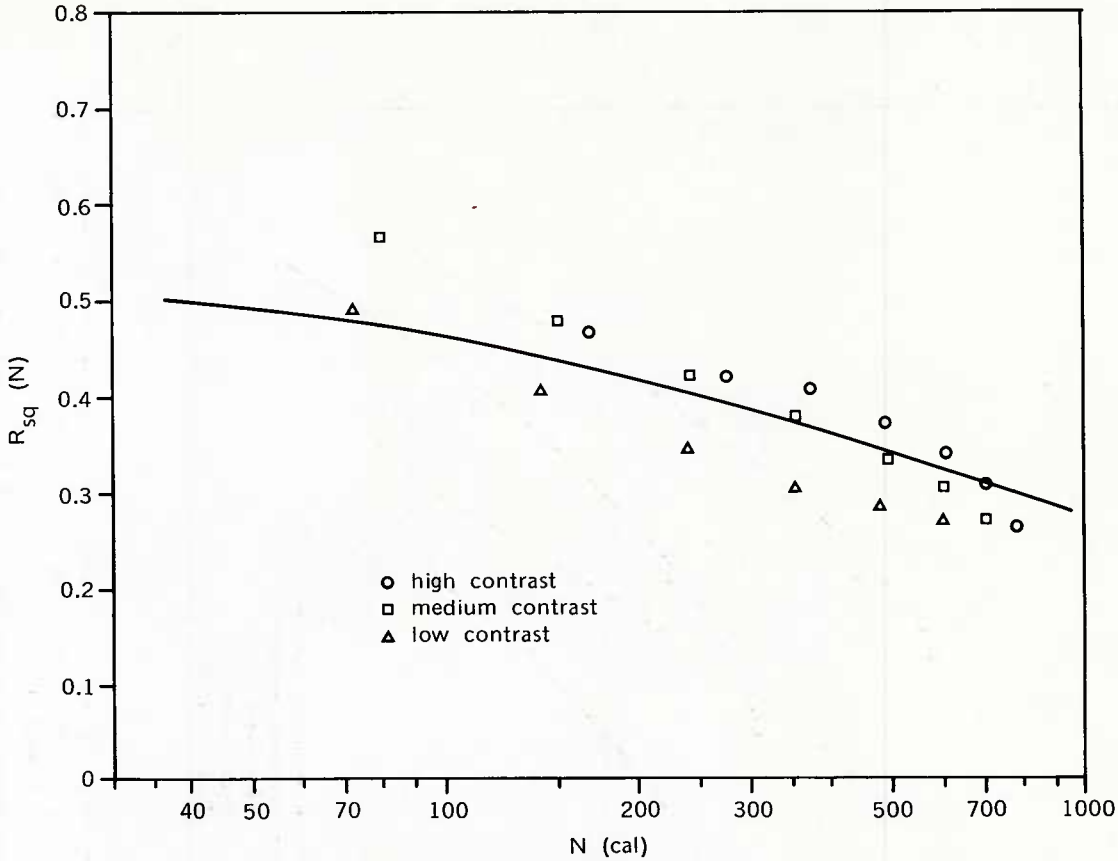

Figure C.7. Estimates of $R_{sq}(N)$ for the polarization-discrimination system in Type II water.

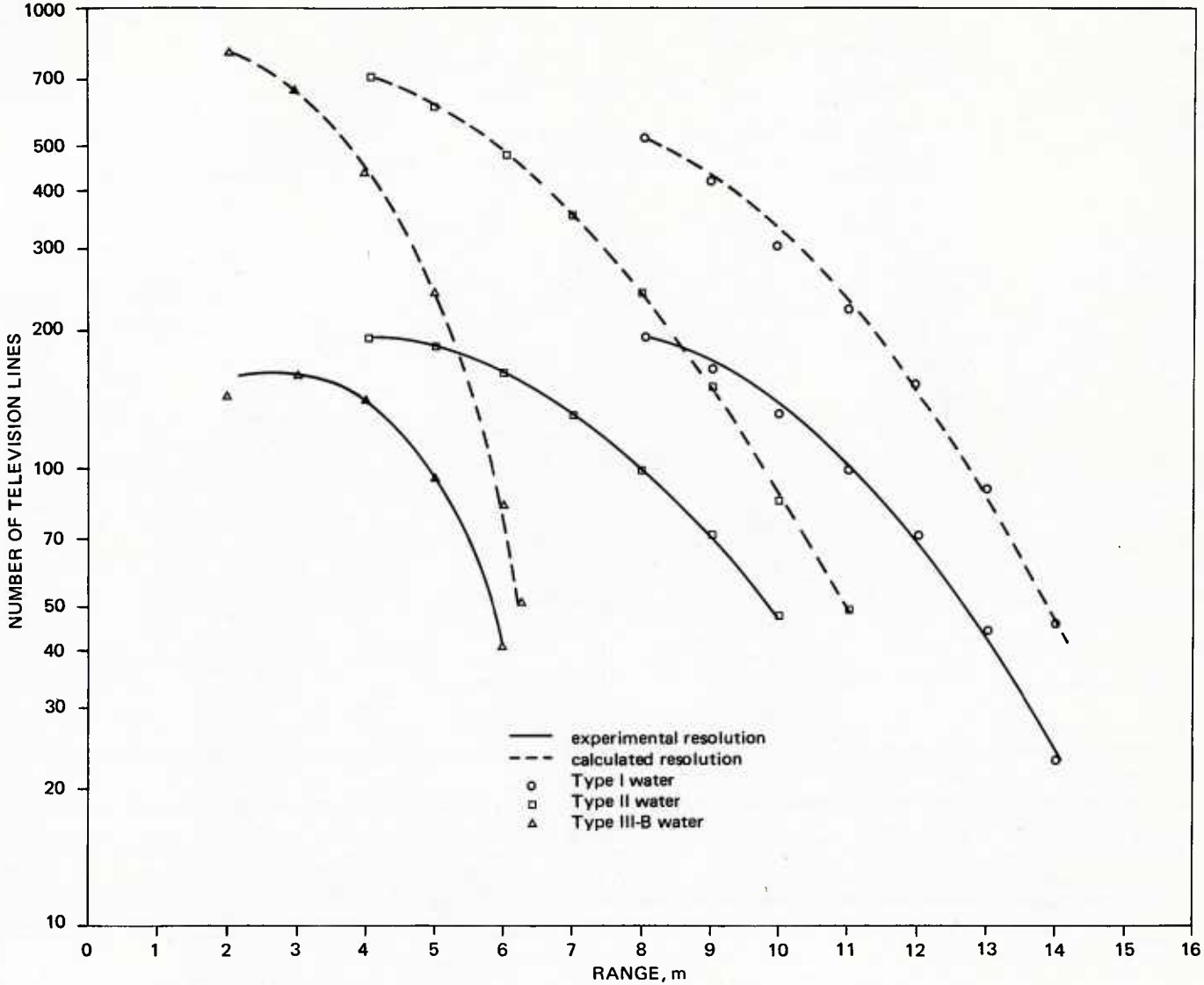

Figure C.8. Comparison of N(exp) and N(cal) for the polarization-discrimination system in Type I, Type II, and Type III-B waters.

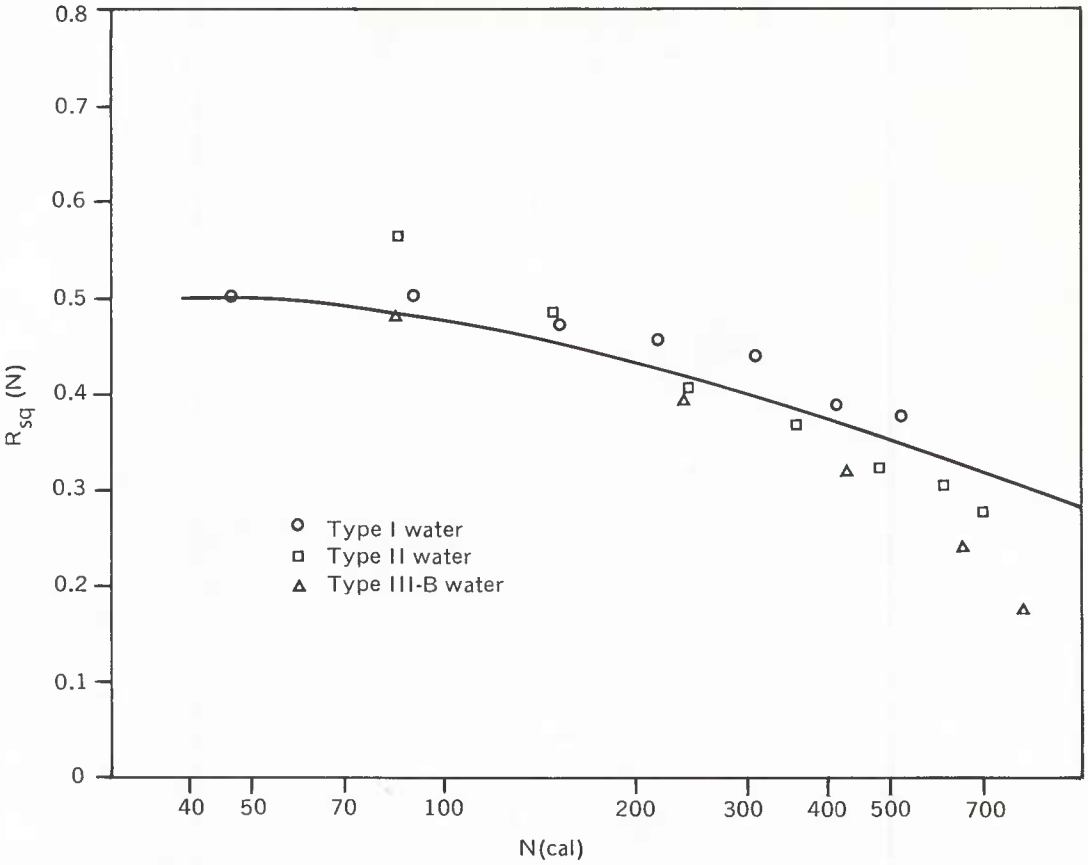

Figure C.9. Estimates of $R_{sq}(N)$ for the polarization-discrimination system in Type I, Type II, and Type III-B waters.

Table C.1. Maximum Experimental Viewing Ranges (m) for the Polarization-Discrimination System Tested at Morris Dam.*

Water Type	Target Contrast		
	High	Medium	Low
I	16.5	14.3	12.5
II	12.3	11.2	9.1
III	7.3	6.7	5.8

*The properties of the different types of water are listed on page C-10.

Table C.2. Maximum Viewing Ranges (m) for the Polarization-Discrimination System Predicted by the System Performance Analysis Method.

Water Type	Target Contrast		
	High	Medium	Low
I	16.0	14.0	12.2
II	12.2	11.0	9.5
III	5.5	4.9	4.5

Table C.3. Optical Properties and Corresponding Predicted Maximum Viewing Ranges for Three Assumed Types of Water.

Water Type	Optical Properties					
	$\alpha(\lambda_0)$	$s(\lambda_0)$	η	s/a	c_1/α	c_3/α
III-A	0.70	0.38	0.032	1.19	0.53	0.53
III-B	0.70	0.38	0.018	1.19	0.53	0.53
III-C	1.00	0.66	0.018	1.94	0.43	1.00

Predicted Maximum Viewing Ranges (m)

Water Type	Target Contrast		
	High	Medium	Low
III-A	6.8	6.1	5.4
III-B	7.0	6.3	5.6
III-C	5.7	5.3	4.6

USER COMMENT RETURN FORM

_____
(date)

From:
To: Deep Ocean Technology Program

Subj: Improvement of Handbook of Underwater Imaging System Design, Suggestions for

1. It is suggested that the handbook could be improved by making the following changes:

2. Reasons for suggested changes are:

3. It is further suggested that the handbook could be made more useful to users by adding material on the following (provide information or indicate sources of information if known):

_____ _____
(signature) (date)

_____
(title, organization)

(Fold so that return address is out, tape, and mail.
No postage required.)

DEPARTMENT OF THE NAVY
NAVAL SHIP ENGINEERING CENTER
HYATTSVILLE, MARYLAND 20782

OFFICIAL BUSINESS

POSTAGE AND FEES PAID
DEPARTMENT OF THE NAVY
DoD-316

U.S.MAIL

Commanding Officer
Naval Ship Engineering Center (Code 6157E)
Hyattsville, Maryland 20782